TR diss
2641

Plasma Etching
for Integrated Silicon Sensor Applications

Plasma Etching for Integrated Silicon Sensor Applications

PROEFSCHRIFT

ter verkrijging van de graad van doctor
aan de Technische Universiteit Delft,
op gezag van de Rector Magnificus Prof. ir. K. F. Wakker,
in het openbaar te verdedigen ten overstaan van een commissie,
door het College van Dekanen aangewezen,
op maandag 16 oktober 1995 te 10:30 uur

door

Yuan Xiong LI

Master of Science
geboren te Fujian, China

Dit proefschrift is goedgekeurd door de promotor:
Prof. dr. ir. S. Middelhoek

Toegevoegd promotor:
Dr. ir. R. F. Wolffenbuttel

Samenstelling promotiecommissie:

Rector Magnificus, voorzitter	Technische Universiteit Delft
Prof. dr. ir. S. Middelhoek	Technische Universiteit Delft
Prof. dr. C. I. M. Beenakker	Technische Universiteit Delft
Prof. dr. J. H. J. Fluitman	Universiteit Twente
Prof. dr. ir. P. P. L. Regtien	Universiteit Twente
Prof. M. Zhang	Shanghai Institute of Metallurgy, Chinese Academy of Sciences
Dr. ir. R. F. Wolffenbuttel	Technische Universiteit Delft
Dr. P. J. French	Technische Universiteit Delft

Published and distributed by:
Delft University Press
Stevinweg 1
2628 CN Delft
The Netherlands
Telephone +31 15 783254
Fax +31 15 781661

CIP-DATA KONINKLIJKE BIBLIOTHEEK, DEN HAAG
Li, Yuan Xiong
Plasma Etching for Integrated Silicon Sensor Applications / Y. X. Li. - Delft : Delft University Press. - Ill.
Thesis Delft University of Technology. - With ref. - With summary in Dutch.
ISBN 90-407-1177-1
NUGI 841
Subject headings: Plasma etching/Silicon sensor/Micromachining

Copyright © 1995 by Y. X. Li
All rights reserved.
No part of the material protected by this copyright notice may be reproduced or utilized in any form or by any means, electronic or mechanical, including photocopying, recording or by any information storage and retrieval system, without permission from the publisher: Delft University Press, Stevinweg 1, 2628 CN Delft, The Netherlands.

Printed in The Netherlands

To my parents and Jing

On the cover: SEM (Scanning Electron Microscope) photograph of etching sidewall profile of an n^- epitaxial layer with an underlying n^+ buried layer on a p-type silicon substrate. The dependence of the sidewall profile on the type and level of the doping has been used to develop a completely "dry" bulk micromachining process - SIMPLE in this study.

Table of Contents

1 **Introduction** **1**

1.1 Introduction **1**

1.2 Silicon micromachining techniques - an overview **3**

1.2.1 Bulk micromachining 3

1.2.2 Surface micromachining 4

1.2.3 Wafer-to-wafer bonding 7

1.2.4 Emerging techniques 9

1.2.5 Compatibility issue in micromachining 10

1.3 Plasma etching for silicon micromachining **12**

1.3.1 The necessity of using plasma etching for micromachining 12

1.3.2 The motivation of plasma etching research for micromachining 13

1.3.3 The status of silicon micromachining using plasma etching 15

1.4 Objective and organization of the thesis **15**

References **16**

2 **Plasma Etching Technique - Some Theoretical and Practical Aspects** **22**

2.1 Introduction **22**

2.2 Plasma state and characteristics of plasma **22**

2.2.1 Basic characteristics of plasma 23

2.2.2 Production of species in plasma 25

2.2.3 Sheath region formation and sheath potential 26

2.2.4 Development of self-bias on RF electrodes 27

2.3 Etching mechanisms **30**

2.4 Plasma etching reactors **31**

2.4.1 Barrel-type reactors 32

2.4.2 Parallel-plate reactors 32

2.4.3 Triode reactors 33

2.4.4 Magnetron and ECR reactors 35

2.5 Plasma etching chemistries 35

2.5.1 Fluorine atom dominant plasma 36

2.5.2 Unsaturated etchant dominant plasma 37

2.5.3 Chlorine and bromine based plasma 38
2.5.4 Importance of gas additives 39
2.6 Summary of the previous most important developments of plasma etching chemistry for micromachining 40
2.6.1 SF_6-based chemistry 40
2.6.2 CF_4-based chemistry 41
2.6.3 Cl_2- and Br_2-based chemistry 43
2.6.4 O_2-based chemistry 44
2.7 Process control and optimization 45
2.7.1 Process requirements 45
2.7.2 Effects of process variables 47
2.7.3 End point detection for process control 54
2.7.4 Process optimization 56
2.8 Problems caused by plasma etching 56
References 57

3 Etching of Poly-Si/Silicon Nitride/Poly-Si Structures Using Multi-Step Approach 61
3.1 Introduction 61
3.2 The tactile image sensor 61
3.3 Experimental details 63
3.4 Development of silicon nitride plasma etching chemistry selective over polysilicon 64
3.4.1 Experimental results 65
3.4.2 Discussions 69
3.5 Multi-step process design for the etching of polysilicon/silicon nitride/polysilicon sandwich structures 74
3.5.1 CF_4 + SF_6 + O_2 chemistry for the top polysilicon etching 74
3.5.2 Two-step process for the top polysilicon and silicon nitride etching 75
3.5.3 Analysis of the two-step process 78
3.6 Problems arising from polymer formation for high selectivity and their solution 81
3.6.1 Experimental methods 81
3.6.2 Results on contact resistance and polymer film formation 82
3.6.3 Results on mechanical adhesion 84
3.7 Conclusions 85
References 86

4 **Applying Plasma Etching for the Planarization of Surface-Micromachined Devices** **89**
4.1 Introduction **89**
4.2 Local planarization technique using PSG spacers **90**
4.2.1 Experimental details 92
4.2.2 Results and discussions 93
4.2.3 Selection of the extra PSG layer thickness 98
4.2.4 Application of the spacer technique in IC technology . 101
4.3 Filling silicon trench by PSG using two-layer resist coating and plasma etching-back **102**
4.3.1 Single-layer photoresist coating using HPR204 resist . 102
4.3.2 Two-layer resist coating technique 103
4.3.3 Plasma etch-back 108
4.3.4 Planarization results and feature size limitation 111
4.4 Conclusions **112**
References **114**

5 **Single Crystal Silicon Etching for Selective Epitaxial Growth and Micro-Tip Fabrication** **117**
5.1 Introduction **117**
5.2 Experimental details **118**
5.3 Results and discussions **118**
5.3.1 Effects of Cl_2 content and mask material on the etching profile and selectivity 118
5.3.2 Optimized silicon etching process for SEG 124
5.3.3 Silicon trench etching process for micro-tip fabrication 124
5.4 Conclusions **129**
References **133**

6 **SIMPLE - A Technique of Silicon Micromachining Using Plasma Etching** **136**
6.1 Introduction **136**
6.2 Experimental details **137**
6.3 Results and discussions **138**
6.3.1 Lateral etching of the n^+ buried layer formed by different n-type dopants 138
6.3.2 Effects of the n^+ doping level on the lateral etch rate . 139

6.3.3 Feature size and time dependence of the lateral etching . . . 140
6.4 Optimization of the Cl_2/BCl_3 plasma etching chemistry 142
6.4.1 Experimental design . . . 143
6.4.2 Results and analysis . . . 144
6.4.3 The optimized etching process for SIMPLE . . . 147
6.5 Compatibility of the SIMPLE process with on-chip circuit fabrication . . . 148
6.5.1 Selection of the dopant for the n^+ buried layer . . . 148
6.5.2 Selection of the doping for the mechanical structures . 151
6.5.3 Passivation of the exposed pn junction . . . 157
6.6 Limitation of the SIMPLE technique . . . 158
6.7 Conclusions . . . 158
References . . . 159

7 Plasma Etching Process Optimization Using Statistical Experimental Design and Data Analysis - a Case Study . . . 162
7.1 Introduction . . . 162
7.2 Experimental design consideration . . . 163
7.2.1 Factorial design . . . 163
7.2.2 Fractional factorial design . . . 163
7.2.3 Determination of the relative importance of factors . . 165
7.3 Development of a SF_6/O_2 plasma etching process for etch-through of silicon membranes using orthogonal design . 168
7.3.1 Process requirements . . . 168
7.3.2 Orthogonal design . . . 169
7.3.3 Experimental details . . . 170
7.3.4 Results . . . 171
7.3.5 Data analysis . . . 171
7.3.6 Optimization of the process . . . 174
7.3.7 Discussions . . . 177
7.4 Modelling and optimization of silicon trench etching processes using Response Surface Methodology (RSM) . . . 178
7.4.1 Response surface designs for quadratic model . . . 179
7.4.2 Experimental details . . . 180
7.4.3 Experimental results and least square regression (LSR) analysis . . . 182
7.4.4 Discussions . . . 185
7.4.5 Optimization of the SF_6/O_2 chemistry for desired

applications 189
7.4.6 Transferability of the optimized process 190
7.4.7 Limitation of the RSM 191
7.5 Conclusions **192**
References **192**

8 Conclusions **195**
8.1 General conclusions **195**
8.2 Perspective **197**

Appendix **199**
Appendix A1 Principle of the least square regression **199**
Appendix A2 Output file of NONLIN for the etch rate **200**
Appendix A3 The output file of NONLIN for the etch rate when some terms of the model are removed as suggested by the "t" statistics of Appendix A2 . . . . **202**
Appendix A4 The calculation of F statistics to test the significance of the model **203**
Appendix A5 Test the lack of fit of the model **205**
Appendix A6 Principles of multi-objective optimization **207**

Summary **210**

Samenvatting **213**

Acknowledgement **217**

List of publications **219**

About the author **221**

Chapter 1 Introduction

1.1 Introduction

Information processing has become an integral part of life of human beings in the modern "information society" because of the increasing dependence on sophisticated systems in, e.g. domestic appliances and transportation. Typically an information processing system consists of an input transducer, a modifier and an output transducer [1.1]. In the input transducer (or sensor) energy carrying signal is converted from non-electrical form (including radiant, mechanical, thermal, magnetic and chemical domain) into an electrical form. In the modifier the electrical signal is modified by signal processing devices such as amplifiers or microprocessors. In the output transducer (or actuator) the electrical signal is again converted into a non-electrical one, which can interact with the non-electrical process or can be detected by human senses.

In the past few decades, the performance of electrical signal processing devices such as microprocessors has been greatly enhanced, with an ever decreasing cost, owing to the continuous and dramatic progresses of planar integrated circuit (IC) technology [1.2]. Therefore, now we have at our disposal an unprecedented signal processing capability for electrical signal at low cost. However, less advance has been made in improving the overall performance of the information processing system due to the relatively slow progress in the sensor and actuator fields [1.3]. Over the past two decades, there have been increasing activities of fabricating sensors and actuators using silicon, so as to apply the highly developed and mature batch-production methods of ICs, making it possible to lower the price of those devices [1.4]. More importantly, with silicon as the starting material, it is feasible to combine sensors and ICs for signal conditioning, amplification, A/D conversion and even a sensor bus on one single chip to achieve integrated sensors or "smart" sensors [1.3]. Therefore, the performance/price ratio of sensors and actuators can be greatly enhanced.

Moreover, the size of silicon sensors can be very small by using the advanced silicon microfabrication techniques. These microsensors can provide unique solutions for many applications where small size is crucial, such as in the medical instrumentation field. Since silicon exhibits many physical effects, which can be used in the conversion of the energetic signal carrier, silicon sensors are compatible with ICs with respect to the material [1.1]. Furthermore, the fabrication technology for silicon sensors can be developed in such a way that it makes use part of the complete IC processing sequence and/or it has little influence on the characteristics of ICs. Therefore, silicon senors can

be compatible to ICs with respect to the fabrication technology used [1.5].

Many silicon sensors can be fabricated using planar IC processing technology without modifications in the standard process sequence, such as silicon magnetic sensors [1.6] and silicon thermal sensors [1.7] based on transistors. In some cases sensors and actuators require three dimensional micromechanical structuring to fabricate beams, cantilevers or membranes. These techniques are usually referred to as "micromachining" techniques. Silicon micromachining is the manufacture of small mechanical components from silicon, and is in principle based on the deposition, photolithography and etching techniques which have been developed for IC production [1.8]. The micromechanical structure is either directly involved in the mechanical transduction or has been applied to enable or improve a non-mechanical transduction. The micromechanical sensor can be based on a direct effect (such as plates in a capacitive accelerometer [1.9]) or on part of a tandem effect (such as a beam with piezoresistors [1.10]). The operation of thermopile-based sensors and magnetic sensors is strongly improved by micromachining techniques because of the removal of part of a thermally or electrically conductive substrate [1.11]. From the mechanical point of view, single-crystal silicon is a very good material [1.12] for its ideal elastic response to force over a large range and therefore very low hysteresis, which is of vital importance in sensing applications where the sensing device is to be free of drift. Its Young's modulus (1.7×10^{11} N/m^2) has a value approaching that of stainless steel or nickel. It has a tensile yield strength (6.9×10^{9} N/cm^2) which is at least three times higher than stainless steel wire and relatively low thermal coefficient of expansion (2.33×10^{-6}/°C), which is approximately half that of quartz.

Two major silicon micromachining technologies have been developed, "bulk" and "surface" micromachining, for the realization of a variety of micromechanical structures in silicon [1.13-1.15]. In bulk micromachining [1.16], single-crystal silicon substrate can be etched from both sides to achieve the desired structures by mainly using crystalline orientation dependent anisotropic "wet" chemical etching, frequently in combination with "dry" plasma etching. In surface micromachining [1.17-1.19], sacrificial and structural materials are sequentially deposited and patterned, mostly by using plasma etching. After removal of the former type of layer, usually with wet chemical etching, free-standing structural layers remain.

In both micromachining approaches, plasma etching plays an important role due to its ability to pattern very small feature size, which is based on the possibility of anisotropic etching in a gaseous chemical environment, and due to its greater controllability over the etching results than conventional wet etching techniques.

The fast growing research and development in silicon micromachined sensors and actuators since the middle of 1980's has resulted in a new category of systems: the microelectro mechanical system (MEMS) [1.20-1.24]. A good example of such a system is the digital micromirror device (DMD) for projection displays [1.25]. This device, which is the result of Texas Instruments's hundreds million investment, is based on surface micromachined tilting aluminium mirrors with MOS addressing circuits at each pixel location monolithically integrated on the same chip. Devices with up to 768×576 pixel resolution have been fabricated on 6'' wafers using standard semiconductor processing. Video projectors using the device have been demonstrated. Due to its batch-fabrication possibility, it can be made in high volume at low cost. In the near future devices of 2048×1152 pixel resolution will be available that will be capable of providing projected images from all currently operational or proposed high definition standards.

1.2 Silicon micromachining techniques - an overview

1.2.1 Bulk micromachining

Bulk micromachining can be implemented using an anisotropic etch (high etch rate in a preferential direction) or an isotropic etch (uniform etch rate in all direction). With anisotropic wet chemical etchants lateral geometries and etch profiles can be controlled more precisely than with isotropic ones, such as HF/HNO_3 solutions. The most commonly used wet anisotropic chemical etchants for bulk micromachining include potassium hydroxide-water (KOH) [1.26], ethylenediamine-pyrocatechol-water (EDP) [1.27], hydrazine-water [1.28] and tetramethylammonium hydroxide (TMAH) [1.29]. All of these etchants are known to exhibit crystalline orientation dependent etching characteristics, i.e. they etch the (100) and the (110) crystal planes much faster (typically several tens to hundreds times) than the (111) planes. With (100) orientation silicon wafers, the sidewalls in the etching openings have a $54.74°$ slope with respect to the surface, whereas with (110) oriented silicon wafers, vertical sidewalls are formed [1.30]. These structures are shown in Figure 1.1. To define the areas to be etched, masking layer such as silicon oxide for EDP etching and silicon nitride for KOH etching is used.

To control the vertical geometries of micromechanical structures, the anisotropic wet etching must be stopped precisely at a designated depth. Several "etch-stop" methods have been developed, such as the boron etch-stop and electrochemical etch-stop.

In the boron etch-stop technique [1.31], a heavily boron-doped p^+ region, where the

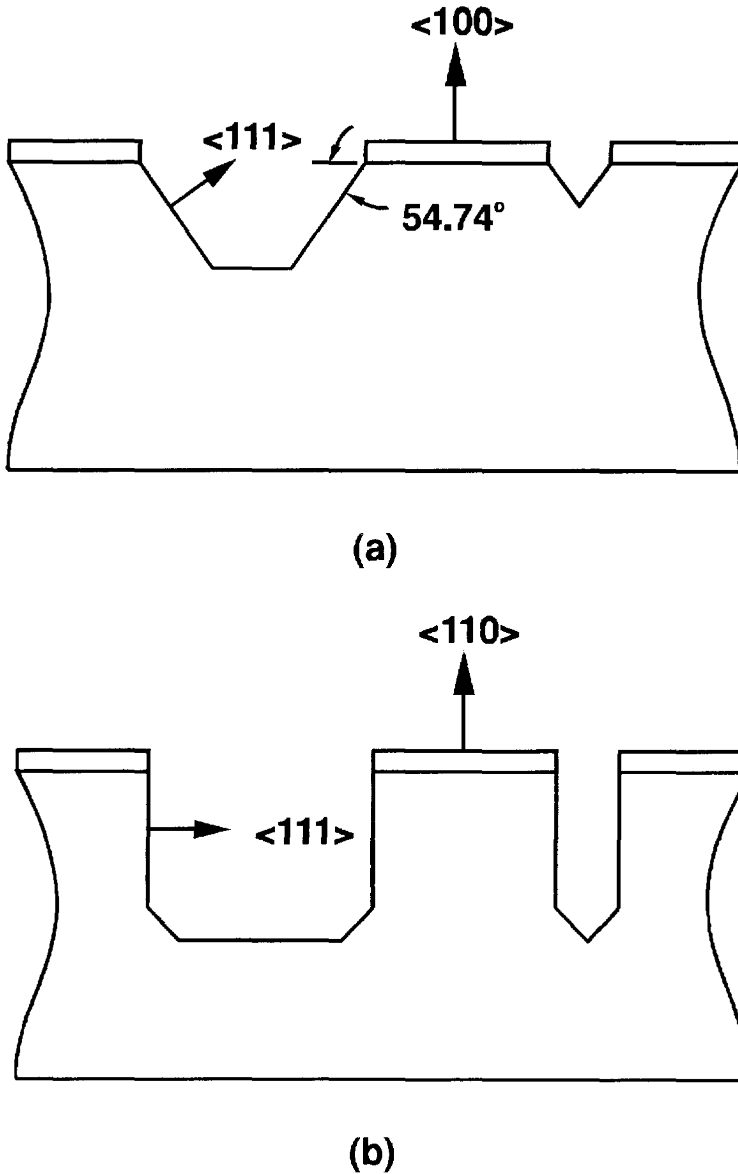

Figure 1.1 *A summary of anisotropically wet etched trench geometries commonly used in micromechanical devices. (a) on (100) orientation surface. (b) on (110) orientation surface.*

boron concentration is greater than approximately 5×10^{19} cm^{-3}, is used. The anisotropic etchants such as EDP or KOH etch n-type or lightly p-type regions of structures but the etch rate is significantly reduced at the interface between the regions and p^{+} region. Although simple, the high doping concentration required in this etch-stop method precludes the possibility of fabricating electronic devices in the area. Severe autodoping takes place due to the high boron concentration if one attempts to form epitaxial layer on top of the etch-stop layer. The high boron doping also introduces considerable mechanical strain, which makes it difficult to grow a high-quality epitaxial layer on top for electronic devices. Furthermore, the high strain level can result in undesired buckling of the structures. These factors limit the application of the high boron etch-stop method.

In the electrochemical etch stop technique [1.32], a reverse-bias voltage is applied during the anisotropic chemical etching to the p-n diode formed between n-type epitaxial layer and p-type substrate. The etching starts from the p-type substrate and when it reaches the p-n junction, the n-type area with anodic passivation voltage is in contact with the etchant, causing an anodic oxidation that stops the etching. This phase of the etching is indicated by a large increase in the current. Therefore, the thickness of the structure obtained is that of the epitaxial layer. This etch-stop approach, although more difficult to implement, offers significant advantages over the former one. Electronic devices can be fabricated in the epitaxial layer (the front side of the wafer) before the substrate anisotropic etching (often at the backside of the wafer), so as to maintain the possibility of on-chip integration. After the wet chemical etching, the epitaxial membrane can be patterned using plasma etching from the front side of the wafer to produce free-standing beams and cantilevers out of the epitaxial membrane.

Wet chemical bulk micromachining suffers from several common limitations:

1. The etching results in tapered sidewalls in case of (100) orientation wafers, which may limit the minimum lateral dimensions of the structures to several tens of microns. Although (110) orientation wafers can be used to produce vertical sidewalls, the sides of the mask must be aligned with the (111) planes, which considerably limits the forms of the structure obtainable [1.33].

2. Corner compensation is required due to extra etching taking place at the convex corners of the structures (corner undercut), making it further difficult to produce small lateral dimension structures [1.34].

3. The etching usually needs to start from the backside of the substrate, requiring special photolithography equipment for backside alignment.

4. The etching characteristics are highly temperature and composition sensitive due to the pure chemical nature of the etching. Precise monitoring and tight control of these two factors is a key issue in obtaining reproducible and well controlled etching results.

Bulk micromachining can also be performed based solely on plasma (dry) etching [1.35]. This technique uses a plasma instead of a liquid as the source of chemical reagents. Plasma etching can be isotropic or anisotropic in nature. With etching chemistries in which chemical reaction is the major etching mechanism, the etching is inherently isotropic, although it can provide high etching selectivity over mask. On the other hand, with chemistries in which energetic ion-bombardment causes crystal damage and therefore induces the etching, the etching is inherently anisotropic but with low selectivity. Therefore, compromises must be made in practical plasma bulk micromachining between etching directionality and maximum etch depth. At present, the plasma micromachining process incorporating high etch rate, anisotropy and selectivity, therefore resulting in anisotropic through-wafer etching, has not yet been found.

1.2.2 Surface micromachining

Three-dimensional micromechanical structures can be built on top of the surface of a wafer by a variety of film deposition and etching techniques. In this surface micromachining, structures are of the three-dimensional type more by their degrees of mechanical freedom than by their dimensions. Almost all these processes use the "sacrificial layer" technique [1.36], which consists of liberating mechanical structures that have been sequentially deposited and patterned by selectively underetching another underlying thin sacrificial layer, as shown in Figure 1.2.

This approach has several advantages over bulk micromachining:

1. It offers large flexibility in the construction of structures. Very complicated micromechanical devices can be fabricated, such as micromotors, where several different structural layers with a variety of shapes are required, since the technique makes use of the well-developed film deposition and patterning techniques for IC processing.

2. The structures can be small since their scale is not related to the thickness of the wafer, but depends on the lithographic abilities.

3. The technique can be more compatible with conventional IC technology. For example, part of the mechanical structural layers can be formed at certain process steps

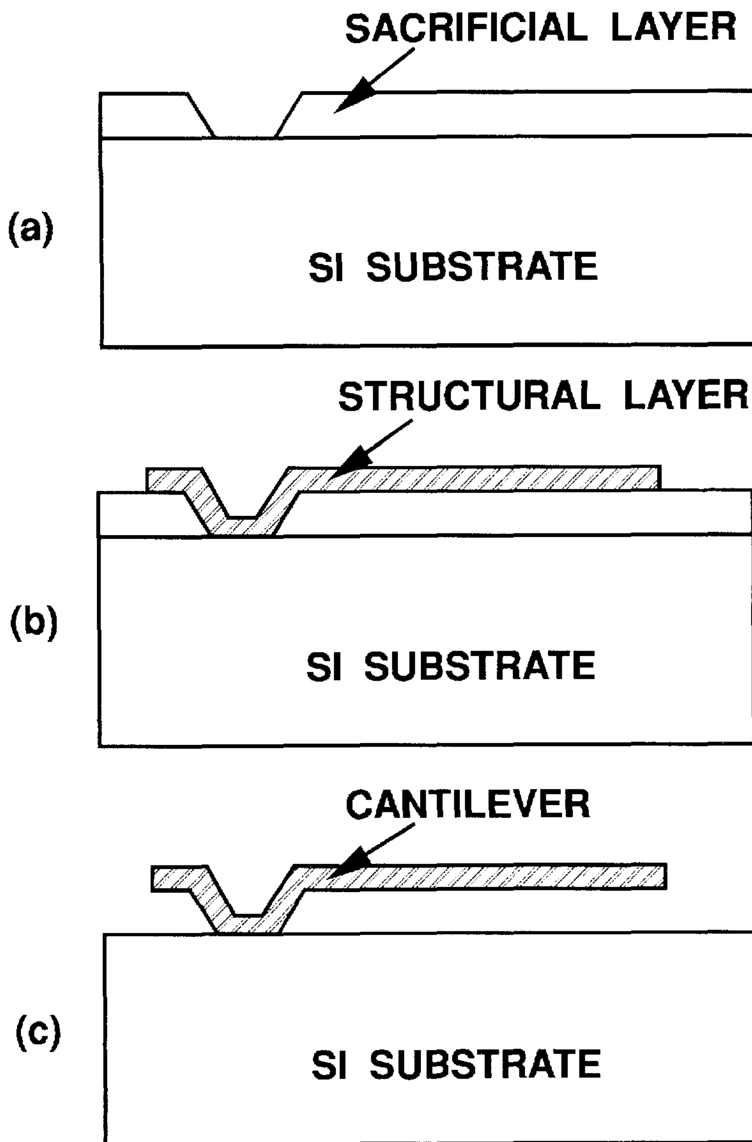

Figure 1.2 *Process sequence of surface micromachining. (a) sacrificial layer deposition and patterning. (b) structural layer deposition and patterning. (c) selective sacrificial layer removal.*

for electronic device processing.

4. Due to its "additive" nature, surface micromachining can be used to produce micromechanical structures above ICs which have been completed in a "classical" silicon foundry. This could favour development of smart sensor concept at a reasonable cost.

However, some disadvantages of the technique limit its application:

1. The mechanical properties of deposited structural films are less well-defined than and sometimes are inferior to those of bulk silicon. In particular, thin structural films are typically in a state of residual strain which affects the mechanical response of the structure. The strain level could cause failure of the structure due to buckling or cause it to crack with excessive compressive or tensile strain, respectively [1.37]. Therefore, measures must be taken, for example annealing at high temperature, to control the residual strain level, which complicates the processing or results in undesired extra thermal budget.

2. The film thickness is practically limited to $\sim 2\ \mu m$ due to the limited film deposition rate. This can result in severe constrains to device applications where relatively large area sidewalls or large mass are required, such as in a capacitive lateral accelerometer.

3. Surface non-planarity becomes a problem with an increasing number of patterned layers.

4. During the drying process after wet sacrificial etching, the surface tension of the rinse water might pull the delicate microstructure to the substrate where a combination of forces keep it firmly attached, resulting in failure of the device [1.38].

1.2.3 Wafer-to-wafer bonding

Wafer-to-wafer bonding techniques are useful in combination with or as possible alternatives to surface/bulk micromachining. One practical wafer bonding technology is silicon to glass bonding [1.39]. In this case, the silicon sensor wafer is brought into contact with a glass wafer whose thermal expansion coefficient should be as close to that of silicon as possible. Corning 7740 glass (Pyrex) is usually used for this purpose. The assembly is raised to a temperature of typically 400 to 600°C and a voltage of 400 to 1000 V is applied with silicon as the anode. Most of the applied voltage is dropped across the silicon-glass interface, inducing a permanent irreversible fusion bond which is stronger than either of the materials individually. Such bonds have been used for a

wide variety of microstructures [1.40-1.41].

Another important technique is silicon fusion bonding (SFB), which has been developed based on bonding of two silicon wafers at a high temperature (near 1000°C) [1.42]. It is simple and does not require the application of an external pressure, electric field, or an intermediate layer. Additionally, the added flexibility in three-dimensional design provided by SFB enables the fabrication of new devices, such as micro-valves [1.43]. However, the relatively high temperature required for SFB can cause compatibility problem.

To maintain compatibility with microelectronic circuits, low-temperature intermediate bonding is developed [1.44-1.45]. Intermediate bonding is based on the addition of a material in between two wafers before pressing these together. This intermediate can be a polymer glue, a low-temperature melting glass or a metal at eutectic temperature. The intermediate bonding usually requires a much lower value of the processing temperature as compared to SFB.

1.2.4 Emerging techniques

Recently some novel silicon micromachining techniques have been proposed to overcome the drawbacks of conventional bulk/surface micromachining. One such a technique is micromachining based on silicon on insulator (SOI) substrate [1.46]. An SOI substrate such as SIMOX (Separation by ion IMplantation of OXygen) wafer provides a silicon dioxide buried layer under a thin single-crystal silicon layer. This buried oxide layer is used as the sacrificial layer in the surface micromachining technique or as etch-stop in bulk micromachining technique.

Surface micromachining using SOI is shown in Figure 1.3. A silicon epitaxial layer is formed on the substrate to obtain a thickened structural layer. An opening is then made in the silicon layer by anisotropic plasma etching and the oxide sacrificial layer is etched in HF solution to obtained free-standing membranes or beams. The technique is very promising due to the following advantages:

1. It maintains all the advantages of surface micromachining such as CMOS compatibility, small lateral dimensions and precise control over the separation between the membrane and the silicon substrate.

2. It eliminates most of the disadvantages of conventional surface micromachining by providing single-crystalline surface layer and freedom on the surface structural thickness by epitaxial process.

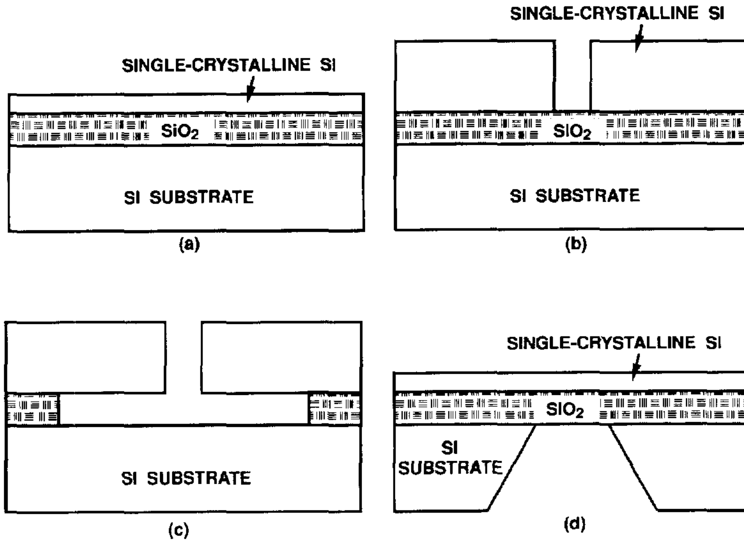

Figure 1.3 *Surface micromachining (a-c) and bulk micromachining (d) using SOI substrate. (a) SIMOX substrate. (b) epitaxial layer growth and hole opening. (c) selective sacrificial layer etching. (d) Buried oxide layer as the etch-stop for bulk micromachining.*

3. The electrical isolation between mechanical structures and the substrate can readily be achieved with the buried oxide layer.

4. The substrate is industrially available.

Capacitive pressure sensors based on a 300 μm diameter diaphragm and lateral capacitive accelerometers have been realized using this technique [1.46]. However, the SOI substrate fabrication requires very high dose oxygen implantation and excessive high temperature annealing, which makes the wafer very expensive. In addition, unlike in conventional surface micromachining technique, no electronic devices under the sacrificial layer (the buried oxide layer) can be made. This implies that electronic circuits cannot be fabricated before hand in a silicon foundry and that electrical contact to the substrate from the front side is very difficult.

Another new silicon micromachining technique is based on selective formation and etching of porous silicon [1.47]. Porous silicon is formed when silicon is electrochemically modified in HF solution under anodic bias [1.48]. The porous silicon has a very large inner surface and therefore can be dissolved by using a rather weak

etchant (e.g. 1% KOH solution at room temperature) which does not attack the rest of the structure. Therefore, porous silicon is a very interesting material for micromachining with following features:

1. It can be etched to form thick layers, which extend to the whole thickness of the wafer.

2. On the porous layer further thin film processes can be performed.

3. It can be generated locally by appropriate masking. Depending on the process parameters, the undercutting can be low or high.

4. An etch stop in silicon can be obtained by doping.

5. Anodization for porous formation is CMOS compatible.

Since the porous layer can be made very thick (tens of microns or more), the gap between the structure and the silicon substrate can be very large, which is advantageous for some thermal sensors in which the gap should provide a thermal isolation. Furthermore, the large gap eliminates the sticking phenomenon caused by small gap (a few microns) of conventional surface micromachining. A flow sensor based on a free-standing polysilicon bridge and a thin film bolometer using a silicon carbide membrane have been fabricated using the porous silicon technology [1.47][1.49]. However, the depth of porous silicon is not uniform and often not repeatable, which causes difficulties in some applications.

Epitaxial lateral overgrowth (ELO) is another novel micromachining technique. In ELO windows are opened in a thick oxide layer. Under certain process conditions, epitaxial layer grows selectively from the silicon seeds in the oxide windows and laterally overgrowth on the oxide layer. The ELO silicon layer can be used as structural layer while the oxide underneath the sacrificial layer for surface micromachining or etch-stop for bulk micromachining [1.50].

Other reported silicon micromachining techniques include those using novel etching methods such as focused ion beams [1.51] and YAG laser-assisted etching [1.52]. The former uses focused Ga^+ ion beams to directly sculpture silicon substrate, while the latter etches silicon using a reactive gas such as SF_6 or NF_3 assisted by the YAG laser irradiation.

1.2.5 Compatibility issue in micromachining

In the development of micromachining techniques, one of the issues of major concern is the compatibility of the technique with conventional IC processing, so that integration of micromechanical structures with microelectronic circuits can be achieved [1.53]. In bulk micromachining, compatibility can be retained by using an electrochemical etch-stop and by postponing the wet anisotropic etching to the very last stage of the process sequence. Because EDP and KOH are not compatible with IC processing laboratory, wafers which have undergone the wet anisotropic etching are usually not allowed to join the IC processing flow. The front side of the wafer must be kept away from the wet chemicals to protect aluminium interconnections by using appropriate cover with a rubber O ring. Also special structure of heavily n-type doping need to be made on the wafer surface to facilitate applying the anodizing voltage. Therefore, plasma bulk micromachining is a more attractive approach.

In surface micromachining, micromechanical structures are usually formed after the completion of most parts of the electronic circuits. Any high temperature cycle in the micromachining for film deposition and annealing for residual stress reduction can alter or degrade the performance of the electronic devices, and therefore should be avoided. Aluminium interconnections must usually be formed after the formation of micromechanical structures since they can stand for thermal processing of lower than 400°C [1.54]. Microelectronic circuits should be protected by using, for example, photoresist during the sacrificial etching with HF solutions, which also attack aluminium interconnections if not properly masked. In wafer-wafer bonding, care must be taken to avoid any possible damage of the on-chip electronic devices, due to high electric field and/or high temperature required for the bonding.

1.3 Plasma etching for silicon micromachining

1.3.1 The necessity of using plasma etching for micromachining

Due to its unique ability to pattern fine ($\sim \mu$m) feature size, which cannot be achieved by conventional wet chemical etching, plasma etching has been applied for IC fabrication for more than two decades. The development of many successful plasma etching techniques for pattern transfer is one of the major technological achievements in microelectronic fabrication, which allow ICs to be continuously improved with regard to device density and feature size. Recently, plasma etching has also received much attention in micromachining applications [1.55-1.56]. Plasma etching presents two main advantages when used for bulk micromachining:

1. The etching results are not dependent of crystalline orientation of the substrate, providing much more design flexibility in terms of the lateral shape of the microstructures.

2. The plasma does not exert large forces on the microstructures, which can be very fragile at certain stage of the processing and easily be broken by further wet processing, such as after the formation of thin membranes. Moreover, plasma etching allows better control over the etching procedure by instrumentational parameters of plasmas than conventional wet chemical etching.

Although surface micromachining can be implemented with wet etching alone, plasma etching is almost exclusively applied whenever possible to take the advantage of the advanced pattern transfer technique - smaller feature size and therefore better device performance. For example, in side-driven electrostatic micromotors, polysilicon rotors and stators must be patterned using anisotropic plasma etching to minimize the gap between them and thus to maximize the electrostatic driving force [1.57]. With directionality of plasma etching, novel device structures can be realized. For example, highly flexible polysilicon beams with high aspect ratio (height/width) can be fabricated by using polysilicon sidewalls formed by anisotropic plasma etching [1.58].

1.3.2 The motivation of plasma etching research for micromachining

Although many plasma etching chemistries have been developed for IC fabrication and some of them can be directly adopted for micromachining (for example, polysilicon etching on oxide), there are several important reasons for plasma etching research for micromachining applications:

1. Plasma etching characteristics are highly equipment dependent and therefore the plasma parameters should be optimized for a specific etching machine.

2. Diversity of materials used in micromachining results in many requirements for the etching selectivities different from those imposed by IC fabrication. In silicon micromachining, all the IC technology compatible silicon-based materials are used, such as silicon, including single crystal and polycrystalline silicon, silicon nitride (stoichiometric or silicon-rich) and silicon oxide (thermal or chemical vapour deposition (CVD) oxide, phosphosilicate glass (PSG) or boro-phosphosilicate glass (BPSG)). In micromachined devices the underlying layer may be one of the other two types. This requires the etching of one material to be selective over one of the other two, as shown in Table 1.1. For instance, silicon nitride needs to be etched selectively over either silicon or silicon oxide. In contrast, in conventional IC technology only silicon oxide

may be present underneath silicon nitride. Also silicon trench depth is limited to a few microns in microelectronic processing, but may exceed tens of microns in micromachining, which makes important the etch selectivity over mask (resist or other film) [1.59]. Therefore, many new plasma etching chemistries need to be developed to meet the requirements.

Table 1.1 Requirements for the etching selectivity over the underlying layer for surface micromachining.

Selectivity requirement		Material to be etched		
		Si	SiO_2	Si_xN_y
Material Underneath	Si		SiO_2 over Si	Si_xN_y over Si
	SiO_2	Si over SiO_2		Si_xN_y over SiO_2
	Si_xN_y	Si over Si_xN_y	SiO_2 over Si_xN_y	

3. Complexity of device structures in micromachining puts further challenges to plasma etching characteristics. Due to the complication of the device structure, sometimes more than one type of material is simultaneously present underneath a film. For example polysilicon etch must stop on both PSG and nitride in a surface micromachining process module [1.60]. This further complicates the etching process development.

In some cases multilayers (e.g. a polysilicon/silicon nitride/polysilicon sandwich layer) are necessary and their etching requires multi-step processes [1.61]. When two conductive layers (e.g. polysilicon layers) need to have electrical contact through windows in an insulating layer (e.g. silicon nitride), the nitride window etching must not leave any surface polymer in order to ensure good electrical contact and mechanical adhesion [1.62].

In surface micromachining, a structural layer may need to cover high steps of sacrificial layer and the way of patterning the sacrificial layer would influence the profile of the steps, and therefore the step coverage of the structural layer as well as mechanical properties of the structure, such as force response of elevated beams [1.63]. When surface areas with large-size (tens of micron or more) patterns need to be planarized for certain sensor applications, the planarization technique, and therefore the plasma etching for it, can be much different from those used for conventional IC planarization in which small-size patterns are usually dominant [1.64]. All these applications require new

plasma etching processes.

4. Novel device structures can be achieved and new micromachining processes can be developed by making use of some etching characteristics which are not desirable, and therefore need to be minimized for conventional IC fabrication. For example, bowing in silicon trench etching can be used for the fabrication of recessed micro-tips in silicon [1.65], which find applications in vacuum microelectronic devices and surface profile sensing devices. Alternatively, isotropic etching of heavily n-doped buried layers in bulk silicon by Cl-containing plasmas can be used for releasing microstructure from substrate, leading to a novel micromachining technique [1.66]. To explore the possibility of micromachining offered by plasma etching, many plasma etching phenomena, which were ignored or suppressed in mainstream microelectronic research, need to be re-examined and developed.

1.3.3 The status of silicon micromachining using plasma etching

Much of the research on plasma etching techniques reported for micromachining applications have been on bulk silicon etching. This is due to the required capability for very deep trench etching with vertical sidewalls, which is very much challenging. Therefore, etching selectivity over the masking material and etching anisotropy, in addition to high etch rate, are crucial. Also the surface roughness should be minimized. To achieve these requirements, both gas composition and masking material itself are important.

Surface micromachining can relatively easily adopt conventional plasma etching for IC fabrication due to their similar etching requirements. Normally, etching selectivity over the underlying layer and uniformity, apart from the anisotropy and surface roughness, are more important issues of concern than etch rate.

The most important developments in silicon micromachining using plasma etching will be summarized in Chapter 2.

1.4 Objective and organization of the thesis

This thesis describes the development of plasma etching chemistries for the fabrication of silicon micromechanical structures for sensor and actuator applications. These chemistries have resulted in successful fabrication of micromachined silicon sensing and actuating devices.

In Chapter 2 some fundamental theoretical and practical aspects of plasma etching are discussed. The understanding of plasma etching chemistry and knowledge of general plasma etching operation are essential for the process development. Subsequently, the most important developments in the research on plasma etching for silicon sensor fabrication are summarized.

Chapters 3 and 4 describe the development of the plasma etching processes for surface micromachining. In Chapter 3 a silicon nitride plasma etching chemistry selective to polysilicon is reported. Subsequently, a two-step etching process for the patterning of polysilicon/silicon nitride/polysilicon sandwich structures is described and process design considerations of the two-step process are presented. The effects of silicon nitride etching chemistry and post-processing on the electrical contact and mechanical adhesion of two polysilicon layers through contact windows in an intermediate silicon nitride layer are described. Chapter 4 reports on two techniques for planarizing substrate topography for surface micromachined devices using PSG spacers and two-layer resist coating followed by plasma etching-back, respectively.

Chapters 5 to 7 describe the development of the plasma etching processes for bulk silicon micromachining. In chapter 5 a bulk silicon trench etching process for application in selective epitaxial growth as well as for the fabrication of recessed silicon tips for vacuum microelectronic devices is presented. Chapter 6 describes the SIMPLE technique (SIilicon Micromachining based on single-step PLasma Etching), which is capable of fabricating high aspect ratio single-crystal silicon micromechanical structures and is compatible with standard electronic circuit fabrication process. Chapter 7 reports the optimization of bulk silicon trench etching processes using statistical experimental design and data analysis, in which orthogonal design and response surface methodology are used.

Finally, in Chapter 8 the conclusions are presented and further research scopes are discussed.

References

[1.1] S. Middelhoek, S. A. Audet, *Silicon Sensors*, Academic Press, London, 1989, Chapter 1, pp. 1-6.

[1.2] S. M. Sze Ed., *VLSI Technology*, McGraw-Hill, New York, 1988.

[1.3] J. H. Huijsing, "Integrated smart sensors," *Sensors and Actuators*, Vol. A-30, pp. 167-174, 1992.

[1.4] S. Middelhoek, "Quo vadis silicon sensors," *Sensors and Actuators*, Vol. A-41, pp. 1-10, 1994.

[1.5] R. F. Wolffenbuttel, "Fabrication compatibility of integrated silicon smart physical sensors," *Sensors and Actuators*, Vol. A-41, pp. 11-28, 1994.

[1.6] A. W. Vinal and N. A. Masnari, "Operating principles of bipolar transistor magnetic sensors," *IEEE Trans. Electron Devices*, Vol. ED-31, pp. 1486-1494, 1984.

[1.7] G. C. M. Meijer, "Thermal sensors based on transistors," *Sensors and Actuators*, Vol. 10, pp. 103-125, 1986.

[1.8] P. Wilson, "Tutorial: silicon micro-machining," *Sensor Review,* Vol. 10, pp. 178-181, 1990.

[1.9] W. H. Ko, in *Sensors and Actuators 10, State of the Art of Sensor Research and Development*, S. Middelhoek and J. Van der Spiegel Eds., Elsevier Sequoia, Lausanne, 1986, pp. 303-320.

[1.10] L. Roylance and J. B. Angell, "A batch-fabricated silicon accelerometer," *IEEE Trans. Electron Devices*, Vol. ED-26, pp. 1911-1917, 1979.

[1.11] P. M. Sarro, H. Yashiro, A. W. van Herwaarden and S. Middelhoek, "An infrared sensing array based on integrated silicon thermopiles," in *the Proc. 4th Intern. Conf. Solid-State Sensors and Actuators (Transducer'87)*, 1987, pp. 227-230.

[1.12] J. C. Greenwood, "Silicon in mechanical sensors," *J. Phys. E: Sci. Instrum.*, Vol. 21, pp. 1114-1128, 1988.

[1.13] W. Benecke, "Silicon micromachining for microsensors and microactuators," *Microelectronic Engineering*, Vol. 11, pp. 73-82, 1990.

[1.14] K. D. Wise, "Silicon micromachining and its application to high-performance integrated sensors," in *Micromachining and Micropackaging of Transducers*, C. D. Fung, P. W. Cheung, W. H. Ko and D. G. Fleming Eds., Elsevier Science Publishers B. V., Amsterdam, 1985, pp. 3-19.

[1.15] G. Delapierre, "Micro-machining: a survey of the most commonly used processes," *Sensors and Actuators*, Vol. 17, pp. 123-138, 1989.

[1.16] K. E. Petersen, "Silicon as a mechanical material," *Proc. IEEE*, Vol. 70, pp. 420-457, 1982.

[1.17] R. T. Howe, "Surface micromachining for microsensors and microactuators," *J. Vac. Sci. Technolo.*, Vol. B6, pp. 1809-1813, 1988.

[1.18] C. Linder, L. Paratte, M-A. Gretillat, V. P. Jaecklin and N. F. de Rooij, "Surface micromachining," *J. Micromech. Microeng.*, Vol. 2, pp. 122-132, 1992.

[1.19] R. T. Howe, "Polycrystalline silicon microstructures," in *Micromachining and Micropackaging of Transducers*, C. D. Fung, P. W. Cheung, W. H. Ko and

D. G. Fleming Eds., Elsevier Science Publishers B. V., Amsterdam, 1985, pp. 169-186.

[1.20] R. T. Howe, R. S. Muller, K. J. Gabriel and W. S. N. Trimmer, "Silicon micromechanics: sensors and actuators on a chip," *IEEE Spectrum,* pp. 29-35, July 1990.

[1.21] K. D. Wise and N. Najafi, "The coming opportunities in microsensor systems," in *the Proc. 6th Intern. Conf. Solid-State Sensors and Actuators (Transducer'91)*, 1991, pp. 2-7.

[1.22] H. Fujita and K. J. Gabriel, "New opportunities for microactuators," in *the Proc. 6th Intern. Conf. Solid-State Sensors and Actuators (Transducer'91)*, 1991, pp. 14-20.

[1.23] K. Najafi, "Silicon integrated microsensors," in *the Proc. SPIE*, Vol. 1793, 1992, pp. 235-246.

[1.24] M. Mehregany, "An overview of microelectromechanical systems," in *the Proc. SPIE*, Vol. 1793, 1992, pp. 2-11.

[1.25] J. B. Sampsell, "The digital micromirror device and its application to projection displays," in *the Proc. 7th Intern. Conf. Solid-State Sensors and Actuators (Transducer'93)*, 1993, pp. 24-27.

[1.26] D. B. Lee, "Anisotropic etching of silicon," *J. Appl. Phys.*, Vol. 40, pp. 4569-4574, 1969.

[1.27] A, Reisman, M. Berkenblit, S. A. Chan, F. B. Kaufman and D. C. Green, "The controlled etching of silicon in catalyzed Ethylenediamine-Pyrocatechol-Water solutions," *J. Electrochem. Soc.*, Vol. 126, pp. 1406-1414, 1979.

[1.28] M. J. Declercq, L. Gerzberg and J. D. Meindl, "Optimization of the hydrazine-water solution for anisotropic etching of silicon in integrated circuit technology," *J. Elelctrochem. Soc.,* Vol. 122, pp. 545-552, 1975.

[1.29] O. Tabata, R. Asahi, H. Funabashi and S. Sugiyama, "Anisotropic etching of silicon in $(CH_3)_4NOH$ solutions," in *the Proc. 6th Intern. Conf. Solid-State Sensors and Actuators (Transducer'91)*, 1991, pp. 811-814.

[1.30] D. L. Kendall and G. R. de Guel, "Orientations of the third kind: the coming of age of (110) silicon," in *Micromachining and Micropackaging of Transducers*, C. D. Fung, P. W. Cheung, W. H. Ko and D. G. Fleming Eds., Elsevier Science Publishers B. V., Amsterdam, 1985, pp. 107-124.

[1.31] A. Bohg, "Ethylene Diamine-Pyrocatechol-Water mixture shows etching anomaly in boron-doped silicon," *J. Electrochem. Soc.*, Vol. 118, pp. 401-402, 1971.

[1.32] T. N. Jackson, M. A. Tischler and K. D. Wise, "An electrochemical p-n junction etchstop for the formation of silicon microstructures," *IEEE Electron Device Letters*, Vol. EDL-2, pp. 44-46, 1981.

[1.33] K. Ohwada, Y. Negoro, Y. Konaka and T. Oguchi, "Groove depth uniformization in (110) Si anisotropic etching by ultrasonic wave and application to accelerometer fabrication," in *the Proc. 1995 IEEE Workshop on Micro Electro Mechanical Systems (MEMS'95)*, 1995, pp. 100-105.

[1.34] H. Sandmaier, H. L. Offereins, K. Kuhl and W. Lang, "Corner compensation techniques in anisotropic etching of (100)-silicon using aqueous KOH," in *the Proc. 6th Intern. Conf. Solid-State Sensors and Actuators (Transducer'91)*, 1991, pp. 456-459.

[1.35] C. D. Fung and J. R. Linkowski, "Deep etching of silicon using plasma," in *Micromachining and Micropackaging of Transducers*, C. D. Fung, P. W. Cheung, W. H. Ko and D. G. Fleming Eds., Elsevier Science Publishers B. V., Amsterdam, 1985, pp. 159-166.

[1.36] H. C. Nathanson, W. E. Newell, R. A. Wickstrom and J. R. Davis, "The resonant gate transistor," *IEEE Trans. Electron Devices*, Vol. ED-14, pp. 117-133, 1967.

[1.37] M. W. Putty, S. C. Chang, R. T. Howe, A. L. Robinson and K. D. Wise, "Process integration for active polysilicon resonant microstructures," *Sensors and Actuators*, Vol. 20, pp. 143-151, 1989.

[1.38] R. L. Alley, G. J. Cuan, R. T. Howe and K. Komvopoulos, "The effect of release-etch processing on surface microstructure stiction," in *the Proc. of IEEE Solid-State Sensor and Actuator Workshop*, 1988, pp. 92-95.

[1.39] W. H. Ko, J. T. Suminto and G. J. Yeh, "Bonding techniques for microsensors," in *Micromachining and Micropackaging of Transducers*, C. D. Fung, P. W. Cheung, W. H. Ko and D. G. Fleming Eds., Elsevier Science Publishers B. V., Amsterdam, 1985, pp. 41-61.

[1.40] M. Esashi, "Micromachining for packaged sensors," in *the Proc. 7th Intern. Conf. Solid-State Sensors and Actuators (Transducer'93)*, 1993, pp. 260-265.

[1.41] B. Ziaie, J. Von Arx, M. Nardin and K. Najafi, "A hermetic packaging technology with multiple feedthroughs for integrated sensors and actuators," in *the Proc. 7th Intern. Conf. Solid-State Sensors and Actuators (Transducer'93)*, 1993, pp. 266-269.

[1.42] K. E. Petersen, P. Barth, J. Poydock, J. Mallon Jr. and J. Bryzek, "Silicon fusion bonding for pressure sensors," in *the Proc. of IEEE Solid-State Sensors and Actuators Workshop*, 1988, pp. 144-147.

[1.43] H. Jerman, "Electrically-activated, normally-closed diaphragm valves," in *the Proc. 6th Intern. Conf. Solid-State Sensors and Actuators (Transducer'91)*, 1991, pp. 1045-1048.

[1.44] R. F. Wolffenbuttel and K. D. Wise, "Low-temperature silicon wafer-to-wafer bonding using gold at eutectic temperature," *Sensors and Actuators*, Vol. A43,

pp. 223-229, 1994.

[1.45] M. Esashi, N. Nakano, S. Shoji and H. Hebiguchi, "Low-temperature silicon-to-silicon anodic bonding with intermediate low melting point glass," *Sensors and Actuators*, Vol. A21-23, pp. 931-934, 1990.

[1.46] B. Diem, M. T. Delaye, F. Michel, S. Renard, G. Delapierre, "SOI (SIMOX) as a substrate for surface micromachining of single crystalline silicon sensors and actuators," in *the Proc. 7th Intern. Conf. Solid-State Sensors and Actuators (Transducer'93)*, 1993, pp. 233-236.

[1.47] W. Lang, P. Steiner A. Richter, K. Marusczyk, G. Weimann and H. Sandmaier, "Application of porous silicon as a sacrificial layer," *Sensors and Actuators*, Vol. A43, pp. 239-242, 1994.

[1.48] R. L. Smith and S. D. Collins, "Porous silicon formation mechanisms," *J. Appl. Phys.*, Vol. 71, pp. R1-R22, 1991.

[1.49] W. Lang, P. Steiner, U. Schaber and A. Richter, "A thin film bolometer using porous silicon technology," *Sensors and Actuators*, Vol. A43, pp. 185-187, 1994.

[1.50] J. J. Pak, A. E. Kabir and G. W. Neudeck, "A micromachining technique for a thin silicon membrane using merged epitaxial lateral overgrowth of silicon and SiO_2 for an etch-stop," in *the Proc. 6th Intern. Conf. Solid-State Sensors and Actuators (Transducer'91)*, 1991, pp. 1028-1031.

[1.51] B. Khamsehpour and S. T. Davies, "Micromachining of semiconductor materials by focused ion beams," *Vacuum*, Vol. 45, pp. 1169-1173, 1994.

[1.52] K. Minami, Y. Wakabayashi, M. Yoshida, K. Watanabe and M. Esashi, "YAG laser- assisted etching of silicon for fabricating sensors and actuators," *J. Micromech. Microeng.*, Vol. 3, pp. 81-86, 1993.

[1.53] P. J. French, "Development of compatible micromachining processes in silicon," in *the Proc. Workshop on Silicon Sensor Realization Compatible with Microelectronic Circuit Fabrication*, Toulouse, France, 29-30 Sept. 1994. pp. 2.1-2.27.

[1.54] R. F. Wolffenbuttel, "On-chip functional integration," in *the Proc. Workshop on Silicon Sensor Realization Compatible with Microelectronic Circuit Fabrication*, Toulouse, France, 29-30 Sept. 1994. pp. 3-40.

[1.55] I. W. Rangelow, S. Skocki, P. Dumania, "Plasma etching for micromechanical sensor applications," *Microelectronic Engineering*, Vol. 23, pp. 365-368, 1994.

[1.56] Y. X. Li, M. R. Wolffenbuttel, P. J. French, M. Laros, P. M. Saro and R. F. Wolffenbuttel, "Reactive ion etching (RIE) techniques for micromachining applications," *Sensors and Actuators*, Vol. A41-42, pp. 317-323, 1994.

[1.57] M. Mehregany, S. D. Senturia, J. H. Lang and P. Nagarkar, "Micromotor

fabrication," *IEEE Trans. Electron Devices*, Vol. ED-39, pp. 2060-2068, 1992.

[1.58] M. W. Judy and R. T. Howe, "Highly compliant lateral suspensions using sidewall beams," in *the Proc. 7th Intern. Conf. Solid-State Sensors and Actuators (Transducer'93)*, 1993, pp. 54-57.

[1.59] C. Linder, T. Tschan and N. F. de Rooij, "Deep dry etching of silicon - a novel micromachining tool," *Sensors and Materials*, Vol. 3, pp. 311-324, 1992.

[1.60] J. Goosen, P. French, Y. Li, D. Poenar, B. van Drieenhuizen, R. Wolffenbuttel, "Surface micromachining module compatible with BIFET microelectronic processing," in *the Book of Abstracts of Eurosensors VIII Conference*, Toulouse, France, 1994, p. 108.

[1.61] Y. X. Li, M. Laros, P. M. Sarro. P. J. French and R. F. Wolffenbuttel, "Process design for plasma etching of polysilicon/silicon nitride/polysilicon sandwich structures for sensor applications," *Microelectronic Engineering*, Vol. 20, pp. 321-328, 1993.

[1.62] Y. X. Li, P. J. French and R. F. Wolffenbuttel, "Effects of plasma etching chemistry and post-processing on the mechanical adhesion and electrical contact of double polysilicon layer structures," *IEEE Trans. Electron Devices*, Vol. ED-48, pp. 64-69, 1995.

[1.63] Q. Meng, M. Mehregany and R. L. Mullen, "Analytical modelling of step-up supports in surface micromachined-beams," in *the Proc. 7th Intern. Conf. Solid-State Sensors and Actuators (Transducer'93)*, 1993, pp. 779-782.

[1.64] Y. X. Li, P. J. French and R. F. Wolffenbuttel, "Plasma planarization for sensor applications," submitted to J. Microelectromechanical Systems.

[1.65] J. A. Foerster, Y. X. Li, M. Bartek, P. J. French and R. F. Wolffenbuttel, "Fabrication of recessed micro-tips in silicon for sensor applications," in *the Proc. Micromechanics Europe 1994 (MME'94)*, 1994, pp. 198-201.

[1.66] Y. X. Li, P. J. French. P. M. Sarro and R. F. Wolffenbuttel, "Fabrication of a single crystalline silicon capacitive lateral accelerometer using micromachining based on single step plasma etching," in *the Proc. 1995 IEEE Workshop on Micro Electro Mechanical Systems (MEMS'95)*, 1995, pp. 398-403.

Chapter 2 Plasma Etching Technique - Some Theoretical and Practical Aspects

2.1 Introduction

Pattern transfer from the masking layer to the substrate is one of the key processes in the fabrication of microelectronic devices. Conventionally this has been achieved using chemically reactive liquid to etch the substrate material not covered by the mask (wet etching). Wet etching techniques are effective when device geometries are relatively large. However, these simple techniques have a number of disadvantages which become obvious as the line-width of the devices is reduced to less than 3 μm:

1. Wet etching is pure chemical reaction and usually has no preferential direction (except for some etchants which etch faster along specific crystal planes of silicon). This leads to isotropic circular profile and thus undercutting of the mask, resulting in the line-width loss.

2. Many wet etching agents often attack the resist and results in ragged edges in the etched material. There is poor dimensional control where the adhesion of the resist to the substrate is lost in wet chemicals.

3. Sometimes bubbles grow during the etching thereby acting as localized masks and resulting in non-uniform substrate removal.

4. Aggressive reagents often exhibit irreproducible delays in the initiation of the etching process, causing problems with regard to process control.

Due to these difficulties, wet etching techniques are not suitable to produce structures with fine feature size. Using plasma etching techniques it is possible to etch substrate material along the direction perpendicular to the substrate surface (anisotropic etching), producing small geometries with minimal undercutting and maintaining accurate dimensional control of the etched features. Plasma etching also avoids the problems of bubble formation and loss of adhesion of the resist layer associated with wet etching.

2.2 Plasma state and characteristics of plasma

2.2.1 Basic characteristics of plasma [2.1]

The simplest plasma reactors usually consist of opposed parallel plate electrodes in a chamber that can be maintained at low pressure, typically ranging from 0.01 to 1 Torr (Fig. 2.1). When a high frequency voltage is applied between the electrodes, current flows forming a plasma, which can be recognized by the emission of a characteristic glow. Reactive radicals are generated by this electrical discharge. Substrate materials on the electrode surfaces are exposed to reactive neutral and charged species. Some of this species combine with the substrate and form volatile products that evaporate, thus etching the substrate.

The plasma environment can be described using some basic characteristics. A plasma is an ionized gas with equal numbers of free positive and negative charges. The free charge is produced by the passage of electric current through the discharge. For most plasmas of interest for etching, the plasma density (i.e. the density of charged particles) is normally in the range of 10^9 - 10^{12} cm^{-3}. In other words, the extend of ionization is very small (one charged particle per 100,000 to 1,000,000 neutral atoms and molecules). The positive charge is mostly in the form of singly ionized neutrals, (i.e. atoms, radicals or molecules) from which a single electron has been stripped. The majority of negatively charged particles are free electrons and these are the main current-carriers because they are light and mobile. They collide with the neutrals in the path from one electrode to the other. Because electrons are much lighter than the neutrals they collide with (generally by a factor of $\sim 5\times10^{-4}$ to 5×10^{-6}), energy transfer from electrons to gas molecules is inefficient and electrons can attain a high average energy, often many electron volts (equivalent to tens of thousands of degree above the gas temperature). The elevated electron temperature permits electron-molecule collisions to excite high temperature type reactions, which form free radicals, in a low temperature neutral gas. Generating the same reactive species without a plasma would require temperature in the range of $\sim 10^3$ - 10^4 K. The coexistence of a warm gas and high temperature active species distinguishes the plasma reactor from conventional thermal processing.

Although formally there are equal number of positive and negative charged particles in a plasma, diffusion of charge to the walls of the reactor and recombination on boundary surfaces tend to deplete charge in the adjacent gas phase, forming a thin boundary layer or sheath. Because electrons are light and have high energy, these diffuse fastest, leaving an excess of positive charge and a plasma potential that is positive relative to

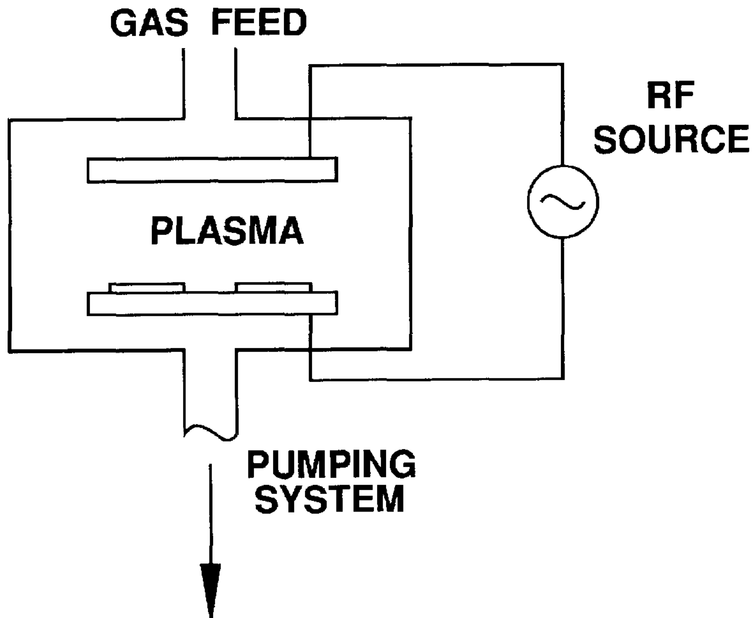

Fig. 2.1 *Basic configuration of a plasma reactor.*

the walls (Fig. 2.2). Since charged particles are most abundant in the central glow of the plasma, it is a fairly good conductor and most of the potential drop appears across the sheath. Voltage across the sheath ranges from a few volts to thousands of volts, depending on other parameters. Positive ions are accelerated through the sheath and strike the walls at near-normal incidence. As show in Fig. 2.2, the sheath thickness is on the order of a Debye length.

In the remaining of this section the two most important processes in plasma which determine the characteristics of plasma etching will be discussed, i.e. production of species and formation of sheath potential. The former produces reactants required for the chemical reaction in plasma etching. The latter creates a potential difference between plasma and substrate, causing energetic ion bombardment in the direction perpendicular to the substrate surface, which enhances or induces the etching.

2.2.2 Production of species in plasma

In a plasma, energetic electron collisions with gas molecules produce species which are required by the etching. An oxygen plasma discharge is a simple example which illustrates the most important types of electron-neutral collisions of plasma chemistry:

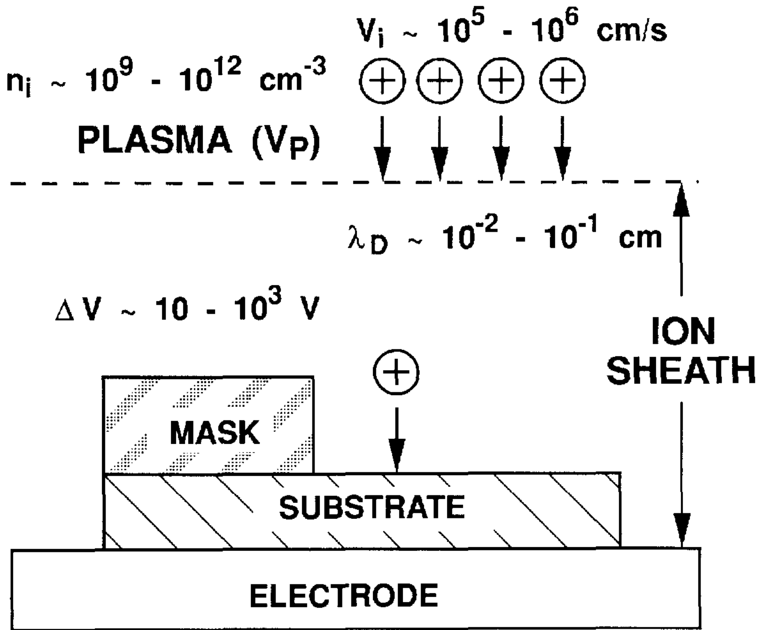

Fig. 2.2 *Typical parameters of plasma and plasma sheath.*

a) ion and electron formation

$$e + O_2 \rightarrow O_2^+ + 2e \tag{2.1}$$

b) atom and radical formation

$$e + O_2 \rightarrow O + O \tag{2.2}$$

c) generation of heat and light

$$e + O_2 \rightarrow O_2^* \tag{2.3}$$

$$O_2^* \rightarrow h\nu + hk + O_2 \tag{2.4}$$

$$e + O \rightarrow O^* \quad (2.5)$$

$$O^* \rightarrow h\nu + hk + O \,, \quad (2.6)$$

where O_2^* and O^* indicate the excited states of O_2 and O, respectively. In these systems, Reaction (2.1) forms the charge carriers that sustain the plasma as well as impinge the substrate surface (the positive ions); reaction (2.2) is responsible for producing atomic oxygen, the active chemical species for e.g. resist stripping or patterning; Reactions (2.3) - (2.6) stimulate characteristic plasma-induced optical emission, which is useful for process control (end point detection).

In the plasma, the formation of the species is balanced by the loss of them due to reaction for the etching and recombination process. The equilibrium between the formation and loss determines the steady concentrations of species in a discharge.

2.2.3 Sheath region formation and sheath potential

Kinetic theory [2.2] shows that random thermal motion of a gas results in a flux of particles to the wall:

$$\bar{j} = n \frac{\bar{v}}{4} = \frac{n}{4} \sqrt{\frac{8kT}{\pi m_i}} \,, \quad (2.7)$$

where n and υ are the density and average velocity of particles, respectively, k is the Boltzman Constant, T is the absolute temperature and m_i is the mass of gas molecules. There are important differences between the ion and electron fluxes. Firstly, the flux of electrons is far greater than that of ions or neutrals,

$$j_e >> j_i \,, j_n \quad (2.8)$$

because $T_e \gg T_g$, T_i and $m_e \ll m_g$, m_i. Thus electrons are much more mobile than ions and hence the plasma can be seen as a rectifier, i.e. only electron flux moves from the plasma to the wall.

Secondly, since electrons carry negative charge, the excess random thermal electron flux over the ion flux (Eq. 2.8) makes insulating walls charged negatively. This negative charge accumulates on the walls until the resulting repulsive electric sheath field is intense enough to reduce electron current to the level of the ion current flux (Fig. 2.3).

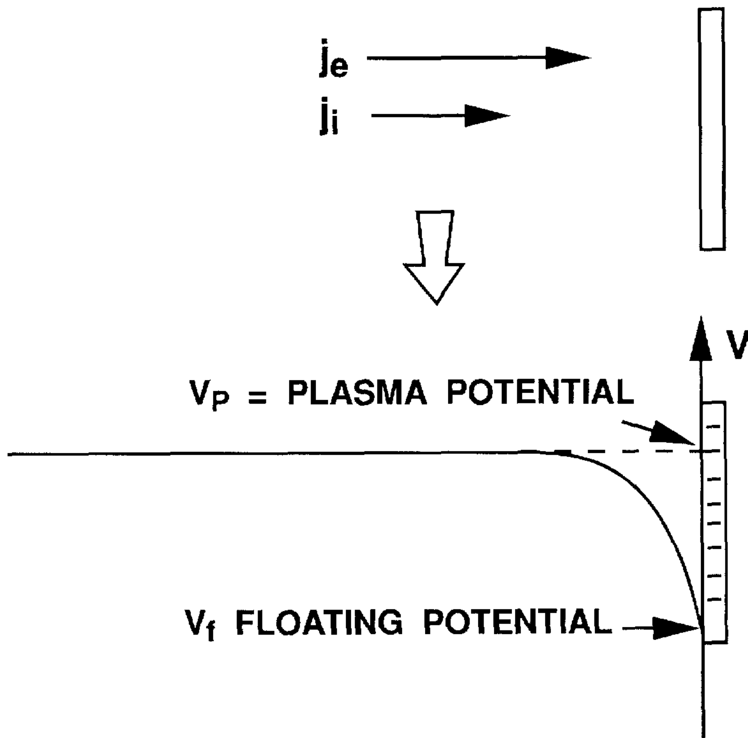

Fig. 2.3 *Establishment of plasma potential and floating potential.*

The wall is then said to be at floating potential; and at this point, the current of electrons entering the boundary layer no longer corresponds to random motion described by Eq. (2.7). This phenomena usually force the average wall potential to be negative relative to the higher density plasma in the (more nearly equipotential) glow region. The potential in the glow is termed the plasma potential. Therefore, a potential difference (also called sheath potential) is built between plasma and floating walls with the latter at a relative negative potential.

2.2.4 Development of self-bias on RF electrodes

In the practical device processing, glow discharge processes are almost exclusively driven by a high-frequency power supplier, usually in the radio frequency (RF) range. The reasons for using RF instead of DC power supplies are to avoid the charging of insulator surfaces often exhibiting in the system and to obtain higher efficiency in promoting ionization and sustaining the discharge.

The fact that electrons are much more mobile than ions has a significant effect in RF discharge - generation of self-bias on the electrodes. Consider the glow discharge circuit shown in Fig. 2.4, where C is the capacitance of an insulating electrode or is a blocking capacitor in the case of a conducting electrode and V_a the (alternating) supply voltage. When V_a is momentarily positive, a vast number of highly mobile electrons are accelerated toward the electrode in this short period of time, causing a rapid accumulation of negative charge. When V_a is momentarily negative, heavy, less mobile ions are accelerated to the electrode. However, significantly fewer ions arrive the electrode during this portion of the sinusoidal period than did electrons on the previous positive part of the RF cycle. Therefore, a net negative charge building-up on the powered electrode occurs and hence the continuous negative DC self-bias is observed on the powered electrode immersed in a plasma, indicated in Fig. 2.4 [2.3].

The self-bias will have a value equal to nearly half the applied RF peak-peak voltage. This value is produced to fulfil the requirement that total charge flow per cycle sums to zero (equal electron and ion current). Because the electrons are much more mobile than ions, only a very short positive fraction of a cycle is required to attract the number of electrons equal to that of ions attracted within the remaining part of a cycle. In other words, most part of a cycle of the voltage at the electrode is negative relative to the plasma, resulting in an ion bombardment of the electrode which is almost continuous.

As excessive electrons are available at both electrodes, the DC offset voltage between the plasma and the electrodes in RF discharge is in principle the same at both electrodes. Consequently, the energy with which ions bombard both electrodes is identical. This situation changes when the area of the electrodes is made different and when a blocking capacitor is used. Larger DC potential is present between the smaller electrode and the plasma [2.4]:

$$\frac{V_1}{V_2} = \left(\frac{A_2}{A_1}\right)^4 \tag{2.9}$$

i.e. the DC off-set voltage V across the sheath is inversely proportional to the fourth power of the electrode area A. Consequently, when the substrate to be etched is on the smaller area electrode, the ions will impinge on the substrate with a larger energy than on the counter electrode. This is of course ideal to enhance the vertical component of the etching and meanwhile to minimize the sputtering effect on the counter electrode. For that reason, the counter electrode and the walls of the reactor chamber are usually connected together as one (grounded) electrode to increase its area.

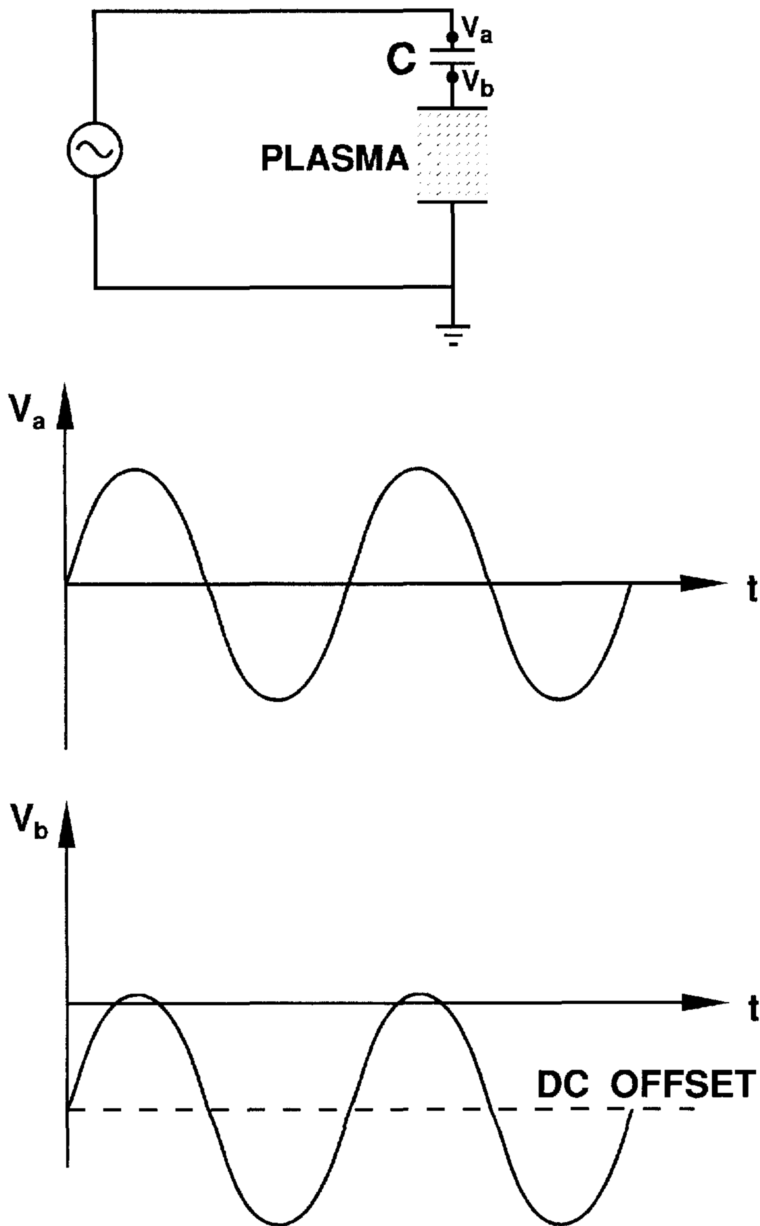

Fig. 2.4 *Self-bias at the RF-excited electrode.*

2.3 Etching mechanisms [2.5]

All known basic plasma etching processes can be grouped into four categories as shown schematically in Fig. 2.5: 1) sputtering, 2) chemical gasification, 3) energetic ion-induced chemistry and 4) inhibitor ion-induced chemistry. In sputtering, ions accelerated across the sheath bombard a surface with high energy. The sudden energy impulse can immediately remove surface atoms. If there is to be a net material removal, however, molecules sputtered from the surface must be prevented from returning. This requires a low gas pressure ($<$ 50 mTorr), yielding a mean free path that is comparable to the vessel dimensions. As a mechanical process, sputtering lacks selectivity. It is sensitive to the magnitude of bonding forces and structure of a surface, rather than its chemical nature.

In chemical etching, gas phase species merely react with a surface according to elementary chemistry. Fluorine atom etching of silicon is a good example of this mechanism. The key, and in fact the only requirement for this kind of process, is that a volatile reaction product be formed. In silicon/F-atom etching, spontaneous reactions between F-atoms and the substrate form SiF_4, a gas. The only purpose of the plasma is to produce the reactive etchant species, F-atoms in this example. Ion bombardment is not essential for the reaction to proceed although it can accelerate the reaction by creating damage on the surface, so that the surface is more susceptible to the etchants. Chemical etching is the most selective kind of process, because it is inherently sensitive to differences in bonds and the chemical consistency of a substrate. However, the process is usually isotropic or non-directional, which is often a disadvantage.

There are two types of directional etching mechanisms that are stimulated by the vertical bombardment by ion flux: energetic ion- and inhibitor ion-induced anisotropy. In energetic ion-induced etching, impinging ions damage the surface, which increases its reactivity. For example, undoped single crystal silicon surface is not etched by Cl_2 or Cl atoms at room temperature. When the surface is simultaneously exposed to a high energy ion flux, however, the result is a rapid reaction that forms silicon chlorides, which removes material much faster than the physical sputtering rate. Here the energetic ion bombardment is essential for the reaction to proceed.

The second class, inhibitor ion-induced etching, requires two conceptually different species: etchants and inhibitors. The substrate and etchants in this mechanism would react spontaneously and etching would proceed isotropically, if it were not for the inhibitor species, which cover the substrate surface. Energetic ion bombardment removes the inhibitors and allows the direct contact between the reactive species with

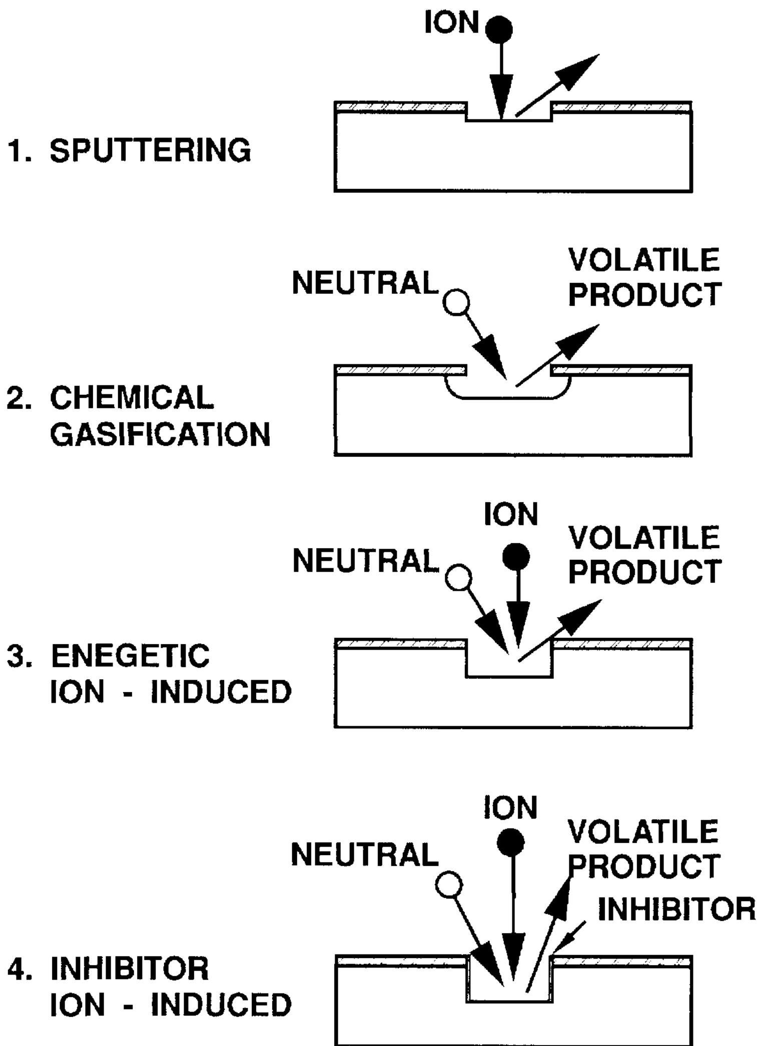

Fig. 2.5 *Four basic plasma etching mechanisms.*

substrate, and therefore the reaction between them. However, the inhibitors form a thin film on vertical surfaces, which receive very little ion bombardment. The film acts as a barrier to etchant and prevents attack of the feature sidewalls, thereby making the process anisotropic. An example of the inhibitor ion-induced etching is the etching of aluminium with Cl_2 + BCl_3 chemistry in which BCl_x radicals form sidewall protecting film against the isotropic Al etching by Cl atoms.

2.4 Plasma etching reactors

A large variety of plasma reactors has been developed. These are all glow discharge systems, but vary considerably in terms of excitation frequency (50 kHz in the LF band to 50 GHz in the MW band), operating pressure (1 mTorr to 1 Torr) and electrode arrangements (external, internal, capacitive and inductive). The early so-called barrel reactors have external electrodes, and are suitable for non-directional etching only. High energy ion bombardment necessary for directional etching is accomplished by placing the electrodes inside the reactor, and bringing the wafer in direct contact with the plasma. A widely employed reactor of this type is the parallel-plate reactor. Recently, magnetic fields have sometimes been introduced in a plasma etcher, combined with microwave excitation, to achieve high plasma density at low pressure, and thereby improve system performance.

2.4.1 Barrel-type reactors

The barrel-type reactor shown schematically in Fig. 2.6 consists of a quartz cylinder (the barrel) with connections for gas lines and vacuum pump. Plate electrodes are strapped to the outside of the cylinder. It usually operates with a 13.56 MHz excitation frequency and at a relatively high pressure (~ 1 Torr). Wafers to be etched are placed on a quartz or metal boat inside the barrel. A metal cage not connected to external

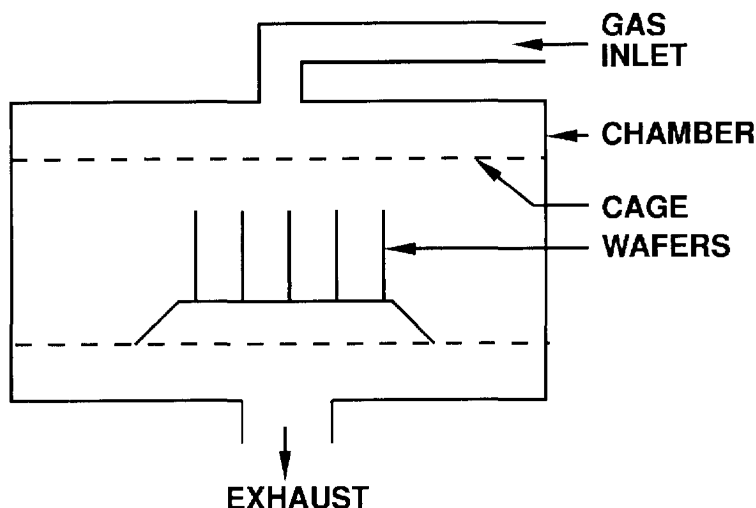

Fig. 2.6 Barrel-type reactor.

circuitry is usually placed around the wafer boat to prevent charged particles from reaching the wafer. Therefore, the etching is limited to the neutral particles diffusing from the discharge zone between the cage and reactor wall to the wafer, and normally leads to an isotropic profile. Other limitations of the reactor are the lack of temperature control of the substrate, wafer contamination due to the sputtering of the cage and high non-uniformity of the etching. This type of reactor was once the most widespread type of plasma etching reactor, but is nowadays mostly used for photoresist stripping and other non-critical applications.

2.4.2 Parallel-plate reactors

The parallel-plate or planar reactor is the most common type in use today. The traditional parallel-plate reactor consists of a high vacuum chamber, in which two plates are positioned parallel to each other. There are two types of parallel plate reactors: the anode-coupled reactor and the cathode-coupled reactor. The anode-coupled reactor is characterized by operation at a fairly high pressure (100 mTorr ~ 1 Torr) and the substrate placed on the grounded electrode (anode), which is usually electrically connected to the chamber walls. Due to the sheath potential developed across the plasma and substrate, ion bombardment results and the etching can be anisotropic under certain conditions. The capability of directional etching is an important improvement over the barrel-type reactor. However, because the substrate electrode area is larger than that of the top electrode, the ion bombardment energy to the substrate is lower than that to the top electrode due to the higher negative bias developed there (refer to Eq. 2.9). This results in the undesirable etching of the top electrode in some cases.

The cathode-coupled reactor operates at a low pressure (10 mTorr ~ 150 mTorr) with the wafer placed on the RF-excited electrode (cathode). Because the area of the electrode is smaller than that of grounded one, high-energy ion bombardment is available with this type. Therefore, etching is greatly enhanced in the direction of incident ions and thus is inherently directional. Very often the cathode-coupled reactor is called RIE (Reactive Ion Etching) reactor to address the importance of ion bombardment. Fig. 2.7 shows schematically a typical parallel-plate RIE reactor (Alcatel GIR300) which will be used in this research. To increase the throughput of parallel-plate reactors, the hexode reactor has been developed in which the electrode surfaces are folded into concentric cylinders and expanded vertically in the third dimension to increase wafer capacity [2.6].

2.4.3 Triode reactors

In the parallel-plate reactors the energy of ion bombardment is amongst others

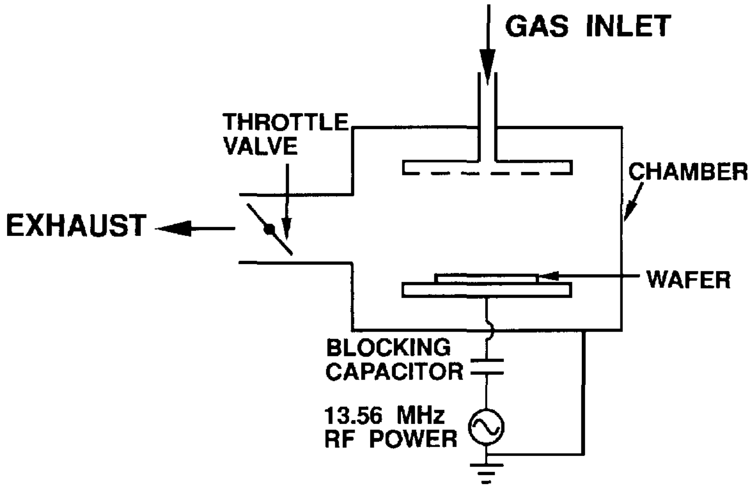

Fig. 2.7 *Parallel-plate reactor.*

determined by the applied RF power. In other words, bombardment energy is strongly coupled with power supply. When high density reactive species are required for high speed etching, high RF-power supply is needed and high self-bias is produced. The resulting excessive high energy ion bombardment can have some detrimental effects such as low selectivity, radiation damage to the substrate and degradation of photoresist. This limitation can be avoided by using the so-called triode reactor design in which the discharge is maintained with two electrodes, and then introducing the wafer on the third electrode that can be powered and therefore biased. As a result, neutral density and bombardment energy can be separately controlled with the triode configuration. Fig. 2.8 shows schematically such a triode reactor (DRYTEK 384T), which will be used in this research. A grounded grid is inserted between two RF-powered electrodes. The automatic matching network can divide the RF power between the two electrodes, according to the desired self-bias on the lower electrode. It can apply all the RF power to the lower electrode (the "RIE mode"), to the upper electrode (the "remote mode"), or any combination of both (the "split-power mode"). Since it is a single wafer system, a relatively high pressure (100 mTorr ~ 300 mTorr) is used in the etching to achieve high etch rate for high throughput.

2.4.4 Magnetron and ECR reactors

When electrons move in both magnetic and electric fields which are perpendicular to each other, they are forced into a helical path. This effect can be employed in plasma etching to reduce the loss of energetic electrons by confining them within the plasma

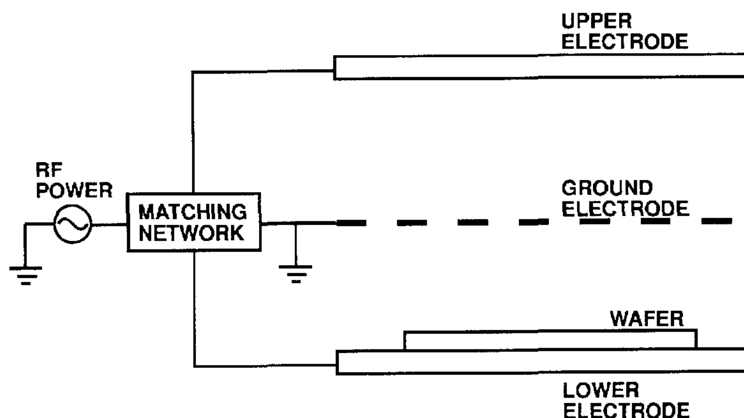

Fig. 2.8 *Triode reactor.*

volume instead of reaching the chamber walls, where these would recombine. With increasing magnetic field strength the DC self-bias, which determines the ion bombardment energy, drops, releasing the problem associated with energetic ion bombardment. This is because the voltage at which the electron current density balances with the ion current density in the sheath is lower [2.7]. At the same time, the plasma density increases, and hence the ion bombardment flux [2.8]. An additional feature of RF discharge with magnetic confinement is that the etcher can operate at a gas pressure of typically 1 ~ 10 mTorr, much lower than usual. Such a dry etching reactor is known as magnetron etcher. Through combination of low pressure and a high magnetic field, it is possible to construct the system in which the dominant etching species are ions rather than reactive neutrals. This can have advantages for processes where high degree of etching directionality is required.

If the excitation frequency is in the same range of the electron cyclotron frequency (which is in the microwave range), resonance effects can occur in plasma, causing an additional increase in the energy transfer efficiency. Reactors based on this principle are called electron cyclotron resonance (ECR) etchers. ECR reactors normally operate with 2.45 GHz microwave power at a pressure less than 1 mTorr. The plasma density can be as high as 10^{11} cm^{-3}.

2.5 Plasma etching chemistries [2.5]

2.5.1 Fluorine atom dominant plasma

The isotropic etching of silicon by fluorine atoms produced in a plasma is one of the most widely used plasma processes. Many different plasma feed gases produce F atoms as the dominant etching species. These include F_2, CF_4, SiF_4, SF_6, NF_3 and ClF_3. Among them CF_4 and SF_6 are probably most often used due to their availability and low toxicity. F atoms are produced through electron impact processes. In CF_4 discharge, e.g., the following processes take place:

1. Dissociative ionization

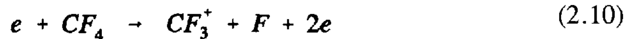

$$e + CF_4 \rightarrow CF_3^+ + F + 2e \tag{2.10}$$

2. Dissociation

$$e + CF_4 \rightarrow CF_3 + F + e \tag{2.11}$$

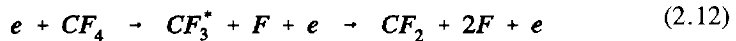

$$e + CF_4 \rightarrow CF_3^* + F + e \rightarrow CF_2 + 2F + e \tag{2.12}$$

3. Dissociative attachment

$$e + CF_4 \rightarrow CF_3 + F^- \tag{2.13}$$

$$e + CF_4 \rightarrow CF_3^* + F^- \rightarrow CF_2 + F + F^- \tag{2.14}$$

followed by detachment

$$e + F^- \rightarrow F + 2e \tag{2.15}$$

When silicon is exposed to the F-atoms produced, it quickly acquires a fluorinated layer that extends about one to five monolayers into the bulk. F atoms penetrate into the fluorinated layer and attack subsurface Si-Si bonds. The attack liberates two gaseous desorption products, *viz*. the free radical SiF_2 and the stable end product SiF_4.

In CF_4 or SF_6 plasma, unsaturated species (C_nF_{2n} radicals derived from CF_2) and fluorosulfur radicals, S_xF_y, are formed which can combine with free F atoms and sometimes can form polymeric residuals. Oxygen is frequently added to these plasmas to suppress the reaction of F atoms with unsaturated species and fluorosulfur radicals. This is because oxygen atoms are produced upon oxygen addition and these react with the unsaturated species, forming F atoms, while depleting these polymer-forming species:

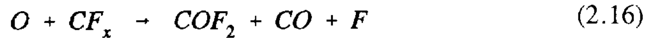

$$O + CF_x \rightarrow COF_2 + CO + F \tag{2.16}$$

This enhances silicon etch rate and improves selectivity over silicon dioxide compared to pure CF_4, because unsaturated species selectively etch SiO_2 at ion bombardment. When enough oxygen is added to the feed, O atoms chemisorb on the silicon surface, competing for surface site with F atoms and thus slowing down the etching [2.9].

Because of the pure chemical nature of the reaction between silicon and F atoms, the etching is isotropic. Furthermore, etch rates often decrease with an increasing amount of etchable substrate material placed in a reactor. This is the so-called loading effect and is the result of gas phase etchant being depleted by reaction with the substrate material.

Besides etching silicon, F atom-based chemistries are used for the etching of silicon oxide, silicon nitride, refractory metals and their silicides. While the etching of silicon oxide and nitride is pure chemical and therefore isotropic with F atoms, the etching of refractory metals and their silicides is ion induced and thus anisotropic.

2.5.2 Unsaturated etchant dominant plasma

Some freons (e.g., C_2F_6, CHF_3, CF_3Cl, CF_3Br) or their mixtures with certain additive gases (such as $CF_4 + H_2$) yield abundant unsaturated polymer-forming species in plasmas. Unsaturated species stand for CF_2 radicals and derivatives (C_2F_4, C_3F_6) formed by chain-building oligomerization when fluorocarbons are involved, or CCl_2 and derivatives (C_2Cl_4 etc.) in chlorocarbon feeds. These simple monomers and oligomers can influence the etching in several ways:

1. These polymerize to form thin films on substrate surfaces, which results in anisotropy by sidewall protection mechanism, such as the anisotropic etching of heavily n-doped silicon by Cl_2/C_2F_6 plasma.

2. These react with F or Cl atoms and reactive molecules by saturation reactions, reducing their concentration and thus the etch rate, such as in CF_4 plasma described

above.

3. These can significantly retard the etching of substrate, such as on silicon substrate in CHF_3 plasma.

Silicon oxide can be etched using feed mixtures that generate abundant unsaturated fluorocarbon species, because polymerization of unsaturated is inhibited by the reaction of the surfaces with fluorocarbon radicals to form volatile products. This reaction can only take place when the surface is simultaneously receiving high energy ion bombardment. Therefore, the reaction is ion-induced and thus inherently anisotropic. It appears that when unsaturated fluorocarbon species impinge on the oxide surface, a thin ($\leq$ 10 Å) fluorocarbon layer is formed and halogen atoms in the layer are transferred to the oxide substrate. With the help of ion bombardment which produces dangling bonds, material in this carbonaceous layer reacts continuously with silicon oxide, forming volatile reaction products such as COF, COF_2, CF_2O [2.10]. Naturally, fluorocarbon layers also form on exposed silicon. Since there are no reactions with silicon that can gasify the carbonaceous film, a fairly thick layer ($\geq$ 100 Å) accumulates on silicon and blocks the attack to silicon. This protective film on silicon provides etching selectivity of silicon oxide over silicon. Experimentally it is shown that the etching selectivity between oxide and silicon in the plasma increases as the C/F ratio of the feed gas, e.g. $C_3F_8 > C_2F_6 > CF_4$ [2.11]. The unsaturated-dominant plasma can also be used to selectively and anisotropically etch silicon nitride over silicon based on a similar mechanism.

2.5.3 Chlorine and bromine based plasma

Chlorine- and bromine-containing plasmas can be used to etch silicon, aluminium and a variety of other substrates. These can provide high selectivity ($>$ 10) over silicon oxide since the latter is etched very slowly ($<$ 200 Å/min) in those plasmas. Chlorine is more widely used because it has a higher vapour pressure, is less corrosive and tends to form less toxic by-products.

Etching of undoped silicon with chlorine-containing plasmas must be accompanied by energetic ion bombardment otherwise Cl atoms and Cl_2 molecules etch undoped silicon very slowly ($\sim$ 100 Å/min below 100°C at 0.1 Torr). Therefore, the etching is inherently anisotropic. However, heavily n-type doped silicon is rapidly and spontaneously etched by Cl atoms. Thus severe undercutting occurs when heavily As- or P-doped layers are etched in Cl_2 plasmas. C_2F_6 or CCl_4 can be added to the plasma to provide sidewall inhibitors to prevent the underetching [2.12]. Mixing F atoms and Cl atoms by adding Cl_2 to ClF_3 plasma can result in a tapered etching profile which is

intermediate between the anisotropic extreme of Cl atom etching and isotropic one of F atom etching [2.13].

Both atomic or molecular chlorine and bromine attack aluminium vigorously and ion bombardment has little influence on the etch rate because spontaneous chemical reaction is very fast. $AlCl_3$ and Al_2Cl_6 are two etch products from chlorine attack. Inhibitor chemistry is necessary for line-width control in Al etching. BCl_3, CCl_4 and $SiCl_4$ are additives that form inhibitors and promote anisotropy in the etching. These additives are also essential to remove the native aluminium oxide, which is always formed on Al surfaces exposed to the air and is not reactive with Cl atoms.

2.5.4 Importance of gas additives

The feed for plasma etching is invariably a mixture of primary gases and additives. While primary gases provide reactive species necessary for the etching, gas additives can change the composition of plasmas and, hence, influence the etching characteristics dramatically. The reasons for applying additives can be grouped as follows:

1. Oxidants are used to increase etchant concentrations or suppress polymer formation. The addition of O_2 or Cl_2 to CF_4, CCl_4 and the other freons are examples.

2. Radical-scavengers such as H_2 in CF_4, which increase the concentration of film formers or reduce etchant concentration.

3. Inhibitor-formers supply unsaturated radicals to form the sidewall films which result in anisotropy. Such as C_2F_6 addition in Cl_2, BCl_3 or $SiCl_4$ in Cl_2.

4. oxide etchants are added to etch the native oxide on substrate because some etchants, such as Cl atoms, do not etch the oxide. Examples are C_2F_6 in Cl_2 for native silicon oxide and BCl_3 in Cl_2 for native aluminium oxide etching.

5. "Inert" gases such as Ar and He can help to stabilize a plasma, enhance anisotropy by ion bombardment or reduce the etching rate by dilution. Helium can also improves heat transfer between wafers and the supporting electrode, due to its high thermal conductivity.

2.6 Summary of the previous most important developments of plasma etching chemistry for micromachining

2.6.1 SF_6-based chemistry

Due to its ability to produce fluorine-rich and carbon-free plasmas, and therefore the potential for high silicon etch rate, SF_6, as well as its mixtures with O_2, has frequently been used to etch bulk silicon for micromachining applications. Early in 1985, Fung and Linkowski [2.14] reported deep silicon etching using SF_6 plasma with a negative DC bias in a reactive ion etching (RIE) reactor, in an attempt to replace wet anisotropic through-wafer etching to provide backside contact vias for chemical transducers. They used Al_2O_3 as the etch mask and the selectivity achieved was as high as 320 with a silicon etch rate of 1.6 μm/min. However, they did not report on the anisotropy of the chemistry. Furthermore, the surface at the trench bottom was rather rough (several microns for a total etching depth of 60 - 100 μm).

Through-wafer plasma etching using SF_6 was also reported by Fischer *et al.* [2.15] for pressure sensor fabrication. Linder *et al.* [2.16] reported about 1 μm/min etch rate using SF_6/O_2 gas mixtures, with a selectivity of 20 ~ 30 for photoresist, 85 for silicon dioxide and > 300 for aluminium. However, the etching showed little anisotropy (with undercutting of the mask versus vertical depth of 0.55, 0.65 and 0.8, respectively for the three types of masks). The isotropy of the chemistries was used to undercut the silicon substrate to obtain free-standing SiO_2 or aluminium beams and bridges. Silicon membranes of about 15 μm thick were obtained by etching originally 360 μm thick silicon wafers with aluminium mask, although a significant surface roughness (15 ~ 20 μm) was measured. Isotropic SF_6 etching was also used in underetching silicon to form a silicon dioxide net, which was subsequently sealed to form a membrane for pressure sensors [2.17], in releasing the rotor of a nickel micromotor from silicon substrate and in fabrication of self-aligned needles [2.18].

With sufficiently high oxygen content the etching of silicon using SF_6/O_2 gas mixtures can be anisotropic, as reported by D'Emic *et al.* [2.19]. In a magnetron ion etching (MIE) system they developed a process containing 25% O_2 to etch 50 μm deep trenches into silicon with 8800 Å/min etch rate and a nearly vertical etch profile using an aluminium mask. The anisotropy results from the sidewall passivation arising from the oxidation of silicon at the trench sidewalls, where ion bombardment is absent. The process was used to fabricate silicon doughnuts of dimensions 25 - 50 μm thick, 50 μm inner diameter, and 100 -200 μm outer diameter. However, the selectivity over the mask was limited to about 9. In a RIE system a process with 60% O_2 content was found

to etch silicon anisotropically with etch rate of 4900 Å/min and selectivity of only about 2.5. Addition of CHF_3 to SF_6/O_2 gas mixtures can improve the surface roughness often occurring with SF_6/O_2 chemistries [2.20].

One possibility for controlled silicon trench sidewall profile with SF_6 plasma was reported by using a gas mixture of SF_6 with carbon-containing mixed halogens (CF_xX_n, in which X is one of halogens except for F) such as CCl_2F_2 [2.21-2.22] and $C_2Cl_3F_3$ [2.23]. It was found that these gases had complementary effects on the trench profile, permitting some flexibility in tailoring the sidewalls. As shown in Figure 2.9, SF_6-dominant chemistry causes the bottom of the trench to be narrower than the top, whereas CCl_2F_2 has the opposite effect, resulting in re-entrant profiles. When the effects of these gases are balanced, near vertical trench sidewalls can be achieved. This optimized chemistry has been used in patterning thick, narrow structures in a bulk silicon dissolved wafer process. Using SF_6/C_2ClF_5 gas mixtures in a RIE reactor, a completely anisotropic etching profile was obtained up to 33 μm deep etching with resist mask. However, a limited selectivity (5 ~ 6) over the mask was achieved [2.24-2.25]. Higher selectivity (25) over resist mask and therefore deeper trench depth (50 μm) has been reported with $SF_6/C_2Cl_3F_3$ gas mixtures [2.23].

Another possibility of obtaining anisotropic SF_6 etching is to use cryogenic substrate electrode. As reported by Murakami *et al.* [2.26], by using a cryogenic RIE system maximum silicon etch rate of 1.6 μm/min was achieved with SF_6 plasma at a cathode temperature of -120 °C. The lateral etch rate was found to be only 2% of the vertical one. The etching selectivity over aluminium mask was over 900. Anisotropic polyamide

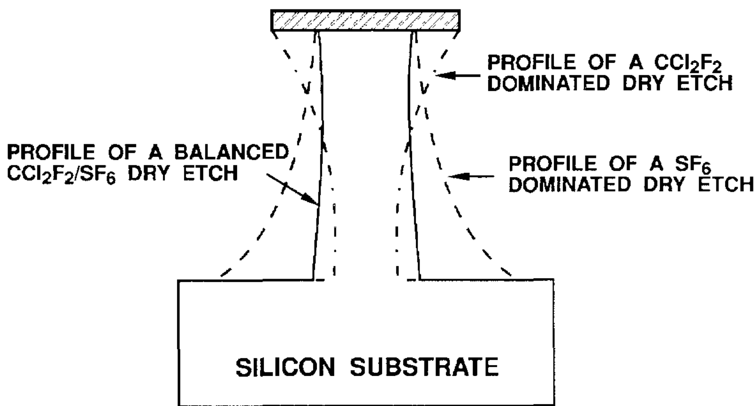

Fig. 2.9 *Illustration of different sidewall profiles using plasma chemistries based on SF_6 and CCl_2F_2 gases.*

film etching was also obtained using the cryogenic SF_6 etching with 1% lateral etching relative to the vertical one. Therefore, the cryogenic etching technique can be used to fabricate 3-dimensional microstructures with very high aspect ratio.

2.6.2 CF_4-based chemistry

A CF_4/O_2 plasma-based micromachining technique to control sidewall angles of silicon trenches was reported by tilting silicon substrate relative to the plate of bottom electrode of plasma etcher [2.27]. When the substrate is tilted, the incident angle of the ion flux is not 90° as usual with untilted substrate. Smooth sidewall with angles varying from 15 - 60° with regard to the normal axis of the wafer were obtained with tilts ranging from 0 - 45°, as a result of surface erosion by the combination of ion milling and neutral chemical etch mechanisms. These silicon structures with tapered sidewalls could find applications in optical reflecting gratings for opto- and micromechanical devices as well as in the fabrication of field emitter cone or ridge cathodes for vacuum microelectronic devices.

In a so-called "light intensity profile method", CF_4/O_2 plasma was used to transfer a specific curved photoresist profile, which was obtained by exposing the resist to a specific energy profile through a dither mask, to the silicon substrate to obtain a dynamic focusing mirror whose deformation is optically ideal due to its thickness profile [2.28]. The plasma etching process must be tailored to remove the photoresist and silicon at the same rate.

In a surface micromachining process CF_4/CHF_3 plasma has been used to etch very thick (~5 μm) PSG anisotropically to obtain vertical sidewalls of PSG. Subsequently, polysilicon sidewall beams were formed by depositing a polysilicon layer on the patterned PSG and anisotropically etch-back the polysilicon layer using also the CF_4/CHF_3 plasma [2.29] or a CCl_4 plasma [2.30]. These polysilicon sidewall beams are very flexible due to their high aspect ratio (height/width), providing highly compliant lateral suspensions for lateral resonators. In addition, polysilicon hollow beams can be fabricated based on the polysilicon sidewall beams, which adds tremendously to micromechanical design possibilities. Removal of inside PSG is not trivial and needs to depend on the permeation of HF solution through the grain boundaries of polysilicon. With hollow beam technology, the surface micromachined structures are less constrained by film thickness and photolithography, thereby allowing the fabrication of devices with very large height/width aspect ratios.

2.6.3 Cl_2- and Br_2-based chemistry

Cl_2- or Br_2-base plasmas usually etch silicon anisotropically with high selectivity over silicon oxide and, therefore, can be used for small lateral feature size bulk silicon micromachining. A micromachining process called SCREAM (Single Crystal Reactive Etching And Metallization) was reported by Zhang and MacDonald [2.31]. An anisotropic Cl_2/BCl_3 plasma has been used to pattern silicon structures and isotropic SF_6/O_2 plasma to undercut and, therefore, release the structures from the substrate. As shown in Figure 2.10, by combining the anisotropic and isotropic plasma etching, submicron silicon beams can be fabricated with high aspect (height to width) ratio. An x-y micro-stage was fabricated using the technique based on sidewall electrostatic driving. However, the technique is quite complicated which involves several film deposition and plasma etching steps. More importantly, the patterning of aluminium electrodes relies on photolithography with very thick (the same as the height of the structures) photoresist in the silicon trench, which requires large (typically more than 5 μm for a 4 μm deep trench) separation between the structures (i.e. the trench width), resulting in very high (more than 200 V) driving voltage in actuating devices using sidewall electrostatic force.

A modified version of the process (SCREAM I) [2.32] eliminates the requirement for the thick resist patterning in the trench and, therefore, can be used to produce structures with very small (~ 1 μm) gap. A lateral accelerometer based on sidewall capacitance sensing was fabricated using the SCREAM I process. However, the electrical isolation between the structures depends on the trenches around the structures. The resulting surface non-planarity due to the trenches make it very difficult to integrate on-chip electronic circuits with mechanical structures.

A somewhat similar technique based on Cl_2/BCl_3 anisotropic silicon plasma etching with selective oxidation and wet etching called COMBAT (Cantilevers by Oxidation for Mechanical Beams And Tips) has been reported by Yao *et al.* [2.33]. In addition to high aspect ratio submicron silicon beams, silicon micro-tips having a nominal diameter of 200 Å can be produced with the process. A two dimensional actuator for scanned probe devices has been fabricated. However, the process is rather complicated and involves very high temperature (1100 °C) processing for the selective oxidation, which causes compatibility problems.

Wolfe *et al.* reported a Br_2 plasma process in a magnetically enhanced triode etching system for the fabrication of large-area silicon membranes for ion projection lithography [2.34]. The process is intrinsically anisotropic for both B- and degenerately P-doped silicon substrates (in contrast to Cl_2-based processes which result in isotropic etching of

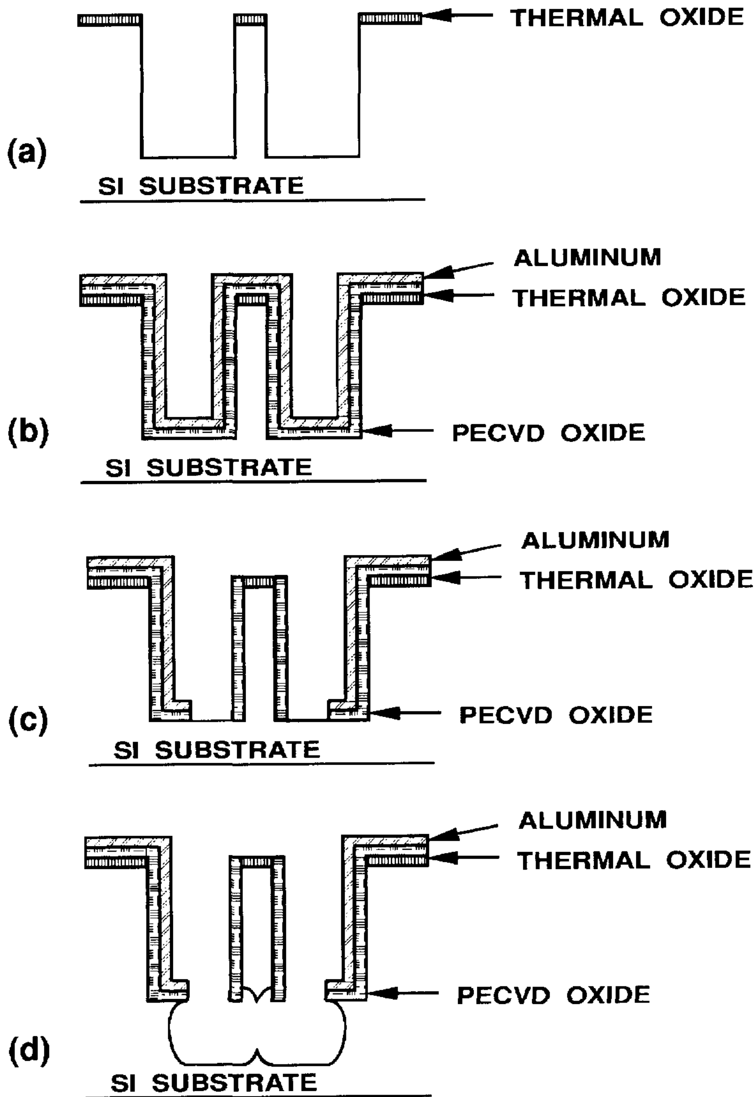

Fig. 2.10 *The SCREAM process [2.31]. (a) Anisotropic deep silicon trench etching using Cl_2/BCl_3 plasma. (b) PECVD oxide and aluminium deposition. (c) Isotropic aluminium etching using Cl_2/BCl_3 plasma and anisotropic PECVD oxide etching using CF_4 plasma. (d) Isotropic silicon etching using SF_6/O_2 plasma.*

heavily P-doped silicon), which are required for low stress ion masks. For the optimized process, the selectivity relative to SiO_2 is as high as 160. The low power density, low self-bias voltage and inertness of SiO_2 to a Br_2 plasma are responsible for the high selectivity. However, the silicon etch rate is very low (400 Å/min).

2.6.4 O_2-based chemistry

O_2 plasma is used for photoresist ashing in IC processing. In micromachining O_2-based plasmas can be used to etch organic materials such as polyamide, which is frequently used as the structural material for micromechanical structures due to its compatibility with silicon processing and unique material properties (such as optical transparency, chemical or thermal resistance). O_2 plasmas have been used in etching fluorinated polyamide to fabricate high aspect ratio microstructures [2.35]. Using a Ti mask in a magnetically controlled RIE system etch rates of 3 - 5 μm/min have been obtained for the polyamide with a selectivity of 2600 over the mask and little underetching. 100 μm high polyamide poles with 15 μm diameter have been produced using the technique, resulting in smooth surface morphology which is suitable for optical device applications. An O_2 plasma was also used to etch polymer with aluminium mask in a dry-release process for surface micromachined large area membranes [2.36].

2.7 Process control and optimization

2.7.1 Process requirements

Plasma etching processes are mainly judged by their etch rate, selectivity, uniformity, anisotropy, surface quality and reproducibility. Production rates and cost are determined by these factors. Usually, application-dependent optimization is possible by a compromise between, e.g. etch rate and selectivity. For some applications such as silicon trench etching for device isolation, the profile of sidewalls and the shape of the trench bottoms are also important.

Etch rate refers to the amount of vertical removal of the substrate per unit time. It determines the utility and cost of a process and needs to be sufficiently high.

Selectivity is defined as the ratio of the etch rate of the material to be etched to that of the materials not to be etched (such as a mask or underlying layer). Roughly the minimum required selectivity over a mask is simply the thickness ratio between the film and the mask. However, a somewhat higher mask selectivity than this simple estimation is required due to the overetching necessary to account for non-uniformities of the

thickness and etch rate for both the mask and the film. The minimum required film-to-substrate selectivity can be determined by the following equation [2.37]:

$$S_s^f = \frac{t_f}{t_{s,\max}} U_s^f , \tag{2.17}$$

where t_f is the film thickness and $t_{s,max}$ is the maximum allowed etch depth to the substrate, and U_s^f is the combined uniformity factor defined as:

$$U_s^f = \frac{(1 + \alpha)(1 + \delta)}{(1 - \beta)} - \frac{(1 - \alpha)}{(1 + \beta)} , \tag{2.18}$$

where α, β are the non-uniformity of the film thickness and etch rate, respectively; δ is the overetching factor to account for other sources of variation, which is usually expressed as a percentage of the total clearing time.

Uniformity refers to the evenness of etching across a wafer or from wafer to wafer in the same reactor. It is usually represented by non-uniformity defined as

$$U = \frac{R_{\max} - R_{\min}}{R_{\max} + R_{\min}} \times 100\% , \tag{2.19}$$

where R_{max} and R_{min} denote the maximum and minimum etch rate, respectively. At any rate, non-uniformity should be kept minimum.

Anisotropy is a measure of the vertical etch rate relative to the lateral one. A definition which is often used is

$$A = 1 - \frac{E_l}{E_v} , \tag{2.20}$$

where E_l and E_v are the lateral and vertical etch rate, respectively. With such a definition a complete anisotropic etching ($E_l = 0$) will lead to $A = 1$, whereas a complete isotropic etching ($E_l = E_v$) corresponds to $A = 0$. The requirement for anisotropy depends on the application. To attain small feature size a high anisotropy is necessary, but a slightly tapered etching profile is better for good step coverage. Sometimes both anisotropic and isotropic etching are required alternatively. For example, during patterning of polysilicon microstructures, an anisotropic process is first

used to clear the planar portion of the film and subsequently an isotropic process is necessary to completely remove the remaining of the thicker polysilicon along sidewalls of PSG steps, as indicated in Fig. 2.11.

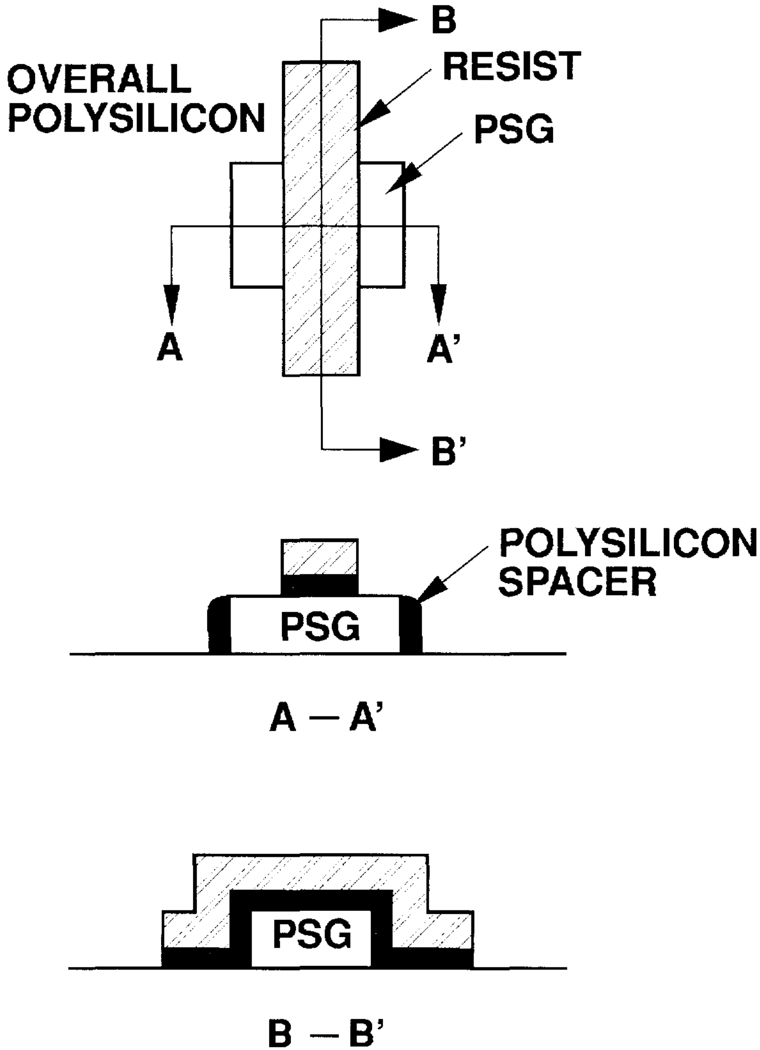

Fig. 2.11 *When patterning a polysilicon structural layer on a PSG step, anisotropic plasma etching alone will result in polysilicon spacers along the sidewalls of the PSG step (cross-sectional view A-A'). A subsequent isotropic plasma etching is necessary to remove the spacers.*

Surface quality mostly refers to the smoothness and degree of electrical damage of a surface after etching and can be influenced by variables such as temperature, power, pressure, etchant and crystallographic orientation. Contamination from sputtering, etch product re-deposition, etch residuals and electrical damage caused by radiation (including ion bombardment) and charging may degrade surface quality.

Reproducibility, at first glance, might appear to be more a matter of process control than an inherent process characteristics. However, etching equipment and processes sometimes have insidious "memory" or hysteresis effects that are difficult to control. The initial condition of the reactor can be influenced by accumulation of etch products, exposure to the ambient atmosphere (with adsorption of air and moisture on reactor surface) and surface modification brought about by reaction with chemical plasmas in the equipment. For example, aluminium etching is sensitive to moisture, oxygen and surface condition. Thus, reproducible aluminium etching was difficult to achieve until reactor design and chemistries were developed to control these hidden variables. Another source of variability is load size, the exposed area on a wafer or the number of wafers in a reactor. When etching reactions consume most of the etchant, the etch rate will be inversely proportional to the number of wafers in the reactor. Process development must be aimed in avoiding this effect.

2.7.2 Effects of process variables

The instrumental process variables which are at the disposal of an operator include reactor pressure, RF excitation frequency, temperature, flow rate, RF input power (or power density), feed gas composition, electrode distance and sometimes, materials of electrodes. When fixed, all these variables uniquely determine the operation of a plasma process. The influence of those process variables on the etching depends on the etching mechanisms involved which are determined by the values of the process variables as well as the substrate material to be etched. The influence of feed gas composition has been discussed in Section 2.5.

a. Pressure effects

The primary effects of pressure are on the mean free path of ions and concentration of species in a plasma. Pressure directly influences major phenomena that control plasma etching. The most important one among these are:

1. The sheath potentials and energy of ions bombarding surfaces.
2. The electron energy.
3. The ion-to-neutral abundance ratio and fluxes of these species to surface.

4. The relative rate of higher to lower order chemical kinetics.

As the gas pressure is lowered the gas density (the number of gas molecules per unit volume) is decreased. This results in reduction of concentration of radicals and ions due to the decrease in collision rates between electrons and gas molecules and between ions and neutrals. As a result, the impedance of the plasma may rise thereby resulting in a higher voltage applied to the discharge at a given power input. As self-bias is proportional to the peak applied voltage, it is raised too. Furthermore, due to the increase in the mean free path of the species in plasma (inversely proportional to pressure), the collisions between ions and neutrals whilst traversing the dark space is reduced. These two effects lead to a higher ion bombardment energy to substrate surface.

For typical plasma etching conditions, the average electron energy ϵ increases with the ratio of electric field to number density (E/N), with the latter being the number of neutral species per unit volume. From the above discussion the average electron energy will increase with lower pressure. In the range of interest, with mean electron energies $< 5 - 8$ eV, many electron-molecule dissociation reaction rates tend to slowly increase with E/N (or lower pressure) because of increasing overlap between elementary reaction cross sections and electron energy distribution functions. As a result, electron-molecule ionization rate constants tend to increase with decreasing pressure, leaving a more efficient ionization process. However, because of compensating effects - the lower neutral reactant concentration (gas density) and a higher diffusive loss rate - the electron number density does not necessarily change much with pressure.

Because the average degree of ionization in most practical etching plasmas ranges between about 10^{10} and 10^{11} cm^{-3}, more or less independent of the operating pressure, the change in pressure (thus neutral density), usually spanning from $\sim$ 1 Torr to 1 mTorr, implies a change in the neutral flux relative to ion flux to the substrate surface up to three orders of magnitude. This, together with the effects on ion energy, allows pressure to determine wether etching will be chiefly chemical, with little or no contribution from ion-assisted reactions (at the higher pressure end), or be predominantly ion-assisted (at the lower pressure end).

Pressure also influences the rate of chemical kinetics in the regime of relatively high pressure. Experimental studies show that in the case of bimolecular reaction (such as the recombination reaction of CF_3 radicals with F atoms to form CF_4 in plasma), the reaction rate between two species can be usually represented as [2.5]

$$\frac{product\ formation}{time} = k(T)n_a n_b \ , \qquad (2.21)$$

where k(T) is the rate constant and depends only on temperature; n_a and n_b are the concentration of species A and B, respectively. For a fixed gas feed mixture, the concentrations, n_i, are given in molar fractions x_i by:

$$n_i = x_i\, p \ , \qquad (2.22)$$

which shows that each of the n_i is proportional to pressure p. Hence the rate is proportional to p^2 (i.e. second order reaction). When the reaction occurs on or near surfaces (as in the case of F atom etching of silicon to form SiF_2), the reaction is a heterogeneous one and the rate is frequently expressed as:

$$\frac{product\ formation}{time} = k(T)n_a A_w \ , \qquad (2.23)$$

where A_w is the surface area. Hence the rate is proportional to p (i.e. first order reaction). Some reactions in plasma can be of a higher order in pressure than two, e.g. the polymerization reaction of CF_2 to form C_3F_6 is of the third order in pressure, since it involves 3 CF_2 radicals. The higher the order of the reaction, the more rapidly the rate changes with the pressure. In the above examples, lower pressure will favour etching, while higher pressure polymerization and recombination.

b. Frequency effects

The excitation frequency alters key discharge characteristics that have an important influence on plasma etching. Among them are the sheath potential, which determines the ion bombardment energy, and energy coupling efficiency, which limits the minimum pressure under which a plasma can be sustained. Fig. 2.12 illustrates the excitation bands commonly used for plasma etching, together with some characteristic frequencies in plasma. In this figure, the electrical plasma decay time is mainly determined by recombination of ions and electrons to the walls of the reactor. The electron plasma frequency ω_e and ion plasma frequency ω_i are determined by the mass of the electrons and ions, respectively. When the frequency of an electromagnetic disturbance is lower than ω_e (ω_i), the plasma electrons (ions) can response fast enough to the disturbance.

In the HF range with the excitation frequencies above the ion plasma frequency, there is not enough time for ions to cross the sheath and reach the electrode in a single cycle. Instead, ions cross the sheath over many periods and experience an electric field which

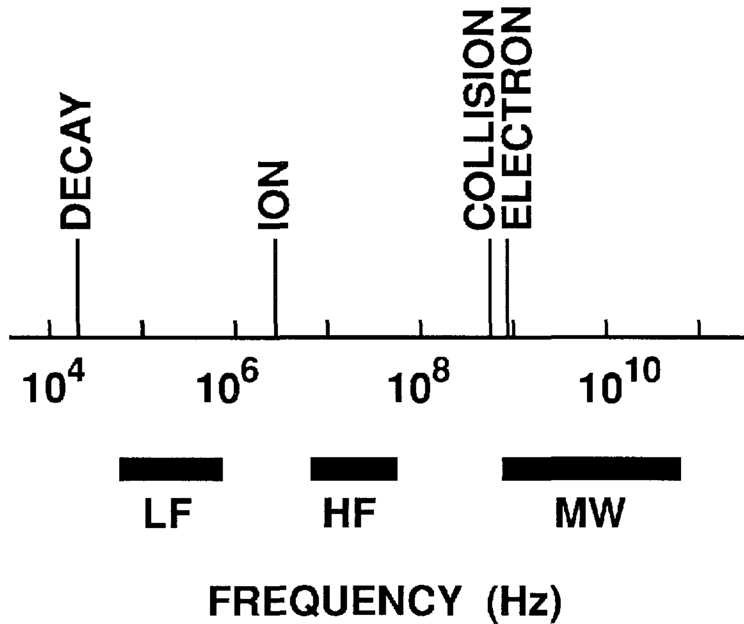

Fig. 2.12 *Characteristic discharge frequencies and operation ranges for plasma etching.*

is averaged over this transit time. It can be shown that the maximum energy a ion can obtain is eV_0/π, in which V_0 is the peak value of the excitation voltage [2.38]. In the LF range, on the other hand, when the excitation frequency is below the ion plasma frequency, ions can transverse the sheath and reach to the wall in a single cycle, obtaining the maximum energy of eV_0. Therefore, as the excitation frequency is lowered through the ion plasma frequency the peak ion energy is increased by more than three-fold.

Furthermore, experiments show a large increase in the discharge-sustaining voltage in the LF range, and in total the peak ion bombardment energy increases by more than a factor of 10. Therefore, using a low excitation frequency promotes damage-driven etching such as silicon etching in chlorine plasma. On the other hand, excitation frequency in microwave (MW) range is far above the electron-neutral collision frequency, and the electrons can undergo many field-induced oscillations before hitting another particle. In the MW band the frequency is high enough to neglect the capacitance impedance of the space charge regions at the plasma-wall interface altogether. Therefore, the voltage drop across the sheath is greatly reduced and thus also the ion bombardment energy. This property is one of the advantages of MW plasma

etching in case the substrate is sensitive to energetic ion bombardment, such as in polysilicon gate etching.

Another significant effect of the excitation frequency is that an increase in operating frequency allows a plasma to be sustained at lower pressure [2.39]. This indicates that there is an extra source of ionization with higher frequency.

c. Temperature effects

Surface temperature has a profound influence on etching chemistry. In the etching involving mainly free radical chemical reaction, an Arrhenius type temperature dependence for the etch rate is found [2.5]:

$$R = C(T)T^{1/2}ne^{-E_A/RT} \tag{2.24}$$

where C(T) is a "pre-exponential" factor which is weakly dependent on temperature, n the concentration of the reactant, R the universal gas constant, T the reaction temperature and E_A the activation energy, which is the height of the energy barrier that reactants must overcome in order for the reaction to proceed. For example, the E_A for Si and SiO_2 etching by F atoms are 2.48 and 3.76 kcal/mole, respectively. The lower activation energy of Si compared to SiO_2 results in a higher etch rate for Si than SiO_2 and thus in a selective etching. Higher selectivity can be achieved by cooling the substrate below room temperature, however, with a decreased etch rate. The dependence of etch rate on temperature will be less significant in processes in which the etching proceeds mainly by ion-induced damage mechanism. In this case the ion impact supplies the activation energy.

In some systems it has been observed that the roughness of the etched silicon surface increases with surface temperature. This may be associated with defects or impurity nuclei in the substrate where chemical reactions proceed excessively.

d. Gas flow rate effects

Below a critical flow rate, there is a depletion of reactants to etch the substrate material and thus a small increase in flow rate can result in rapid increase in the etch rate. Alternatively, if the flow rate is further increased with an accompanying increase in pumping speed to keep a constant pressure of operation, it is possible that the active species produced in the plasma can be pumped away before they have the opportunity to react due to too short residence time expressed as

$$\tau = \frac{V}{S}, \tag{2.25}$$

where V is the volume of the chamber and S is the pumping speed which is the ratio of the flow rate to pressure. The gas residence time relative to the average lifetime of etchant species (determined by loss process such as gas phase reactions) is therefore very important to obtain a stable process. If the lifetime is significantly shorter than the residence time, changing the flow rate over a limited range should have a minimal effect on the process because the concentration of active species is not affected. When the intrinsic lifetime is longer than the residence time, the effective lifetime value in the reaction chamber will be equivalent to the residence time. In this case the concentration of active species is controlled primarily by the starting composition of the feed gas. Consequently, changing flow rate can change the etch rate and observed loading effects. For example, increasing flow rate will decrease etch rate as well as loading effects [2.40]. Rapid surface reaction rates combined with long residence time should be avoided because this leads to loading effects, depletion of reactants across the substrate leading to non-uniformity, possibility of undesired polymer formation and re-deposition.

e. Power effects

At constant pressure the plasma density can be raised by increasing the power input into the plasma. The increase in power will cause a rise in the applied voltage particularly at low pressures [2.41], thus increasing the sheath potential and therefore the ion bombardment energy. At the same time, the formation rate of plasma products such as free radicals is also increased due to the higher current which gives a more intensive dissociation processes. As a result, etch rate is generally increased, while selectivity is reduced due to the enhanced ion bombardment. Any polymer formation from free radicals will be suppressed at the substrate surface by the higher ion bombardment energy. Substrate damage caused by plasma radiation is certainly increased with power.

f. Electrode distance effects

With some parallel-plate plasma etchers, the distance between the two electrodes can be changed. Increasing the electrode spacing may increase the plasma volume in contact with the vessel walls and if these walls are at ground potential, then the ground electrode area will increase with respect to RF-driven electrode area. As a result, the negative DC bias formed on the RF electrode will increase, resulting in higher ion bombardment energy. Also the applied RF voltage need to be increased with electrode distance, which further increases the ion bombardment energy. This is because the

higher plasma recombination events between the electrodes increase the plasma impedance, and hence a higher potential is required to maintain the same charge flow.

g. Electrode material effects

The ionization conditions of plasma can be changed by changing electrode material. An electrode material with lower second electron emission coefficient (e.g. stainless steel with respect to aluminium) may need a higher voltage to maintain the same plasma density. Electrodes made of aluminium appear to increase the likelihood of surface polymerization compared to that for stainless steel electrodes. This is believed to be caused by aluminium halides in the plasma, which increase the molecular weight of the polymer-forming free radical species. By pre-conditioning the plasma chamber with gases of high C/F ratio such as C_4F_8, a polymer film can be formed on the chamber walls which may reduce any metal electrode effects during the etching.

2.7.3 End point detection for process control [2.42]

For a tight process control it is important to determine the time when the film is etched through (the end point). Although the end point can be estimated straightforward by the film thickness divided by etch rate, this method is rather unreliable, since the end point is also affected by non-uniformity of both the film thickness and etch rate, and the substrate area exposed to the plasma. Sometimes a thin native oxide layer or residual mask layer gives an unpredictable delay of the etching. Thus, end point detection is an important part of process control. Detection of the end point can be achieved by monitoring signal intensity changes corresponding to etchants or etching products of either film or substrate. Usually when the film is etched through, the signal intensity for the etchant increases due to the decrease in the consumption of the etchant and that for the etching product of the film (or substrate) decreases (or increases). There are a variety of phenomena from which signals can be derived to mark the end point. These mainly include pressure change, self-bias change, species change (monitored by mass spectrometry or emission spectroscopy) and thickness change measured by laser interferometry.

The pressure increase observed as the film clears at the end point with fixed pumping speed has been employed for some early batch reactors. This is because the gas-solid reactions during the etching usually cause a decrease in the number of gas molecules, so system pressure is lower than when the film is etch through. Although this method requires no special equipment, chamber pressure in modern etching reactors is usually maintained by an automatic "throttle" valve which regulates the pumping speed. This configuration improves process control, but excludes the possibility of using pressure

as an end point indicator.

A self-bias change is observed as the plasma composition changes during the etch cycle, because the plasma impedance and sheath characteristics change. In some processes this change is large enough to allow end point detection. This method is very attractive in automated systems due to its ease of implementation and the intrinsic large signal.

Mass spectroscopy can be used to monitor the change of species associated with the end of an etch cycle. Often the concentration of a particular constituent in the chemistry can be used to track the progress of an etch. For example, in the etching of Si_3N_4 film on a SiO_2 substrate with CF_4 chemistry, volatile SiF_4 forms from the reaction between F-atoms and Si_3N_4. When the Si_3N_4 is etched through and the SiO_2 is exposed, the SiF_4 in the plasma is reduced due to a slower reaction between F-atoms and SiO_2. Therefore a sharp drop in the intensity of SiF_3^+ (which is formed by electron impact-induced fragmentation of SiF_4 in the instrument's ionizer) will occur at the etch end point. Mass spectrometry can be used to detect the concentration of such specific species. However, the method is very expensive and requires operation skill.

Optical emissions from species excited by the plasma are widely used as a sensitive and effective end point monitor. Emission can emanate from etchants, etch products, or their fragments with a characteristic wavelength corresponding to a particular species. An optical spectrometer can be set to the wavelength of interest and be used to monitor its intensity during an etch cycle. Take the same example as in mass spectroscopy, either 704 or 674 nm peak intensity associated with F-atoms (reactants) or N atoms (products), respectively, can be traced. Very often, signal intensities associated with more than one species are monitored through a multichannel approach and certain algorithm can be used to manipulate the intensity data so that maximum signal change is obtained. The optical method is less expensive and easier to use than mass spectroscopy. However, light from the plasma contains emissions from many species that cover a wide spectral range. Sometimes it is difficult to separate a characteristic line from the intense background.

When monochromatic light rays transmitted the front surface and reflected from underlying interface of a thin transparent film interact, constructive and destructive interference takes place, which is characteristic of the light wavelength and the film thickness. This effect can be used to monitor the (remaining) thickness of etched materials such as polysilicon, silicon oxide and silicon nitride, which are transparent in a wavelength region. This technique permits real-time monitoring, so that etch rate changes caused by variations in the composition of the film with depth, or a diffuse interface between film layers, can be automatically detected and corrected. A major

limitation of the technique stems from the small spot size needed to obtain a distinct interferogram (~ 10 μm in diameter). Since the end point determination is made from sensing a small area, non-uniformities in the film thickness or etch rate are not detected.

2.7.4 Process optimization

Plasma process optimization involves finding the setting for each of plasma variables that optimizes the etching results (responses of the variables) to meet the requirement for the etching process. Moreover, at the optimum setting the change of the responses with plasma variables should be gradual to avoid major non-reproducibility at a minor drift of the setting. A plasma etching system contains several variables, as described previously, to be adjusted and usually more than one etching requirements need to be met simultaneously.

However, the plasma is a very complex system and many of the details of physical and chemical interactions within the plasma and with substrate surface are not yet fully understood. Thus kinetic modelling of plasma etching process from a fundamental approach is generally very difficult. As a result, empirical approaches (parametric modelling) are often used. Because process optimization may involve five or more independent variables and some of the variables may interact with each other, some systematic procedure needs to be used for the optimization. Statistical experimental design procedures and data analysis techniques, such as response surface methodology (RSM) [2.43], are powerful tools to explore unknown regions of parameter space, to obtain initial information on important variables and to refine the information, so that optimum conditions can be determined.

2.8 Problems caused by plasma etching

Because the substrate in a plasma is exposed to energetic particle and photon bombardment, radiation damage of the substrate surface can be caused and thereby electrical characteristics of devices may be altered or degraded. Much of these radiation damage caused by energetic ions, electrons and photons can be removed by thermal annealing up to 900°C provided by thermal cycling in device fabrication. However, soft x-ray damage from plasma may require an annealing temperature as high as 1000°C. Such a high temperature cycling is not acceptable in the fabrication of small size devices with shallow junctions.

There are some effects occurring in plasma which cannot be readily removed without special care. One of these is contamination during critical operations such as etching

SiO_2 windows for metallization. To obtain certain selectivity over the underlying layer (polysilicon or silicon substrate) a chemistry is chosen which can produce a thin polymer film on silicon. Sometimes foreign material, such as sputtered reactor material, enters an opened contact window. If these surface contamination is not removed properly, it will later be covered by metallization. The result is high contact resistance, which cannot be corrected. Hence control of reaction products from the plasma chemistry, particularly polymeric products, is essential. One another source of irreversible damage is electrostatic breakdown of thin insulating films caused by charge accumulation during the plasma process cycle [2.44].

References

[2.1] D. L. Flamm and G. K. Herb, "Plasma etching technology - an overview," in *Plasma Etching - An Introduction*, D. M. Maros and D. L. Flamm Eds., Academic Press, Inc., California, 1989, pp. 14-17.

[2.2] E. W. McDaniel, in *Collision Phenomena in Ionized Gases*, John Wiley and Sons, New York, 1964, p. 120.

[2.3] B. Chapman, "RF discharges," in *Glow Discharge Processes*, John Wiley & Sons, New York, 1980, pp. 139-176.

[2.4] H. R. Koening and L. I. Maissel, "Application of rf discharges to sputtering," *IBM J. Res. Develop.*, Vol. 14, pp. 168-171, 1970.

[2.5] D. L. Flamm, "Introduction to plasma chemistry," in *Plasma Etching - An Introduction*, D. M. Maros and D. L. Flamm Eds., Academic Press, Inc., California, 1989, pp. 91-184.

[2.6] D. N. K. Wang, D. Maydan and H. J. Levinstein, "Reactive sputtering etching and its applications," *Solid State Technol.*, Vol. 23 (8), pp. 122-126, 1980.

[2.7] K. Hirobe and H. Azuma, "Reduction of radiation damage on silicon substrate in magnetron reactive ion etching," *J. Electrochem. Soc.*, Vol. 132, pp. 938-942, 1985.

[2.8] A. D. Kuyers and H. J. Hopman, "Measurement of ion energy distributions at the powered RF electrode in a variable magnetic field," *J. Appl. Phys.*, Vol. 67, pp. 1229-1240, 1990.

[2.9] C. J. Mogab, A. C. Adams and D. L. Flamm, "Plasma etching of Si and SiO_2 - the effect of oxygen additions to CF_4 plasmas," *J. Appl. Phys.* Vol. 49, pp. 3796-3803, 1979.

[2.10] J. W. Coburn, "*In situ* Auger electron spectroscopy of Si and SiO_2 surfaces plasma etched in CF_4-H_2 glow discharges," *J. Appl. Phys.*, Vol. 50, pp. 5210-5213, 1979.

[2.11] J. W. Coburn and E. Kay, "Some chemical aspects of the fluorocarbon plasma etching of silicon and its compounds," *Solid State Technol.*, Vol. 22(4), pp. 117-124, 1979.

[2.12] A. C. Adams and C. D. Capio, "Edge profiles in the plasma etching of polycrystalline silicon," *J. Electrochem. Soc.*, Vol. 128, pp. 366-370, 1981.

[2.13] D. L. Flamm, D. N. K. Wang and D. Maydan, "Multiple-etchant loading effect and silicon etching in ClF_3 and related mixtures," *J. Electrochem. Soc.*, Vol. 129, pp. 2755-2760, 1982.

[2.14] C. D. Fung and J. R. Linkowski, "Deep etching of silicon using plasma," in *Micromachining and Micropackaging of Transducers*, C. D. Fung, P. W. Cheung, W. H. Ko and D. G. Fleming Eds., Elsevier Science Publishers B. V., Amsterdam, 1985, pp. 159-166.

[2.15] K. Fischer, R. Hoffmann, J. Müller, "Design and fabrication of a micromechanical integrated optical pressure sensor," in *Micro System Technology 91*, R. Krahn and H. Reichl Eds., 1991, pp. 425-431.

[2.16] C. Linder, T. Tschan and N. F. de Rooij, "Deep dry etching techniques as a new IC compatible tool for silicon micromachining," in *the Proc. 6th Intern. Conf. Solid-State Sensors and Actuators (Transducer'91)*, 1991, pp. 524-527.

[2.17] S. Adams, U. Hilleringmann and K. Goser, "CMOS compatible micromachining by dry silicon-etching techniques," *Microelectronic Engineering*, Vol. 19, pp. 191-194, 1992.

[2.18] T. Hirono, T. Furuhata and H. Fujita, "Dry released nickel micromotors and their friction characteristics," in *the Proc. 7th Intern. Conf. Solid-State Sensors and Actuators (Transducer'93)*, 1993, pp 80-83.

[2.19] C. P. D'Emic, K. K. Chan and J. Blum, "Deep trench plasma etching of single crystal silicon using SF_6/O_2 gas mixtures," *J. Vac. Sci. Technol.*, Vol. B10, pp. 1105-1110, 1992.

[2.20] H. Jansen, M. de Boer, R. Legtenberg and M. Elwenspoek, "The black silicon method, a universal method for determining the parameter setting of a fluorine based reactive ion etcher in deep silicon trench etching with profile control," in *the Proc. Micro Mechanics Europe 1994 (MME'94)*, 1994, pp. 60-64.

[2.21] I. W. Rangelow, S. Skocki, P. Dumania, "Plasma etching for micromechanical sensor applications," *Microelectronic Engineering*, Vol. 23, pp. 365-368, 1994.

[2.22] Y. Gianchandani and K. Najafi, "A Bulk silicon dissolved wafer process for microelectromechanical devices," *J. Microelectromechanical Sys.*, Vol. 1, pp. 77-85, 1992.

[2.23] V. A. Yunkin, D. Fisher and E. Voges, "Highly anisotropic selective reactive ion etching of deep trench in silicon," *Microelectronic Engineering*, Vol. 23,

pp. 373-376, 1994.

[2.24] C. Linder, T. Tschan and N. F. de Rooij, "Deep dry etching of silicon - a novel micromachining tool," *Sensors and Materials*, Vol. 3, pp. 311-324, 1992.

[2.25] E. Cabruja and M. Schreiner, "Deep trenches in silicon using photoresist as a mask," *Sensors and Actuators*, Vol. A37-38, pp. 766-771, 1993.

[2.26] K. Murakami, Y. Wakabayashi, K. Minami and M. Esashi, "Cryogenic dry etching for high aspect ratio microstructures," in *the Proc. 1993 IEEE Workshop on Micro Electro Mechanical Systems (MEMS'93)*, 1993, pp. 65-70.

[2.27] J. M. Kim, W. N. Carr, R. J. Zeto and L. Poli, "Reactive ion etching techniques for silicon sidewall angle control in micromachining," *J. Electrochem. Soc.*, Vol. 139, pp. 1700-1705, 1992.

[2.28] M. Hisanaga, T. Koumura and T. Hattoro, "Fabrication of 3-dimensionally shaped Si diaphragm dynamic focusing mirror," in *the Proc. 1993 IEEE Workshop on Micro Electro Mechanical Systems (MEMS'93)*, 1993, pp. 30-35.

[2.29] M. W. Judy and R. T. Howe, "Polysilicon hollow beam lateral resonators," in *the Proc. 1993 IEEE Workshop on Micro Electro Mechanical Systems (MEMS'93)*, 1993, pp. 265-271.

[2.30] M. W. Judy and R. T. Howe, "Highly compliant lateral suspensions using sidewall beams," in *the Proc. 7th Intern. Conf. Solid-State Sensors and Actuators (Transducer'93)*, 1993, pp. 54-57.

[2.31] Z. L. Zhang and N. C. MacDonald, "An RIE process for submicron, silicon electromechanical structures," in *the Proc. 7th Intern. Conf. Solid-State Sensors and Actuators (Transducer'91)*, 1991, pp. 520-523.

[2.32] K. A. Shaw, Z. L. Zhang and N. C. MacDonald, "SCREAM I: a single mask, single-crystal silicon, reactive ion etching process for microelectromechanical structures," *Sensors and Actuators*, Vol. A40, pp. 63-70, 1994.

[2.33] J. J. Yao, S. C. Arney and N. C. MacDonald, "Fabrication of high frequency two-dimensional nanoactuators for scanned probe devices," *J. Microelectromechanical Systems*, Vol. 1, pp. 14-22, 1992.

[2.34] J. C. Wolfe, S. Sen and S. V. Pendharkar, "Magnetically enhanced triode etching of large area silicon membranes in a molecular bromine plasma," *J. Vac. Sci. Technol.*, Vol. B10, pp. 2716-2719, 1992.

[2.35] A. Furuya, F. Shimokawa, T. Matsuura and R. Sawada, "Micro-grid fabrication of fluorinated polyamide by using magnetically controlled reactive ion etching (MC-RIE)," in *the Proc. 1993 IEEE Workshop on Micro Electro Mechanical Systems (MEMS'93)*, 1993, pp. 59-64.

[2.36] C. H. Mastrangelo and G. S. Saloka, "A dry-release method based on polymer columns for microstructure fabrication," in *the Proc. 1993 IEEE Workshop on*

Micro Electro Mechanical Systems (MEMS'93), 1993, pp. 77-81.

[2.37] C. J. Mogab, "Dry Etching," in *VLSI Technology*, S. M. Sze, Ed., McGraw-Hill, New York, 1983, pp. 303-345.

[2.38] V. M. Donnelly, D. L. Flamm and R. H. Bruce, "Effects of frequency on optical emission, electrical, ion and etching characteristics of a radio frequency chlorine plasma," *J. Appl. Phys.*, Vol. 58, pp. 2135-2144, 1985.

[2.39] H. Norstrom, "Experimental and design information for calculating impedance matching networks for use in RF sputtering and plasma chemistry," *Vacuum*, Vol. 29, pp. 341-350, 1979.

[2.40] B. N. Chapman and V. J. Minkiewicz, "Flow rate effects in plasma etching," *J. Vac. Sci. Technol.*, Vol. 15, pp. 329-332, 1978.

[2.41] R. A. Morgan, "The RF voltage/current characteristics and related dc negative bias properties of an electrotech flat bed plasma etcher," *Vacuum*, Vol. 32, pp. 297-303, 1982.

[2.42] D. M. Manos and H. F. Dylla, "Diagnostics of plasmas for materials processing," in *Plasma Etching - An Introduction*, D. M. Maros and D. L. Flamm Eds., Academic Press, Inc., California, 1989, pp. 259-338.

[2.43] M. W. Jekins, M. T. Mocella, K. D. Allen and H. H. Sawin, "The modelling of plasma etching processes using response surface methodology," *Solid State Technol.*, Vol. 29 (4), pp. 175-182, 1986.

[2.44] T. Watanabe and Y. Yoshida, "Dielectric breakdown of gate insulator due to reactive ion etching," *Solid State Technol.*, Vol. 27 (4), pp. 263-266, 1984.

Chapter 3 Etching of Poly-Si/Silicon Nitride/Poly-Si Structures Using Multi-Step Approach

3.1 Introduction

In surface micromachining polysilicon/silicon nitride/polysilicon sandwich structures are required as structural layers of sensors, such as in tactile imagers [3.1] and Fabry-Perot light interferometers [3.2]. Mechanically the sandwich structure is more rigid than a polysilicon layer alone of the same thickness since silicon nitride has a higher Young's modulus (3.85×10^{11} N/m^2 for single crystal silicon nitride) than silicon (1.9×10^{11} N/m^2 for single crystal silicon). Furthermore, the symmetry of the structure helps to avoid buckling of the membrane due to residual strain in the layers. Optical transmission and reflection of the membrane can be well-controlled by defining the individual thickness of the sandwich, which is essential to light interferometry.

The anisotropic etching ability of plasma is especially important in patterning such a sandwich structure, in order to precisely define the lateral dimensions of the membrane and the narrow beams usually required to support the membrane. The beam dimension determines the spring constant of the system and therefore the flexibility of the membrane, which in turn determines the sensitivity of the tactile image sensor and controllability of the movement of the membrane using electrostatic force in the interferometer.

In this chapter plasma etching process development for the patterning of polysilicon/silicon nitride/polysilicon sandwich structure is described. A silicon nitride etching chemistry selective over polysilicon using CHF_3 with N_2 addition is developed. Subsequently a multi-step etching process featuring in high selectivity and good uniformity is designed for the patterning of the sandwich structure. Finally possible problems arising from high selectivity with regard to the surface quality of the etched film are investigated and a solution using post-processing is proposed and experimentally verified.

3.2 The tactile image sensor

A tactile image sensor usually consists of a matrix of force-sensitive cells. When used for force-sensing, a capacitive sensor is one or two orders of magnitude more sensitive with a much lower temperature coefficient than a piezoresistive device [3.3]. The

surface micromachining technique is very suitable for the fabrication of such a capacitive tactile image sensor, because (1) the sensing elements can be made very small and densely packed to obtain high spatial resolution (finer than 1 mm); (2) interfacing electronic circuits for multiplexing and capacitance-detecting can be fabricated together with the sensing cells on the same chip to reduce the number of external wiring and to enhance the system performance.

In the surface micromachined capacitive tactile image sensor design [3.1], the sensing capacitance is composed of a base plane on the silicon substrate and an elevated membrane formed by sacrificial layer technique, as shown in Fig. 3.1. When a force is applied to the membrane, the displacement of the membrane relative to the base plane results in change in the capacitance value, which can be detected by the on-chip electronic circuit. The membrane consists of a 1400 Å polysilicon/1700 Å silicon nitride/1400 Å polysilicon sandwich structure. The lower polysilicon film functions as one electrode of the capacitance and the upper polysilicon film acts as a shielding film against electromagnetic interference. The silicon nitride film provides electrical isolation between the two polysilicon layers and enhances the rigidity of the membrane.

To electrically contact the lower polysilicon layer, the upper polysilicon and the silicon nitride layer must be etched. In addition to high etching uniformity, high selectivity of nitride etching over the lower polysilicon layer is essential during the plasma etching to maintain the integrity of the lower polysilicon. Furthermore, the etching should not result in any surface contamination to the lower polysilicon surface to ensure good electrical contact of the polysilicon layer with the subsequently deposited conductive film.

3.3 Experimental details

All the plasma etching experiments were performed in a commercial parallel-plate RIE machine (Alcatel GIR300), described in Chapter 2. The RF power (frequency 13.56 MHz) and gas pressure were varied from 50 - 70 W and 22.5 - 52.5 mTorr (0.03 - 0.07 mBar), respectively. Both the upper and lower electrodes were 15 cm in diameter with a 6.5 cm spacing. This electrode configuration resulted in the power density of 0.28 - 0.4 W/cm^2. The flow rates of reaction gases were regulated by mass flow controllers. Unless otherwise stated, a 1.3 μm HPR204 photoresist was used as the mask for the etching. The etch rate of the films was determined by measuring the thickness change due to etching using a Leitz MPV-SP Optical Measurement System.

The silicon nitride used in the experiment was deposited on a (100) p-type 5 Ω•cm

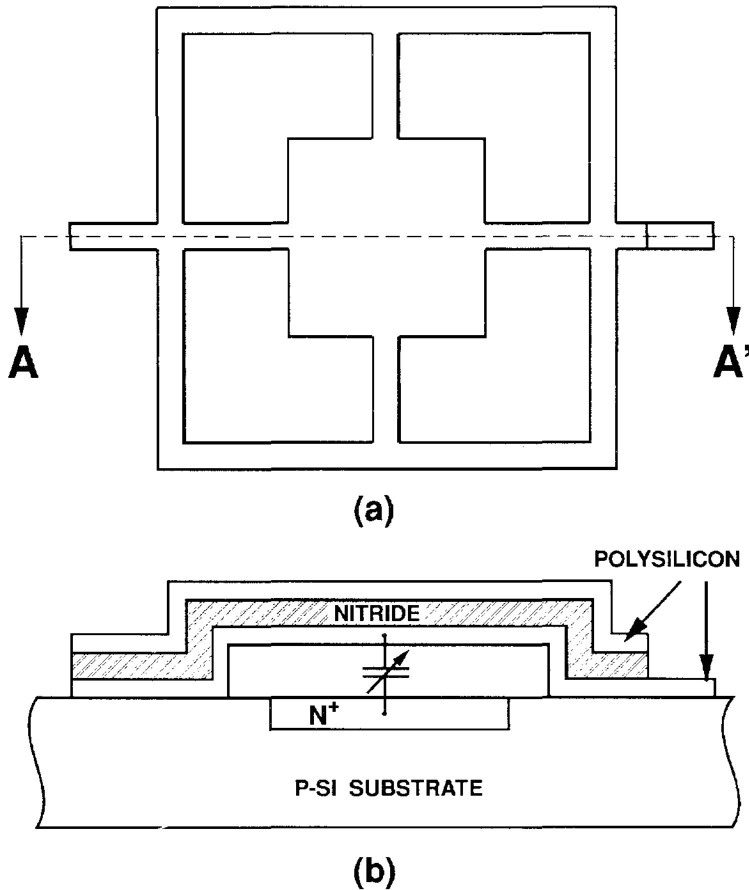

Fig. 3.1 *Schematic view of the sandwich structure for a tactile image sensor. (a) top view. (b) cross-sectional view.*

silicon substrate using a Low-Pressure Chemical Vapour Deposition (LPCVD) system (Tempress Omega M) operating at 850°C and 150 mTorr. The reaction takes place between SiH_2Cl_2 (170 sccm) and NH_3 (30 sccm) in a 15 cm diameter quartz tube to form silicon nitride, which is silicon-rich (Si/N ratio of 0.82) and exhibits low tensile stress (300 μstrain). The polysilicon films of 3000 Å were formed in a similar LPCVD system in which silane decomposition took place at 575°C and 150 mTorr. The polysilicon film was doped by phosphorus implantation of 5×10^{15} cm^{-2} at 80 keV and subsequently thermally annealed at 850°C for 30 minutes in a N_2 atmosphere. This resulted in a sheet resistance of about 200 $\Omega/\square$. The silicon dioxide film was formed by oxidation in dry oxygen at 1100°C.

3.4 Development of silicon nitride plasma etching chemistry selective over polysilicon

Conventionally, silicon nitride can be patterned using wet chemicals such as hot phosphoric acid, which provides high selectivity over silicon dioxide. However, plasma etching is used almost exclusively in modern microelectronic fabrication owing to its etching anisotropy. As discussed in Chapter 2, the anisotropy results from the ion bombardment to the substrate surface during the etching, which enhances the etching in the vertical direction. However, the substrate underneath the nitride (silicon or silicon dioxide) may also be etched during the etching. This is because the chemistry usually used in the nitride etching also etches either silicon or silicon dioxide. As a result, selectivity is one of the issues of major concern in the development of etching chemistry.

To obtain a high selectivity over silicon, generally a chemistry such as CHF_3 [3.4-3.6] or CF_4/H_2 [3.7] is chosen, which contains both reactive species such as F atoms and CF_x^+ (x=1-3) ions and polymer-forming precursors such as CF_y (y=1-3) radicals. The reactive species etch nitride with the help of energetic ion bombardment, while the CF_y radicals form a C-F polymer layer on the silicon substrate, which retards the etching of the substrate by the reactive species. Many gas mixtures providing such etching characteristics have been used, including CHF_3 + O_2 and CHF_3 + CO_2 [3.4], CHF_3 + CH_4 and CF_4 + CH_4 [3.8], CF_4 + H_2 + He [3.9], SiF_4 + O_2 [3.10]. With these chemistries selectivities of 10 - 12 have been achieved. Using a downstream plasma etcher with SF_6 + H_2 + He, a selectivity as high as 40 has been reported [3.9]. However, the etching was isotropic because the downstream reactor configuration resulted in pure chemical reactions only. Using feed gases with high C/F ratio such as C_2F_6 [3.11], C_2F_6 + C_2H_4 [3.12], cyclo-C_4F_8 [3.12], and C_3F_8 [3.13], selectivities of 10 - 20 have been reported.

It has been pointed out that molecular nitrogen is the major nitrogen-containing reaction product of silicon nitride etching. However, the distance between the adjacent nitrogen atoms in Si_3N_4 (~2.8 Å) is larger than that of a N-N single bond (~1.5 Å). Thus adjacent nitrogen atoms, in a silicon depleted Si_3N_4 structure, are not in sufficiently close proximity to form a bond. In other words, desorption of nitrogen atoms on Si_3N_4 surface is a factor which limits the etch rate [3.14]. If additional nitrogen atoms are introduced in the system, it is expected that these may combine with the nitrogen atoms attached to the surface, thus enhancing the nitride etching. Therefore, a plasma etching chemistry using N_2 addition in CHF_3 has been developed, as described below. It is shown that the etch rate of the nitride and selectivity over polysilicon increase with the

N_2 content, leading to the maximum selectivity of 16.

3.4.1 Experimental results

a. The effects of N_2 content in CHF_3 + N_2 gas mixtures

Fig. 3.2 shows the dependence of etch rate of the silicon nitride, silicon dioxide and polysilicon and the selectivity of nitride over polysilicon on N_2 content in the gas mixtures of CHF_3 + N_2. The power, pressure and total gas flow rate were fixed at 60 W, 37.5 mTorr and 50 sccm, respectively. Note that without N_2, a pure CHF_3 chemistry etches the nitride with an etch rate of 70 Å/min and a selectivity of 4 over the polysilicon. The etch rate for the nitride increases dramatically with the N_2 content in the range of 0 - 85% and drops when the content is further increased. However, no change of the etch rate of the polysilicon could be measured. Therefore, the selectivity increases with N_2 content, which reaches its maximum of 16 at 85% (42.5 sccm) N_2. This gas composition (7.5 sccm CHF_3 + 42.5 sccm N_2) was further used in the remaining experiments with regard to RF power, gas pressure, mask materials, nitride composition and residual stress in nitride. The N_2 content has been limited to 95% due to the fact that at an N_2 content above 95%, the plasma cannot be ignited as a result of

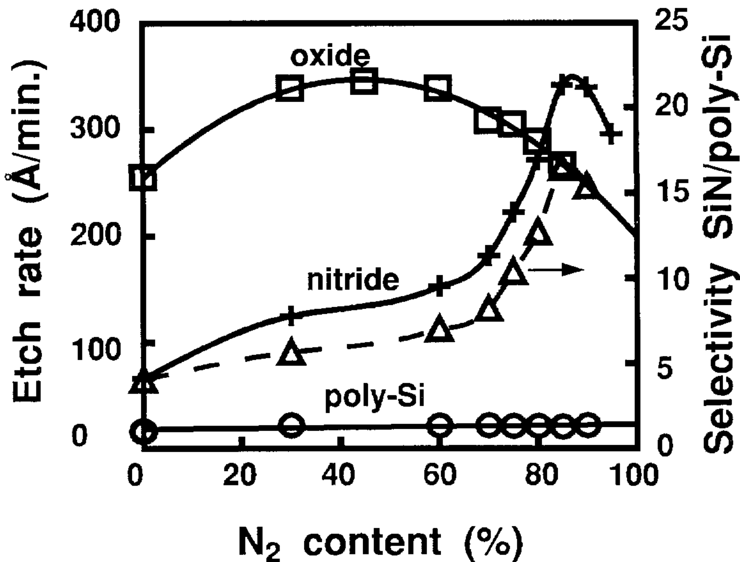

Fig. 3.2 *Etch rates of poly-Si, SiN and SiO_2 as well as selectivity of SiN over poly-Si versus N_2 content in the CHF_3 + N_2 chemistry. RF power = 60 W, pressure = 37.5 mTorr, the total gas flow rate = 50 sccm.*

the limited range of adjustment of the automatic network matching system. The etch rate for the oxide varies with the N_2 content in the similar way as that for the nitride. However, the oxide etch rate without N_2 addition is higher and reaches its maximum at lower N_2 content (45%) compared to the nitride etch rate.

b. The effects of RF power and gas pressure

Fig. 3.3 and Fig. 3.4 show the etch rates of the nitride and polysilicon and the selectivity versus RF power and gas pressure, respectively. The pressure used in the experiment for Fig. 3.3 is 37.5 mTorr and the power in Fig. 3.4 is 60 W. Clearly the etch rate for the nitride increases with the power, while that for the polysilicon remains essentially unchanged. This etch rate dependence on the power results in the increase of the selectivity with the power, as indicated in Fig. 3.3. Fig. 3.4 shows that the etch rate of the nitride decreases with the pressure, resulting in the selectivity variation with the same trend because the etch rate of the polysilicon is not significantly influenced.

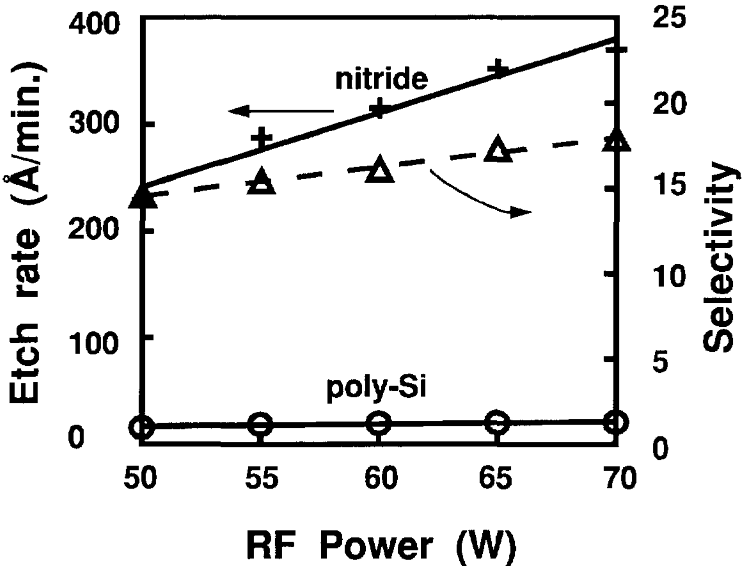

Fig. 3.3 *Effects of RF power on the etch rates of SiN and poly-Si and the selectivity. Pressure = 37.5 mTorr, CHF_3 = 7.5 sccm, N_2 = 42.5 sccm.*

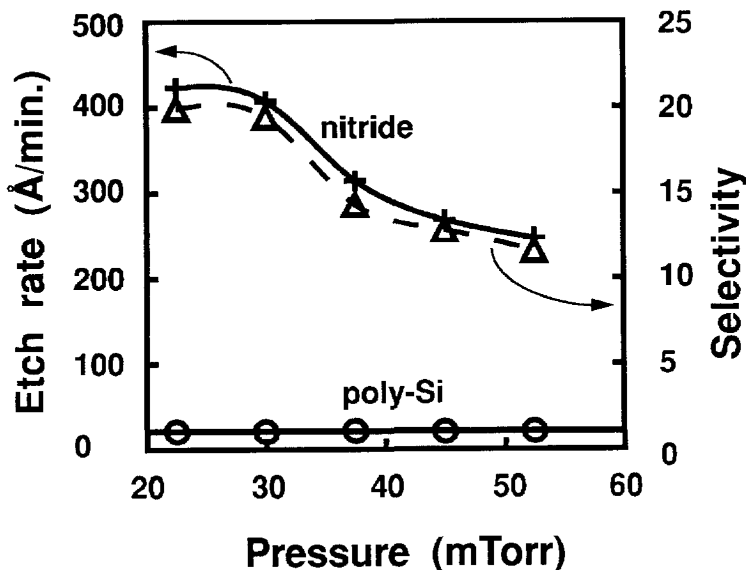

Fig. 3.4 *Effects of pressure on the etch rates of SiN and poly-Si and the selectivity. Power = 60 W, CHF_3 = 7.5 sccm, N_2 = 42.5 sccm.*

c. The effects of helium addition instead of N_2

For comparison helium was also used instead of N_2 as the additive gas to CHF_3. Helium is an inert gas and its main role is dilution only. Fig. 3.5 shows the etch rate of the nitride and polysilicon and the selectivity versus helium content. The RF power, gas pressure and total gas flow rate were the same as those for Fig. 3.2. It can be seen that both etch rates for the nitride and polysilicon increase with the helium content. The selectivity increases with the helium content due to the fact that the nitride etch rate increases more compared to the polysilicon etch rate. The selectivity increase is similar to the results as in the case of N_2 addition. However, The maximum selectivity (5.5 at 90% He content) is much less than that with the N_2 addition (16).

d. The effects of mask materials

To examine the influence of masking materials on the etch rates of both the silicon nitride and polysilicon layer, a 6000 Å aluminium and a 3000 Å nitride layer, in addition to 1.3 μm photoresist, were also used as the mask. The aluminium mask was formed by wet etching of a sputtered pure aluminium layer with a photoresist mask, followed by resist stripping. The etching of nitride with nitride mask was carried out,

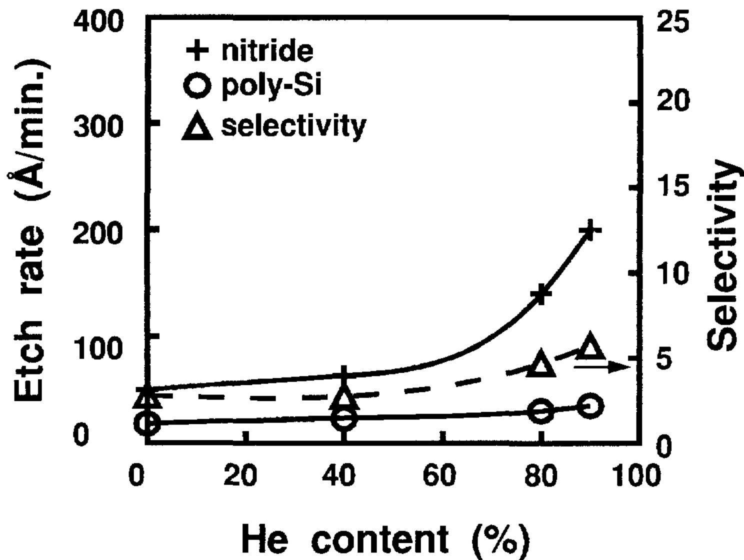

Fig. 3.5 *Etch rates of poly-Si and SiN as well as the selectivity versus He content in the CHF_3 + He chemistry. RF power = 60 W, pressure = 37.5 mTorr, the total flow rate = 50 sccm.*

in fact, with a wafer covered completely with silicon nitride. The nitride mask on polysilicon was prepared by first etching a nitride layer on polysilicon using plasma etching with a resist mask until a very thin (200 Å) nitride layer was left, and then removing the resist and stripping the remaining thin nitride layer in a HF solution. The two-step process was necessary to eliminate any influence of plasma etching on the initial state of polysilicon surface originally underneath the nitride layer.

Table 3.1 lists the etch rates for the nitride and polysilicon and the selectivities with all the three mask materials. It is shown that the etch rate for the nitride is basically not affected by the mask materials while that of polysilicon with the resist mask is lower than that with either Al or nitride mask, leading to the highest selectivity among the three mask materials.

e. The effects of NH_3/SiH_2Cl_2 ratio during nitride deposition

To examine the effects of nitride composition (Si/N ratio) on the etching characteristics, the flow rate ratio of NH_3 to SiH_2Cl_2 for the LPCVD reaction was varied while keeping the total flow rate to a constant 200 sccm. The lower end of the ratio (30/170) resulted in a nitride film with a Si/N ratio of 0.82, while the higher end of the ratio (150/50) a

Table 3.1 *Effects of mask materials on the etch rate and selectivity of SiN over poly-Si. Power = 60 W, pressure = 37.5 mTorr, CHF_3 = 7.5 sccm, N_2 = 42.5 sccm.*

Mask	Etch rate (Å/min)		Selectivity SiN/poly-Si
	Nitride	Polysilicon	
Resist	350	25	14
Al	350	100	3.5
Nitride	380	90	4.2

Si/N ratio of 0.73. Fig. 3.6 shows the etch rate dependence on the NH_3/SiH_2Cl_2 ratio, indicating that the etch rate decreases with increasing NH_3/SiH_2Cl_2 ratio.

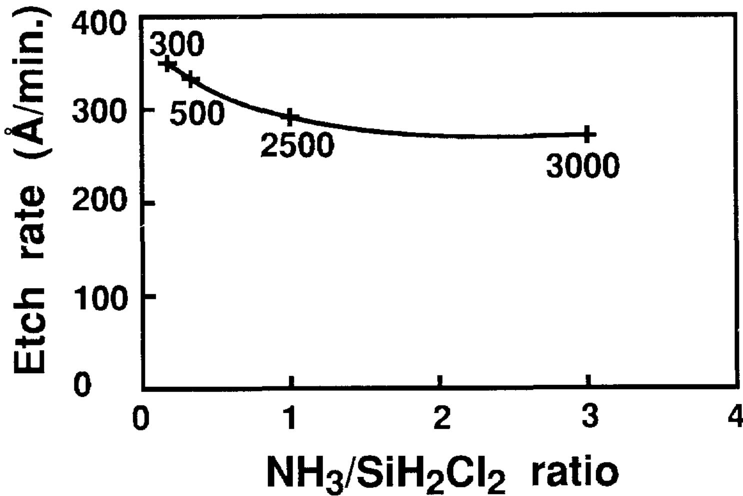

Fig. 3.6 *Silicon nitride etch rate dependence on the NH_3/SiH_2Cl_2 flow rate ratio during deposition. The plasma etching conditions are: RF power = 60W, pressure = 37.5 mTorr, CHF_3 = 7.5 sccm, N_2 = 42.5 sccm. The conditions for the LPCVD nitride deposition are: temperature = 850 °C, pressure = 150 mTorr, total flow rate of SiH_2Cl_2 + NH_3 = 200 sccm. The values next to each data point are corresponding residual stress levels in μstrain.*

f. The effects of residual stress in the nitride film

CVD stoichiometric silicon nitride usually has a tensile residual strain of approximately 3000 μstrain. The Si-rich low-stress silicon nitride used in the experiment has a tensile residual strain of 300 μstrain. It has been shown that annealing at high temperature (> 850 °C) can significantly increase the residual stress level in the low-stress nitride film, but does not change the Si/N ratio of the film [3.15]. To investigate the effect of the residual stress level on the nitride etch rate, anneals had been carried out at 850 °C and 1000 °C, respectively for 45 minutes in Ar atmosphere before the film was etched. The annealing resulted in a residual stress level of 400 and 1000 μstrain, respectively. It was found that there was no measurable difference in the etch rate between the as-deposited and the annealed films, indicating that the residual stress level does not influence the nitride etch rate.

3.4.2 Discussions

a. Etching mechanism

In a CHF_3-based plasma, the following ionization processes take place as a result of high-energy electron collisions with the CHF_3 molecules [3.4][3.6]:

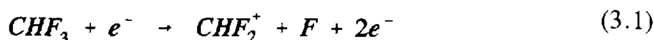

$$CHF_3 + e^- \rightarrow CHF_2^+ + F + 2e^- \tag{3.1}$$

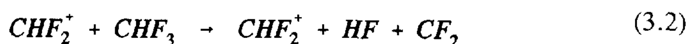

$$CHF_2^+ + CHF_3 \rightarrow CHF_2^+ + HF + CF_2 \tag{3.2}$$

These ionization processes produce reactive species such as F atoms, CF_2 radicals and CHF_2^+ ions, which react with the nitride when adsorbing on the nitride surface.

In the case of F atoms, the reaction proceeds according to the similar consecutive processes as oxide etching [3.14]. The reaction takes place spontaneously but is enhanced by energetic ion bombardment [3.16]. High-energy ion bombardment is required to induce the reaction with CF_2 or CHF_2^+. A coordinatively unsaturated nitrogen site, occurring naturally or created through the process of Si removal with F atoms may be the site of CF_2 attack. In the case of CHF_2^+ ions, the following reaction takes place [3.17]:

$$2Si_3N_4 + 6CHF_2^+ \rightarrow 6SiF_2 + 6CN + N_2 + 3H_2 \quad (3.3)$$

In addition to the reactions described above, a surface polymerization process takes place at the same time due to the reaction between the polymer-forming radicals [3.4]:

$$CF_2 + CF_2 \rightarrow C_2F_4 \quad (3.4)$$

$$C_2F_4 + CF_2 \rightarrow C_3F_6 \quad (3.5)$$

$$C_3F_6 + CF_2 \rightarrow C_4F_8 \quad (3.6)$$

This surface polymerization tends to retard the reaction by keeping the reactive species from making contact with the substrate surface. However, with the help of energetic ion bombardment, part of the nitrogen atoms in the nitride (or oxygen atoms in the oxide) will react with the polymer-forming radicals and form volatile products, reducing the polymer film thickness and ensuring the etching to proceed. Because oxygen atoms are more reactive than nitrogen atoms [3.17] and therefore thinner polymer film is present on oxide surface than on nitride surface, the etch rate of oxide in a pure CHF_3 plasma is higher than that of nitride, as indicated in Fig. 3.2. However, surface polymerization takes place significantly on a silicon surface, resulting in a low silicon etch rate and thus in a high selectivity of the nitride (or oxide) etching over polysilicon. The formation of polymer layer on polysilicon surface is confirmed in the polysilicon/polysilicon contact test described later in this chapter.

From above description of the etching mechanism, it is clear that energetic ion bombardment plays a key role in enhancing and/or inducing the nitride reactions as well as in preventing surface polymerization. This argument is supported by the results in Fig. 3.3 and Fig. 3.4, showing that with either higher power or lower pressure the etch rate for the nitride is increased. Higher power produces higher potential difference between the plasma and substrate and lower pressure results in a longer mean free path of ions. As a result, the kinetic energy of ions which bombard the substrate surface increases.

b. Role of N_2 addition

One of the straightforward effects of N_2 addition is the dilution. It has been pointed out that N_2 plays a very minor chemical role in fluorocarbon plasmas and can be thought

of as essentially a diluent gas [3.18]. On the one hand, the dilution lowers the concentration of polymer-forming radicals and, therefore, reduces the thickness of the etch-retarding polymer film and enhances the etch rate. On the other hand, if the dilution is so high that the concentration of the reactive species is significantly reduced, the etch rate will be reduced. The effect of dilution is obvious for the oxide etching results shown in Fig. 3.2, in which the etch rate increases at first with the N_2 content up to 45% and then drops significantly. However, the dilution effect alone cannot account for the dramatic increase of the nitride etch rate with the N_2 content since the peak etch rate for the nitride corresponds to the much higher N_2 content (85%) compared to the peak for the oxide. Note at this N_2 content, CHF_3 content is only 15%. Note also that dilution of CHF_3 by adding the inert He gas results in only a moderate increase of the nitride etch rate, as indicated in Fig. 3.5.

It is inferred, therefore, that there might be some additional mechanisms responsible for the rapid increase of nitride etch rate with N_2 content. Note, that apart from the surface polymerization, another rate-limiting process during the nitride etching is the desorption of N atoms adsorbed on the surface, which are left as a result of reaction of silicon with, for example, F atoms and subsequent SiF_2 desorption [3.14]. Silicon nitride obtained by CVD process is generally a polymorphous crystalline compound. At deposition temperatures below 1150°C, which is the case with the LPCVD process used, the nitride exhibits the stable α crystal modification related to hexagonal structures of the phenacite type, as shown in Fig. 3.7 [3.19]. The distance between the N atoms in the α modification nitride ranges between 2.7 and 3 Å, which is larger than that in a N_2 molecule (a N-N single bond distance, which is in the order of 1.5 Å). In the case of the low-stress nitride, which is silicon-rich, the N atom distance is even larger than in the stoichiometric Si_3N_4. Therefore the N atoms left on the nitride surface during the etching are not likely to spontaneously combine with the adjacent N atoms to form volatile N_2 molecules. Instead they tend to remain attached to the surface and consequently retarding the reaction.

The formation of a N_2 molecule during the etching can take place only if a surface rearrangement resulting in N_2 evolution is brought out by, for example, energetic ion bombardment [3.14]. The argument that the desorption of nitrogen atoms is rate-limiting is supported by the experimental results shown in Fig. 3.6, where the etch rate of the nitride decreases with increasing NH_3/SiH_2Cl_2 ratio, i.e. with increasing nitrogen composition in the nitride film. Since the residual stress level does not affect the nitride etch rate, it is reasonable to assume that the change in the etch rate in Fig. 3.6 is caused by the change in the film composition (Si/N ratio) rather than the change in the residual stress level, which is another consequence of change in the NH_3/SiH_2Cl_2 ratio. When N_2 is added to the CHF_3, abundant nitrogen atoms are generated by the dissociation

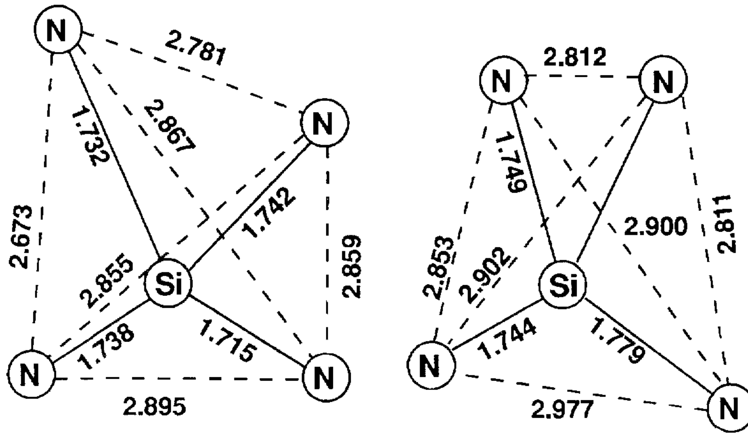

Fig. 3.7 *Unit cell of stoichiometric α-Si_3N_4. The numbers indicate the distance between atoms in Å.*

process:

$$N_2 + e^- \rightarrow 2N + e^- \quad (3.7)$$

The nitrogen atoms can diffuse to the substrate surface and combine with the nitrogen atoms adsorbed there, forming volatile N_2 molecules and therefore making the etching of the nitride faster.

Because of the significant increase of the nitride etch rate with the N_2 content compared to the moderate increase with the He addition, it is suggested that the diffusion and combination of the nitrogen atoms produced by dissociation is also a major factor which enhances the reaction in addition to the dilution effect.

c. Importance of photoresist

It is shown that when the Al or nitride mask is used instead of the photoresist for the nitride etching, the selectivity is reduced due to the increase of the polysilicon etch rate, as indicated in Table 3.1. The result implies that photoresist plays an important role in providing sufficient polymer-forming radicals to form the polymer film on the silicon substrate. Photoresist generally consists of resin which is carbon-hydrogen compound. During the plasma etching, photoresist is also etched by reactive species such as F atoms [3.16]. The carbon-containing reaction products can help the formation of C-F polymer film by providing more precursors in the reaction system.

3.5 Multi-step process design for the etching of polysilicon/silicon nitride/polysilicon sandwich structures

As discussed in the previous section, the etch rate for the nitride increased dramatically with the N_2 addition in CHF_3 and moderately with the He addition, while that of the polysilicon was essentially not changed, resulting in a maximum selectivity of 16 with 42.5 sccm N_2 added to 7.5 sccm CHF_3 (85% N_2 content) at 60 W and 37.5 mTorr. Higher power or lower pressure enhanced the nitride etch rate but did not change the polysilicon etch rate significantly. The nitride etch rate was found to be independent of the mask materials, while that of the polysilicon was reduced when using a resist mask. The etch rate for the nitride consisting of more nitrogen was lower than that consisting of less nitrogen. Intrinsic stress level was found to have little influence on the nitride etch rate within the range measured.

Based on this selective silicon nitride etching process, a two-step process has been designed for the patterning of the upper polysilicon and silicon nitride layers of the sandwich structure shown in Fig. 3.1.

3.5.1 CF_4 + SF_6 + O_2 chemistry for the top polysilicon etching

CF_4/O_2 gas mixtures are frequently used for silicon etching due to their availability, non-toxic nature and relatively well-understood chemistry. Although the etching of silicon in the plasma of these gas mixtures is mainly based on chemical reaction of F atoms, which results in non-directional etching, the chemistries are still quite useful in the etching of polysilicon layer in the sandwich structure, where the polysilicon film is very thin (1400 Å) and, therefore, the underetching does not change the feature size significantly. SF_6 is added to the gas mixture in view of more F-atoms and less C-F polymer-forming radicals with the gas compared to CF_4, to achieve high etch rate.

Fig. 3.8 shows the etch rates of polysilicon and silicon nitride, using gas mixtures of 70 sccm CF_4 + 10 sccm SF_6 with O_2 varied in the range of 0 to 15 sccm. The RF power and gas pressure were fixed at 60 W and 37.5 mTorr, respectively. The etch rates of both polysilicon and nitride increase with oxygen content. The etch rate for the nitride is lower than that for the polysilicon over the applied oxygen content range. The typical non-uniformity of the polysilicon and nitride etching is 6%.

In CF_4- and SF_6-based gas mixtures, such as used in the experiment, F atoms are well

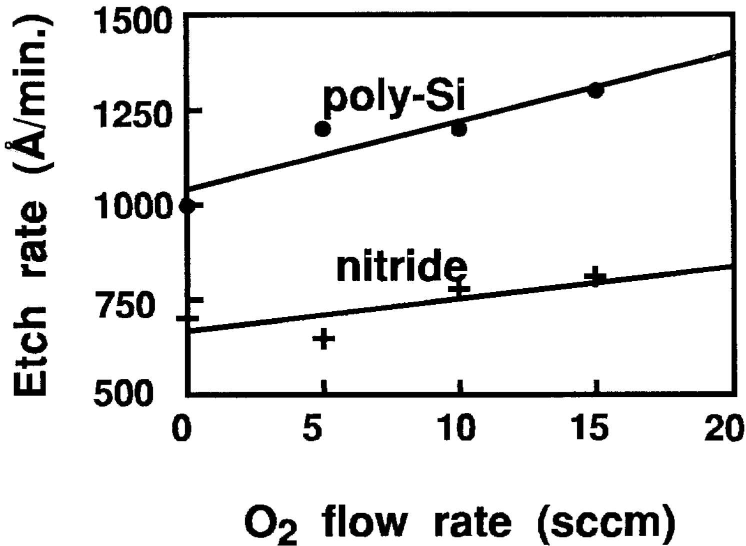

Fig. 3.8 *Poly-Si and SiN etch rates versus O_2 flow rate using CF_4 (70 sccm) + SF_6 (10 sccm) + O_2 plasmas. RF power = 60 W, Pressure = 37.5 mTorr.*

known to be the main reactive species for both silicon nitride and polysilicon [3.20]. The major rate limiting step in the chemistry is the chemical reaction of the F atoms with silicon atoms. The concentration of the F atoms is limited because fluorocarbon radicals in the plasma tend to combine with them. When oxygen is added to the plasma, the concentration of the F atoms increases, because oxygen atoms will react with fluorocarbon species and produce F atoms [3.20], as discussed in Chapter 2. Therefore, both the polysilicon and nitride etch rates increase with oxygen addition in the experiment. Because F atoms are consumed due to the etching, the F concentration in the plasma at the centre of the wafer is lower than that at the outer part of the wafer, leading to a lower etch rate at the central part of the wafer and thus a non-uniformity in the etch rate across the wafer (6% in the experiments). Consequently, overetching is necessary to insure that the film on all of the wafer area is etched.

The higher etch rate for the polysilicon compared to that for the nitride is due to the lower activation energy for the reaction of F atoms with silicon (0.13 eV) than that with silicon nitride (0.18 eV) [3.21]. Therefore, the chemistry provides no selectivity between the nitride and polysilicon etching. If 10 sccm O_2 flow rate is used, the selectivity is 0.7 only. As a result, although the gas mixture can be used for the etching of the top polysilicon layer of the sandwich structure with reasonable uniformity and

high etch rate, it is not suitable for the etching of the nitride layer as well.

3.5.2 Two-step process for the top polysilicon and silicon nitride etching

Selective etching of the nitride over polysilicon can be obtained with the gas mixture of CHF_3 + N_2, as described in Section 3.4. In this chemistry, the reduction of polymer film thickness is one of the major factors determining the nitride etch rate, instead of the F atom concentration. Energetic ion bombardment is essential to induce the polymer removal. Since the size of the electrode of the etcher (20 cm) is much larger than that of the wafer (10 cm), the ion bombardment on the wafer area is expected to be rather uniform. Experimentally, a non-uniformity of 3% in the nitride etch rate has been achieved, which is much better than that using the gas mixture of CF_4 + SF_6 + O_2 (6%).

An optimum RIE process has been designed based on the above experimental results. The top two layers of the sandwich structure were etched using the following two-step process. Firstly the top polysilicon layer was etched with the gas mixture of CF_4 (70 sccm) + SF_6 (10 sccm) + O_2 (10 sccm). Secondly, as soon as the top polysilicon layer was etched completely, the chemistry is changed *in situ* to the gas mixture of CHF_3 (7.5 sccm) + N_2 (42.5 sccm) for the etching of the nitride layer so that high selectivity (16) over the lower polysilicon was obtained. In such a way the top two layers were etched, while the attack of the lower polysilicon layer was minimized. Fig. 3.9 shows SEM photo's of the membrane patterned with the two-step process which is used for the surface micromachined tactile sensor.

It is very important to determine the end point during the etching of the top polysilicon layer, so that the etching can be switched to the second step as soon as the film is etched through. This was achieved by using an EG&G Optical Multichannel Analyzer (OMA), with which optical spectrum of plasma glow can be analyzed. Fig. 3.10 shows the change of the 704 nm signal corresponding to F atoms when the sandwich structure was etched through completely with the gas mixture for the first step. More F atoms are consumed for the etching of the polysilicon than for that of the nitride since the etch rate for the polysilicon is higher than that for the nitride. Therefore, the sharp increase of the signal at the end of the top polysilicon etching is a good indication that the film is etched completely.

After completion of the two-step etching the resist left was sufficiently thick to etch the lower polysilicon layer, if desired. Therefore, a three-step process for etching the total sandwich structure, to define the membrane, is a simple extension of the two-step by repeating the first chemistry for the lower polysilicon layer. Although the entire stack

(a)

(b)

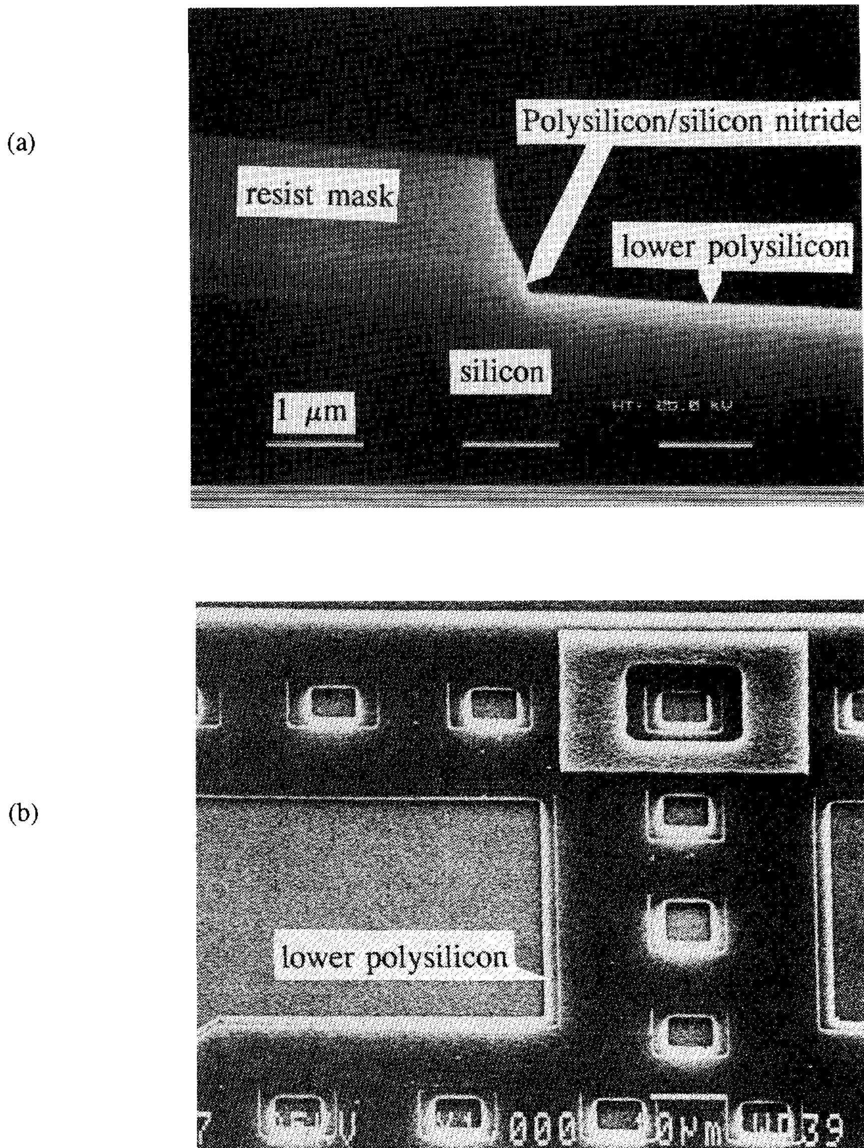

Fig. 3.9 *Poly-Si/SiN/poly-Si membrane for a tactile sensor patterned using the two-step process. (a) cross-sectional view, (b) top view.*

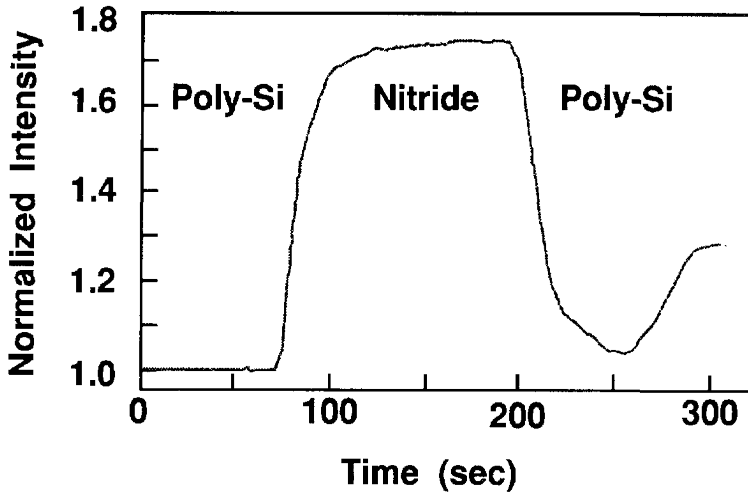

Fig. 3.10 *704 nm signal change during the etching of the sandwich with the gas mixture of 70 sccm CF_4 + 10 sccm SF_6 + 10 sccm O_2. RF power = 60 W, Pressure = 37.5 mTorr.*

could be etched in one step based solely on the $CF_4/SF_6/O_2$ chemistry, as used in the etching of the upper polysilicon layer, significant underetching and non-uniformity would result since the etching basically depends on the chemical reaction of the F atoms with the films.

3.5.3 Analysis of the two-step process

When no end point signal can be detected, the appropriate etching time for a given sandwich structure with the two-step process can be calculated by straightforward analysis of the film thickness and the etch rate as well as uniformity data. Assuming the worst case, i.e. area of the greatest thickness corresponding to the lowest etch rate, the required maximum etch time can be estimated. Using the symbols defined in Table 3.2, the etch time t_1 for the first step must be:

$$t_1 = \frac{T_{1max}}{V_{1min}} = \frac{T_1(1 + U_{T1})}{V_{11}(1-U_{V11})} \tag{3.8}$$

However, at the position of the lowest polysilicon thickness corresponding to the highest etch rate, polysilicon has been etch through at the time of:

Table 3.2 *Definition of symbols and their value for the analysis of the two-step process.*

Symbol	Definition	Value
T_1	Thickness of the upper poly-Si	1400 Å
T_2	Thickness of the nitride	1700 Å
T_3	Thickness of the lower poly-Si	1400 Å
V_{11}	Average etch rate of poly-Si, Step 1	1300 Å/min
V_{21}	Average etch rate of nitride, Step 1	700 Å/min
V_{12}	Average etch rate of poly-Si, Step 2	25 Å/min
V_{22}	Average etch rate of nitride, Step 2	400 Å/min
U_{T1}	Non-uniformity of T_1	5%
U_{T2}	Non-uniformity of T_2	5%
U_{V11}	Non-uniformity of V_{11}	6.5%
U_{V22}	Non-uniformity of V_{22}	3%

$$t_1' = \frac{T_1(1 - U_{T1})}{V_{11}(1 + U_{V11})} \tag{3.9}$$

Afterwards silicon nitride starts to be etched at this position until time t_1. Thus the maximum thickness of the etched nitride film during step 1 is

$$T_{21} = V_{21}(t_1 - t_1') \tag{3.10}$$

assuming a complete uniform etch rate for silicon nitride during step 1.

Similarly, in step 2 the etch time t_2 must be chosen as

$$t_2 = \frac{T_{2max}}{V_{2min}} = \frac{T_2(1 + U_{T2})}{V_{22}(1 - U_{V22})} \tag{3.11}$$

The time when the nitride is etched through with the highest etch rate at the position of the lowest nitride thickness (original minimum nitride thickness due to the non-uniform deposition minus the maximum etched thickness during step 1) is

$$t_2' = \frac{T_2(1 - U_{T2}) - T_{21}}{V_{22}(1 + U_{V22})} \tag{3.12}$$

At this position the lower polysilicon layer starts to be etched until the end of step 2. Thus the maximum thickness of the etched lower polysilicon film during step 2 is

$$T_{32} = V_{12}(t_2 - t_2') \tag{3.13}$$

Substitution of Eq.'s (3.8) - (3.12) into the Eq. (3.13) yields:

$$T_{32} = \frac{1}{S}\left[\frac{T_2(1+U_{T2})}{1-U_{V22}} - \frac{T_2(1-U_{T2}) - V_{21}\left[\frac{T_1(1+U_{T1})}{V_{11}(1-U_{V11})} - \frac{T_1(1-U_{T1})}{V_{11}(1+U_{V11})}\right]}{1+U_{V22}}\right], \tag{3.14}$$

where $S=V_{22}/V_{12}$ is the selectivity of the nitride etching over polysilicon during step two. Therefore, the etched thickness of the lower polysilicon layer is inversely proportional to the etching selectivity in the second step. Using the values defined in Table 3.2, T_{32} can be further expressed as:

$$T_{32} = 440/S \tag{3.15}$$

Since S is about 16 in the second step of the developed two-step process, the attack on the lower polysilicon with such a process will be about 27.5 Å. The etching time needed for the second step as calculated was 4.6 minutes. A 10% overetch is often applied in plasma etching and this will result in an extra 11.5 Å etching of the lower polysilicon layer. Thus the maximum etched thickness of the lower polysilicon layer will be about 38.5 Å, being 2.8% of the total thickness of the lower polysilicon. On the other hand, if the chemistry of the first step only were used (S = 7/13), the etched thickness of the lower polysilicon layer would be about 820 Å, according to Eq. (3.14), even without any further overetching period. This is more than half of the original film thickness, which is obviously not acceptable.

3.6 Problems arising from polymer formation for high selectivity and their solution

In applications such as micromotors [3.22] and tuneable light interferometers [3.2], double polysilicon layer structures with both good mechanical adhesion and electrical contact in-between are required. Often the intermediate layer is an insulating film such as silicon nitride or silicon dioxide. When this layer is patterned with plasma etching, as described in previous sections, a chemistry which produces an etch-inhibiting layer on the surface of the underneath polysilicon layer must be used to obtain high selectivity. Therefore, it is expected that both the etching chemistry and post-processing after etching can have a significant influence on the surface quality of the lower polysilicon layer and, therefore on the mechanical adhesion and electrical contact to the subsequently deposited second polysilicon layer.

3.6.1 Experimental methods

A 1400 Å polysilicon layer, doped and annealed as described in Section 3.3, and a 1700 Å silicon nitride layer were initially deposited. Three different plasma etching chemistries were used to etch the silicon nitride, as described below. Some samples were subjected to an *in situ* oxygen plasma processing after the plasma etching of the nitride layer. Control wafers were wet etched in 20% HF solution. Wafers were dip-etched in buffered HF solution for 30 seconds before the deposition of the second 1400 Å polysilicon layer, doped and annealed as the first polysilicon layer. For comparison, the dip-etching was not performed in a group of control wafers subjected to the same processing sequences. After patterning of the second polysilicon, the sheet resistance of the polysilicon layer and electrical contact resistance between the two polysilicon layers were measured with Van der Pauw test structure and Kelvin test structure [3.23], respectively, using the HP4145B semiconductor parameter analyzer. The mechanical adhesion of the two polysilicon layers was examined by applying mechanical leverage on the second polysilicon and observing the crack formation, using scanning electron microscope (SEM), model Philips SEM525M.

Plasma etching and post-processing were carried out with RF power and the chamber pressure fixed at 60 W and 37.5 mTorr, respectively. The three types of chemistry as well as the post-processing used are summarized in Table 3.3. After the RIE etching, the remaining photoresist was removed in a barrel-type plasma asher (Technics Plasma GmbH Tepla plasma ashing system) using O_2 and Ar gas mixture.

Table 3.3 *Plasma etching conditions and post-processing for three groups of wafers.*

Group	Type	Etching chemistry for the nitride	Post-process after the nitride etching
1	A	CF_4 (70 sccm) + SF_6 (10 sccm) + O_2 (10 sccm) Selectivity 0.7	No
	B		O_2 (50 sccm), 3 min
2	A	CHF_3 (25 sccm) + CF_4 (25 sccm) + He (40 sccm) Selectivity 3	No
	B		O_2 (50 sccm), 3 min
3	A	CHF_3 (7.5 sccm) + N_2 (42.5 sccm) Selectivity 16	No
	B		O_2 (50 sccm), 3 min

3.6.2 Results on contact resistance and polymer film formation

It was found that the contact resistance between the two polysilicon layers was very high ($2 \sim 5 \times 10^6$ Ω on a 4×4 μm^2 window at 100 V voltage) in the wafers without dip-etching before the second polysilicon deposition, irrespective of nitride etching history (wet or plasma etching). The poor electrical contact was most likely to be due to the native oxide layer on the first polysilicon layer. The contact exhibited breakdown characteristics when the applied voltage was above 100 V, after which the contact resistance was reduced to about 200 Ω, which is a further indication that the problem was due to a thin oxide layer. Therefore, dip-etching was essential to obtain a good electrical contact between the two polysilicon layers. Table 3.4 shows the measurement results of the contact resistance between two polysilicon layers via a 4×4 μm^2 hole. These values are averaged measurements over 10 randomly selected dice. Note that the contact resistance measurement for the wafers with dip-etching before the second polysilicon deposition was carried out with 5 V voltage, which is much lower than the voltage value for the same measurement for the wafers without dip-etching.

From Table 3.4 it can be seen that:

1. For groups one and two, there is little difference (less than 6%) in the contact resistance between type A and type B, as defined in Table 3.3. For group three the contact resistance for type A exceeded the measurement range ($> 10^{12}$ Ω) whereas for type B the resistance is slightly higher than that of the groups one and two.

Table 3.4 Measured contact resistance (R_c) between two polysilicon layers

Group		1		2		3		Control
Type		A	B	A	B	A	B	
R_c (Ω)	mean	80	85	89	93	$\sim 10^{12}$	100	89
	standard deviation	3.11	3.19	4.45	1.74		5.55	4.77
	Without dip-etching ($\times 10^6$)	2	4	2	5	2	2	3

2. All the contact resistances for type B of the three groups are essentially the same as that of the control group, although there appears to be a slight increase in contact resistance with increasing etch selectivity.

The value of the contact resistance is a measure of the surface quality of the lower polysilicon layer. Contact resistance depends on the materials forming the contact, doping level and quality of the contact interface. For all the wafers the materials between which contact is made are polysilicon. Although a slight difference in surface doping level may result from the difference in the overetching of the lower polysilicon, the implantation for the upper polysilicon ensures this difference is negligible. Therefore, any difference in the contact resistance indicates a difference in contact interface quality. During the nitride plasma etching, radiation damage caused by high energy ion bombardment and polymer formation on the surface are two major factors, apart from the etching of the underlying polysilicon due to insufficient selectivity, that modify the quality of the contact interface. Since the radiation damage can be removed effectively by high temperature annealing, which is performed after the ion implantation of the upper polysilicon layer, any increase in the contact resistance can safely be assumed to originate from insulating thin film formation on the lower polysilicon surface during the plasma etching.

The above results show that there is no measurable polymer film formation, as far as contact resistance is concerned, for both group one and two. As discussed in Section 3.4, the $CF_4/SF_6/O_2$ etching chemistry for the group one wafers is unlikely to have created any fluorocarbon layer on either nitride or polysilicon surface. Although the reasonably high selectivity (3) indicates that a polymer layer has been formed on the surface of the lower polysilicon layer with the $CHF_3/CF_4/He$ chemistry for the etching

of group two wafers, this polymer layer is probably sufficiently thin or it has been removed during the plasma ashing to remove the remaining photoresist after the nitride etching. Therefore, the contact resistance is basically independent of post-processing since the polymer layer is automatically removed.

The extremely high contact resistance of the type A of group three suggests that significant polymer film is formed on the surface of the polysilicon when the nitride is etched through with the CHF_3/N_2 chemistry. This polymer layer is thick enough to become an insulating layer between the two polysilicon layers. Although the wafers were cleaned after the plasma etching using the barrel-type oxygen plasma asher to remove photoresist followed by cleaning in 100% HNO_3 for 5 minutes and 65% HNO_3 for 15 minutes, the polymer film appears not to have been removed. Further measurements showed that the contact exhibited breakdown characteristics only after the applied voltage was as high as about 50 V. After breakdown and removing the applied voltage, the insulating layer is broken-through and the contact becomes permanently resistive with a contact resistance of about 300 Ω, which is still about two times higher than its counterparts in group one and two. The similar contact resistance of the type B of group three wafers compared to that of the other two groups is an indication that this insulating layer can be effectively removed by post-processing using oxygen plasma maintained in a RIE reactor, in which a self-bias of 300 V was produced.

The fact that polymer film could not be removed in the barrel-type reactor, in which no ion bombardment takes place, suggests that high-energy ion bombardment plays a very important role in the reaction of the oxygen atoms with the carbon in the polymer film. Volatile carbon oxide would be formed, thus removing the polymer film from the polysilicon surface.

3.6.3 Results on mechanical adhesion

The two polysilicon layers exhibit good mechanical adhesion irrespective of etching chemistry applied for the nitride etching. Good mechanical adhesion is an obvious requirement for stable electrical contact. Since groups one, two and type B of three yield good electrical contact characteristics, no problems with the mechanical adhesion between the two polysilicon layers were expected. Indeed, the double polysilicon structure was examined for its mechanical adhesion under SEM. Firstly the nitride between the two polysilicon layers in the area other than the contact windows was removed by etching in 20% HF. The resulting gap between the two polysilicon layers was subjected to mechanical leverage. Both optical and SEM observation showed that no cracking had taken place at the interlayer contact due to the mechanical leverage, indicating that all the wafers had good mechanical adhesion between the two polysilicon

layers. Experiments demonstrated, surprisingly, that type A of the group three, with polymer film between the two polysilicon layer, also showed a good mechanical adhesion. Fig. 3.11 (a) shows the cross-sectional view of the double polysilicon structure for type A of group three wafers directly after the nitride has been removed by wet etching. Fig. 3.11 (b) shows the same structure after mechanical leverage has been carried out. It can be seen in Fig. 3.11 (b) that the upper polysilicon layer remains fixed to the lower one in the contact area despite the breaking-off of the overhanging part of the upper polysilicon by mechanical leverage.

3.7 Conclusions

Polysilicon/silicon nitride/polysilicon sandwich structures are important as structural layers for surface micromachined sensors. A multi-step RIE process is designed for patterning of the sandwiches for surface micromachined tactile image sensors. In the first step the top polysilicon layer is etched using a gas mixture of 70 sccm CF_4 + 10 sccm SF_6 + 10 sccm O_2. In the second step a gas mixture of 7.5 sccm CHF_3 with 42.5 sccm N_2 addition is applied to etch the nitride layer, which provides high selectivity over lower polysilicon. Improved uniformity is achieved in the nitride etching with the CHF_3-based chemistry (3%) than with the CF_4-based (6%), although the nitride could also be etched with the latter. Therefore, the top two layers of the sandwich structure are etched with good uniformity, while the integrity of the lower polysilicon layer is maintained with the two-step process. The three layers can be etched with the same resist mask, if desired, by repeating the first chemistry.

Surface quality of the lower polysilicon of the sandwich after plasma etching of the nitride layer is investigated. it is concluded:

1. No polymer film is formed on the surface of the lower polysilicon layer when the nitride layer on top is etched through with the $CF_4/SF_6/O_2$ chemistry.

2. Although some polymer film is formed with the $CHF_3/CF_4/He$ chemistry, the film is sufficiently thin or has been removed readily during the subsequent plasma ashing of the photoresist, so that the contact resistance is not significantly affected.

3. There is significant polymer film deposition on the lower polysilicon layer with the CHF_3/N_2 chemistry and the film is thick enough to actually insulate the two polysilicon layers. This polymer film could be effectively removed by using the *in situ* oxygen plasma post-processing, in which high energy ion bombardment plays a very important role.

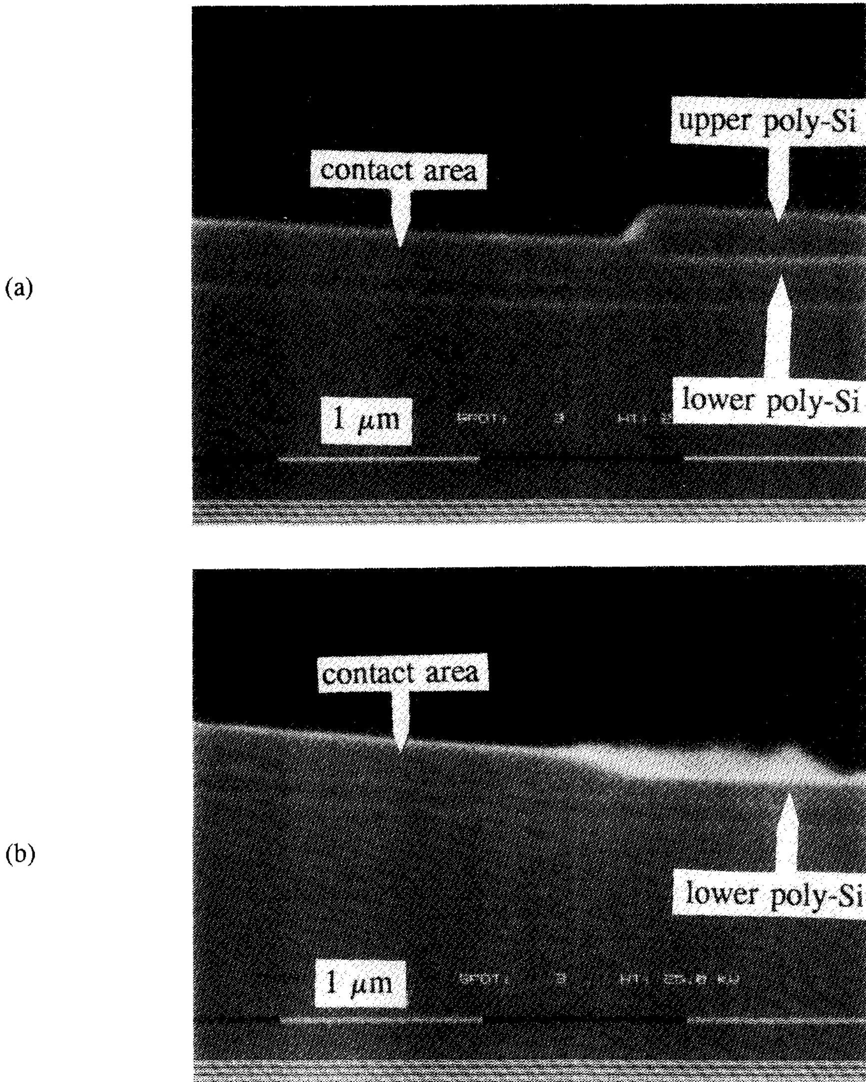

Fig. 3.11 *SEM photographs of cross-sectional views of the double poly-Si structure for the type A of wafer group three: (a) after the nitride between the two poly-Si layers has been removed by lateral underetching using 20% HF, and (b) after mechanical leverage has been applied to the resulting overhanging section. The contact windows between the two poly-Si layers was previously etched using the selective 7.5 sccm CHF_3 + 42.5 sccm N_2 plasma without post-processing.*

References

[3.1] M. R. Wolffenbuttel, Y. X. Li, D. Poenar, P. J. French, P. P. L. Regtien and R. F. Wolffenbuttel, "Multilayer membranes for a tactile image sensor, using surface micromachining and RIE," in *the Proc. 7th Intern. Conf. Solid-State Sensors and Actuators (Transducer'93)*, 1993, pp. 284-287.

[3.2] K. Aratani, P. J. French, P. M. Sarro, D. Poenar, R. F. Wolffenbuttel and S. Middelhoek, "Surface micromachined tuneable interferometer array," *Sensors and Actuators,* Vol. A43, 1994, pp. 17-23.

[3.3] H. L. Chau and K. D. Wise, "Scaling limits in batch-fabricated silicon pressure sensors," *IEEE Trans. Electron Devices*, Vol. ED-34, pp 850-858, 1987.

[3.4] T. C. Mele, J. Nulman and J. P. Krusius, "Selective and anisotropic reactive ion etch of LPCVD silicon nitride with CHF_3 based gases," *J. Vac. Sci. Technol.,* Vol. B2, pp. 684-687, 1984.

[3.5] T. Kure, Y. Kawamoto, N. Hashimoto and T. Takaichi, "VLSI device fabrication using a unique, high-selective Si_3N_4 dry etching," in *the Technical Digest of 1983 Intern. Electron Device Meeting (IEDM 1983)*, pp. 757-759.

[3.6] H. W. Lehmann and R. Widmer, "Profile control by reactive sputter etching," *J. Vac. Sci. Technol.*, Vol. 15, pp. 319-326, 1978.

[3.7] J. L. Linstrom, G. S. Oehrlein and W. A. Lanford, "RIE of silicon nitride deposited by different methods in CF_4/H_2 plasmas," *J. Electrochem. Soc.*, Vol. 139, pp. 317-320, 1992.

[3.8] H. Norstrom, R. Buchta, F. Ronovc and P. Wiklund, "RIE of SiO_2 in doped and undoped fluorocarbon plasmas," *Vacuum*, Vol. 32, pp. 737-745, 1982.

[3.9] L. M. Loewenstein, "Selective etching of silicon nitride using remote plasmas of CF_4 and SF_6," *J. Vac. Sci. Technol.,* Vol. A7, pp. 686-690, 1989.

[3.10] H. Boyd and M. S. Tang, "Applications for silicon tetrafluoride in plasma etching," *Solid State Technol.*, Vol. 22 (4), pp. 133-139, 1979.

[3.11] S. Matsuo, "Etching characteristics of various materials by plasma reactive sputter etching," *Jpn. J. Appl. Phys.*, Vol. 17, pp. 235-236, 1978.

[3.12] S. Matsuo, "Selective etching of SiO_2 relative to Si by plasma reactive sputter etching," *J. Vac. Sci. Technol.*, Vol. 17, pp. 587-594, 1980.

[3.13] R. A. H. Heineke, "Control of relative etch rates of SiO_2 and Si in plasma etching," *Solid State Electronics*, Vol. 18, pp. 1146-1147, 1975.

[3.14] P. E. Clarke, D. Field, A. J. Hydes, D. F. Klemperer and M. J. Seakins, "Mass spectrometric studies of plasma etching of silicon nitride," *J. Vac. Sci. Technol.*, Vol. B3, pp. 1614-1619, 1985.

[3.15] P. J. French, R. F. Wolffenbuttel, R. Mallee and P. M. Sarro, "Optimization

of a low stress silicon nitride process for surface micromachining applications," in *the Book of Abstract of EUROSENSORS VIII Conference*, 1994, p. 205.

[3.16] D. L. Flamm, "Introduction to plasma chemistry," in *Plasma Etching - An Introduction*, D. M. Maros and D. L. Flamm eds., Academic Press, Inc., San Diago, U. S. A., Chap. 2, pp. 91-184, 1989.

[3.17] J. Dulak, B. J. Howard and Ch. Steinbruchel, "Etch mechanism in the reactive ion etching of silicon nitride," *J. Vac. Sci. Technol.*, Vol. A9, pp. 775-778, 1991.

[3.18] J. W. Coburn and E. Kay, "Some chemical aspects of the fluorocarbon plasma etching of silicon and its compounds," *Solid State Technol.*, Vol. 22 (4), pp. 117-124, 1979.

[3.19] V. I. Belyi, L. L. Vasilyeva and A. S. Ginovker, "Structure and chemical composition of silicon nitride," in *Silicon Nitride in Electronics*, Elservier Materials Science Monographs 34, Chapter 4.

[3.20] C. J. Mogab, A. C. Adams, and D. L. Flamm, "Plasma etching of Si and SiO_2 - the effect of oxygen additions to CF_4 plasmas," *J. Appl. Phys.*, Vol. 49, pp. 3796-3803, 1978.

[3.21] T. Enomoto, M. Denda, A. Yasuoka, and H. Nakata, "Loading effect and temperature dependence of etch rate in CF_4 plasma," *Jpn. J. Appl. Phys.*, Vol. 18, pp. 155-163, 1979.

[3.22] M. Mehregany, S. D. Senturia, J. H. Lang, and P. Nagarkar, "Micromotor fabrication," *IEEE Trans. Electron Devices,* Vol. ED-39, pp. 2060-2068, 1992.

[3.23] T. C. Shen, G. B. Gao, and H. Morkoc, "Recent developments in ohmic contacts for III-V compound semiconductors," *J. Vac. sci. Technol.*, Vol. B 10, pp. 2113-2132, 1992.

Chapter 4 Applying Plasma Etching for the Planarization of Surface-Micromachined Devices

4.1 Introduction

During the fabrication of micromechanical structures using silicon micromachining, the topography of the substrate is increasingly non-planer. In conventional surface micromachining, phosphosilicate glass (PSG) of 0.5 - 2 μm is often used as the sacrificial layer. Etching of the PSG layer could cause sharp corners of PSG patterns and surface non-planarity.

Dry etching of PSG layer usually results in anisotropic profile and therefore steep sidewalls and sharp corners of PSG patterns. Although a quarter-circle profile results in priciple if wet etching proceeds just to the etching end point, in practice wet etching frequently produces a vertical sidewall profile due to the required overetching. Although LPCVD polysilicon film, which is frequently used as structural layers of surface micromachined devices, usually exhibits good step coverage, the sharp corners of PSG can cause step coverage problems of some other deposited film, such as sputtered aluminium. The steep sidewalls of PSG can result in undesired residuals of the subsequently deposited structural layer along the sidewalls (usually called filament) during anisotropic plasma etching of the layer. The edge sharpness can also cause local stress concentration and therefore degrade the mechanical properties of the structure on top of PSG due to an abrupt change in the cross-sectional shape of the structure.

Moreover, the patterning of the PSG layer creates surface non-planarity. The problem is compounded if two sacrificial PSG layers are required for given device application, as shown in Fig. 4.1a. The non-planarity results in complications in subsequent processing associated with lithography, as in the case of modern IC fabrication [4.1]. These difficulties include variations in resolution and line-width in the vicinity of high steps, due to the limited depth of focus of wafer steppers [4.2]. In micromechanics, this surface non-planarity will result in elevated (step-up) beams, which may introduce deviations from the double-clamped beam theory in modelling the beam [4.3]. Placing the lower PSG layer in recesses in the silicon substrate by etching a trench in the bulk silicon followed by a PSG filling, not only greatly improves the surface planarity, but also makes the beam between the two PSG layers genuinely double-clamped, as shown in Fig. 4.1b. Therefore, planarization is important in sensor fabrication, and provides

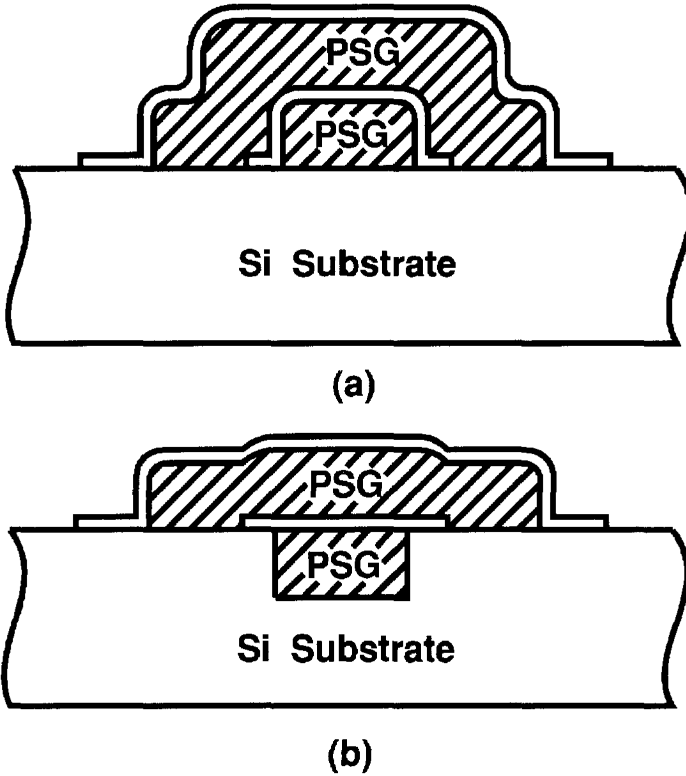

Fig. 4.1 *Multilayer surface micromachining process: (a) conventional and (b) using PSG filled trenches.*

many possibilities for sensor and actuator structuring.

Many techniques for planarizing a substrate surface to be used for IC fabrication have been developed. Basically the techniques can be classified into two groups: local and global planarization. Local planarization techniques can smoothen the sharp corners. However, the surface level across the wafer due to the substrate topography remains essentially unchanged. Therefore, these can be used to improve the step coverage and to eliminate residual filament; but are not applicable to such micromachining applications as filling silicon trenches by PSG. The global planarization, on the other hand, is able to provide a fully planarized substrate surface. It is expected that filling silicon trenches by PSG can be achieved using this approach.

In this chapter two planarization techniques for surface micromachining using plasma etching are developed. Firstly a local planarization technique using PSG spacers based

on an extra PSG layer deposition and subsequent anisotropic plasma etching-back is presented. The effects of cross-sectional shape of PSG steps on the step coverage of both aluminium and polysilicon films are investigated. Secondly a global plasma planarization technique, providing fully planarized PSG filling in large area silicon trenches, is described. This planarization technique involves two-layer-resist coating and plasma etching-back.

4.2 Local planarization technique using PSG spacers

Local PSG planarization techniques include reflow [4.4], laser melting [4.5], plasma etch-back of single-layer resist coating [4.6] as well as oxide spacer approach [4.7]. Reflow of PSG requires high temperature (1000 - 1100°C). Although borophosphosilicate glass (BPSG) reflows at a lower temperature, it suffers from much lower etch rate in HF solutions, which is not desirable in micromachining [4.8]. Laser melting is a method of very low throughput and requires special equipment. Plasma etching-back of single-resist coating usually results in reduced PSG thickness, which is not acceptable in surface micromachining, since the thickness of the sacrificial PSG layer determines the distance between the structural layer and the substrate, and must be accurately controlled in many applications. Some researchers have also proposed to wet-etch or dry-etch the upper part of the PSG layer isotropically before a subsequent anisotropic dry etching, to round-off the edges of the step, as shown in Fig. 4.2a [4.9]. However, the interface between the PSG surface and the isotropic etching profile is still sharp with an angle of about 90°. To solve this problem, a pre-treatment has been applied, which used Ar^+ implantation to damage the surface of the PSG layer, enhancing the etch rate of the PSG there during wet etching and therefore making the edge of the step less sharp [4.10]. However, since this method is based on wet etching, it is not useful when small feature sizes are desired.

Yao and his co-workers introduced a method using plasma deposited oxide spacers along the vertical sidewalls of aluminium interconnections to obtain local planarization, as shown in Fig. 4.2b [4.7]. This method is ideal for surface micromachining planarization in which high temperature processing and wet etching as well as any reduction of PSG thickness should be avoided. Therefore, a technique based on the spacer method by depositing an extra PSG layer on the patterned sacrificial PSG layer and anisotropic plasma etching-back has been developed. The resulting cross-sectional shape of the PSG steps is round, making possible an excellent step coverage on high PSG steps and releasing the problem associated with the filament formation of structural films. Gas composition of the etching chemistry for the PSG spacer formation has been optimized. The relevant criteria used for the selection of the thickness of the extra PSG

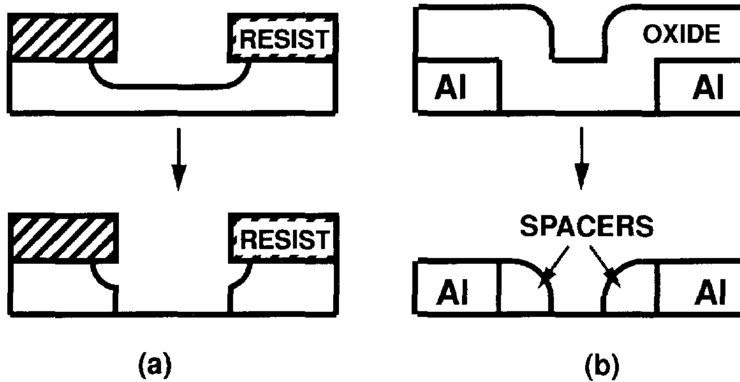

Fig. 4.2 *Schematic process sequence for the improvement of step coverage: (a) the isotropic etching followed by anisotropic etching technique and (b) the oxide spacer technique.*

layer are discussed.

4.2.1 Experimental details

A 2 μm PSG layer (with about 8% wt. phosphorus) was deposited on 4'' (100) silicon substrates, using LPCVD based on a SiH_4, O_2 and PH_3 reaction. Althogh pratically silicon nitride overall coating is present underneath the PSG, the silicon substrate was found to be appropriate for the development of PSG plasma etching chemistry. An anneal at 850°C for 30 minutes in N_2 atmosphere was performed to densify the PSG. Subsequently, the layer was patterned using different methods as shown in Table 4.1. The PSG layer on Group 1 through 3 wafers were first plasma-etched to the end point. Group 2 wafers were subsequently annealed at a temperature of 1050°C for 45 minutes in N_2 atmosphere for PSG to reflow. On the Group 3 wafers another 2 μm PSG layer was deposited and was densified using the same procedure as described for the first PSG layer. Subsequently, the second PSG layer was plasma-etched to form spacers along the sidewalls of the first PSG patterns. Group 4 wafers were first wet-etched in BHF solution to remove half of the film and then plasma-etched to remove the remaining thickness, referring Fig. 4.2a. Finally on all the wafers either a 6000 Å aluminium (with 1% silicon) or a 2000 Å polysilicon layer was deposited by sputtering and LPCVD, respectively. Step coverage of the layers on the PSG steps was examined using SEM.

Plasma etching was carried out in a commercial triode etcher (Drytek 384T), as described in Chapter 2. A 1.3 μm HPR204 photoresist layer was used as the mask. The

Table 4.1 Etching methods for PSG patterning.

	Group 1	Group 2	Group 3	Group 4
Etching method	plasma	plasma	plasma	wet + plasma
Post processing		reflow	spacer formation	

RF power (13.56 MHz), the chamber pressure, the total gas flow rate, the electrode temperature and He pressure for backside cooling were fixed to 300 W, 180 mTorr, 180 sccm, 12°C and 12 Torr, respectively. The gas mixture investigated was CHF_3 + C_2F_6. The end point of the PSG etching was determined using a multichannel optical analyzer, which is integrated in the etcher. For the etching selectivity experiments, either LPCVD silicon nitride or polysilicon film (doped by P^+ implantation of 5×10^{15} cm^{-2} at 80 keV followed by 850°C, 30 min annealing in N_2) was used since they are often present under the sacrificial PSG layer. Etch rate was determined by measuring the change in the film thickness due to the etching using a Leitz-SP optical measurement system.

4.2.2 Results and discussions

a. Optimization of plasma etching process for PSG spacer formation

The main requirements for plasma etching chemistry for PSG spacer formation are anisotropy and selectivity. Initial experiments were performed to characterize plasma etching chemistry of CHF_3 + C_2F_6 in terms the etch rate, selectivity over either the nitride or polysilicon, anisotropy and linewidth loss. The flow rate of C_2F_6 in the gas mixture was varied with a total gas flow rate of 180 sccm.

Fig. 4.3 shows the etch rates of the PSG, silicon nitride, polysilicon and photoresist as a function of C_2F_6 content and Fig. 4.4 shows the selectivities of the PSG etching over the other materials. It can be seen that all the etch rates increase monotonically with C_2F_6 content while all the selectivities are reduced.

The variations in the etch rates and selectivities result from the increased F and decreased fluorocarbon concentration in the plasma at increasing C_2F_6 content. During plasma etching process, the substrate surface is subjected to fluxes of several different reactive species. In fluorocarbon plasmas, such as used in the experiments, the species

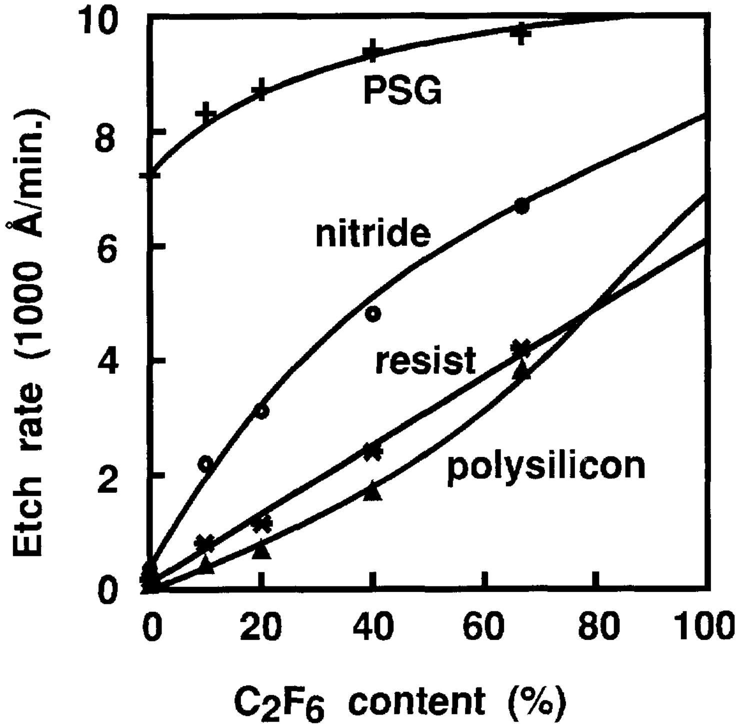

Fig. 4.3 *Etch rate versus C_2F_6 content. RF power = 300 W, pressure = 180 mTorr, total flow rate of CHF_3 + C_2F_6 = 180 sccm.*

striking the substrate surface include F, CF_y (y=0 - 3) and energetic CF_x^+ (x=0 - 3). As described in Chapter 3, unselective and isotropic etching of oxide results if F atoms are the major reactive species, such as in a pure CF_4 or SF_6 plasma. Selective and anisotropic etching of oxide can be achieved if CF_y radicals are dominant to F atoms, such as in pure CHF_3 plasma. In addition to enhance the reaction of CF_y radicals, energetic molecular ions (CF_x^+) can remove a larger number of oxide molecules than noble gas ions like Ar^+ [4.11]. Therefore, the relative concentration of the species in the plasma determines the etching characteristics. With the plasma containing pure CHF_3 in the experiments, the etch rate for the polysilicon is very low compared to that for the PSG, resulting in very high selectivity of about 100. Compared with nitrogen, oxygen is more reactive to the fluorocarbons. This results in a higher etch rate of the PSG than that of the nitride, leading to an etching selectivity of about 20.

When C_2F_6 is added to CHF_3, more F atoms are available for etching. Consequently, all the etch rates increase with the increasing C_2F_6 content as shown in Fig. 4.3. Due

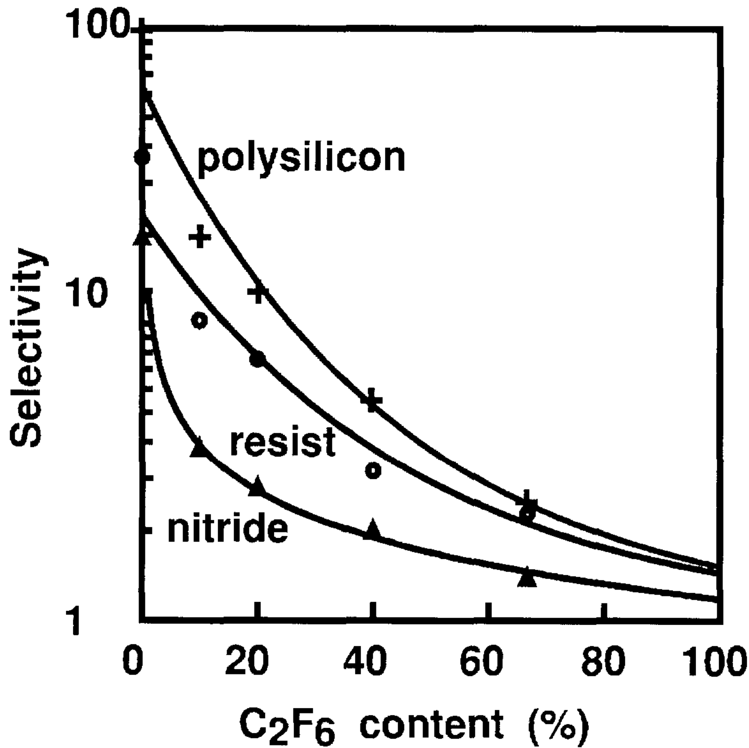

Fig. 4.4 *Selectivity of PSG etching over polysilicon, silicon nitride and resist versus C_2F_6 content. RF power = 300 W, pressure = 180 mTorr, total flow rate of CHF_3 + C_2F_6 = 180 sccm.*

to the recombination of F atoms with the fluorocarbon radicals, the relative concentration of the fluorocarbon radicals is reduced. Thus carbonaceous layer deposited on both the polysilicon and photoresist is thinner. This leads to a rapid increase in the etch rate for these layers and a corresponding decrease in the etching selectivities. Since F atoms react with nitride more easily than with oxide (the activation energy is 4.0 Kcal/mol and 4.2 Kcal/mol, respectively), etch rate for the nitride increases more rapidly at increasing C_2F_6, resulting in a decrease in the etching selectivity.

It was found that all the gas mixtures lead to a highly anisotropic etching profile for PSG. Fig. 4.5 shows the SEM photographs of the cross-sections of the etched 1.5 μm line and spacing with different C_2F_6 contents. The anisotropy found in the etching is the result of energetic ion-induced reaction of the PSG with reactive species, which is dominant in the etching. Although F atoms can etch silicon dioxide spontaneously, the

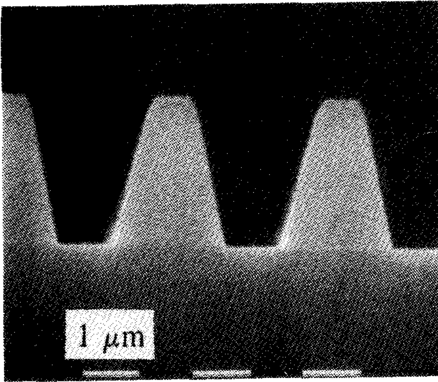

(a)

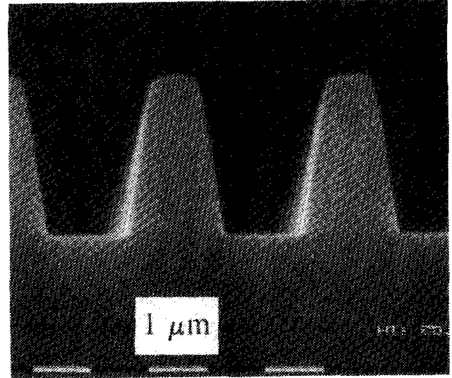

(b)

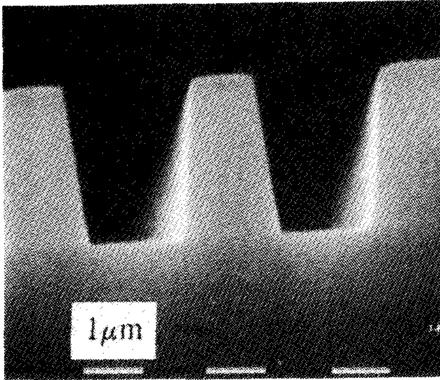

(c)

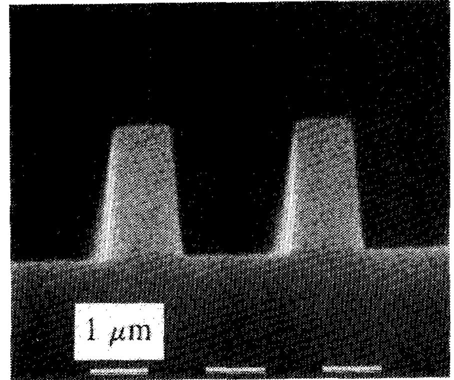

(d)

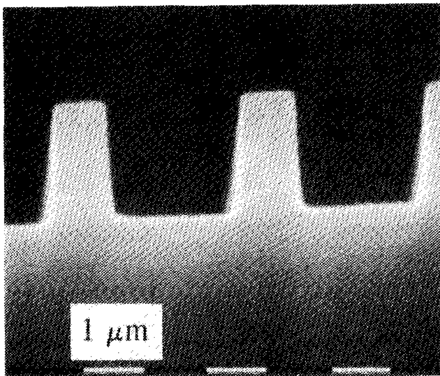

(e)

Fig. 4.5 *SEM photographs of the profile of the PSG steps with C_2F_6 content of (a) 0, (b) 10%, (c) 20%, (d) 40% and (e) 66.7%. Power = 300 W, pressure = 180 mTorr, CHF_3 + C_2F_6 = 180 sccm.*

etch rate based on such a mechanism would be far less than that observed. In fact, the very high etch rate for the oxide in fluorocarbon plasmas can be explained by taking into account also the reaction of the oxide with CF_y radicals induced by the energetic ion bombardment of CF_x^+. Since the ion bombardment is highly directional, the etching proceeds only in the same direction as the incident ions, that is, anisotropy is achieved.

As the C_2F_6 content increases, the angle of the etched profile more and more approaches 90°, while the line-width variation changes from negative (line-width increase) to positive (line-width decrease), as can be seen in Fig. 4.6. The line-width variation is defined as the original nominal line-width of photoresist (1.5 μm) minus the real line-width at the bottom of the line. The line-width variation is the result of the decreased carbonaceous film deposition on the photoresist and increased etching of the photoresist by F atoms with increasing C_2F_6. When the C_2F_6 content is zero, the etch rate for the photoresist is very low since the amount of the F atoms is small and there is much carbonaceous film deposition on the resist. The angle of the PSG profile is only 80° with zero C_2F_6 content. Note that the angle of the original photoresist profile is about 85°. The increase in line-width and reduction in the profile angle are probably due to the deposition of the carbonaceous film on the sidewalls of both the resist and the PSG pattern, which is subjected to less ion bombardment than the planar surface [4.12]. With C_2F_6 added to CHF_3, more F atoms are generated to etch the photoresist, while less fluorocarbon is available for the protection of the surface and sidewalls of the photoresist. As a result, the etch rate for the photoresist is increased. Since the original photoresist profile is not vertical, thinning of the resist results in line-width reduction. This effect, together with the weakening of the sidewall protection, leads to a significant line-width loss at a C_2F_6 content larger than 40%, as indicated in Fig. 4.5 and Fig. 4.6.

The above experimental results clearly indicate that a compromise must be made for the optimized C_2F_6 content so that high etch rate can be achieved with sufficient high selectivity over either the nitride or polysilicon, nearly vertical etching profile and good line-width control. A 10% C_2F_6 content is chosen for the actual PSG etching. With this chemistry, a PSG etch rate of 8300 Å/min is obtained with selectivity of 3.8 over the silicon nitride, which is practically frequently present underneath PSG layer. The selectivities over the polysilicon and resist are 19.7 and 10.3, respectively. The angle of the PSG profile is 82° and line-width variation at the bottom of 1.5 μm lines for 2 μm thick PSG etching is within 1500 Å.

b. Step coverage of the aluminium and polysilicon layer

The step coverage of the 6000 Å Al film on the 4 types of 2 μm PSG steps is examined by SEM and the results are shown in Fig. 4.7. The step formed by anisotropic plasma

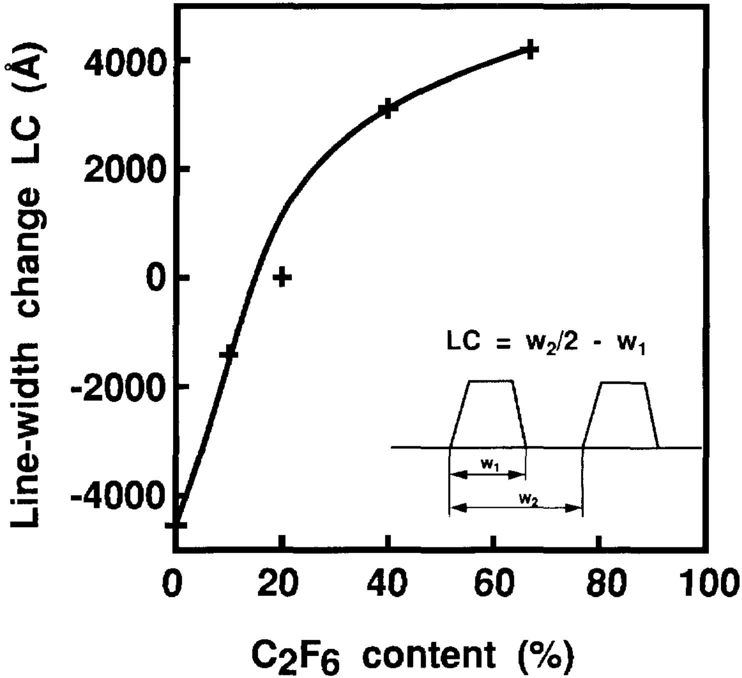

Fig. 4.6 *Line-width change of 1.5 μm line measured with SEM. Negative values mean line-width increase.*

etching results in poor step coverage, as can been seen from the very thin Al film on the sidewall of the PSG step (Fig. 4.7a). Reflow of PSG improves the Al coverage, as is evident from the thicker Al film on the sidewall shown in Fig. 4.7b compared to Fig. 4.7a. Both the PSG spacer method and wet plus plasma etching of the PSG result in good Al coverage on the step, as shown in Fig. 4.7c and Fig. 4.7d.

Fig. 4.8 shows the SEM photographs of the cross-sectional views of 2000 Å polysilicon on PSG steps of 2 μm. It turns out that good coverage of polysilicon can be obtained with each of the etching methods for PSG listed in Table 4.1. This is the result of the very good step coverage properties of the LPCVD polysilicon process. It can be seen that the PSG spacer method produces a round corner of the PSG step and consequently a gradual transition of the polysilicon coverage. Reflow of the PSG can also produce a less sharp corner of the PSG steps than without reflow. On the other hand, the anisotropic plasma etching of PSG leads to a very sharp corner of the PSG step, making an abrupt transition of the polysilicon coverage. Similar sharp corners are found in the case where the PSG was wet etched first, followed by anisotropic plasma etching.

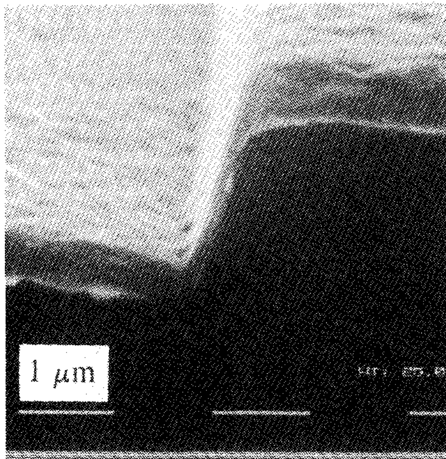

(a)

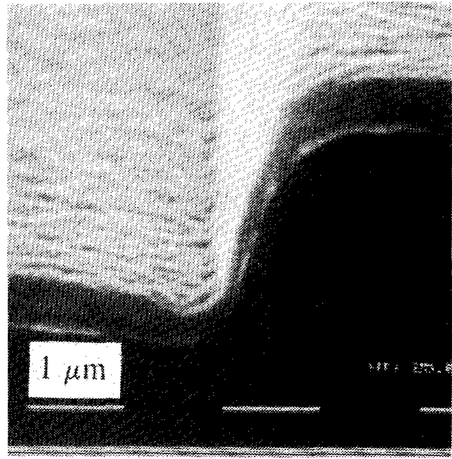

(b)

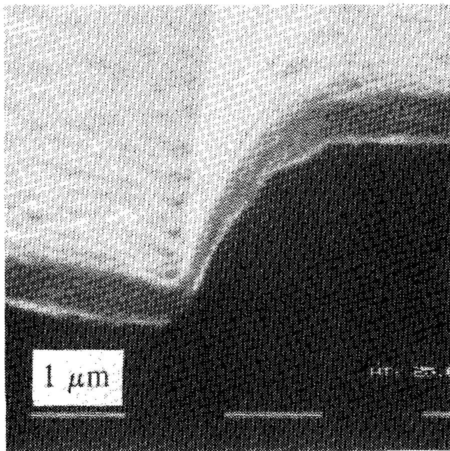

(c)

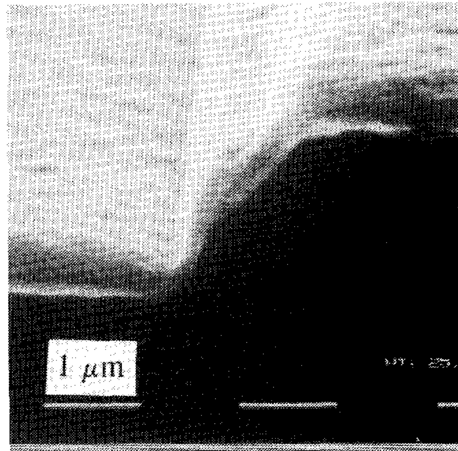

(d)

Fig. 4.7 *SEM photographs of the sputtered aluminium coverage on the steps of (a) wafer group one with plasma etching only, (b) group two with PSG reflow, (c) group three with the PSG sidewall, and (d) group four with wet etching followed by plasma etching.*

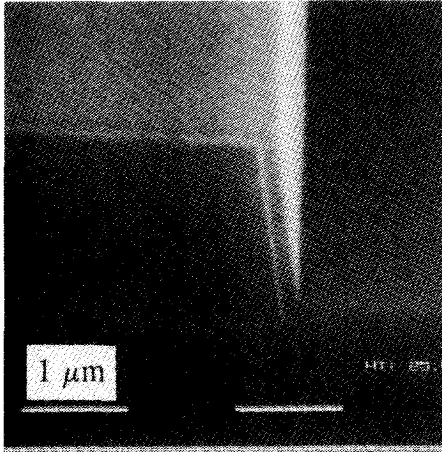

(a)

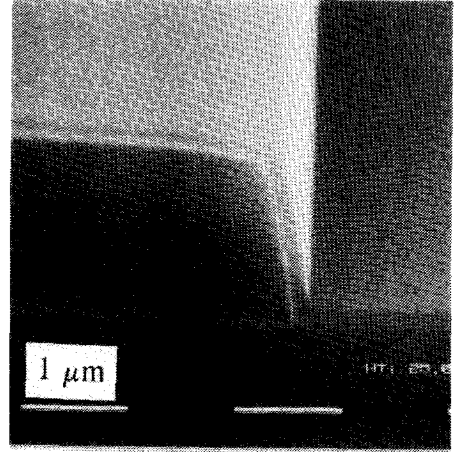

(b)

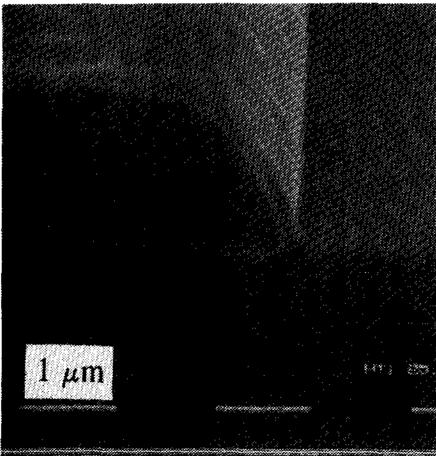

(c)

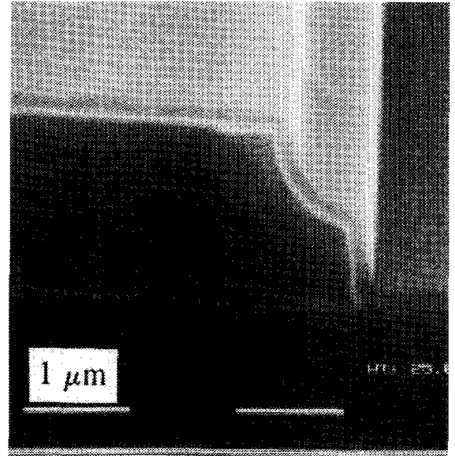

(d)

Fig. 4.8 *SEM photographs of the LPCVD polysilicon coverage on the steps of (a) wafer group one with plasma etching only, (b) group two with PSG reflow, (c) group three with the PSG sidewall and (d) group four with wet etching followed by plasma etching.*

4.2.3 Selection of the extra PSG layer thickness

The thickness of the extra PSG layer will determine the width of the PSG spacer and, therefore, the degree of roundness of PSG corners. As shown in Fig. 4.9, suppose the deposition of the PSG layer is completely conformal (i.e. the deposition rate is identical along all directions) and etching-back proceeds only in the vertical direction, the thickness of the PSG spacer after etch-back which is stopped just at the end point is

$$T = t(1 - \cos\alpha), \tag{4.1}$$

where t is the thickness of the extra PSG layer and α is the angle of the original PSG steps. In the experiments, t is 2 μm and α is 82° and thus a spacer thickness of about 1.7 μm results, according to Eq. (4.1). SEM observation reveals that the thickness calculated with the simple model is in good agreement with the actual etching result. Therefore, the required thickness of the extra PSG layer can be determined easily using Eq. (4.1) as a function of desired spacer thickness.

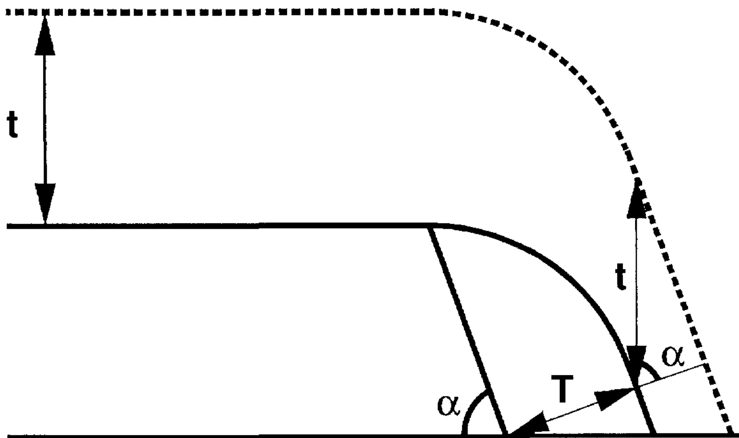

Fig. 4.9 *Model for the calculation of the remaining thickness of the PSG spacer.*

4.2.4 Application of the spacer technique in IC technology

The PSG spacer method can be applied not only in improving step coverage of micromechanical structures, but also in achieving good coverage of metallization such as aluminium on PSG steps in conventional silicon integrated circuit technology. With this method, the high temperature treatment necessary for the reflow of PSG can be eliminated, relieving problems such as extra junction diffusion and, therefore, punchthrough in short channel MOS transistors. Furthermore, the method provides a solution of producing windows with the size smaller than obtainable with the available lithography ability. This can be realized as shown in Fig. 4.2b. After the formation of windows using normal lithographic and plasma etching techniques, PSG (or other dielectric materials, such as silicon nitride) spacers are formed along the sidewalls of the window, making the opening smaller. The final size of the window can be easily adjusted by choosing the thickness of the extra PSG layer, using Eq. (4.1). This method is very useful when extremely small openings are desired for certain applications, such as in very high cut-off frequency bipolar transistors where emitter width should be as small as 0.5 μm [4.13].

4.3 Filling silicon trench by PSG using two-layer resist coating and plasma etching-back

Althogh the PSG spacer technique relieves the step coverage problem, the difference between global surface topography remains the same. Reduction of the difference requires global planarization techniques, such as chemical mechanical polishing (CMP) and plasma planarization, which provide possibilities of a completely planarized surface across the wafer. CMP has emerged recently as a new method of achieving globle planarization for submicron VLSI applications [4.14-4.15]. However, this method suffers from difficulties in planarity control (feature size dependency, hollow formation in wide features, over-polishing of large array areas and residual contaminations). In plasma planarization [4.6], a low viscosity sacrificial layer (usually photoresist or polyamide) is used to coat the uneven substrate surface to obtain a practically flat surface. Subsequently, plasma etching is used to etch-back the sacrificial coating layer, during which the etch rate of substrate and sacrificial layer should be equal, to form a planar surface after the etching. Filling silicon trenches by PSG has been achieved using this approach.

4.3.1 Single-layer photoresist coating using HPR204 resist

It has been reported that HPR204 photoresist provides good surface planarization

performance because of its superior spin-on planarization properties and its flow at a relatively low temperature (~150°C) [4.16-4.17]. However, the effectiveness of such a single photoresist coating in planarization is feature-size dependent. Small and/or periodic features are planarized to a larger degree than larger and/or isolated features. Table 4.2 shows the measured step height of a wide (150 μm) isolated trench and those of 50 and 20 μm periodic line-and-space patterns with 2 μm HPR204 coating on 2 μm deep trenches. The step height measured after the resist has been subjected to a 250°C, 30 minutes thermal cure is also shown.

It can be seen that with the 2 μm resist coating, the step height of the isolated trench remains the same as the original trench depth in the substrate, while that of the periodic line-and-space trenches is reduced, depending on the feature size. After the thermal cure, the step height of the isolated line remains basically unchanged, while that of the periodic patterns is increased. This is probably due to more shrinkage of the thicker resist (on the space area) than the thinner resist (on the line area). Increasing the thickness of the resist to 4 μm by spinning-on additional 2 μm HPR204 does not change the step height of the isolated line, although that of the periodic line-and-space is significantly reduced, as indicated in Table 4.2.

These results are in agreement with previously reported observations [4.6][4.16][4.18-4.19]. Usually the second coating mixes or dissolves a portion of the initial coating, which increases the viscosity and the relative solid component of the polymer solution at the interface between the coatings. This change in solution properties could adversely affect the spin-on planarization properties of the subsequent coating. Since in sensor applications the pattern is often large (tens of microns or more) and usually with large separation, single-layer HPR204 resist coating up to 4 μm together with thermal cure is insufficient to provide a completely planarized surface.

4.3.2 Two-layer resist coating technique

To obtain a near flat surface coating, it is desirable to fill the trenches first. This has been achieved by a two-resist-layer planarization scheme proposed by Schiltz *et al.* [4.20] and applied for VLSI fabrication [4.21-4.22]. However, these studies used the same resist for the first coating as for the trench patterning. An additional mask, which is the negative of the mask used to realize the original pattern, has to be used to expose the first resist layer. This drawback has been overcome by the following new planarization process using image reversal photoresist shown in Fig. 4.10. Firstly a PSG layer is deposited with a thickness the same as the depth of the trenches (a). An AZ5214 image reversal photoresist layer is then spun-on (b) and patterned through

Table 4.2 Step height (μm) of original approximately 2 μm trenches with single HPR204 resist coating.

Test patterns	Step height		
	After 2 μm resist coating	After 250 °C, 15 min thermal cure	After second 2 μm resist coating
150 μm isolated line	2.1	2.1	2.1
50 μm periodic line-and-space	1.2	1.5	0.7
20 μm periodic line-and-space	0.7	1.1	0.4

image-reversal using the same mask as that for the trench etching of the silicon substrate (c). Then the photoresist is thermally cured (d), and a 1.3 μm HPR204 photoresist layer is applied (e). After baking to remove the solvent in the upper photoresist, the surface of the wafer is etched-back to leave a PSG filled trench (f).

The application of image reversal resist in the proposed process eliminates the requirement for the extra mask. If the AZ5214 resist is processed in a normal processing sequence, i.e. coat, soft bake, expose, develop and hard bake, a normal positive image is obtained. If, on the other hand, a post-exposure bake sequence is added, the tonal quality of this resist reverses from a positive to a negative one at a post-exposure bake temperature of 90°C. The inversion process seems to be best explained by a cross-linking mechanism [4.23]. Upon exposure, the photoactive compound generates an acidic compound. Following the relatively high temperature post-exposure bake, this acid diffuses through the resin system of the film and causes acid catalyzed cross-linking. Therefore, the exposed area becomes insoluble in the developer. A flood exposure is used to make the unexposed area soluble in the developer. As a result, the final resist pattern after the development is complementary of the silicon trench, i.e. photoresist is left at the trench areas, resulting in filling of the trench.

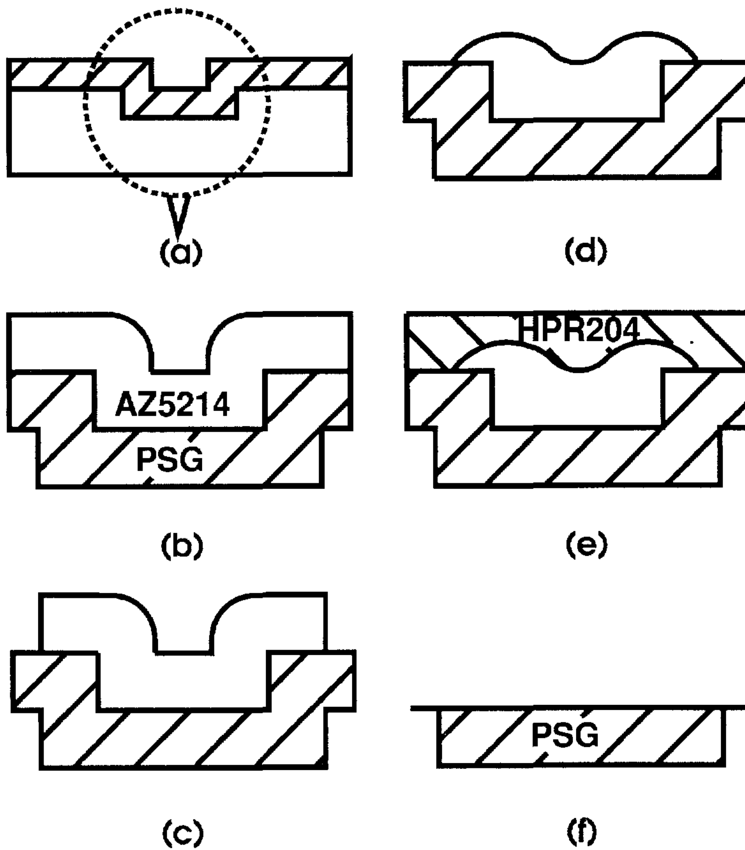

Fig. 4.10 *Processing steps of the planarization technique. (a) PSG deposition, (b) AZ5214 image reversal resist coating, (c) resist patterning, (d) thermal cure, (e) HPR204 resist coating and (f) plasma etching back.*

a. Coating and patterning of AZ5214 resist

The thickness of the image reversal resist must be the same as the depth of the silicon trench to obtain optimum trench filling, and the line-width control of the resist is also important. These two properties are determined by the spin-on speed, exposure energy of the stepper and duration of flood exposure. The spin-on speed is the most important factor to determine the resist thickness. Fig. 4.11 shows the measured thickness of AZ5214 resist versus spin-on speed, which is in good agreement with the theoretical model of the inversely proportional relation between the thickness and the square root of the spinning speed [4.24].

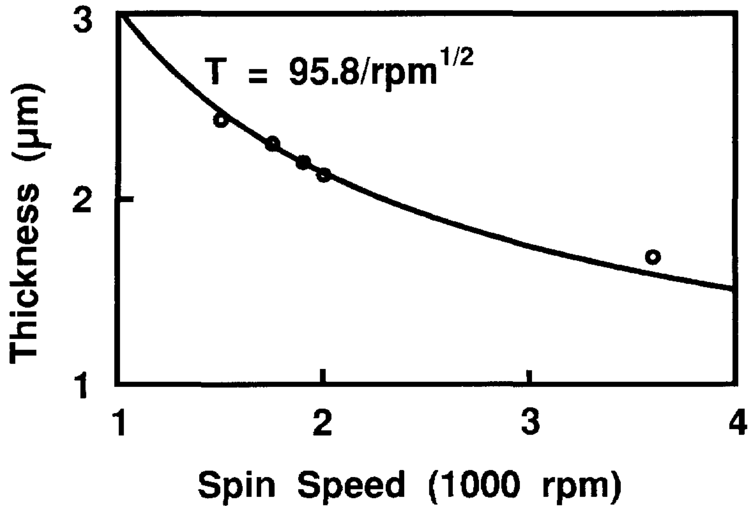

Fig. 4.11 *Dependence of AZ5214 thickness on the spin-on speed.*

Exposure energy of the stepper and the time needed for the flood exposure are essential for the feature size control and are determined according to the requirement of feature size. High exposure energy of the stepper and short flood exposure time tend to increase the feature size. To compensate for the misalignment of the stepper, a slightly larger resist feature size than the trench is desirable. This is achieved by using the optimized exposure energy of the stepper and flood exposure time of 80 mJ/cm^2 and 10 seconds (with an energy density of 10 mJ/cm^2 and a wavelength range of 3650 - 4630 Å), respectively. Fig. 4.12 shows the SEM photograph of 2 μm AZ5214 resist filling on 2 μm trench. It can be seen that at the edge of the trench, the resist is about half micron thicker than in the centre of the trench due to an abrupt change of the surface topography in the substrate.

b. Thermal curing of AZ5214 resist

After developing, the image reversal resist is thermally cured. Such a thermal cure is necessary for three main reasons:

1. to improve planarization by increased thermal flow, so that the resist profile at the edge of the trench (shown in Fig. 4.12) is smoothened;

2. to compensate for misalignment of the resist block with respect to corresponding trench due to limited alignment accuracy of the stepper; and

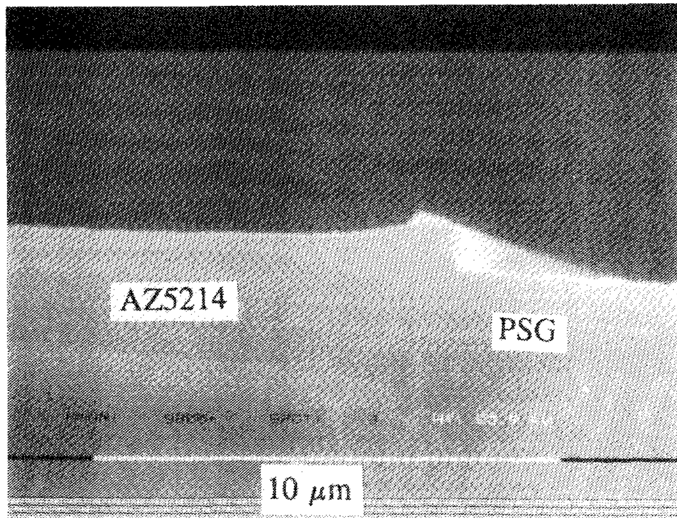

Fig. 4.12 *Filling of 2 μm deep PSG recess by 2 μm AZ5214 image reversal resist using the optimized coating process: spinning speed 2220 rpm, exposure energy of the stepper 80 mJ/cm², flood exposure time 10 seconds. The protruding of the resist at the edge is due to the abrupt change in the substrate topography.*

3. to enhance the cross-linking of the resist to prevent any interface problem associated with dissolving of the lower resist during the coating of the upper resist [4.25].

During the thermal cure, shrinkage of the AZ5214 resist takes place due to the evaporation of the solvent. This effect must be taken into account in the determination of the original thickness of the resist coating. The degree of shrinkage has been examined at a temperature range of 100 - 250°C (Fig. 4.13) for a cure time between 2.5 - 30 minutes (Fig. 4.14). The relative shrinkage in Fig. 4.13 and 4.14 is defined as the ratio of the thickness reduction to the original thickness.

It can be seen from Fig. 4.13 that the shrinkage is strongly dependent on the temperature and from Fig. 4.14 that at 200 and 250°C the shrinkage saturates after 10 and 2.5 minutes, respectively. The optimized curing temperature is experimentally determined by evaluating the reflow of the resist at different temperatures. Fig. 4.15 shows the cross-sectional view of the resist filling at 4 temperatures. It can be seen that basically no reflow has taken place at 100°C and that the reflow at 150°C is not sufficient to smoothen the interface between the resist and the trench. A smooth

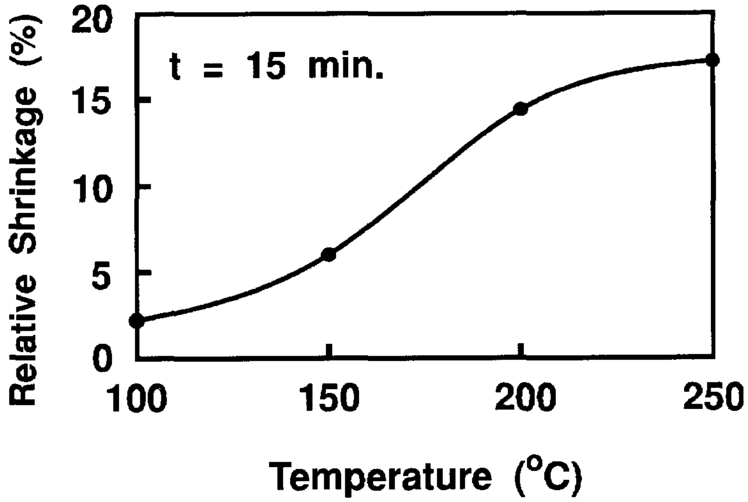

Fig. 4.13 *Relative shrinkage of the AZ5214 resist after thermal cure vers temperature for 15 minute cure time.*

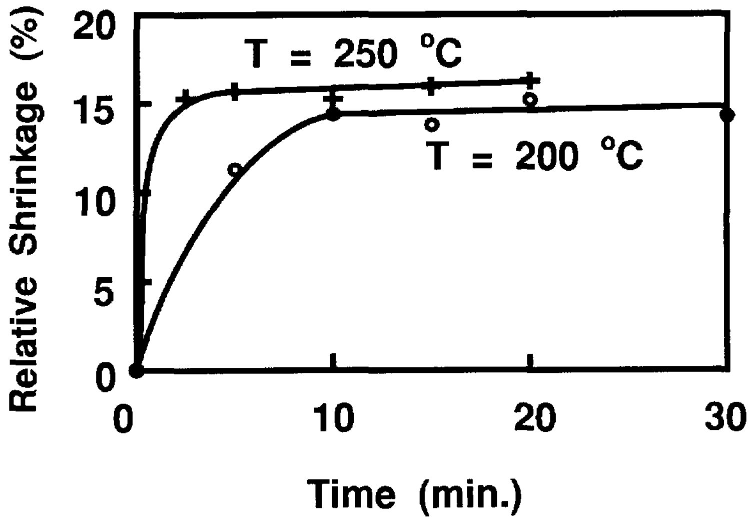

Fig. 4.14 *Relative shrinkage of the AZ5214 resist versus the cure time at 20 and 250°C.*

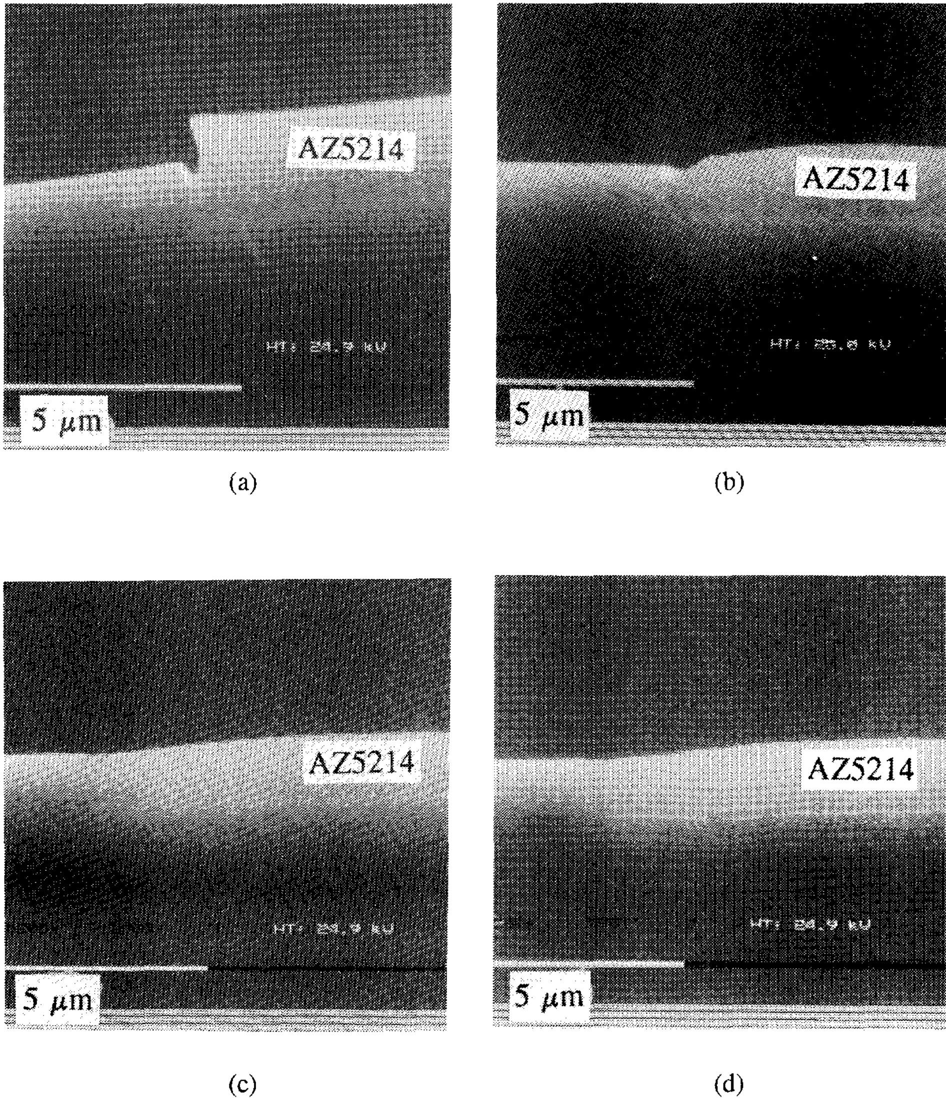

Fig. 4.15 *SEM photographs of the cross-sectional view of the AZ5214 resist filling in trenches subjected to thermal cure at different temperature for 15 minutes, (a) 100°C, without reflow. Note the hollow of the resist due to misalignment. (b) 150°C, insufficient reflow, (c) 200°C and (d) 250°, sufficient reflow.*

interface is obtained at 200°C due to the reflow. It is obvious that the protruding part of the resist at the edge of the trench is completely flattened after the cure. Similar reflow effects are found at 250°C. Therefore, the cure temperature is chosen to be 250°C to ensure a wide process window and sufficient cross-linking [4.26]. A cure time of 15 minutes is used for stable resist thickness. The shrinkage of the resist at this cure condition is about 16%.

A 1.3 μm HPR204 resist coating is applied after the thermal cure for the AZ5214 image reversal resist. This finally leads to a very planar surface, as shown in Fig. 4.16.

4.3.3 Plasma etch-back

The planarized surface profile is transferred to the substrate using plasma etch-back. There are several required properties of etch-back. Firstly, the etch rates for the resist and PSG layer must be equal. Secondly, the etching selectivity over the underlying layer must be high. Thirdly, good uniformity must be achieved during the etching-back, and finally, the surface roughness introduced by the etching-back must be minimized. In other words, any form of redeposition from the plasma to the substrate must be eliminated.

Generally, CF_4-based chemistries can be used for PSG etching and oxygen can be added to the chemistry to adjust the etch rate ratio between the PSG and photoresist [4.6]. However, the selectivity over silicon or silicon nitride is poor because the dominant reactive species in these chemistries are F atoms. A CHF_3-based chemistry, on the other hand, can also be used to etch the PSG. As discussed in the previous section, this type of chemistry usually etches silicon or silicon nitride with a lower etch rate than PSG, thus selective etching can be achieved.

Therefore, the gas mixture of 162 sccm CHF_3 with 18 sccm C_2F_6 addition optimized for PSG spacer formation was chosen for the etching-back experiment. However, the etch rate for PSG with this chemistry is much higher than that for the resist. For this reason, oxygen was used to tailor the etch rate ratio of PSG and resist. Fig. 4.17 shows the dependence of the etch rates of PSG and two types of resist on O_2 addition in the gas mixture. The etch rate for the resists increases linearly because the resist reacts readily with oxygen atoms, and that of PSG decreases linearly with increasing O_2 ratio, mainly because of dillution effects. Note also that the etch rate for AZ5214 is higher than that for HPR204. With 14% O_2 content (25 sccm), the etch rate for the PSG becomes almost the same as that for the AZ5214 resist (about 7300 Å/min). Therefore, this O_2 content was used for the etching-back of the planarized surface. This chemistry results in a selectivity over polysilicon and silicon nitride of about 20 and 4, respectively.

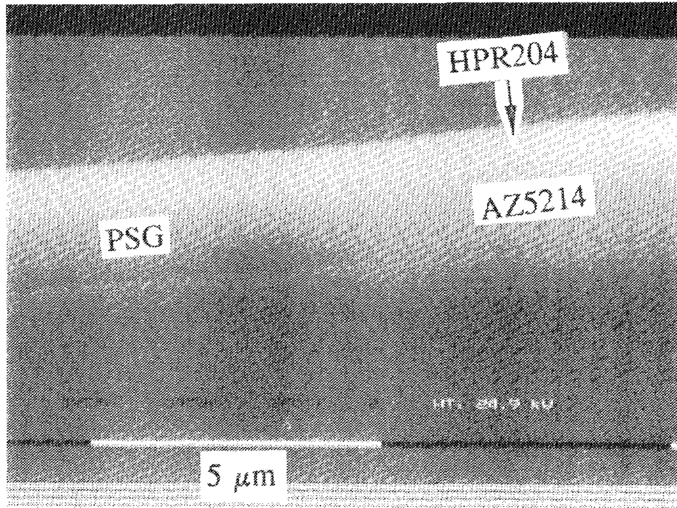

Fig. 4.16 *Cross sectional view of the final planarized surface using the two-layer resist technique.*

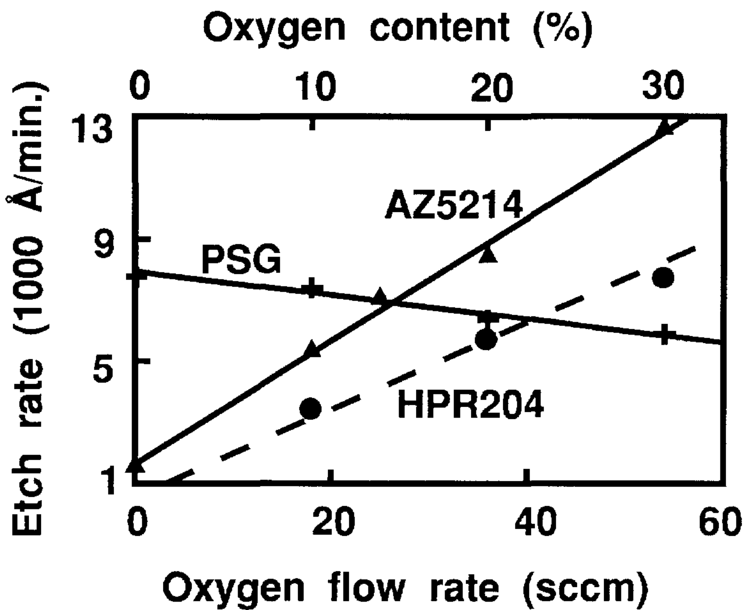

Fig. 4.17 *Etch rate of PSG and resist versus O_2 content in the CHF_3/C_2F_6 chemistry. RF power = 300 W, pressure = 180 mTorr. C_2F_6 = 18 sccm, total flow rate of $CHF_3 + C_2F_6 + O_2$ = 180 sccm.*

4.3.4 Planarization results and feature size limitation

Fig. 4.18 shows the cross-sectional view of PSG filling in the silicon trench after the plasma etching-back. It is clear that planarized PSG filling of the silicon trenches results. The PSG outside the trenches was removed completely and the boundary between the PSG and the trench edge was rather smooth. A concavity in the PSG filling near the trench edge can be seen. This was most probably due to the extra etching of the resist at the interface between the resist and the PSG. During the plasma etching-back, oxygen was released as a result of reaction of reactive radicals with silicon atoms in PSG subjected to energetic ion bombardment. Therefore, the local concentration of oxygen at the interface between the PSG and resist was enhanced, which increased the etch rate of the resist. This argument is supported by the observation that a concavity of the resist appears at the interface during the etching-back, as shown in Fig. 4.19. This concavity leads to a local surface unevenness of about 0.2 μm for a 2 μm deep silicon trench after the planarization. This technique, therefore, represents a considerable improvement in planarity. The global non-uniformity of the planarization is found to be about 6%, i.e. the maximal difference in non-planarity across the substrate surface is about 250 Å.

If the width of the trench in the substrate is less than two times of the trench depth, the PSG at the two opposite trench sidewalls will merge together during the deposition due to the conformal nature of PSG deposition (refer to Fig. 4.10a). Therefore, the approach of using image reversal resist coating and patterning is applicable only when the width of the substrate trench is much larger than the depth of the trench, which is the case in most micromachining applications.

4.4 Conclusions

A method for local planarization and thus improving the coverage of thin deposited structural layers on high PSG steps for micromachining has been developed. Althogh LPCVD polysilicon film usually exhibits excellent step coverage, this technique is very effective in relieving step coverage problem of other deposited films such as sputtered aluminium. The method involves deposition of an extra PSG layer and etching-back anisotropically using plasma. It features in rounded-off corners of PSG steps, thus releasing stress concentration problems caused by sharp PSG corners in conventional surface micromachining. No high temperature treatment or wet etching, and no thickness change in sacrificial layer take place. It was found that a 10% C_2F_6 content in CHF_3 gas is most appropriate for the PSG etching. A simple model has been proposed as a guidance of selection of the extra PSG layer thickness and the calculated

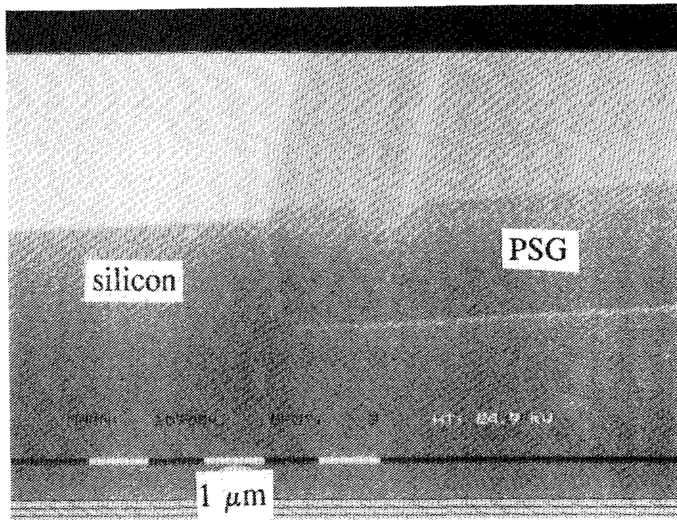

Fig. 4.18 *SEM photograph of 1.85 μm silicon trench filled with PSG using the optimized two-layer resist coating and plasma etching-back. The interface between the PSG and silicon substrate is very smooth. The recess on the PSG surface near the trench edge is caused by enhanced etching of the resist.*

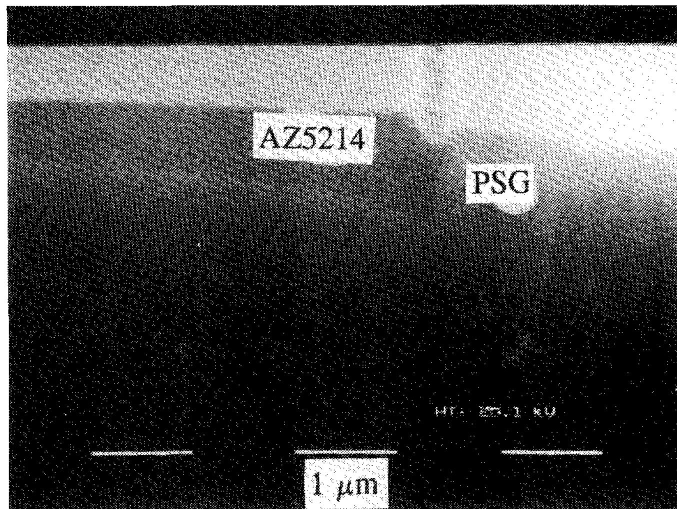

Fig. 4.19 *SEM photograph indicating the enhancement of resist etching (hollow formation) at the interface of the resist and PSG.*

result is in good agreement with experiments. This method can also be applied in IC technology, where high temperature reflow process is not acceptable or when extremely small windows are required.

A global planarization technique for filling PSG in silicon trenches has been developed and tested for 2 μm deep silicon trenches. The technique involves depositing 2 μm PSG layer on the silicon substrate with the trench, planarizing the surface topography using two-layer resist coating and finally, plasma etching-back to transfer the flat surface to the silicon substrate. The application of image reversal photoresist as the first resist coating eliminates the requirement for an extra mask. The technique results in a planarized substrate surface with PSG filled trenches, which is very suitable for sensor applications where wide trenches in the substrate must be planarized, such as in the fabrication of silicon micro-vacuum tubes [4.27].

References

[4.1] A. G. Sabnis, "Multilevel metallization schemes," in *VLSI Electronics - Microstructure Science*, N. G. Einspruch, S. S. Cohen and G. S. Gildenblat, Eds., Vol. 15, Chapter 7, Academic Press, Inc., New York, 1987, pp. 293-343.

[4.2] M. W. Horn, "Antireflection layers and planarization for microlithography," *Solid State Technology*, Vol. 34 (11), pp. 57-62, 1991.

[4.3] Q. Meng, M. Mehregany and R. L. Mullen, "Analytical modelling of step-up supports in surface-micromachined beams," in *The Proc. 7th Int. Conf. Solid-State Sensors and Actuators (Transducer'93)*, 1993, pp. 779-782.

[4.4] W. Kern and R. K. Smeltzer, "Borophosphosilicate glasses for integrated circuits," *Solid State Technology*, Vol. 28 (6), pp. 171-179, 1985.

[4.5] L. Delfino, " Phosphosilicate glass flow over aluminium in integrated circuit devices," *IEEE Electron Device Lett.*, Vol. EDL-4, pp. 54-56, 1983.

[4.6] A. C. Adams, "Plasma planarization," *Solid State Technology*, Vol. 24 (4), pp. 178-181, 1981.

[4.7] W. W. Yao, I. W. Wu, R. T. Fulks and H. A. van der Plas, "Metal step coverage improvement in double-level metal with oxide spacers," in *Proc. 2nd IEEE Int. VLSI Multilevel Interconnections Conf.*, 1985, pp. 38-44.

[4.8] P. J. French and R. F. Wolffenbuttel, "Reflow of BPSG for sensor applications," *J. Micromech. Microeng.*, Vol. 3, pp. 135-137, 1993.

[4.9] W. G. M. Van den Hoek, T. E. Wicker and B. F. Westlund, "Isotropic plasma etching of doped and undoped silicon dioxide for contact holes and

vias," *J. Vac. Sci. Technolo.*, Vol. A7, pp. 670-675, 1989.

[4.10] J. C. North, T. E. McGahan, D. W. Rice and A. C. Adams, "Tapered windows in phosphorus-doped SiO_2 by ion implantation," *IEEE Trans. Electron Devices*, Vol. ED-25, pp. 809-812, 1978.

[4.11] T. M. Mayer and R. A. Barker, "Simulation of plasma-assisted etching processes by ion-beam techniques," *J. Vac. Sci. Technol.*, Vol. 21, pp. 757-763, 1982.

[4.12] R. J. Schutz, "Reactive plasma etching," in *VLSI Technology*, S. M. Sze Ed., Chapter 5, McGraw-Hill Book Company, New York, 1988, pp. 184-232.

[4.13] L. K. Nanver, "Bipolar process research," in *DIMES Annual Report 1994 - Sector IC Devices and Processing*, Delft Institute of Microelectronics and Submicrontechnology (DIMES), pp. 22-23.

[4.14] B. Roberts, "Chemical mechanical planarization," in *the Proc. IEEE/SEMI Advanced Semiconductor Manufacturing Conference and Workshop 1992*, 1992, pp. 206-210.

[4.15] R. Tolles, H. M. Bath, B. Doris, R. Jairath, R. Leggett and S. Siviaram, "Polishing characteristics of different glass films," in *the Proc. SPIE - Intern. Soc. Opt. Eng.*, Vol. 1805, 1993, pp. 42-51.

[4.16] L. K. White, "Planarization properties of resist and polyamide coatings," *J. Electrochem. Soc.*, Vol. 130, pp. 1543-1548, 1983.

[4.17] A. C. Adams and C. D. Capio, "Planarization of phosphorus-doped silicon dioxide," *J. Electrochem. Soc.*, Vol. 128, pp. 423-429, 1981.

[4.18] E. Bassous, L. M. Ephrath, G. Pepper and D. J. Mikalsen, "A three-layer resist system for deep U. V. and RIE microlithography on nonplanar surface," *J. Electrochem. Soc.*, Vol. 130, pp. 478-484, 1983.

[4.19] L. B. Rothman, "Properties of thin polyamide films," *J. Electrochem. Soc.*, Vol. 127, pp. 2216-2220, 1980.

[4.20] A. Schiltz and M. Pons, "Two-layer planarization process," *J. Electrochem. Soc.*, Vol. 133, pp. 178-181, 1986.

[4.21] S. Fujii, M. Fukumoto, G. Fuse and T. Ohzone, "A planarization technology using a bias-deposited dielectric film and an etch-back process," *IEEE Trans. Electron Devices*, Vol. ED-35, pp. 1829-1833, 1988.

[4.22] T. H. Daubenspeck, J. K. DeBrosse, C. W. Koburger, M. Armacost and J. R. Abernathey, "Planarization of ULSI topography over variable pattern densities," *J. Electrochem. Soc.*, Vol. 138, pp. 506-509, 1991.

[4.23] M. L. Long and J. Newman, "Image reversal techniques with standard positive photoresist," in *the Proc. SPIE - Intern. Soc. Opt. Eng.*, Vol. 469, 1984, pp. 189-193.

[4.24] W. J. Daughton and F. L. Givens, "An investigation of the thickness variation

of spun-on thin films commonly associated with the semiconductor industry," *J. Electrochem. Soc.*, Vol. 129, pp. 173-179, 1982.

[4.25] S. Crapella and F. Gualandris, "Planarization by two-resist level," *J. Electrochem. Soc.*, Vol. 135, pp. 683-685, 1988.

[4.26] W. W. Moreau, "Surface preparation and coating," in *Semiconductor Lithography, Principles, Practices and Materials*, Plenum Press, New York, 1988, Chapter 11, pp. 545-566.

[4.27] J. A. Foerster, Y. X. Li, M. Bartek, P. J. French and R. F. Wolffenbuttel, "Fabrication of recessed micro-tips in silicon for sensor applications," in *the Proc. Micro Mechanics Europe 1994 (MME94)*, pp. 198-201.

Chapter 5 Single Crystal Silicon Etching for Selective Epitaxial Growth and Micro-Tip Fabrication

5.1 Introduction

As indicated already in the previous chapter, etching of single crystal silicon is necessary for the fabrication of many microstructures for sensors and actuators [5.1-5.2]. One particular application of silicon etching that is discussed in detail in this chapter is the selective epitaxial growth (SEG) process. Silicon etching and subsequent refill with crystal SEG open new opportunities in the monolithic integration of sensors and readout electronics [5.3]. The depth and sidewall profile of the etching are the main issues of concern in the plasma etching process development for SEG. The etching must be several microns deep, depending on the desired applications, and with vertical sidewalls. High directionality of the etching to realize the vertical sidewalls is required, so that an oxide layer can be formed, either by thermal oxidation or CVD, and etched-back anisotropically, to remove the oxide at the base of the etching while leaving the oxide at the sidewalls unetched. These oxide spacers are essential to ensure SEG selectively from the silicon substrate.

Anisotropic silicon etching has been one of the major efforts in plasma etching process development due to its importance in trench isolation of conventional IC's. Generally Cl_2- or Br_2-based chemistries are used for silicon etching due to their higher anisotropy and selectivity over oxide mask than F-based chemistries [5.4-5.7]. This is because silicon reacts with Cl atoms/Cl_2 molecules and Br atoms/Br_2 molecules only through the simultaneous energetic ion bombardment and silicon oxide is rather inert to those reactive species, as described in Chapter 2. However, Br_2-based chemistries are not preferred due to its toxicity and Cl_2-based chemistries usually depend on substrate doping concentration [5.8-5.9] and frequently result in bowing (i.e. excessive lateral etching at the etching sidewall) in the sidewall profile [5.10-5.12]. Alternatively, CF_4- or SF_6-based chemistries can be used in silicon etching. Although F atoms etch silicon spontaneously and therefore result in severe underetching, anisotropic etching can be achieved under certain circumstances, such as sufficient sidewall protection due to, for example O_2 [5.13-5.14], C_2ClF_5 [5.15] or CF_3Br [5.16] additions in SF_6 chemistry or due to carbon-containing reaction products of photoresist.

Etching silicon towards a controlled degree of bowing is a rather new topic and very little has been reported in the literature. This is because the bowing is usually not

acceptable in the trench isolation and therefore needs to be eliminate. However, recently an important application of single crystal silicon plasma etching is the fabrication of silicon micro-tips. In contrast to the requirements for the SEG application, certain degree of bowing is required in the sidewall profile of the etching, so that silicon cones can be formed and subsequently sharpened, yielding micro-tips. Therefore, etching chemistry must be carefully tuned so that the sidewall profile of the etching can be well-controlled.

In this chapter the effects of Cl_2 addition on the sidewall profile in the silicon etching process using a gas mixture of CF_4 + Cl_2 are investigated. A silicon etching process featuring vertical sidewalls and a sufficient selectivity over the mask has been developed for SEG-silicon in bulk silicon. By making use of bowing in the etching profile followed by thermal oxidation, recessed silicon micro-tips can be fabricated which are used as the cathode of vacuum microelectronic devices. The depth and sharpness of the tip can be determined by correct selection of the Cl_2 content in the chemistry.

5.2 Experimental details

The Drytek 384T triode RIE etcher described in Chapter 2 was used for the etching of silicon with an applied RF power of 175 W and the gas pressure of 165 mTorr. A 1 μm thermal oxide layer was first formed on 4'' (100) 2-5 Ω•cm p-type wafers. The oxide layer was patterned in the same etcher using an optimized CHF_3 + C_2F_6 chemistry, described in Chapter 4, with 1.3 μm HPR204 photoresist. This patterned oxide layer together with the remaining photoresist ($\sim$1 μm thick) was used as the mask during the subsequent silicon etching. The gas mixture investigated was CF_4 + Cl_2 with a total gas flow rate of 220 sccm.

5.3 Results and discussions

5.3.1 Effects of Cl_2 content and mask material on the etching profile and selectivity

Fig. 5.1 and 5.2 show SEM photographs of cross-sectional views of the etched silicon trenches using CF_4/Cl_2 gas mixtures with Cl_2 contents ranging from 0 to 50%. The composite mask of the resist and oxide layer was used in the experiments for Fig. 5.1, while only the oxide mask for Fig. 5.2. Fig. 5.3 shows the silicon etch rate and selectivity versus Cl_2 content over the photoresist and oxide mask, respectively.

It can be seen from Fig. 5.1(a) that at a zero Cl_2 content, the etching is anisotropic but the angle of the trench profile to the substrate plane is about 80° instead of 90°, which

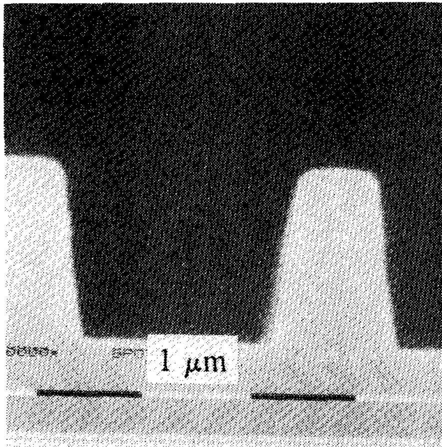

(a)

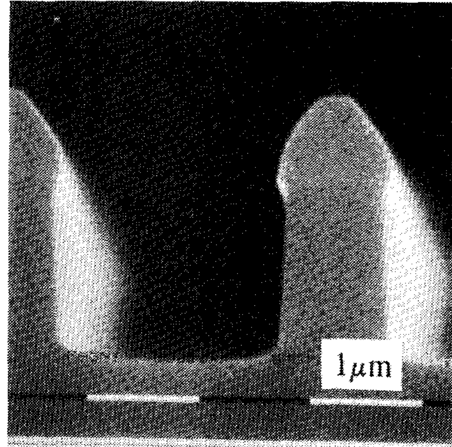

(b)

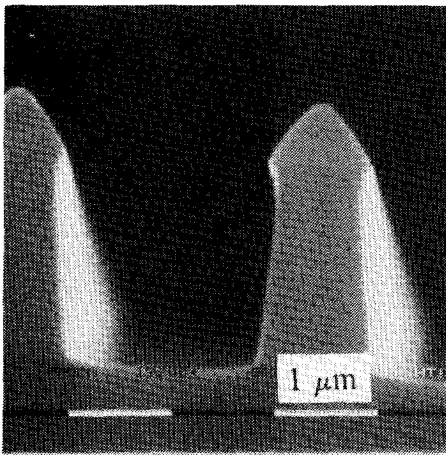

(c)

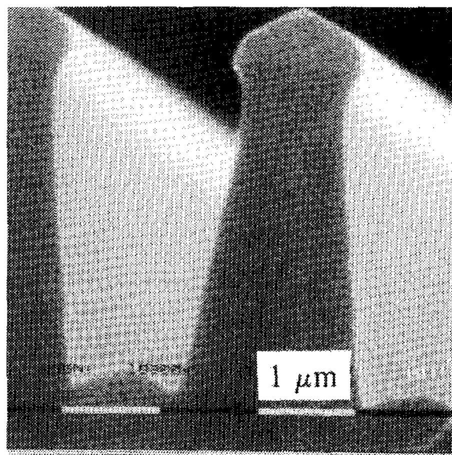

(d)

Figure 5.1 *SEM photographs of the cross-sectional view of silicon trenches etched using the composite mask of resist and oxide. The Cl_2 additions are (a) 0, (b) 10 sccm, (c) 20 sccm and (d) 110 sccm. The total flow rate of Cl_2 + CF_4 is 220 sccm. Power = 170 W, Pressure = 165 mTorr.*

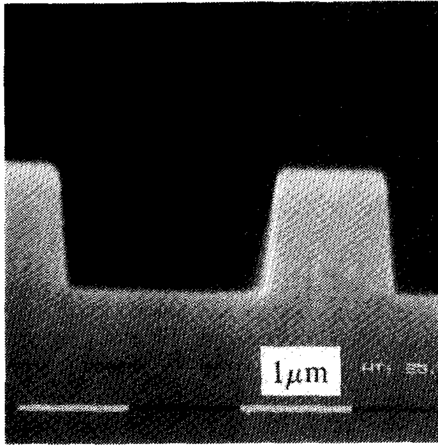

(a)

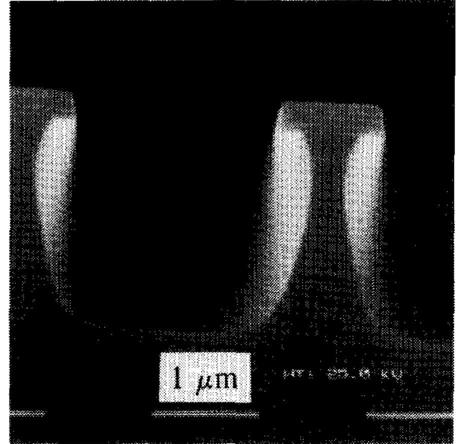

(b)

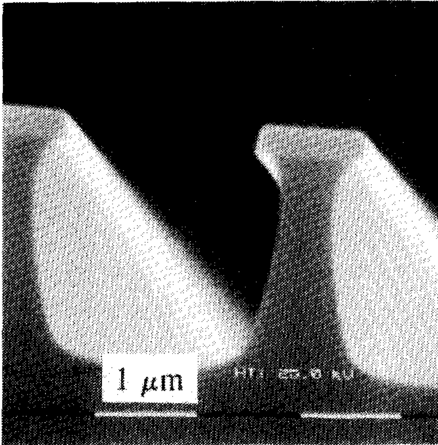

(c)

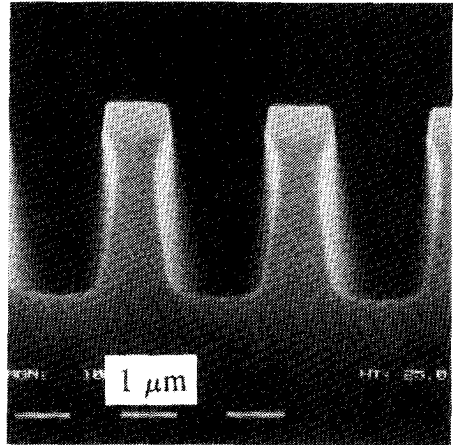

(d)

Figure 5.2 *SEM photographs of the cross-sectional view of silicon trenches etched using oxide mask. The Cl_2 additions are (a) 0, (b) 10 sccm, (c) 20 sccm and (d) 110 sccm. The total flow rate of Cl_2 + CF_4 is 220 sccm. Power = 170 W, Pressure = 165 mTorr.*

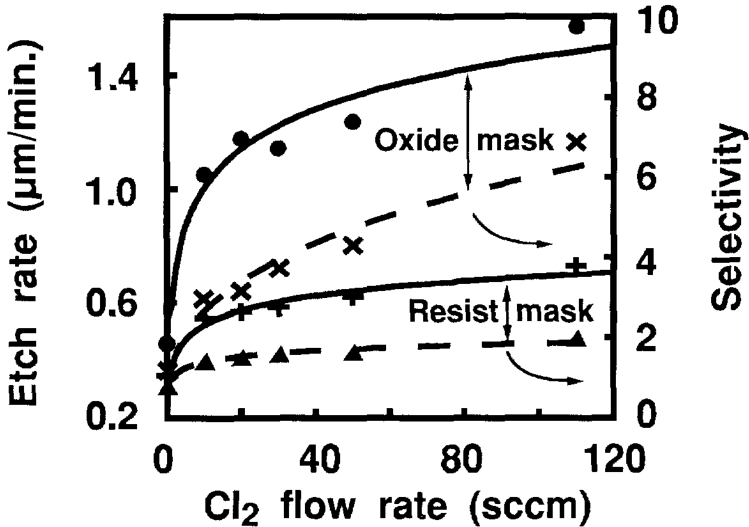

Figure 5.3 *Etch rate and selectivity of the silicon trench etching versus Cl_2 content in CF_4 + Cl_2 chemistry. The total flow rate of Cl_2 + CF_4 is 220 sccm. Power = 170 W, Pressure = 165 mTorr.*

would make it difficult for oxide spacers to be formed by conformal oxide growth/deposition and subsequent anisotropic plasma etching-back.

One of the reasons for the non-vertical profile is the etching of the masking photoresist and oxide layer. As shown in Fig. 5.3, the etching selectivity over the photoresist and oxide with zero Cl_2 content is only 0.82 and 1.2, respectively. In the pure CF_4 plasma, F atoms are the main reactive etchant for the etching. The F atoms etch both the photoresist and the silicon substrate spontaneously. With the help of ion bombardment, F atoms also attack oxide layer. Because the original sidewall of the photoresist mask for the oxide patterning is not vertical, the resulting oxide sidewall is also tapered (with a sidewall angle of about 80°, referring to Fig. 4.5b of Chapter 4). This non-vertical sidewall profile of the masking photoresist and oxide is again transferred to the silicon substrate during the trench etching, because the masking photoresist and oxide are also etched simultaneously.

A further reason for the tapered sidewall profile is probably the deposition of polymer forming C-F radicals (such as CF_2 and CF_3) in the CF_4 plasma on the trench sidewalls [5.17]. Due to the fact that the pure CF_4 chemistry results in anisotropic etching profile as indicated in Fig. 5.1(a), it is inferred that sidewall protection by polymer forming radicals is significant. These radicals originate from the ionization of CF_4 and from

reaction products of the photoresist etching in the plasma. As discussed in Chapter 3, the polymer formation on the polysilicon surface plays a major role in highly selective silicon nitride etching over polysilicon. In the silicon trench etching, due to the lack of ion bombardment on the vertical trench sidewalls, the deposited polymer film serves as a local passivation layer and prevents etching of the sidewalls. This sidewall passivation improves the anisotropy of the trench etching but also leads to a tapered sidewall, as indicated in Fig. 5.4.

Adding 10 sccm Cl_2 to CF_4 resulted in an almost vertical sidewall of the trench, although slight underetching was still found, as shown in Fig. 5.1(b). Further increasing Cl_2 addition to CF_4 resulted in a slight bow to appear at the upper part of the trench and a tapered shape at the remaining part of the trench. The bow in the etch profile is not desirable for the SEG, because it prevents a complete coverage by CVD oxide of the trench step. The tapered part causes problems similar to those discussed at zero Cl_2 content (i.e. difficulties in oxide spacer formation by anisotropic plasma etching-back). The etch rate for the silicon and selectivity over the mask increased with Cl_2 addition. However, at a Cl_2 content higher than 50 sccm, crevices (i.e. extra etching along the bottom of the sidewalls) were formed.

The effects of Cl_2 addition can be understood by considering the reaction of C-F radicals in CF_4 plasmas with Cl atoms generated by energetic electron collision, as proposed in [5.18]. In pure CF_4 plasma, F atoms, CF_2 and CF_3 radicals are present:

$$CF_4 + e \rightarrow CF_3 + F + e \quad (5.1)$$

$$CF_3 + e \rightarrow CF_2 + F + e \quad (5.2)$$

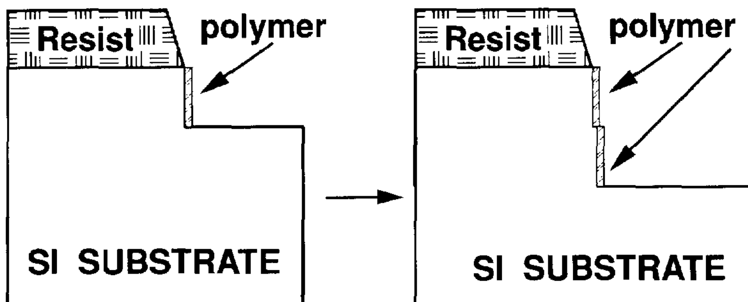

Figure 5.4 Mechanisms of tapered sidewall formation by polymer deposition.

The F atoms etch silicon spontaneously, while the CF_2 and CF_3 radicals form a thin polymer film at the sidewall of the etch profile.

With Cl_2 addition, Cl atoms, Cl^+ and Cl_2^+ ions are formed:

$$Cl_2 + e \rightarrow 2Cl + e \quad (5.3)$$

$$Cl_2 + e \rightarrow Cl_2^+ + 2e \quad (5.4)$$

$$Cl_2 + e \rightarrow 2Cl^+ + 3e \quad (5.5)$$

Cl atoms can etch silicon with the help of ion bombardment:

$$xCl + Si \rightarrow SiCl_x \uparrow \quad (5.6)$$

On the other hand, Cl atoms play a role of oxidant in the chemistry, as discussed in Chapter 2. In other words, they may recombine with the C-F radicals, consuming part of polymer-forming precursors [5.18]:

$$CF_3 + Cl \rightarrow CF_3Cl \uparrow \quad (5.7)$$

The reaction product is volatile and, therefore is readily removed from the plasma by pumping.

Furthermore, due to the scattering caused by the collision with the neutral radicals in the plasma sheath or with the tapered oxide masking sidewalls, part of the Cl^+ and Cl_2^+ ions will deviate from their vertical trajectory and impinge onto the trench sidewalls [5.10-5.12]. The reduced density of the C-F radicals due to the recombination reaction (5.7) and Cl^+ and Cl_2^+ ion impinging onto the sidewalls will weaken the sidewall deposition of the C-F radicals, resulting in, on the one hand, the less tapered (or more vertical) sidewalls and, on the other hand, an enhancement of lateral underetching of the F atoms to the silicon substrate, as observed in Fig. 5.1(b). Simultaneously, the etch rate of the silicon substrate increases because of the reduction of the C-F radicals, which tend to deposit on the silicon surface and retard the etching, thus improving the selectivity of the etching over the mask, as indicated in Fig. 5.3.

Increasing the Cl_2 content further results in more Cl atoms and ions. Due to the severe off-vertical Cl^+ and Cl_2^+ ion bombardment onto the sidewall, the bow and crevices are

formed in the trench profile. In addition to thinning the polymer layer on the sidewall, the ion bombardment will also cause crystal damage in the silicon and make the silicon chemically more susceptible to the etchants. As a result, chemical reaction takes place significantly also at the part of the sidewall which receives the off-vertical ion bombardment, resulting in bow profile. Furthermore, the Cl^+ and Cl_2^+ ions incident to the bowed sidewall can slip to the base of the trench. Some of them may still be sufficiently energetic to cause additional etching in the bulk silicon along the bottom of the sidewall, resulting in the extra etching there (crevices) , as shown in Fig. 5.5.

From Fig. 5.2 it can be seen that significant undercutting took place in the trench etching with oxide mask only. This implies that the reaction products of photoresist etching are essential to provide sufficient polymer forming radicals for sidewall protection, which ensure the anisotropy. Therefore, a composite mask of both photoresist and oxide is necessary to obtain the desired vertical trench profile for SEG.

5.3.2 Optimized silicon etching process for SEG

Based on the above experimental results, the gas mixture of 10 sccm Cl_2 + 210 sccm

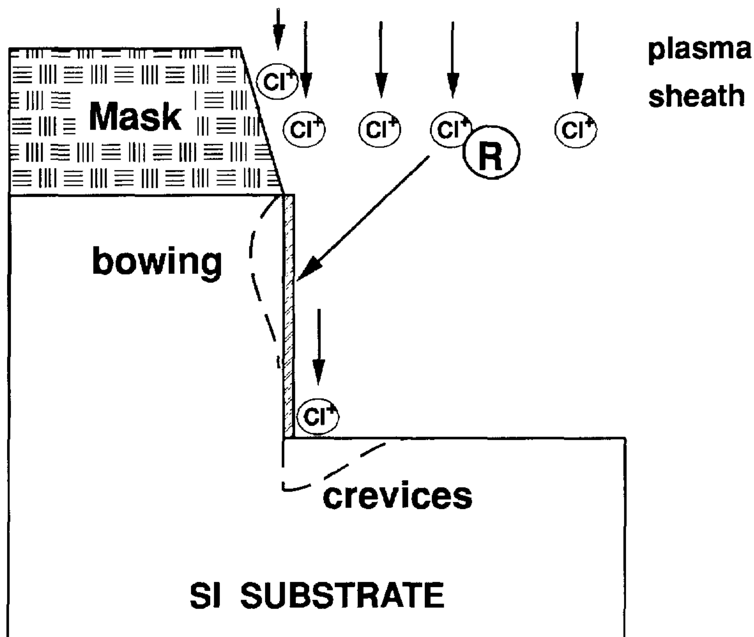

Figure 5.5 *Off-vertical bombardment of Cl^+ ions on the sidewall results in bowing and crevices.*

CF_4 was chosen for the silicon etching so as to achieve vertical etching profile. The composite mask of photoresist and oxide must be used. Using this gas mixture, the silicon etch rate is 5260 Å/min and 1.05 μm/min with the resist and oxide mask, respectively. The selectivity over the two types of masks is 1.44 and 2.98, respectively. These selectivity values are sufficient to etch 3 μm or more silicon using the composite mask of 1 μm resist and 1 μm thermal oxide. Fig 5.6 shows SEM photo of a 3 μm silicon trench etched using the optimized chemistry and Fig. 5.7 is a SEM photo showing the refilled silicon trench with SEG.

The chemistry has been applied in SEG for the fabrication of an integrated colour sensor [5.3]. The detail process sequence is shown in Fig. 5.8. Firstly, a trench is etched in the n-type epitaxial layer on a p-type silicon substrate, using the optimized etching process (Fig. 5.8a). Secondly, an oxide layer is formed by either thermal oxidation or LPCVD (Fig. 5.8b). Thirdly, the oxide layer on the trench base is removed by anisotropic plasma etching, followed by boron implantation to form a p^+ region in the trench base. Subsequently, an n^-- and an n-SEG layer are formed (Fig. 5.8c). Finally, npn transistors are fabricated on the n-type normal epitaxial layer and photo-diodes on the n-type SEG layer (Fig. 5.8d). In this particular example, there are 3 photo-diodes with different junction depth. The lower photo-diode is formed between the p^+ buried layer and the n-type normal epitaxial layer underneath, which detects the red light component. The middle diode is formed between the p^+ buried layer and the n^--SEG layer above, which senses the green light component. The upper photo-diode

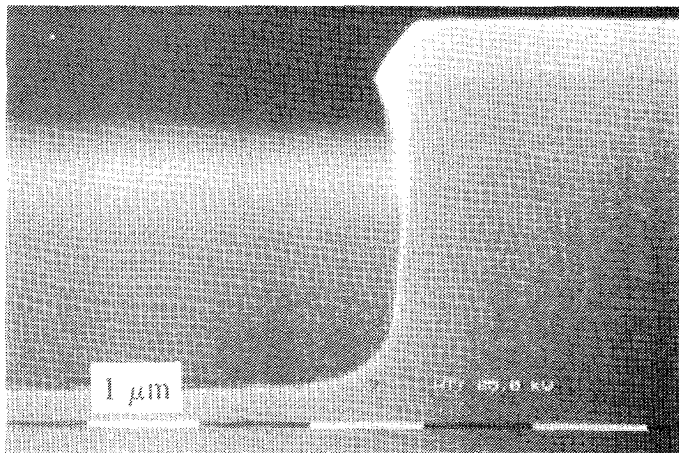

Figure 5.6 *3 μm deep silicon trench with vertical sidewall etched using the resist and oxide composite mask and the gas mixture of 10 sccm Cl_2 addition to 210 sccm CF_4. Power = 170 W, Pressure = 165 mTorr.*

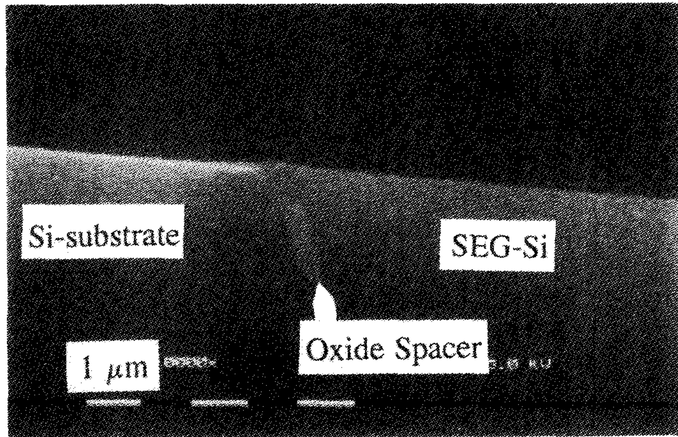

Figure 5.7 *SEG-refilled silicon trench.*

is a shallow junction formed between the n-SEG layer and p^+ region above, which responses to the blue light component.

5.3.3 Silicon trench etching process for micro-tip fabrication

Silicon micro-tips are used in surface profiling devices such as atomic force microscopy (AFM), sensing devices [5.19-5.20] and vacuum microelectronic devices such as field emission arrays. Micro-tips in silicon have been fabricated generally by using two-step processes. The first step is to form a silicon cone using isotropic or anisotropic etching and the second step is to sharpen the cone and therefore produce the tip. Isotropic wet etching in HF/HNO_3 solution [5.21-5.22], isotropic plasma etching using SF_6 [5.23], anisotropic plasma etching using C_2ClF_5/SF_6 gas mixtures [5.24-5.25], plasma etching using SF_6/Ar, $SF_6/CCl_2F_2/Ar$ or $BCl_3/Cl_2/Br_2$ gas mixtures [5.27] are some examples of the process for the first step. The top diameter of silicon cones fabricated is in the range of 300 to 5000 Å. Dry etching based on pure physical bombardment [5.21], anisotropic wet etching [5.22], isotropic wet etching using $HF/HNO_3/CH_3COOH$ solutions [5.24-5.25] and dry oxidation followed by HF stripping of oxide [5.23][5.26 are some methods of sharpening silicon cones. Tips with radius of 10 to 200 Å have been achieved after sharpening.

Based on the bowing in silicon trenches etched using the CF_4 + Cl_2 chemistries shown in Fig. 5.2, a fabrication process for silicon micro-tips has been developed and tested As shown in Fig. 5.9, a silicon cone was formed using the plasma etching with round shape mask. Subsequently, dry oxidation was used to consume the remaining silicon a the narrowest part of the cone. Due to the stress resulting from volume increase during oxidation of silicon, the oxide growth rate at the narrow part of the cone is lower

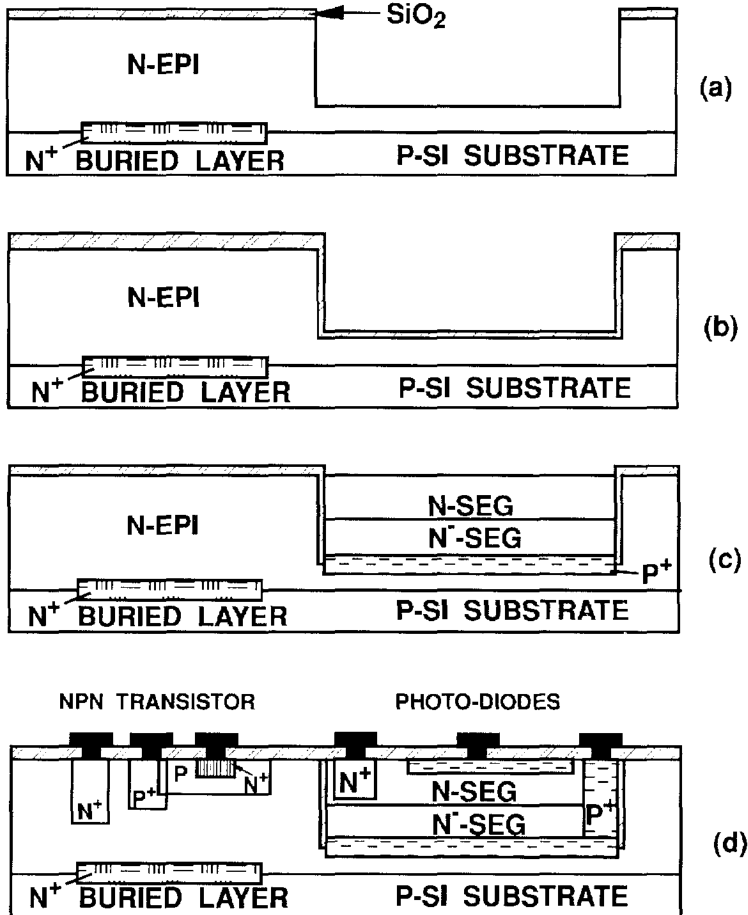

Figure 5.8 *Selective epitaxial growth (SEG) for on-chip integration of sensors with electronic circuits. (a) Deep trench formation. (b) Conformal oxide deposition/growth. (c) Anisotropic oxide etch-back to form oxide spacers and subsequent SEG. (d) Fabrication of electronic circuits and photo-diodes.*

compared with that at the remaining part of the cone. This effect leads to sharpening of the silicon cone during oxidation [5.26]. HF solution was used to strip the oxide layer and yield a silicon micro-tip.

In this process control of the degree of bowing in the silicon trench is a key issue because it determines the position of the tip end relative to the top surface and the minimum diameter of the cone and, therefore sharpness of the tip. Fig. 5.10

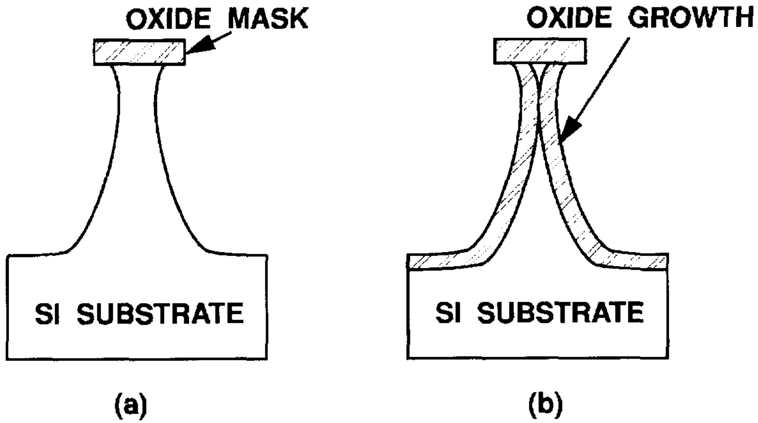

Figure 5.9 *Formation of silicon cones using plasma etching (a) and oxidation sharpening to produce micro-tips (b).*

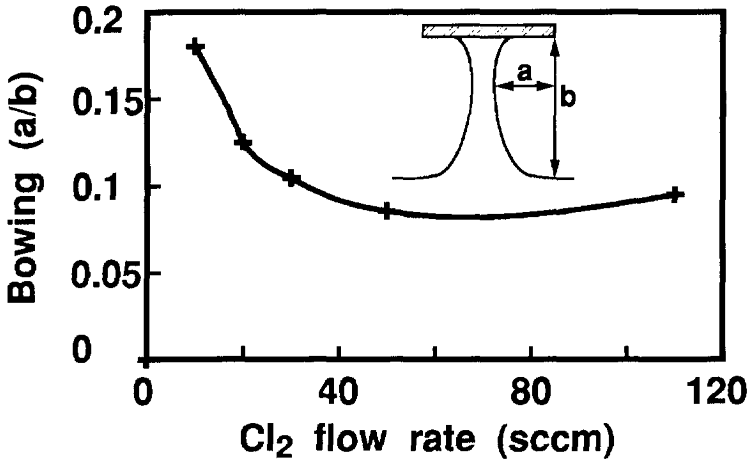

Figure 5.10 *The degree of bowing (ratio of the maximum lateral etching to the vertical depth of the trench) versus Cl_2 content in the CF_4/Cl_2 chemistry with oxide mask.*

summarizes the degree of bowing (measured by the ratio of the maximum lateral etching at the sidewalls to the depth of the vertical trench) with the chemistry when oxide only is used as the mask. The zero Cl_2 content is a limiting case due to the completely anisotropic (but tapered) sidewall profile. In the range of 10 - 50 sccm Cl_2 flow rate, the degree of bowing decreases with increasing Cl_2 content, resulting in increased tip sharpness with increasing Cl_2 content in the etching chemistry. Therefore, by suitable selection of Cl_2 flow rate in the chemistry, the sharpness of the tip can be determined, with the maximum sharpness corresponding to 50 sccm Cl_2. The ability to adjust the tip sharpness is of significance in the optimization of the tip for desired applications.

Fig. 5.11 shows the position of the tip end relative to the wafer surface as a function of Cl_2 content in the chemistry. Note that at zero Cl_2 content, the position is actually at the wafer surface due to the fact that no bowing takes place. With increasing Cl_2 content in the chemistry, the position of the tip end is lowered due to the downward displacement of the point of the maximum bowing. Since the tip end is located below the silicon surface, the tip is much less vulnerable during further processing compared to those fabricated using the previously reported methods, which are on top of the wafer surface. Furthermore, the recession of the tip can facilitate formation of gate and anode by sequential film deposition in a vacuum micro-triode, which uses the tip as the cathode [5.19]. The detailed process sequence of the device is shown in Fig. 5.12. Firstly the tip is produced as described above. Secondly, a PSG layer is deposited as

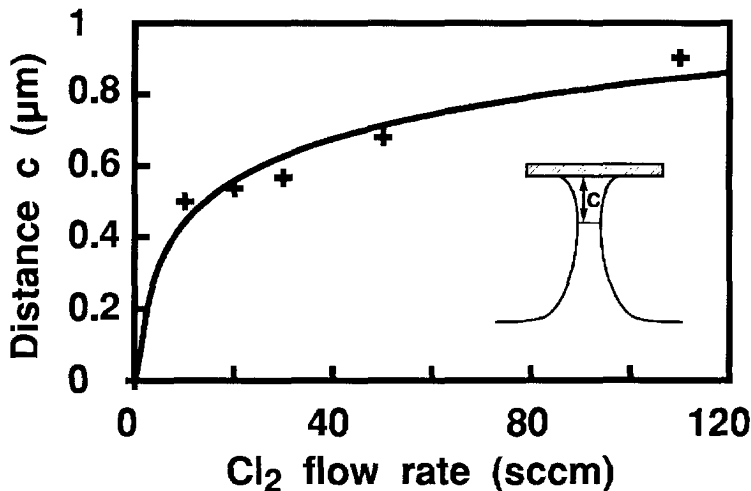

Figure 5.11 *The distance of the position relative to the wafer surface corresponding to the minimum diameter of silicon cone as a function of Cl_2 content in the CF_4/Cl_2 chemistry with oxide mask.*

the insulating layer, followed by the deposition and doping of a polysilicon film, which will be patterned later to form the gate of the triode. Thirdly, a thick BPSG was deposited and reflowed to planarize the surface before a second polysilicon layer is deposited and patterned to form the anode of the triode.

Fig. 5.13 shows the SEM photo of a silicon tip fabricated using the proposed plasma etching and oxidation method, with oxide being not yet removed. The method has been used to produce silicon tips with a radius of curvature of less than 100 Å. This is indicated in Fig. 5.14, which is a close view of the micro-tip. A vacuum diode array has been fabricated based on this method and a high emission current has been observed, indicating the micro-tips are very promising in device applications such as vacuum triode or pressure sensors based on field emission array [5.19].

5.4 Conclusions

Effects of Cl_2 content on the etching profile in a CF_4/Cl_2 plasma etching chemistry for silicon etching have been investigated. It was found that by adding 10 sccm Cl_2 to 210 sccm CF_4, vertical sidewall profile of the silicon trench can be obtained, although with a slight undercutting. This gas composition was most suitable to etch bulk silicon for SEG applications when a composite mask of photoresist and oxide was used. Bowing of the sidewall profile appeared at increasing Cl_2 addition. Moreover, crevices (extra etching along the bottom of the trenched sidewall) took place when more than 50 sccm Cl_2 was added to the CF_4 gas. It is argued that two mechanisms are responsible for the observed bowing and crevices. One is the recombination of Cl atoms with polymer-forming C-F radicals, which deposit on the trench sidewall and result in anisotropy. The other is the Cl^+ or Cl_2^+ ion bombardment onto the trench sidewall, which attacks the sidewall protection film and induce chemical reaction there. Photoresist was found essential to provide sufficient polymer forming radicals for the trench sidewall protection.

By using 170 sccm CF_4 + 50 sccm Cl_2 with round-shape oxide mask, silicon micro-tips have been fabricated. The process involved formation of silicon cones by making use of the bowing in the sidewall profile and sharpening of the cone using thermal oxidation. It was found that the sharpness of the tip and the position of the tip end relative to the wafer surface can be adjusted by changing Cl_2 content in the chemistry. Very sharp recessed silicon tips with a radius of curvature of about 100 Å have been achieved and applied in a vacuum diode array.

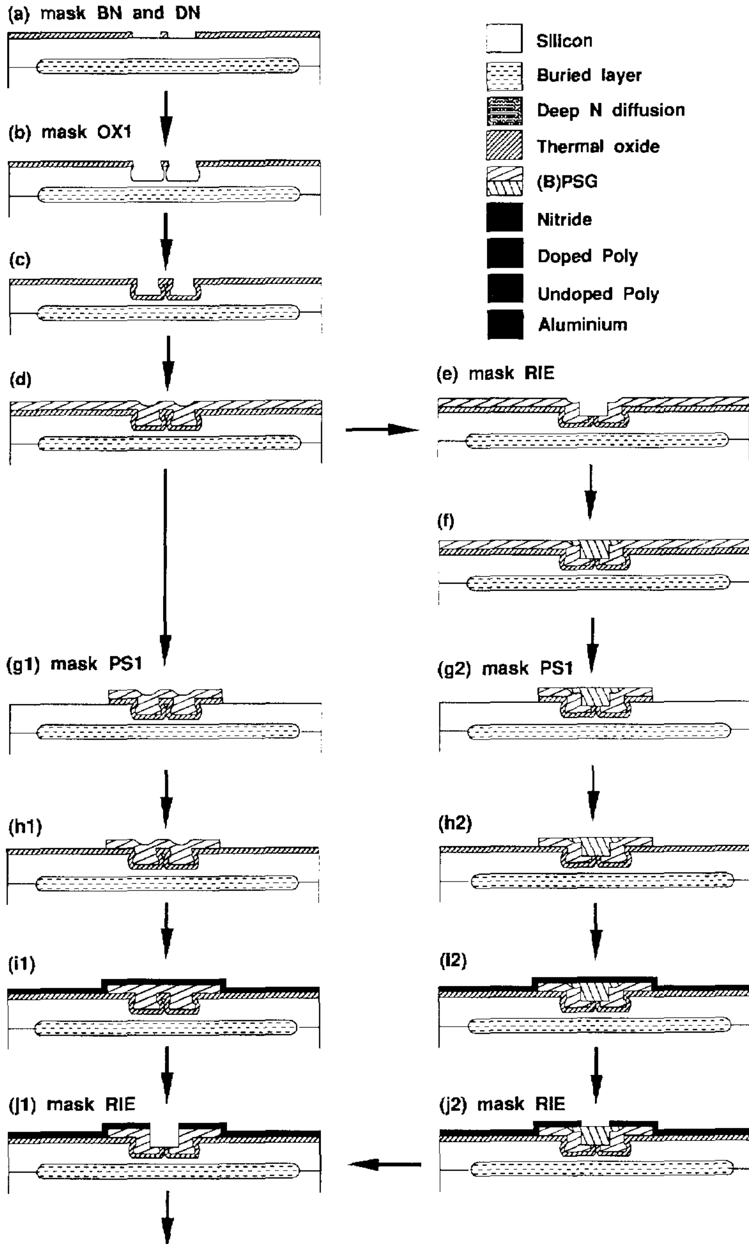
(a) mask BN and DN
(b) mask OX1
(c)
(d)
(e) mask RIE
(f)
(g1) mask PS1
(g2) mask PS1
(h1)
(h2)
(i1)
(i2)
(j1) mask RIE
(j2) mask RIE
Silicon
Buried layer
Deep N diffusion
Thermal oxide
(B)PSG
Nitride
Doped Poly
Undoped Poly
Aluminium

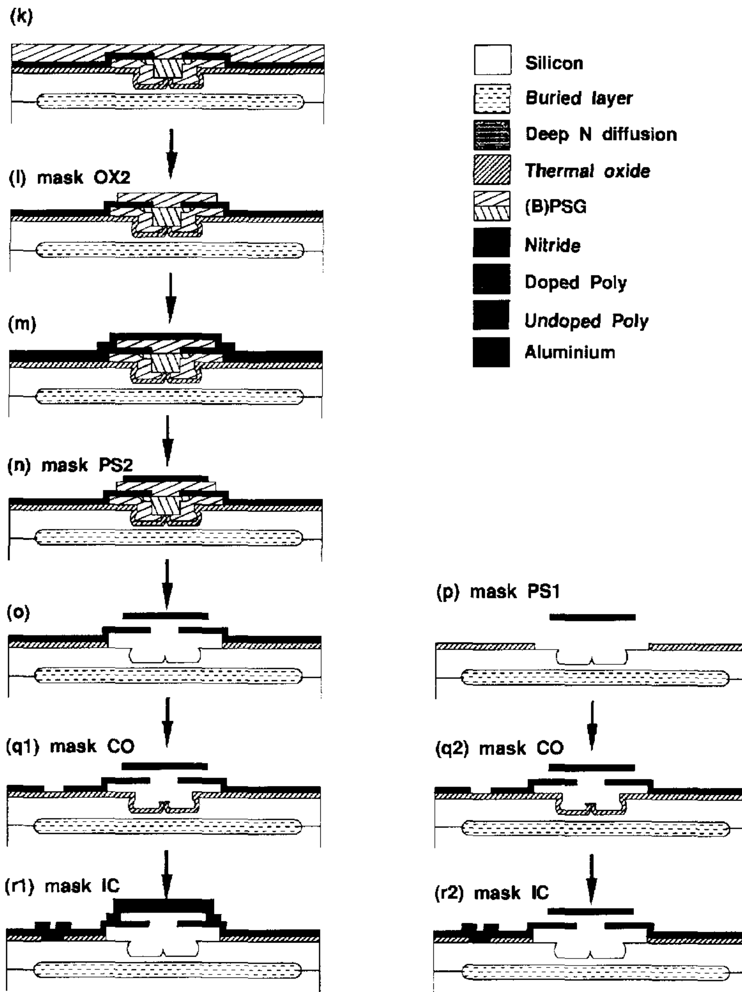

Fig. 5.12 *Process sequence of vacuum micro-triode fabrication based on the silicon tip. (a - c) Mico-tip formation; (d - j) Polysilicon gate formation; (k - q) Polysilicon anode formation; (r) Aluminium interconnection.*

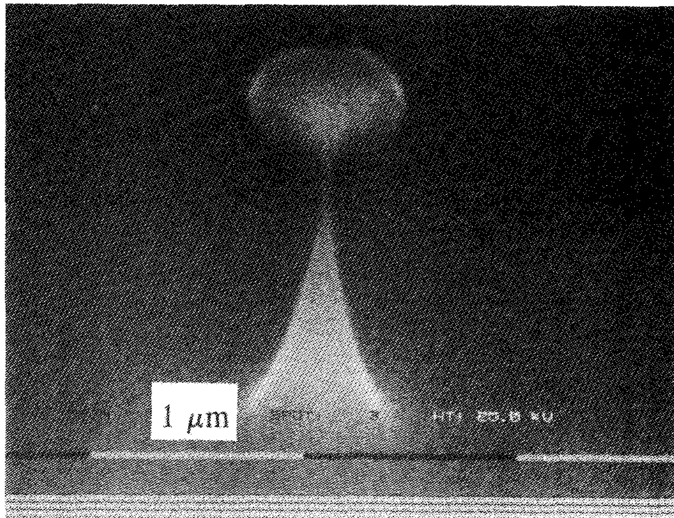

Figure 5.13 *SEM photo of oxidized silicon cone with thermal oxide layer not removed yet. The condition for plasma etching is: Power = 170 W, pressure = 165 mTorr, CF_4 = 170 sccm, Cl_2 = 50 sccm. Oxidation was performed at 1100°C for 45 min, which forms about 3200 Å oxide.*

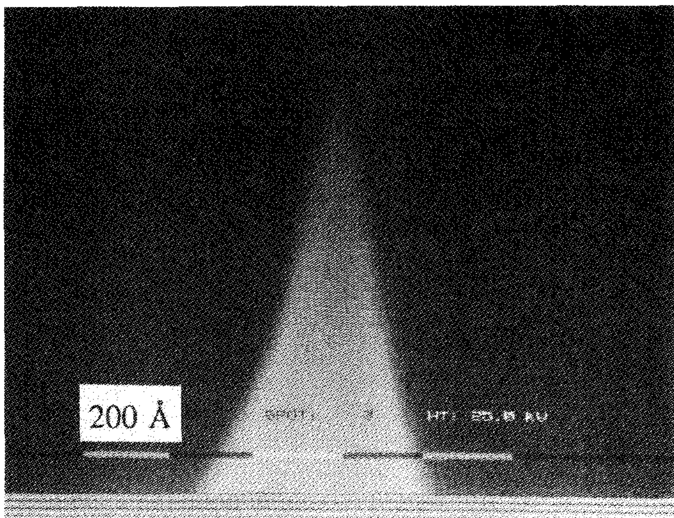

Figure 5.14 *A close view of the silicon micro-tip formed by the plasma etching and oxidation method.*

References

[5.1] C. Linder, T. Tschan and N. F. de Rooij, "Deep trench etching techniques as a new IC compatible tool for silicon micromachining," in *the Proc. 6th Intern. Conf. Solid-State Sensors and Actuators (Transducer'91)*, 1991, pp. 524-526.

[5.2] S. Adams, U. Hilleringmann and K. Goser, "CMOS compatible micromachining by dry silicon-etching techniques," *Microelectron. Eng.*, Vol. 19, pp.191-194, 1992.

[5.3] M. Bartek, P. T. J. Hennissen, E. J. Blaauw, P. M. Sarro, P. J. French and R. F. Wolffenbuttel, "A novel silicon colour sensor using selective epitaxial growth process," in *the Proc. 7th Intern. Conf. Solid-State Sensors and Actuators (Transducer'93)*, 1993, pp. 144-147.

[5.4] R. N. Charlile, V. C. Liang and M. M. Smadi, "High quality trench etches in silicon," *Solid State Technol.*, Vol. 32 (4), pp. 119-123, 1989.

[5.5] M. Sato and Y. Arita, "Etch shape control of single-crystal silicon in reactive ion etching using chlorine," *J. Electrochem. Soc.*, Vol. 134, pp. 2856-2862, 1987.

[5.6] R. N. Charlile, V. C. Liang, O. A. Palusinski and M. M. Smadi, "Trench etches in silicon with controllable sidewall angles," *J. Electrochem. Soc.*, Vol. 135, pp. 2058-2064, 1988.

[5.7] A. M. El-Masry, F. O. Fong and J. C. Wolf, "Magnetically enhanced reactive ion etching of silicon in bromine plasmas," *J. Vac. Sci. Technol.*, Vol. B6, pp. 257-262, 1988.

[5.8] G. C. Schwartz and P. M. Schaible, "The effects of arsenic doping in reactive ion etching of silicon in chlorinated plasmas," *J. Electrochem. Soc.*, Vol. 130, pp. 1898-1905, 1983.

[5.9] G. R. Powell and A. A. Chambers, "Deep Si trench etching with a high rate process through a $n/n^+/p$ type structure, using a triode configured reactor," in *Proc. 2nd Symp. ULSI Sci. and Technol.*, The Electrochem. Soc., ECS Proc. Vol. 89-9, 1989, p. 498.

[5.10] S. W. Pang, J. N. Raudall and M. W. Geis, "Sub-100-nm-wide, deep trenches defined by reactive ion etching," *J. Vac. Sci. Technol.*, Vol. B4, pp. 341-344, 1986.

[5.11] J. I. Ulacin F., C. J. Petti and J. P. McVittie, "Crystal orientation dependent etch rates and a trench model for dry etching," *J. Electrochem. Soc.*, Vol. 135, pp. 1521-1525, 1988.

[5.12] S. Ohki, M. Oda, H. Akiya and T. Shibata, "Cavernous undercuts appearing in reactive ion etched submicron-wide deep trenches," *J. Vac. Sci. Technol.*, Vol. B5, pp. 1611-1616, 1987.

[5.13] C. P. D'Emic, K. K. Chan and J. Blum, "Deep trench plasma etching of single crystal silicon using SF_6/O_2 gas mixture," *J. Vac. Sci. Technol.*, Vol. B10, pp. 1105-1110, 1992.

[5.14] T. Syau, B. J. Baliga and R. W. Hamaker, "Reactive ion etching of silicon trenches using SF_6/O_2 gas mixtures," *J. Electrochem. Soc.*, Vol. 138, pp. 3076-3081, 1991.

[5.15] J. P. McVittie and C. Gozalez, "Anisotropic etching of Si using SF_6 with C_2ClF_5 and other mixed halocarbons," in *the Proc. 5th Symp. Plasma Processing*, The Electrochem Soc., Vol. 85-1, 1985, pp. 552-567.

[5.16] Y. H. Lee and Z. H. Zhou, "Feature size dependence of etch rate in reactive ion etching," *J. Electrochem. Soc.*, Vol. 138, pp. 2439-2445, 1991.

[5.17] R. J. Schutz, "Dry Etching," in *VLSI Technology*, S. M. Sze Ed., McGraw-Hill, New York, 1988, pp. 185-232.

[5.18] C. J. Mogab and H. J. Levinstein, "Anisotropic plasma etching of polysilicon," *J. Vac. Sci. Technol.*, Vol. 17, pp. 721-730, 1980.

[5.19] J. A. Foerster, Y. X. Li, M. Bartek and R. F. Wolffenbuttel, "Fabrication of recessed micro-tips in silicon for sensor applications," in *the Proc. 1994 Workshop on Micro Mechanics Europe (MME'94)*, 1994, pp. 198-201.

[5.20] H. C. Lee and R. J. Huang, "A study on field-emission array pressure sensors," Sensors and Actuators, Vol. A34, pp. 137-154, 1992.

[5.21] H. C. Lee and R. J. Huang, "A novel field emission array pressure sensor," in *the Proc. 6th Intern. Conf. Solid-State Sensors and Actuators (Transducer'91),* 1991, pp. 241-244.

[5.22] P. C. Allen, "Silicon field emitter arrays: fabrication and operation," in *Proc. 2nd Intern. Conf. Vacuum Microelectronics*, 1989, pp. 17-20.

[5.23] J. J. Yao, S. C. Arney and N. C. MacDonald, "Fabrication of high frequency two-dimensional nanoactuators for scanned probe devices," *J. Microelectromechanical Sys.*, Vol. 1, pp. 14-22, 1992.

[5.24] C. Linder, "Deep dry etching of silicon - a novel micromachining tool," *Sensors and Materials*, pp. 311-324, 1992.

[5.25] R. A. Buser, J. Brugger, C. Linder and N. F. de Rooij, "Micromachined silicon cantilevers and tips for bidirectional force microscopy," in *the Proc. 6th Intern. Conf. Solid-State Sensors and Actuators (Transducer'91),* 1991, pp. 249-252.

[5.26] K. K. Chin and R. B. Marcus, "Field emitter tips for vacuum microelectronic devices," *J. Vac. Sci. Technol.*, Vol. A8, pp. 3586-3590, 1990.

[5.27] I. W. Rangelow, "Sharp silicon tips for AFM and field emission," *Microelectronic Eng.*, Vol. 23, pp. 369-372, 1994.

Chapter 6 SIMPLE - A Technique of Silicon Micromachining Using Plasma Etching

6.1 Introduction

The key technologies in silicon micromachining, *viz* bulk micromachining [6.1] and surface micromachining [6.2-6.4], have already been discussed in Chapter 1. As indicated bulk micromachining features a sculpturing capability in three dimensions, however, at the expense of tapered sidewalls and limited aspect ratio of structures. Surface micromachining enables the fabrication of microstructures of a small feature size, however, with a structural thickness limited to that of the deposited film. Many devices exhibit a sensitivity depending on the mass of a suspended microstructure (accelerometer, gyroscope etc.) and large but closely separated opposing areas are required for effective capacitive sensing or electrostatic actuating. Neither conventional bulk micromachining nor surface micromachining is suitable for fabrication of such structures and high aspect ratio deep plasma etching techniques offer a huge potential in this respect.

Basically, it is desirable to micromachine bulk silicon with directional plasma etching so as to achieve both small lateral dimensions and large structural layer thickness. Although the SCREAM process [6.5] fulfils these requirements, it is a rather complicated process involving several film deposition and etching steps. Furthermore, the electrical isolation between the structures depends on trenches around them. The resulting surface non-planarity makes it very difficult to integrate on-chip electronic circuits.

In this chapter, a novel bulk micromachining technique - SIMPLE (Silicon Micromachining by Plasma Etching) is described. This technique uses a Cl_2/BCl_3 plasma chemistry which etches p- or lightly n-doped silicon anisotropically but heavily n-doped silicon laterally [6.6]. As shown in Fig. 6.1, an n^+ buried layer is formed on the substrate before the growth of an lightly n-doped epitaxial layer. The Cl_2/BCl_3 plasma etches the epitaxial layer anisotropically but lateral etching occurs when the n^+ buried layer is exposed to the plasma. Thus the silicon beam with vertical sidewalls can be patterned and released from the substrate in a single plasma etching due to the lateral etching of the n^+ layer.

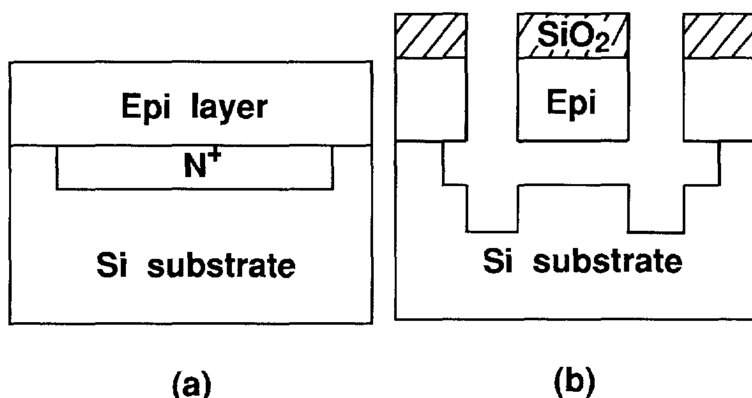

Fig. 6.1 *The SIMPLE process. (a) after n^+ buried layer formation and epitaxial growth. (b) after plasma etching to pattern and release the beam. Note that the height of the beam is the same as the epitaxial layer thickness.*

6.2 Experimental details

The SIMPLE technique has been experimentally optimized to maximize the lateral etching of the n^+ buried layer, while maintaining vertical etching of the epitaxial silicon layer. In these experiments B-doped (100) wafers with 1 - 5 Ω•cm resistivity were used as the starting material. The n^+ buried layer was formed by ion implantation of n-type dopants, using phosphorus, arsenic or antimony, followed by thermal anneal to remove the crystal damage and to activate the implanted dopant. Subsequently, a 4 μm silicon epitaxial layer doped with 1×10^{16} cm^{-3} arsenic was formed. After deposition and plasma patterning of a 2 μm thick PECVD oxide mask, the wafers were etched in the Alcatel GIR300 Reactive Ion Etching (RIE) machine (described in Chapter 2) using a two-step process.

The first step of the plasma etching, which used 15 sccm BCl_3 with 0.34 W/cm^2 RF (13.56 MHz) power density and 22.5 mTorr pressure, was necessary to remove any residual oxide in the windows to eliminate non-uniform silicon etching in the second step. The second step for the bulk silicon etching, used a gas mixture of 20 sccm Cl_2 + 5 sccm BCl_3 with 0.57 W/cm^2 power density and 15 mTorr pressure. After the etching the wafer was cleaved and the etch rate and sidewall profile were examined using a Philips SEM525E scanning electron microscope.

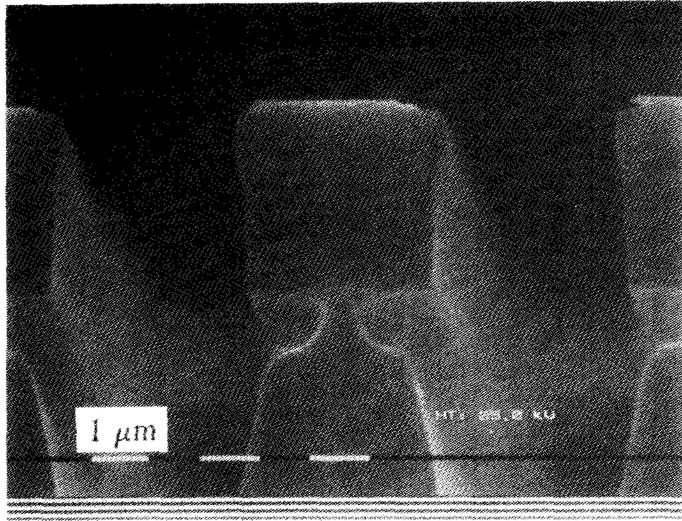

Fig. 6.2 *SEM photograph showing the vertical (anisotropic) etching of the lightly n-doped epitaxial layer and the p-type substrate as well as the lateral etching of the n^+ buried layer. The etching is stopped intendedly before the underetching from the two sides merges together to facilitate SEM operation.*

6.3 Results and discussions

6.3.1 Lateral etching of the n^+ buried layer formed by different n-type dopants

Fig. 6.2 shows the cross-sectional view of a typical microbeam formed by the plasma etching of the 4 μm epitaxial layer on an n^+ buried layer. The buried layer was formed by 180 keV, 1×10^{16} cm^{-2} arsenic implantation followed by 1200°C, 4 hours thermal anneal in $N_2 + O_2$ (flow rate of $N_2/O_2 = 10:1$) atmosphere. It can be seen that vertical (anisotropic) etching takes place in the epitaxial layer, which is lightly arsenic-doped, while lateral etching takes place in the heavily arsenic-doped buried layer. After the buried layer is vertically etched through, the p-type substrate is etched anisotropically and the n^+ buried layer continues to be etched laterally.

Similar lateral etching was observed in n^+ buried layers formed by phosphorus implantation and anneal. However, no significant lateral etching was found in buried layers formed by antimony implantation up to a dose of 2.5×10^{16} cm^{-2} followed by the same thermal anneal as for the arsenic buried layers. Furthermore, no lateral etching

took place in all the 3 types of the buried layers which were not thermally annealed. The reasons for the anisotropic etching of the antimony-doped or unannealed buried layers will be discussed later.

In principle undoped or lightly doped silicon is not etched by Cl atoms or Cl_2 molecules unless energetic ion bombardment to the substrate in a Cl-containing plasma is present [6.7]. The ion bombardment causes damage in the silicon crystal and therefore induces chemical reactions between the silicon atoms and Cl atoms and/or Cl_2 molecules. In other words, the etching takes place only along the direction of ion bombardment, which is perpendicular to the substrate. This is the reason why the lightly n-doped epitaxial layer is etched anisotropically in the experiments. Using the Cl_2/BCl_3 chemistry, the vertical etch rate of lightly doped silicon is ~2000 Å/min. By contrast heavily n-doped silicon reacts rapidly and spontaneously with Cl atoms, thus etching takes place also on the surface of the buried layer which does not receive energetic ion bombardment, leading to the lateral etching observed. This spontaneous reaction is related to the concentration of active n-type carriers, rather than the chemical identity of the dopant [6.8-6.9]. Therefore, no lateral etching was found in the unannealed buried layers.

Some mechanisms have been proposed to explain the spontaneous etching of n^+ silicon in Cl plasmas [6.10]. It is generally agreed that n-type doping raises the Fermi level and thereby reduces the energy barrier for charge transfer to chemisorbed chlorine. As shown in Fig. 6.3, Cl atoms are covalently bound to specific sites in case of an undoped silicon surface. Steric hindrance impedes impinging Cl atoms from penetrating the surface to reach sub-surface Si-Si bonds. However, a more ionic Si-Cl surface bond is formed on an n^+ silicon surface due to the n-type doping and enhanced electron transfer, providing additional chemisorption sites and facilitating Cl penetration into the substrate lattice. This makes it possible for impinging Cl atoms to chemisorb, penetrate the lattice and react more readily. Therefore, on the surface of n^+ silicon Cl atoms can react with silicon spontaneously, resulting in lateral etching of the n^+ buried layer shown in Fig. 6.2.

6.3.2 Effects of the n^+ doping level on the lateral etch rate

Fig. 6.4 shows the lateral etch rate of n^+ buried layer formed by arsenic implantation, after anneal. The etch rate increases linearly with the logarithm of the implantation dose. With doses less than 1×10^{15} cm^{-2} no significant lateral etching can be observed. This implantation dose corresponds to a peak carrier concentration of about 8×10^{19} cm^{-3} according to the process simulation using SUPREM3 [6.11]. Experiments with annealed phosphorus-implanted buried layer result in similar etching.

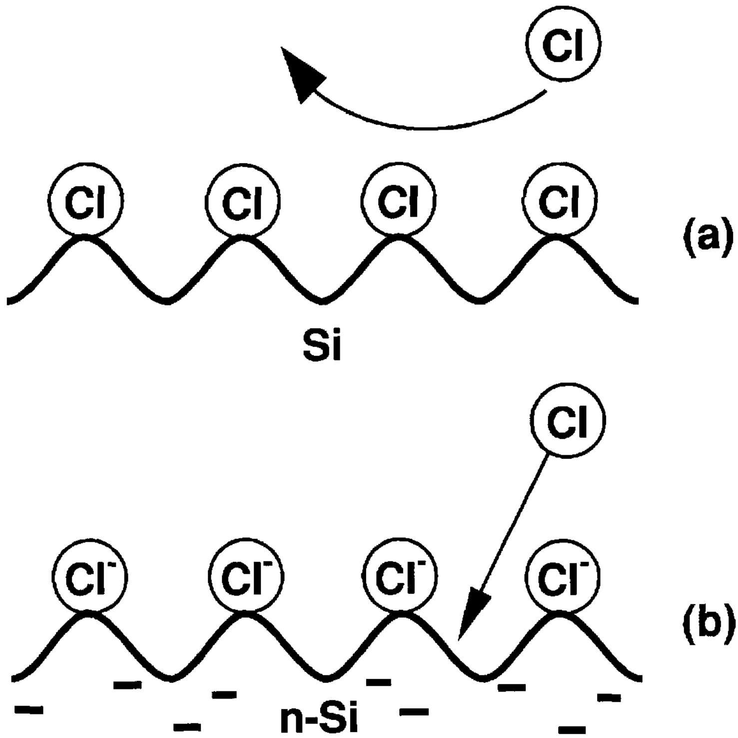

Fig. 6.3 *Steric hindrance impedes Cl atoms from reaching subsurface Si-Si bonds on the undoped silicon surface (a). The higher Fermi level in the doped material promotes charge transfer, and a more ionic Cl-Si bond allows the Cl access to additional sites (b).*

The results indicate that the lateral etching takes place only when the carrier concentration is above a threshold. Note the maximum solid solubility of antimony in silicon is 7×10^{19} cm^{-3} and its electrically active surface concentration is limited to 2 - 5×10^{19} cm^{-3} [6.12]. This carrier concentration is below the threshold concentration indicated, therefore, preventing the etching.

6.3.3 Feature size and time dependence of the lateral etching

The lateral etch rate of the n^+ buried layer has been examined as a function of spacing between structures (i.e. the trench width) and as a function of etching time. The results are shown in Fig. 6.5 and Fig. 6.6, respectively. It is clear from Fig. 6.5 that the etch rate drops slightly for trench widths below 3 μm. With higher dose (or higher etch rate) the reduction of the etch rate at a decreasing trench width is more significant. Fig.

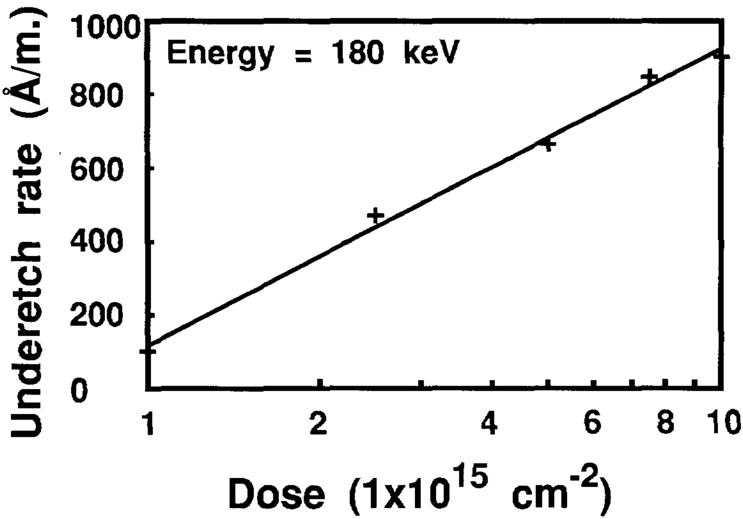

Fig. 6.4 *The lateral etch rate versus implantation dose of the As^+ implanted buried layer. Thermal anneal was performed at 1000°C for 45 min in Ar atmosphere.*

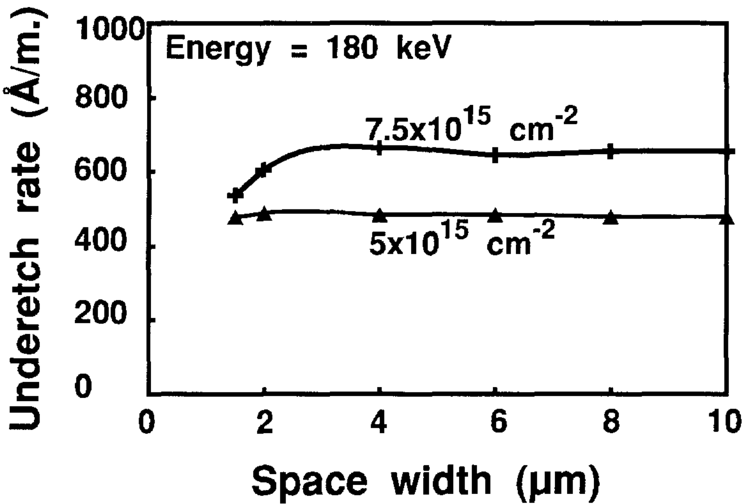

Fig. 6.5 *Dependence of the lateral etch rate on the spacing between the beams. The buried layer was formed by 180 keV As^+ implantation followed by 1000°C, 45 min anneal.*

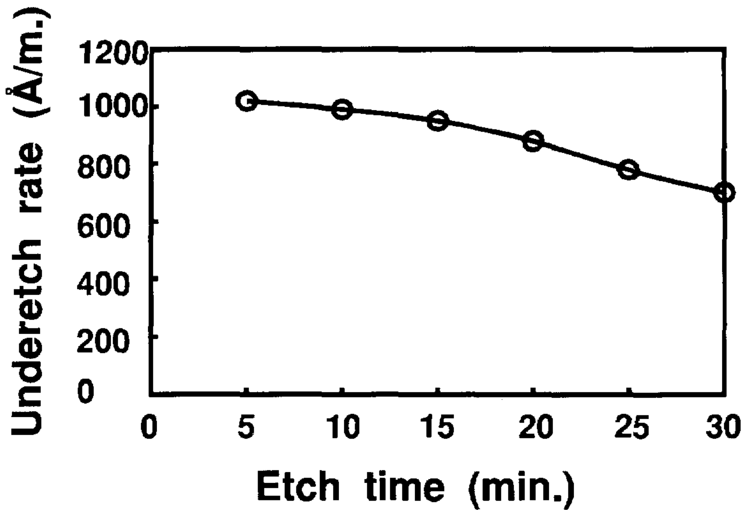

Fig. 6.6 *Time average lateral etch rate versus etch time. The buried layer was formed by 180 keV, 7.5×10^{15} cm^{-2} As^{+} implantation followed by 1000°C, 45 min anneal.*

6.6 shows that the etch rate also decreases over etch time.

The feature size and time dependence of the lateral etching is due to the fact that the etching is the result of spontaneous chemical reactions, which are related to the concentration of reactive Cl atoms on the reaction surface and to the rate of desorption of reaction products. When the trench is narrower than a certain width (3 μm in these experiments) or as the etching time increases (i.e. the reaction surface moves inward), the transportation of the reactive agents as well as the reaction products starts to be limited severely, resulting in the reduction of the etch rate. With higher doping level of the buried layer (higher lateral etch rate) the number of reactive agents needed and the reaction products created is higher than in the case of lower doping level. Therefore, the transportation limitation is more significant, as depicted in Fig. 6.5. The feature size dependency of the underetching practically limits the minimum spacing of microbeams to about 2 μm.

6.4 Optimization of the Cl_2/BCl_3 plasma etching chemistry

Although Cl atoms and Cl_2 molecules are the major reactants in the Cl_2/BCl_3 plasma, BCl_3 addition plays a key role in determining the etching characteristics for the

following two reasons.

1. Cl atoms etch silicon dioxide very slowly and this low etch rate often causes "black silicon" (surface roughness due to the non-uniform silicon etching caused by local masking effect of native oxide) [6.13]. Addition of BCl_3 enhances ion bombardment by providing BCl_x^+ ions [6.14], which removes the native silicon dioxide and therefore ensures the uniform etching.

2. BCl_3 is necessary to provide BCl_y radicals acting to inhibit sidewall etching and therfore, reduce bowing (additional etching at the upper part of the trench sidewalls) [6.15].

In the SIMPLE technique, Cl_2/BCl_3 chemistry was used to etch, on one hand, the lightly n-doped epitaxial layer anisotropically and, on the other hand, the heavily n-doped silicon isotropically. For this micromachining application, process variables of the etching chemistry must be carefully chosen to meet the two somewhat contradictory requirements. Since BCl_3 addition in the chemistry is meant to enhance ion bombardment and to provide the inhibitor for sidewall protection, it is expected that the BCl_3 content has a significant influence on the lateral etch rate of the heavily doped buried layer.

An orthogonal experimental design (which will be discussed in detail in Chapter 7) was carried out to understand the influence of RF power, chamber pressure, total gas flow rate and BCl_3 content on the etching characteristics, in particular the lateral etch rate of the n^+-doped silicon. The lightly n-doped silicon substrates for vertical etch rate experiments are (100) wafers with $\sim 1 \times 10^{16}$ cm^{-3} phosphorus doping. The heavily n-doped layer was formed by 180 keV, 7.5×10^{15} cm^{-2} arsenic implantation, followed by 1000°C, 45 min annealing in Ar atmosphere. The mask used were 5000 Å PECVD oxide.

6.4.1 Experimental design

The 4 variable, 3 level orthogonal design table $L_9 3^4$ (refer to Table 7.1) was chosen to construct the experiments. Starting with a baseline process using an RF power density of 0.57 W/cm^2, a pressure of 15 mTorr, a total gas flow rate of 25 sccm and a BCl_3/total gas flow rate ratio of 20%, a level variation using one higher level and one lower level was determined, yielding 3 level settings for each input variable. The input variables and the level settings chosen are summarized in Table 6.1.

The output functions of interest are the vertical etch rate of the lightly n-doped silicon

Table 6.1 *The input variables and their level settings for the Cl_2/BCl_3 plasma etching process optimization.*

Level setting	Input variable			
	Power (W/cm^2)	Pressure (mTorr)	Flow rate (sccm)	BCl_3 content (%)
1	0.43	11.25	20	10
2	0.57	15	25	20
3	0.71	18.75	30	30

R_v, the lateral etch rate of the heavily n-doped silicon R_l, the non-uniformity of the vertical etch rate U, the selectivity over the mask S_v and S_l for the vertical and lateral etching, respectively, the degree of bowing, B, and the Relative Linewidth Loss, RLL. Fig. 6.7 depicts the definition of B and RLL.

6.4.2 Results and analysis

Table 6.2 lists the etching results of all the experimental runs of the $L_9 3^4$ orthogonal table, together with an replicate of run 1, which is run 10, added to enable the estimation of the experimental errors. Note that all the data represents 10 min etching. Therefore, the lateral etch rate, which is time dependent, is the time average value.

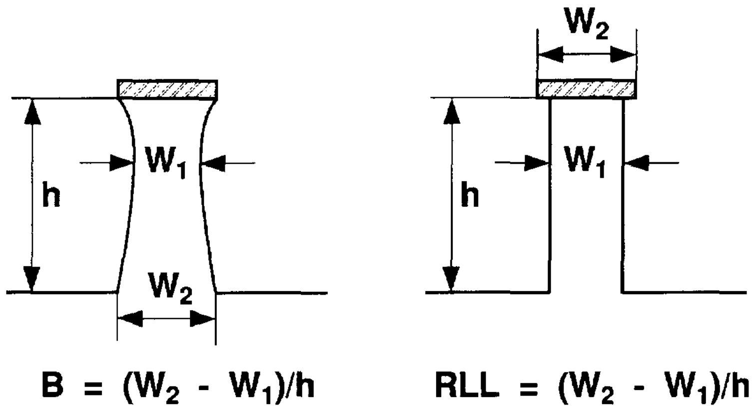

Fig. 6.7 *Definition of the degree of bowing B and Relative Linewidth Loss RLL.*

Table 6.2 *Experimental results of the orthogonal design for the Cl_2/BCl_3 chemistry.*

Experiments				Results						
P	p	F	C	R_v*	R_l*	U(%)	S_v	S_l	B	RLL
1	1	1	1	1854	892	2.1	8.2	4.0	.13	.15
1	2	2	2	1709	994	3.8	8.3	4.8	.045	.18
1	3	3	3	1538	153	2.6	7.5	.75	.10	.23
2	1	2	3	2121	497	.66	6.7	1.6	.11	.14
2	2	3	1	2646	1543	.84	8.7	5.1	.14	.12
2	3	1	2	2532	1541	2.2	8.7	5.3	.091	.15
3	1	3	2	2673	1286	.54	6.8	3.3	.069	.13
3	2	1	3	2866	1075	.73	7.2	2.7	.074	.088
3	3	2	1	3258	2038	2.1	8.7	5.5	.13	.12
1	1	1	1	1997	1083	1.3	8.9	4.8	.12	.14

* in Å/min.

Following the same data analysis procedure described in Section 7.3, the output function averages and the difference between the maximum and minimum values for each set of output function averages are obtained and listed in Table 6.3. The former indicates the trend of the first order effect of an input variable and the latter quantifies the significance of each input variable on the output functions.

a. Vertical etch rate

It is seen from the data of R_v1, R_v2 and R_v3 (the vertical etch rate averages of level setting 1, 2 and 3, respectively), that the vertical etch rate of the lightly n-doped silicon increases with the power, pressure and decreases with total flow rate and BCl_3 content. Among 4 ΔR_v's the one corresponding to the power is much higher than the others, indicating that the power is the most significant input variable determining the vertical etch rate.

Table 6.3 *Output function averages and the difference between the maximum and minimum values for each set of output function averages.*

Output average	Power	pressure	flow rate	BCl_3%
R_v1	1700	2216	2417	2586
R_v2	2433	2407	2363	2305
R_v3	2932	2443	2286	2175
ΔR_v	1232	227	132	411
R_l1	680	892	1169	1491
R_l2	1194	1204	1176	1274
R_l3	1466	1244	994	575
ΔR_l	787	352	182	916
U1	2.82	1.09	1.66	1.65
U2	1.23	1.8	2.18	2.18
U3	1.11	2.27	1.32	1.32
ΔU	1.72	1.18	0.86	0.86
S_v1	8.02	7.25	8.05	8.54
S_v2	8.03	8.07	7.91	7.93
S_v3	7.58	8.31	7.66	7.16
ΔS_v	0.45	1.06	0.39	1.38
S_l1	3.18	2.94	3.99	4.82
S_l2	3.98	4.2	3.95	4.47
S_l3	3.81	3.83	3.03	1.68
ΔS_l	0.8	1.26	0.96	3.14
B1	0.091	0.103	0.098	0.133
B2	0.114	0.087	0.095	0.068
B3	0.091	0.107	0.103	0.095
ΔB	0.024	0.02	0.0083	0.064
RLL1	0.185	0.138	0.130	0.128
RLL2	0.136	0.129	0.146	0.153
RLL3	0.110	0.165	0.156	0.151
ΔRLL	0.075	0.036	0.026	0.025

b. Lateral etch rate

From the data of R_l's it is known that the lateral etch rate of the heavily n-doped silicon

increases with the power, pressure but decreases with the total flow rate and BCl_3 content, similar to the results of the vertical etch rate of the lightly n-doped silicon. However, the BCl_3 content, in addition to the power, is the most important factor determining the lateral etch rate. This result implies that BCl_3 content indeed plays a key role in sidewall protection, which, on the one hand, keeps anisotropic etching of the lightly n-doped silicon and on the other hand, retards the lateral etching of the heavily n-doped silicon.

c. Uniformity of the vertical etch rate

It was found that the non-uniformity averages are rather small ($\leq 2.82\%$), as seen in Table 6.3. The good uniformity of the etching process is the result of the etching mechanism - ion bombardment-induced etching.

d. Selectivity of the vertical etching over the PECVD oxide mask

Data of S_v's show that the selectivity of vertical etching over the PECVD oxide mask is mainly determined by the pressure and BCl_3 content. It increases with pressure but decreases with the other 3 input variables. Higher pressure enhances the vertical etching, as shown above, while reduces ion bombardment energy and therefore reduces the oxide etch rate.

e. Selectivity of the lateral etching over the PECVD oxide mask

As shown in Table 6.3, the major input variables which influence the selectivity of lateral etching over the PECVD oxide mask are pressure and BCl_3 content, similar to the results of the selectivity of the vertical etching. The maximum selectivity occurs at the lower level of the BCl_3 content but the central level of the pressure.

f. Bowing and relative linewidth loss

The bowing and relative linewidth loss are important when small ($\sim\mu$m) feature sizes are desired. It can be seen from Table 6.3 that the degree of bowing and relative linewidth loss are rather small, indicating the Cl_2/BCl_3 chemistry presents very good anisotropic etching characteristics for the lightly n-doped silicon in the ranges of input variables used in the experiments.

6.4.3 The optimized etching process for SIMPLE

To maximize the width of the structure which can be made free-standing by laterally

etching the heavily n-doped buried layer underneath, the process recipe which may result in the highest lateral etch rate of the heavily n-doped silicon is preferable. Based on the above experimental results, the level settings of 3, 3, 2, 1 for power, pressure, total flow rate and BCl_3 content were chosen. This recipe is coincidentally one of the experimental runs of the orthogonal design (run 9). This recipe yielded a lateral etch rate of 2038 Å/min, which was indeed higher than obtained with any other runs. The vertical etch rate, the selectivity of the vertical etching and the selectivity of the lateral etching are 3258 Å/min, 8.71 and 5.45, respectively. The non-uniformity, the bowing and the Relative Linewidth Loss are 2.1%, 0.13 and 0.12, respectively, which are found to be satisfactory for the intended applications. Fig. 6.8 shows cross-sectional views of the etching profile with the optimized recipe.

6.5 Compatibility of the SIMPLE process with on-chip circuit fabrication

The SIMPLE technique can be readily incorporated in a standard bipolar process (DIMES01) [6.16] so that micromechanical structures can be fabricated on a single chip with electronic circuits. The on-chip integration will greatly enhance the performance of microelectromechanical systems. As shown in Fig. 6.9, the n^+ buried layer required for the mechanical structures can be formed as an additional step before epitaxial growth. Subsequently, all the processing steps necessary for the bipolar device are performed until aluminium interconnection. At the same time, the area for mechanical structures can be doped by diffusion (or implantation), if necessary. Then a 2 μm PECVD oxide is deposited at 350°C and patterned to serve as the mask for the final Cl-plasma etching to form the free-standing mechanical structures. Because the plasma etching is carried out as the final stage of the device fabrication, surface planarity necessary for the on-chip circuit fabrication is maintained.

6.5.1 Selection of the dopant for the n^+ buried layer

Care must be taken in selecting the dopant for the n^+ buried layer. As described previously, both phosphorus and arsenic doping can result in lateral etching of the buried layer. However, it is expected that arsenic is more suitable due to its much lower diffusivity (e.g. ~ 10^{-14} cm^2/s at 1050°C) than that of phosphorus (~ 10^{-13} cm^2/s at the same temperature). The high diffusivity of phosphorus may cause severe autodoping in the epitaxial growth, making it very difficult to control the resistivity of the overall epitaxial layer. Furthermore, phosphorus will diffuse out due to the thermal cycle in the subsequent processing steps. Fig. 6.10 shows the simulated doping profile of both arsenic- and phosphorus-doped buried layer after the complete DIMES01 process for

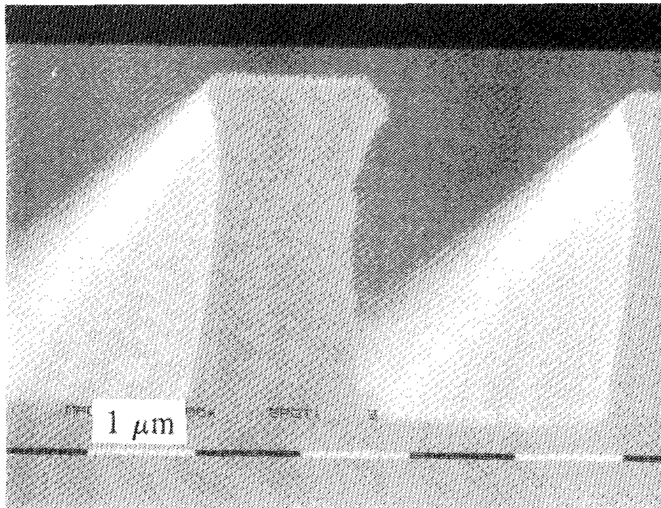

(a)

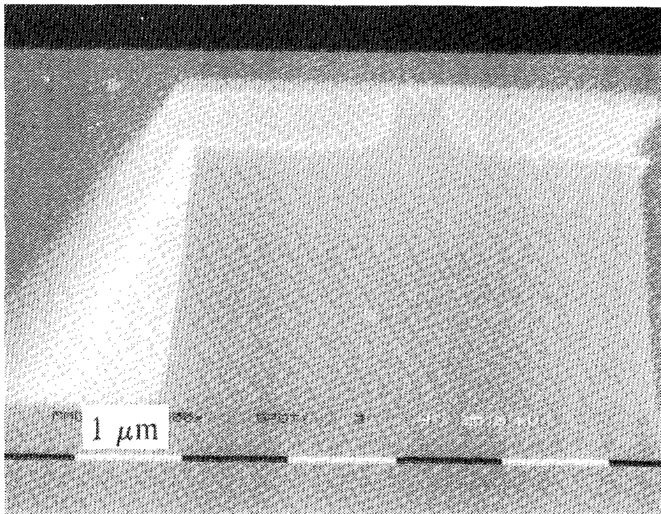

(b)

Fig. 6.8 *Cross-sectional views of the etching profile of lightly n-doped silicon (a) and heavily n-doped silicon (b) using the optimized plasma etching recipe: 0.71 W/cm² RF power density, 18.75 mTorr chamber pressure, 25 sccm total flow rate and 10% BCl_3 content.*

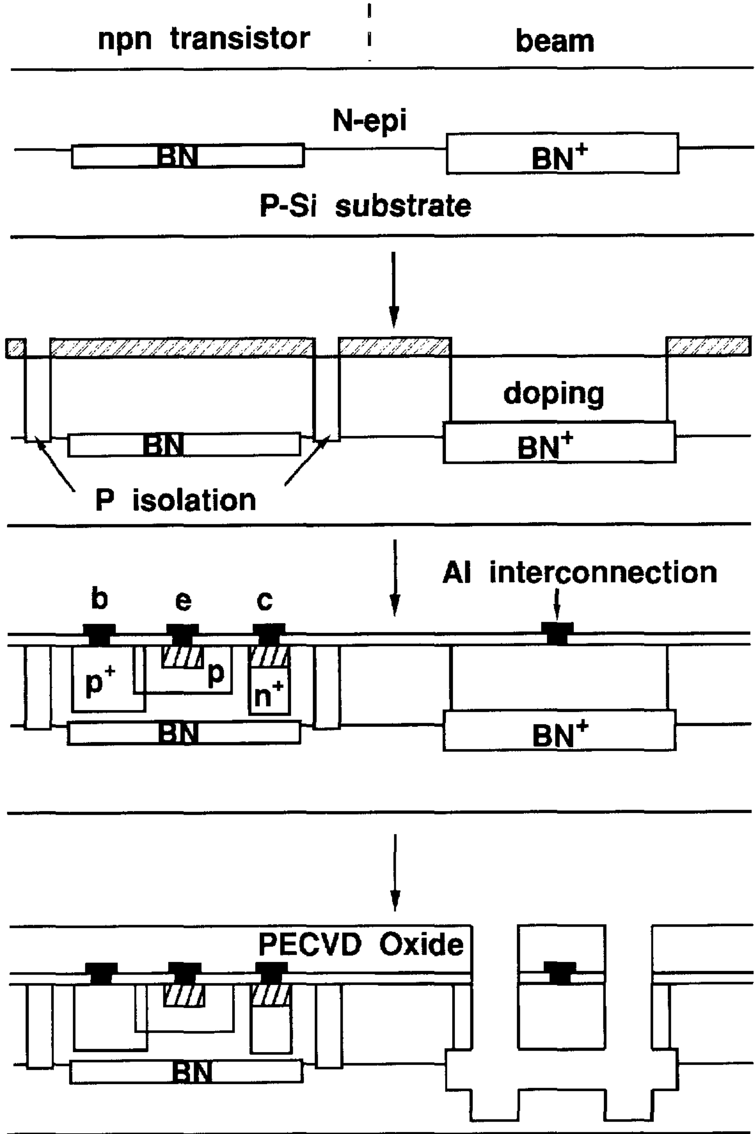

Fig. 6.9 *Process sequence of on-chip integration of microbeams with bipolar transistors by the SIMPLE and DIMES01 process.*

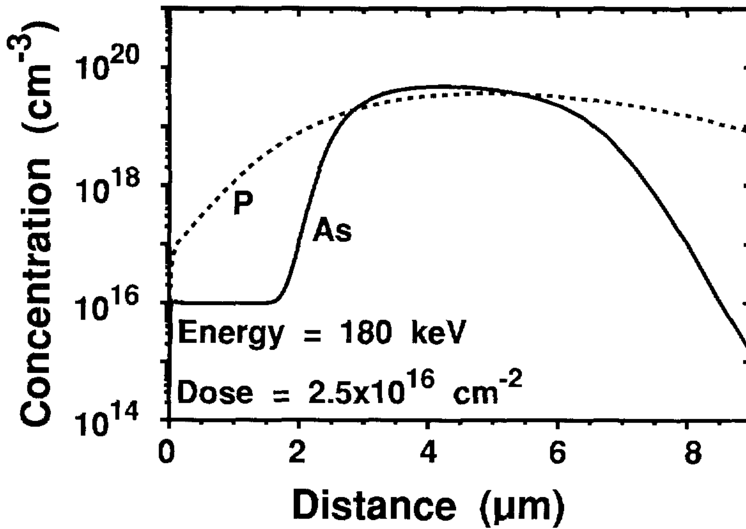

Fig. 6.10 *SUPREM3 simulation results of out-diffusion of the buried layer subjected to the standard DIMES01 bipolar process sequence.*

bipolar transistor fabrication is performed. It is seen that the out-diffusion of phosphorus is considerably more than that of arsenic. This out-diffusion may result in undesired doping to the active micromechanical structures above the buried layer and a reduction of the peak doping level of the buried layer, even below the threshold concentration of the lateral etching.

Even if arsenic is used, the high doping required for the underetching (~ 10^{20} cm^{-3}) may still result in significant autodoping in the epitaxial growth. Table 6.4 shows the effects of arsenic implantation dose of the n^+ buried layer on sheet resistance of the epitaxial layer and current gain of transistors fabricated using the DIMES01 process. It should be pointed out that the sheet resistance and the current gain were measured with the standard buried layer (antimony, 80 keV, 3×10^{15} cm^{-2}) underneath. The temperature for the epitaxial growth was 975 °C. It is evident that the sheet resistance, as well as the current gain, is significantly changed due to the autodoping. Such a modification of resistivity and transistor gain can alter or degrade circuit performance. Therefore, a cap layer (an encapsulating layer which prevents the dopant from out-diffusion during the epitaxial growth) [6.17] or lower temperature for the epitaxial growth should be used to suppress the autodoping.

Table 6.4 *The measured influence of implantation dose of the n^+ buried layer on the sheet resistance of the epitaxial layer and current gain of transistors above standard DIMES01 buried layer.*

Dose (cm^{-2}) (energy 180 keV)	$R_{\square}$ of epi ($\Omega/\square$)	h_{FE}	
		vertical npn	lateral pnp
As, 7.5×10^{15}	889.7		64.6
As, 1×10^{16}	791.2		63.8
As, 2.5×10^{16}	511.8	123.6	54.4
Sb, 80 keV, 3×10^{15} (DIMES01 process)	1200-1500	100	75

6.5.2 Selection of the doping for the mechanical structures

In principle both p-type and n-type doping can be used for the mechanical structures, as long as the concentration of the latter is not above the threshold of the lateral etching (8×10^{19} cm^{-3}). P-type doped structures have the advantages of self-isolating because the epitaxial layer is n-doped, which facilitates the structural design. However, in some applications the p-type doping is required to extend the whole epitaxial thickness to obtain, e.g. the maximum sidewall capacitance of the structure. The p-type area, together with the n^+ buried layer, will form a p-n^+ diode, whose breakdown voltage will be low if high doping is used for the p-type area. Fig. 6.11 shows the carrier concentration profile of such a p^+-n^+ diode, in which the p^+ region is formed using the same boron diffusion as that for the transistor isolation in DIMES01 process. It is seen that the doping level at the two sides of the diode is as high as $\sim10^{20}$ cm^{-3}. The breakdown voltage of such diode was found to be $2\sim3$ volts only and thus the p^+-n^+ junction should be avoided.

Another limitation of using the high concentration p-type doping for the mechanical structure is the residual strain profile caused by the non-uniform profile of high boron doping. Because the radius of boron atoms (0.88 Å) is smaller than that of silicon (1.17 Å), high boron doping level ($\geq 7\times10^{19}$ cm^{-3}) produces tensile strain [6.18] in the layer, which is not uniform along the depth the layer because of the non-uniform doping profile (shown in Fig. 6.11). The strain profile of the p^+ region has been characterized using Raman scattering spectroscopy [6.19].

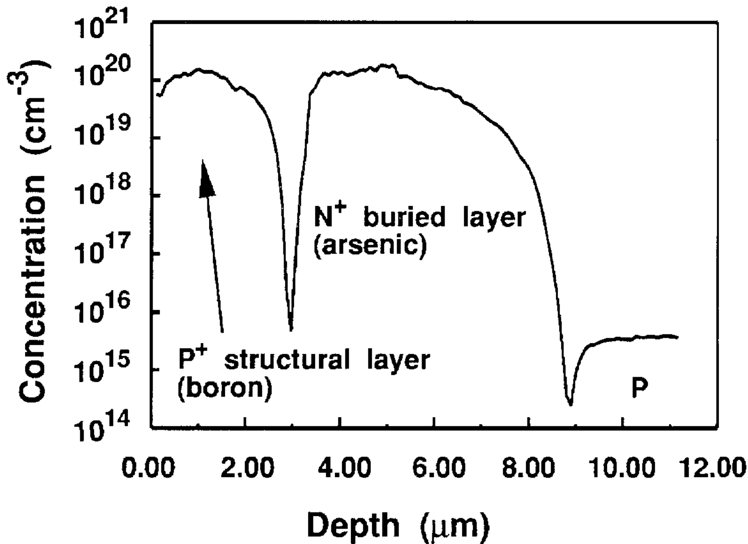

Fig. 6.11 *Carrier concentration profile of the deep boron diffusion for transistor isolation of DIMES01 process with an n^+ buried layer underneath.*

Fig. 6.12 shows the Raman spectrum of the p^+-doped layer, together with the carrier concentration profile of the sample. The broadening and the asymmetry of the peaks up to 4 μm from the surface is mainly due to the doping. It is seen that the position of the peaks up to 4 μm distance from the surface is shifted compared with that of the remaining peaks, which is a combined effects of both high carrier (hole) concentration and the residual strain [6.19]. Using a so-called Fano-type line shape fitting [6.20] which takes into account the effect of the free carrier alone, the effects of the residual strain on the frequency shift can be separated and the net, strain-related frequency shifts are listed in Table 6.4. It is seen that the largest shift, and thus the highest residual strain, takes place at the depth of ~ 2 μm from the surface. After released from the substrate, the structure will buckle if the residual strain is high enough. Such buckling is evident with the p^+ structure with a doping profile shown in Fig. 6.11, as shown in Fig. 6.13. Although it has been reported that high temperature (1100°C) oxidation could significantly modify the residual stress distribution and therefore may release the buckle problem [6.21], the required high-budget thermal processing will result in severe out-diffusion of the n^+ buried layer. Therefore, p-type doping is useful for the micromechanical structure only when the depth of the doping is restricted not to extend to the n^+ buried layer and only when the doping level is not high enough to cause significant residual strain profile ($< 7 \times 10^{19}$ cm^{-3}).

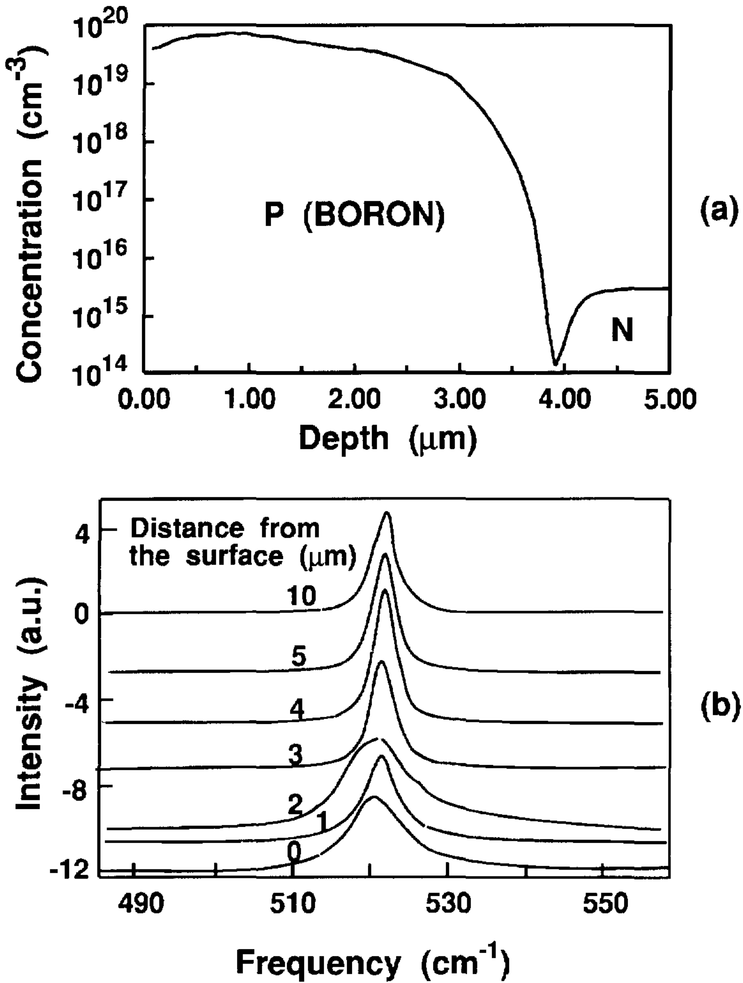

Fig. 6.12 *Raman scattering spectrum of the silicon substrate with the 4 μm deep boron diffusion for transistor isolation. (a) carrier concentration profile. (b) the Raman spectrum.*

N-type doping (of a concentration lower than the threshold for lateral etching) of the mechanical structure is an alternative which provides possibility of extending the depth of the doping to the whole epitaxial thickness. Since the structure and the buried layer are both n-type, the breakdown voltage of such an n-n$^+$ structure when reversely biased relative to the p-type substrate is solely determined by the doping level of the substrate, which was found as high as ~30 volts. However, since the epitaxial layer is also of the n-type, proper measures must be taken to electrically isolate the mechanical structure

Table 6.5 *Shift of the peak frequency of the spectrum (S) due to the residual strain as a function of the distance from the wafer surface (D).*

D (μm)	1	2	3	4	5	10
S* (cm^{-1})	-0.5	-2.0	-0.3	-0.1	0.1	0

*Measurement uncertainty is of the order of 0.3 cm^{-1}.

from each other, e.g. by using the same deep boron diffusion as that for transistor isolation, in combination with trench isolation provided by the trench etching of epitaxial layer. This isolation scheme is shown in plane view in Fig. 6.14. The requirement for the extra isolation results in restriction to the form of the structure.

Fig. 6.15 shows the SEM photo of a free-standing microbridge without buckling, which is doped by 180 keV, 1×10^{15} cm^{-2} phosphorus ion implantation, followed by 1000°C, 43 min steam oxidation and 45 min annealing in Ar. The carrier concentration profile of such a structure obtained by spreading resistance measurement is shown in Fig. 6.16. It can be seen that the doping level is well below the threshold (8×10^{19} cm^{-3}) and the doping extends only about half of the epitaxial thickness due to the limited implantation depth.

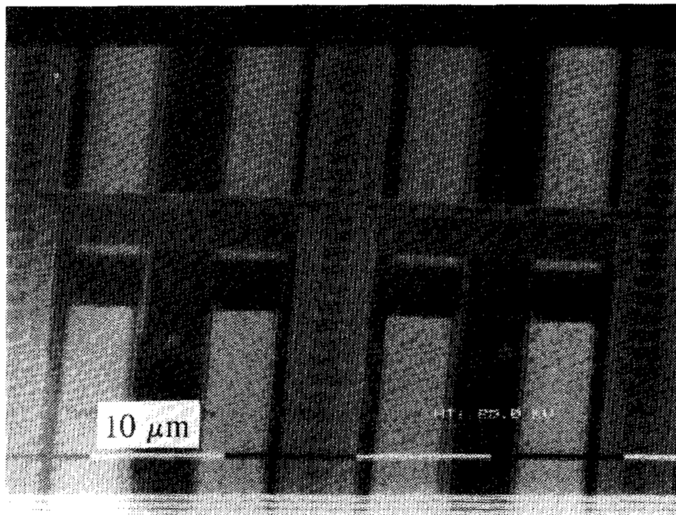

Fig. 6.13 *SEM photograph showing buckling microbridge doped with deep boron diffusion.*

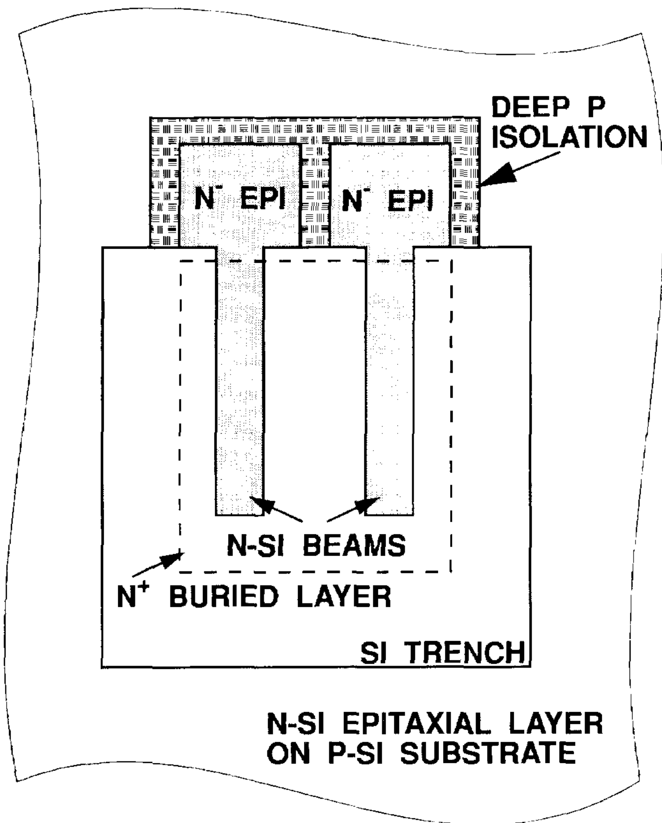

Fig. 6.14 *Isolation scheme for n-type microbeams using the combination of deep boron diffusion and trench etching.*

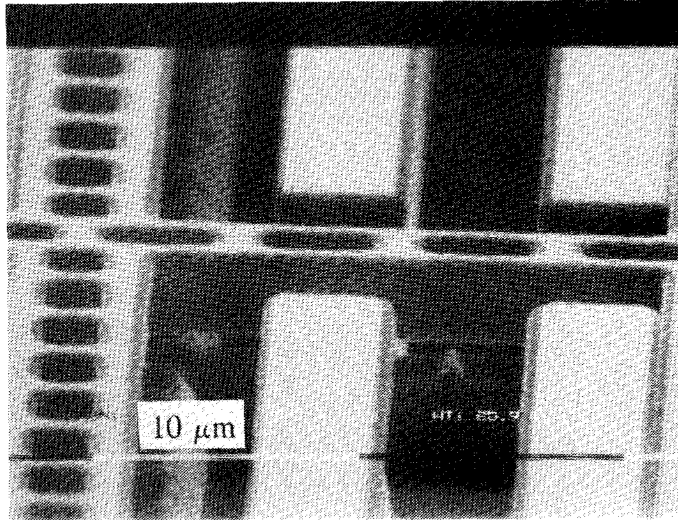

Fig. 6.15 *SEM photograph of microbridge doped with 180 keV, 1×10^{15} cm^{-2} phosphorus implantation without buckling.*

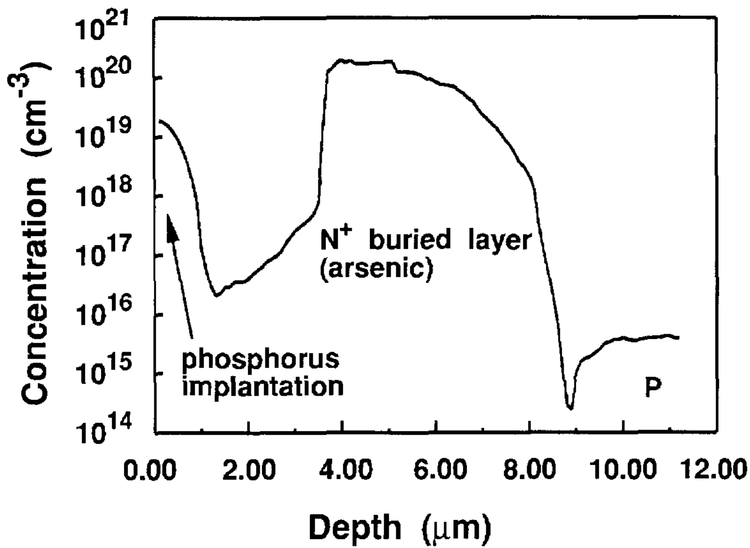

Fig. 6.16 *Measured carrier concentration profile of the 180 keV, 1×10^{15} cm^{-2} phosphorus implantation and the n^{+} buried layer on p-type substrate.*

6.5.3 Passivation of the exposed pn junction

During the lateral etching, the n^+ buried layer is simultaneously etched vertically. As a result, the pn junction formed by the n^+ region and p-type substrate will be etched-through and the sidewall of the junction is therefore exposed to the air. If there is no further passivation step, the exposure of the junction will result in surface leakage current, which degrades the isolation performance of the junction and even causes failure of the device.

Therefore, after the plasma etching, a thin (~1000 Å) PECVD oxide layer was conformally deposited to cover the sidewall of the pn junction and therefore to reduce the leakage current. It was found that the leakage current of a pn junction with ~2500 μm long exposed sidewalls was greatly reduced from 300 μA to 25 μA. A subsequent maskless plasma etching-back using CHF_3/CF_4 chemistry is necessary to remove the PECVD oxide on top of aluminium surface to facilitate final bonding of the device. Due to the anisotropy of the plasma etching-back, the passivating PECVD oxide on the sidewalls of the exposed junction is maintained.

6.6 Limitation of the SIMPLE technique

The release of micromechanical structures from the silicon substrate relies on the plasma lateral etching of the heavily n-doped buried layer. As described previously, PECVD oxide is used as the mask for both the vertical etching-through of the epitaxial layer and the lateral etching. The PECVD oxide thickness is usually ~2 μm. To etch through the 4 μm epitaxial layer approximately 0.5 μm PECVD oxide is removed due to the limited selectivity (~ 8). Therefore, the maximum underetching time with the remaining 1.5 μm PECVD oxide mask is about 37 minutes (etch rate for the PECVD oxide is about 400 Å/min). As was shown in Fig. 6.6, the lateral etch rate tends to decrease as the etching proceeds. Therefore, practical limitations cause the beam width which can be achieved to be limited to ~ 4 μm (i.e. 2 μm underetching from each side of the beam). Larger widths would require unacceptably long etching time and thick mask layer. If wider beams or membranes are desired, additional windows need to be opened inside the structure to facilitate the underetching.

6.7 Conclusions

A technique for the fabrication of silicon micromechanical structures by plasma etching (SIMPLE) has been developed. The technique involves formation of an n^+ buried layer before epitaxial growth and a single plasma etching which etches the epitaxial layer

anisotropically but the n^+ buried layer laterally. Free-standing single-crystal microbeams with vertical sidewalls can be produced. The height of the beam is the same as the thickness of the epitaxial layer while the lateral feature size of the beam can be very small (~ 1 μm). In such a way high aspect ratio (height to width) and closely separated microbeams can be realized, which are very suitable for sensor and actuator applications based on sidewall electrostatic driving or capacitive detection. Since the releasing of the micromechanical structure is performed in a plasma (dry) environment, sticking problems normally associated with wet sacrificial etching in conventional surface micromachining can be eliminated.

The lateral etching of n^+ buried layer is dependent on the concentration of the electrically activated dopants, with a threshold concentration of approximately 8×10^{19} cm^{-3}. The lateral etch rate reduces when the spacing between the beams is less than 3 μm and with increasing etch time. Arsenic is found to be the most suitable dopant for the n^+ buried layer. This is because the maximum electrically active concentration of antimony (2 - 5×10^{19} cm^{-3}) is below the threshold concentration and phosphorus has a much higher diffusivity than arsenic, which causes problems of autodoping during subsequent epitaxial growth and out-diffusion in the high temperature cycles.

The Cl_2/BCl_3 chemistry used for the plasma etching has been characterized using an orthogonal experimental design. It was found that high pressure, low BCl_3 content and high RF power are beneficial to the lateral etching of the n^+ buried layer, while the total gas flow rate has minor influence on the etching. The optimized chemistry, which uses 125 W power, 18.75 mTorr pressure, 25 sccm total flow rate and 10% BCl_3 content, results in anisotropic etching of the epitaxial layer with an etch rate of 3258 Å/min and lateral etching of the n^+ buried layer with an etch rate of 2038 Å/min.

The SIMPLE technique can be readily combined with standard bipolar processing to realize on-chip integration of microstructures with electronic circuits. The n^+ buried layer can be formed as an additional step before epitaxial growth. Although extra electrical isolation scheme is required, n-type doping for the micromechanical structure is preferred to p-type doping as the latter may lead to high residual strain in the structural layer and low breakdown voltage of the isolating pn-junction. After the formation of the free-standing microstructures, a PECVD oxide passivation layer is needed to cover the exposed sidewalls of the pn-junction formed between the structural layer and the substrate. Although the beam achieved is less than 4 μm wide due to the limited lateral etch rate, additional windows can be opened in the beam to facilitate underetching if wider beams are desired in a way similar to surface micromachining technique.

References

[6.1] K. E. Petersen, "Silicon as a mechanical material," *Proc. IEEE*, Vol. 70, pp. 420-457, 1982.

[6.2] R. T. Howe, "Surface micromachining for microsensors and microactuators," *J. Vac. Sci. Technol.*, Vol. B6, pp. 1809-1813, 1988.

[6.3] M. Mehregany, S. D. Senturia, J. H. Lang and P. Nagarkar, "Micromotor fabrication," *IEEE Trans. Electron Devices*, Vol. ED-39, pp. 2060-2068, 1992.

[6.4] T. C. Core, W. K. Tsang and S. J. Sherman, "Fabrication technology for an integrated surface-micromachined sensor," *Solid State Technol.*, Vol. 36, pp. 39-47, Oct. 1993.

[6.5] K. A. Shaw, Z. L. Zhang and N. C. MacDonald, "SCREAM I: A single mask, single-crystal silicon, reactive ion etching process for microelectromechanical structures," *Sensors and Actuators*, Vol. A40, pp. 63-70, 1994.

[6.6] G. C. Schwartz and P. M. Schaible, "Reactive ion etching of silicon," *J. Vac. Sci. Technol.*, Vol. 16, pp. 410-413, 1979.

[6.7] D. L. Flamm, "Introduction to plasma chemistry," in *Plasma Etching - an Introduction*, D. M. Maros and D. Flamm, Eds., Academic Press, California, 1989, pp. 91-184.

[6.8] C. J. Mogab and H. L. Levenstein, "Anisotropic plasma etching of polysilicon," *J. Vac. Sci. Technol.*, Vol. 17, pp. 721-730, 1980.

[6.9] S. Berg, C. Nender, R. Buchta and H. Norstrom, "Dry etching of n- and p-type polysilicon: parameters affecting the etch rate," *J. Vac. Sci. Technol.*, Vol. A5, pp. 1600-1603, 1987.

[6.10] D. L. Flamm and V. M. Donnelly, "Anisotropic etching in chlorine-containing plasmas," *Solid State Technol.*, Vol. 24, pp. 161-166, April 1984.

[6.11] *TMA SUPREM-3, One-Dimensional Process Analysis Program*, Technology Modelling Associates, Inc., California, December, 1988.

[6.12] Ghandhi, in *VLSI Fabrication Principles, Silicon and Gallium Arsenide*, John Wiley & Sons, New York, 1983, pp. 70-170.

[6.13] T. M. Krawiec and N. J. Giammarco, "Reactive ion etching of deep isolation trenches using sulphur hexafluoride, chlorine, helium and oxygen," in *the Proc. of SPIE*, Vol. 1392, 1990, pp. 265-271.

[6.14] D. L. Flamm, "Introduction to plasma chemistry," in *Plasma Etching - an Introduction*, D. M. Maros and D. Flamm, Eds., Academic Press, California, 1989, pp. 146-153.

[6.15] J. S. Maa, H. Gossenberger and L. Hammer, "Effects on sidewall profile of

Si etched in BCl_3/Cl_2 chemistry," *J. Vac. Sci. Technol.*, Vol. B8, pp. 581-585, 1990.

[6.16] L. K. Nanver, E. J. G. Goudena and H. W. van Zeijl, "DIMES01, a baseline BIFET process for smart sensor experimentation," *Sensors and Actuators*, Vol. A36, pp. 139-147, 1993.

[6.17] T. Ishii, K. Takahashi, A. Kondo and K. Shirahata, "Silicon epitaxial wafer with abrupt interface by two-step epitaxial growth technique," *J. Electrochem. Soc.*, Vol. 122, pp. 1523-1531, 1975.

[6.18] W. H. Chu and M. Mehregany, "A study of residual stress distribution through the thickness of p^+ silicon films," *IEEE Trans. Electron Devices*, Vol. ED-40, pp. 1245-1251, 1993.

[6.19] E. Anastassakis, "Strain characterization in semiconductor structures and superlattices," in *Light Scattering in Semiconductor Structures and Superlattices*, D. J. Lockwood and J. Y. Young, Eds., Plenum Press, 1991, pp. 173-196.

[6.20] M. Jouanne, M. A. Kanehisa, J. F. Morhange, N. M. Ravindra and M. Balkanski, "Bound state energy and line width due to the resonant interaction between optical phonon and electronic transitions in degenerate silicon," *Solid-State Electronics*, Vol. 28, pp. 39-45, 1985.

[6.21] W. H. Chu and M. Mehregany, "A study of residual stress distribution through the thickness of p^+ silicon film," *IEEE Trans. Electron Devices*, Vol. ED-40, pp. 1245-1250, 1993.

Chapter 7 Plasma Etching Process Optimization Using Statistical Experimental Design and Data Analysis - a Case Study

7.1 Introduction

Despite its widespread use, plasma etching remains a poorly understood process. The plasma chemistry of even simple etch systems involves many chemical reactions and is complicated by the strong interaction between electrical and physical effects, thus creating an operation space that is difficult to characterize. Plasma modelling from fundamental chemical and physical standpoints has had limited success. All potentially significant plasma reactions can be mathematically represented, and the creation, transport and loss of species can be modelled from a continuum approach [7.1] and/or by Monte Carlo simulation [7.2]. However, the rate coefficients and/or cross-sections for most reactions are unknown. Due to the extremely complex nature of particle dynamics within a plasma, the connection between these microscopic models and macroscopic characteristics such as etch rate has yet to be clearly distinguished.

Therefore, practical etcher operation is carried out primarily through process recipes. Functional relationships between manipulated instrumentational variables (or input variables, such as power, chamber pressure, reactant flow rate, etchant composition etc.), plasma process variables (such as electron density, electron energy distribution, plasma species density, ion energy, ion flux etc.) and performance variables or responses (such as etch rate, selectivity, uniformity, anisotropy etc.) are not well-established. Many process variables are not directly or easily measurable, and thus have been ignored in process development. Therefore, levels of each input variable are found which produce acceptable responses through a process of trial and error. The established recipes are not always transferable between different etch chemistries or from one reactor to the other.

Since it is presently not possible to model plasma process from a fundamental approach, parametric (empirical) modelling techniques are both necessary and appropriate. Statistical experimental design and data analysis methods such as orthogonal design [7.3] and Response Surface Methodology (RSM) [7.4-7.5] are very powerful tools in this aspect. These techniques have been used to obtain statistical models of etch rates of various thin films [7.6-7.8], to develop techniques for real-time monitoring and control in plasma etching of silicon and silicon dioxide using CF_4/O_2 and CF_4/H_2, respectively

[7.9], and to obtain a comprehensive set of empirical models for etch rates, selectivity, uniformity and anisotropy of n^+-polysilicon etching using a $CCl_4/He/O_2$ plasma [7.10]. In this chapter, both orthogonal design and RSM are explored to characterize and optimize SF_6/O_2 plasmas for silicon trench etching required in silicon sensor fabrication.

7.2 Experimental design consideration

Because of the large number of input variables (factors), plasma process development should usually be considered as a multi-dimensional problem. A process is in practice often developed by varying one factor at a time, while holding all other factors at some constant level (the so-called one dimensional search). This approach does not require a statistical design and can results in successful process development if an appropriate base-line recipe is already available, as can be seen from previous chapters. However, it is expensive and can yield incomplete and often misleading results. This type of experimentation requires testing at many factor levels, does not account for experimental errors and ignores interactions among independent input variables. Therefore, a structured strategy of experimental design needs to be implemented to extracting as much information as possible from a limited number of experiments. The unifying feature of statistically designed experiments is that all factors are varied simultaneously, in contrast to the one dimensional search. Statistical experimental designs include mainly factorial designs and fractional factorial designs.

7.2.1 Factorial design

Factorial designs consist of statistical experiments using all combinations of level settings for all input variables [7.11]. The experimental results are analyzed to understand the correlations between these variables and the performance variables, including the effects of individual input variables and also the effects of interactions between the variables [7.12]. Although factorial designs are thorough in a sense of covering all possibilities of input variable combinations, these contain a large number of experiments, which makes this method very expensive. The total number of experiments for k factors at m levels is m^k. For example, in the case of 4 factors at 3 levels, 81 (3^4) runs are required. The exponential increase in the total number of experiments with the number of variables prevents this design to be practical when k is larger than 4, which is often the case in plasma process development.

7.2.2 Fractional factorial design

Fractional factorial designs are a subset of factorial designs that reduce the number of

experiments to be performed by exploring only a fraction (such as one-half) of the input variable space in a systematic manner. A number of fractional factorial design approaches have been developed, including orthogonal designs [7.13], the Face-Centred Cube (FCC) designs, Box-Behnken designs and Central Composite designs [7.11][7.14-7.15].

In orthogonal designs, certain representative combinations of level settings for input variables are selected. These level settings fit into orthogonal tables. As an example, such a table for 4 factors at 3 levels is shown in Table 7.1. The factor level codings of 1, 2 and 3 designate the lower, central and upper level of the variables, respectively. By following the orthogonal tables, the optimum compromise is obtained between the maximum information and the least number of experiments [7.3]. Statistical analysis of the resulting data emphasizes first order effects, i.e., the main effects of each individual input variable on performance variables. In the case of 4 factors at 3 levels, only 9 experimental runs are required. Factor interaction can be obtained by using one column of the orthogonal tables as the interaction column [7.16]. However, there are only certain numbers of input variables and level settings for which orthogonal tables can be derived. This limits the application of orthogonal designs.

Table 7.1 *The orthogonal table designated for 4 factors at 3 levels $L_9 3^4$.*

Run	Manipulated variable			
	1	2	3	4
1	1	1	1	1
2	1	2	2	2
3	1	3	3	3
4	2	1	2	3
5	2	2	3	1
6	2	3	1	2
7	3	1	3	2
8	3	2	1	3
9	3	3	2	1

Common designs for 3 variable case are illustrated in Fig. 7.1: (a) the Box-Behnken design with 15 runs, and (b) the FFC design with 17 runs. The factor level codings of -1, 0 and +1 represent the lower, central and upper level of the variables, respectively. Both designs include replicates of the test which uses the centre settings for all the factors, aiding the quality of the prediction by allowing estimation of experimental errors. Furthermore, these designs have a number of degrees of freedom (the number of experiments minus the number of coefficients in an empirical model) to estimate residual error. The designs are easily extended to cases involving a larger number of factors.

With Central Composite designs experiments are carried out with five levels per factor. It is a variation of the FCC design with the trials at the centres of the faces pushed outward a distance of $2^{k/4}$, in which k is the number of factors, thereby sampling at positions all equally spaced from the centre. The 3 factor Central Composite design is shown in Fig. 7.2. The design generally requires fewer trials than the Box-Behnken or FCC design for large numbers of factors, but has the disadvantage of not covering the primary region of interest (-1 to +1) as well.

7.2.3 Determination of the relative importance of factors

In a plasma process, as discussed in chapter 2, a large number (≥ 7) of input variables exist. Even if a fractional experimental design is applied, the required number of experiments is overwhelming. Although possible, it is time consuming and very costly to carry out all the experiments required on all input variables. Therefore, a strategy to determine the relative importance of factors, and thus to allow the selection of the factors that influence each performance most, is necessary.

A physical understanding of the process can suggest which factors are important. However, the complexity of plasma etching process typically makes *a priori* decisions about the significance of variables difficult. Preliminary testing is often used to select the most significant variables to determine the feasible ranges of input parameters and to observe the process sensitivity to each variable.

A very effective method to facilitate the selection of the most significant variables is one based on screening designs. Screening designs are experimental designs developed to test a large number of variables with few experiments [7.15]. These designs are run and analyzed by fitting the results to a linear model. The most significant variables are selected as those with the largest absolute coefficients. Table 7.2 shows an example of screening designs with twelve runs for up to eleven factors, together with the supposed results of the 12 run experiments. If the data are fitted into a linear model, the

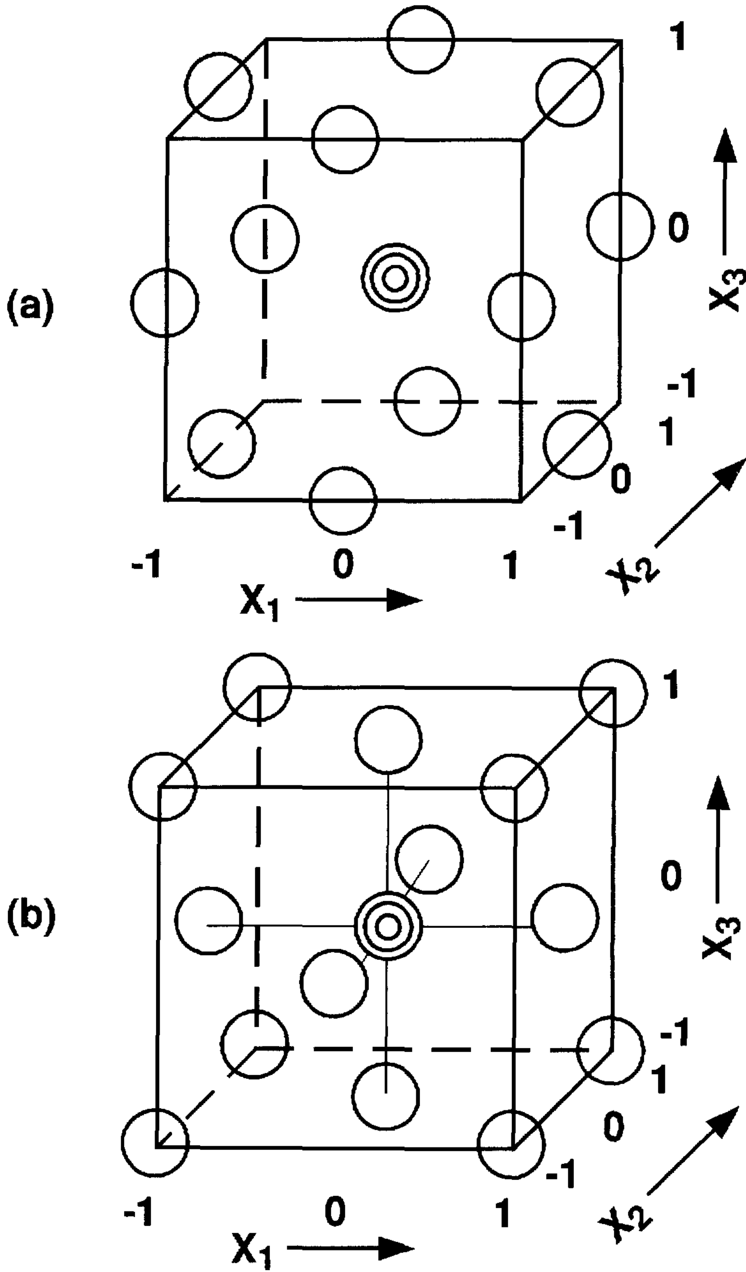

Fig. 7.1 *Geometric representation of experimental designs with 3 variables: Box-Behnken design (a) and Face-Centre-Cube design (FCC) (b).*

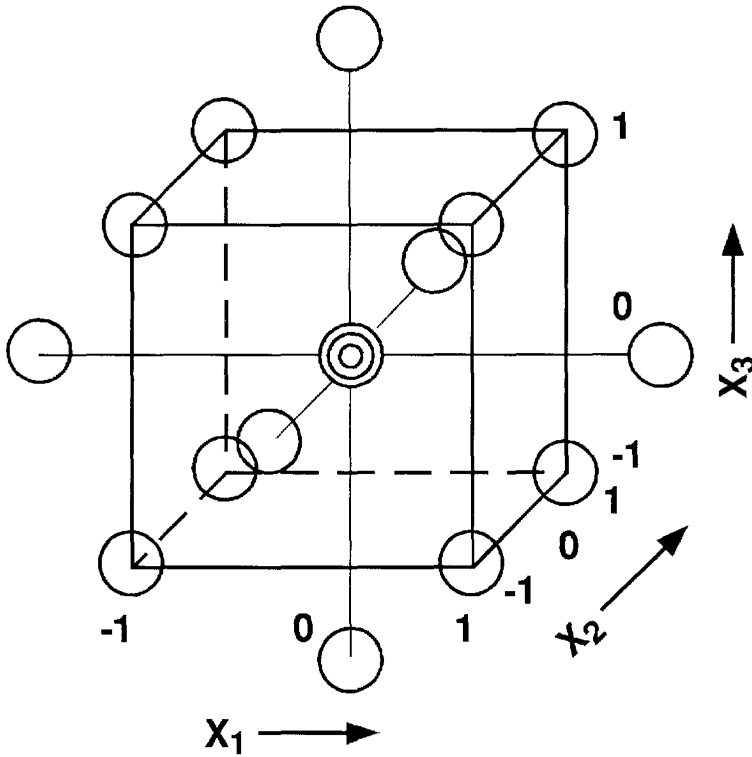

Fig. 7.2 *Geometric representation of the Central Composite design of 3 variables.*

following expression is resulted:

$$R = 8.28 + 2.423\times A - 0.943\times B - 4.093\times C + 0.46\times D + 0.52\times E + 0.3\times F + 3.26\times G + 2.68\times H - 1.577\times I - 5.41\times J + 0.407\times K \quad (7.1)$$

Obviously the factors B, D, E, F and K are less important than the remaining ones since the coefficients corresponding to them are small. Screening designs exist for 4C - 1 factors in 4C runs for any integer C. However, not all screening designs exist for all values of k (the number of factors).

Table 7.2 *Twelve-run screening design for 11 factors.*

	Factors											Result
	A	B	C	D	E	F	G	H	I	J	K	
1	+	+	-	+	+	+	-	-	-	+	-	5.63
2	+	-	+	+	+	-	-	-	+	-	+	6.42
3	-	+	+	+	-	-	-	+	-	+	+	1.38
4	+	+	+	-	-	-	+	-	+	+	-	1.94
5	+	+	-	-	-	+	-	+	+	-	+	11.5
6	+	-	-	-	+	-	+	+	-	+	+	12.1
7	-	-	-	+	-	+	+	-	+	+	+	5.72
8	-	-	+	-	+	+	-	+	+	+	-	0.7
9	-	+	-	+	+	-	+	+	+	-	-	12.6
10	+	-	+	+	-	+	+	+	-	-	-	13.3
11	-	+	+	-	+	+	+	-	-	-	+	7.73
12	-	-	-	-	-	-	-	-	-	-	-	8.28

7.3 Development of a SF_6/O_2 plasma etching process for etch-through of silicon membranes using orthogonal design

7.3.1 Process requirements

In bulk micromachining, formation of many micromechanical structures requires plasma etching-through of silicon membranes, which are usually formed by wet anisotropic etching in, e.g. KOH solutions. Fig. 7.3 shows such an example in which a silicon membrane needs to be patterned to form supporting beams (springs) for a bulk-micromachined accelerometer [7.17]. To facilitate the process, it is desirable to use photoresist as the mask for the etching-through. Etching selectivity over the resist mask is the major concern in the process development. Since the membrane can be as thick as 8 μm, the selectivity must be at least 4 for a standard resist thickness of 2 μm. Furthermore, etch rate must be high (preferably more than 3000 Å/min) and the non-uniformity of the etch rate must be minimized. The anisotropy of the process is not very critical since linewidth loss due to lateral etching can be compensated by proper mask

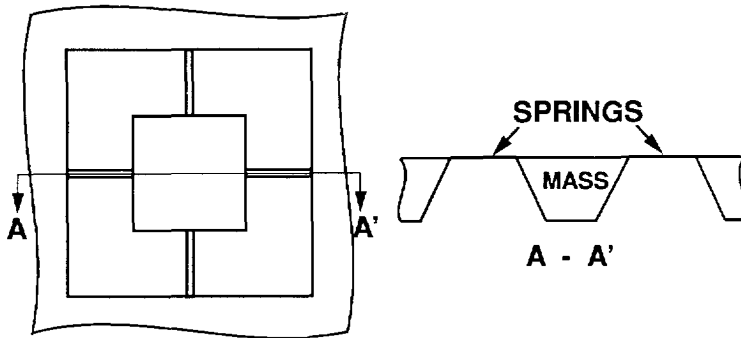

Fig. 7.3 *Schematic view of a bulk-micromachined accelerometer showing the necessity of plasma etching-through of the silicon membrane to form the supporting beams.*

design, if desired.

In the remaining part of the Section 7.3, the procedure outlined in [7.3] will be closely followed to carry out a set of orthogonal design to optimize a SF_6/O_2 chemistry for the membrane etching-through.

7.3.2 Orthogonal design

As shown in Table 7.1, an orthogonal table consists of a left hand column and a top row, with various numbers at the intersections of each column and row. Each element in the top row represents an independent input variable, and each element in the left hand column represents an experimental run. The elements in the intersections indicate the level settings that apply to that input variables for that experimental run.

A matrix can be called orthogonal if and only if the following requirements are met [7.3]:

1. The number of occurrences of each level setting must be equal within each column.

2. All rows having identical level settings in a given column must have an equal number of occurrences of all other level settings in the other columns.

3. The matrix for a given number of columns must be the one with the minimal number of rows that satisfy the above conditions.

For example, consider the orthogonal table designated $L_9 3^4$ (Table 7.1). This table applies to 4 input variables, each of which can be varied over 3 level settings. Nine experimental runs are required to complete the matrix.

It is the property of orthogonality, as defined above, that allows statistical analysis of the data that, in effect, fills in the "blanks" in the full factorial analysis that are not run as experiments in the orthogonal design. When the average value of an output function is taken for a group of runs having the same level setting for a given input variable, the first order effects of the other input variables cancel out, since the level settings for the other input variables occur with equal frequency within this set of experiments. Thus the first order correlation between the level settings of the input variables and output function values can be explicitly obtained without the necessity of completing the much larger number of experiments required by the full factorial analysis.

7.3.3 Experimental details

The etching was performed in the Alcatel GIR300 RIE machine described in Chapter 2, using gas mixtures of SF_6/O_2. SF_6 was chosen as the primary etching gas in view of possible high etch rate of silicon. Oxygen was added to increase the F atom concentration, which is responsible for the etching, and thus to enhance the silicon etch rate. Oxygen can also provide sidewall passivation so that the etching anisotropy is improved. Moreover, helium was used in the chemistry to stabilize the SF_6/O_2 plasma. The flow rate of helium was always kept the same as that of SF_6. The starting silicon substrates were 4'' p-type wafers with resistivity of 2 - 5 Ω•cm. The masking layer was either 1.3 μm HPR204 photoresist or 1 μm thermal SiO_2. The latter was used in order to explore the possibility of etching-though very thick ($\geq$ 10 μm) silicon membranes, which is required in, e.g. a 3-axial tactile sensor fabrication [7.18].

Although it is possible to vary also the electrode spacing and the cathode material of the RIE machine, it is decided to vary the RF power applied to the cathode, the pressure in the reaction chamber, the total gas flow rate and the ratio between O_2 to the total gas flow rate. This is because these 4 variables are relatively easy to be varied and accurately controlled. Thus these 4 variables serves as the 4 inputs for the orthogonal table $L_9 3^4$, shown in Table 7.1. Starting with a baseline process using an RF power of 75 W, a pressure of 45 mTorr, a SF_6 + O_2 total flow rate of 35 sccm and a ratio of O_2 to the total flow rate of 10%, a level variation using one higher level and one lower level was determined, yielding 3 level settings for each input variable. The input variables and level settings chosen are summarized in Table 7.3.

The output functions of interest are the etch rate for silicon R, the non-uniformity of the

etch rate U, the selectivity over the mask Sr and So for the resist and thermal oxide, respectively and the anisotropy A. The anisotropy, although it is not critical for the intended application, needs to be known so that appropriate compensation to the lateral etching can be taken into account in designing the mask.

Table 7.3 Input variables and level settings of the experimental design

Level setting	Input variables			
	Power (W)	Pressure (mTorr)	Flow rate (sccm)	O_2 content (%)
1	50	22.5	20	0
2	75	45	35	10
3	100	67.5	50	20

7.3.4 Results

In Table 7.4a the experimental results for each of the 9 runs required by the $L_9 3^4$ matrix are listed, plus two extra runs, which are listed underneath the $L_9 3^4$ matrix. These are repeats of the first run of the orthogonal design and give a useful gauge of the random variation in the process. It must be pointed out that the experiments have been carried out in a randomized manner to minimize the effects of system drift.

Looking at the experiment listed in the first row of Table 7.4a, run 1, the conditions chosen were level setting 1 for each of the input variables, or 50 W, 22.5 mTorr, 20 sccm and 0%. These conditions resulted in an etch rate of 1617 Å/min, a selectivity over the resist of 2.31, a selectivity over the oxide of 4.11, a uniformity of 4.4% and an anisotropy of 1. Similarly, the data for each of the other experimental conditions are listed. It can be seen that there is a substantial variation in all the output functions among the various experiments, indicating that considerable flexibility exists in optimizing a desired process.

7.3.5 Data analysis

The first order data analysis proceeds as follows: The output function averages (arithmetic means) for each level setting for each input variable are determined. Thus the etch rate average for power setting 1 of 50 W (runs 1, 2 and 3) is given by the

Table 7.4a Experimental results of the $L_9 3^4$ orthogonal design.

Experiments				Results				
P	p	F	C	R*	Sr	So	U (%)	A
1	1	1	1	1617	2.31	4.11	4.4	1
1	2	2	2	2533	3.53	7.99	7.2	0.69
1	3	3	3	3073	4.25	11.2	8.3	0.79
2	1	2	3	1733	1.18	3.24	4.1	1
2	2	3	1	3017	2.62	5.67	5.7	0.79
2	3	1	2	4007	3.76	9.10	6.3	0.63
3	1	3	2	1857	1.43	2.83	3.5	1
3	2	1	3	3233	2.00	5.69	5.6	0.71
3	3	2	1	4007	3.28	7.15	6.6	0.67
1	1	1	1	1750	2.50	4.20	5.1	1
1	1	1	1	1715	2.28	4.05	4.8	1
Standard Deviation				56.3	0.097	0.06	0.29	0

* in Å/min.

average of R1 (1617 Å/min), R2 (2533 Å/min) and R3 (3073 Å/min), which is 2408 Å/min. Similarly, the etch rate average for power setting 2 (75 W) is given by the average of the etch rates for experiments 4, 5 and 6 and is 2919 Å/min. The average etch rate for power level setting 3 is 3056 Å/min.

Note that for each level setting of the power, the orthogonal property of the matrix randomizes the settings for pressure, total flow rate and oxygen content, so that the effects of each of these variables tend to cancel out. From the values of R1, R2 and R3 it is concluded that the first order effects of increasing the power level are to increase the etch rate. This is of course, the expected results since the enhancement of etching by increasing power is quite well-known. Continuing in the same manner, the output function averages for each of the input variable levels can be calculated for all the output functions. The results are shown in Table 7.4b. Each output function average is arrayed in the column corresponding to the input variable to which it applies.

Table 7.4b *Output function averages and the difference between the maximum and minimum values for each set of output function averages.*

Output average	Power	pressure	flow rate	O_2%
R1	2408	1736	2952	2904
R2	2919	2928	2718	2799
R3	3056	3719	2649	2680
ΔR	648	1983	303	224
Sr1	3.36	1.64	2.69	2.74
Sr2	2.52	2.72	2.66	2.91
Sr3	2.24	3.76	2.77	2.48
ΔSr	1.13	2.12	0.1	0.43
So1	7.76	3.39	6.30	5.64
So2	6.00	6.45	6.13	6.64
So3	5.52	9.14	6.56	6.70
ΔSo	2.53	5.75	0.43	1.06
U1	6.63	4.00	5.43	5.57
U2	5.37	6.16	5.97	5.67
U3	5.23	7.07	5.83	6.00
ΔU	1.4	3.07	0.53	0.43
A1	0.83	1.00	0.78	0.82
A2	0.81	0.73	0.79	0.77
A3	0.79	0.70	0.86	0.83
ΔA	0.03	0.3	0.08	0.06

The simplified approach to quantify the effects of each input variable on the output functions is to calculate the difference between the maximum and minimum values for each set of output function averages (ΔR, ΔSr, ΔSo, ΔU and ΔA). The etch rate difference for power is 3056 - 2408 = 648 Å/min. Similarly, the etch rate difference for pressure is given by 3719 - 1736 = 1983 Å/min. By comparing the four differences for etch rate, it is possible to quantify the relative effects of each input variable on the etch rate over the level setting range chosen for that variable.

It can be seen that the largest difference for etch rate (ΔR) is 1983 Å/min, which is due to the pressure. This can be understood on the basis of the change in reactive neutral

density due to the pressure variation, referring to Chapter 2. In the SF_6/O_2 chemistry, the dominant etch mechanism is the ion enhanced chemical reaction of F-atoms with the silicon substrate. Higher pressure results in more F-atoms per unit volume in the plasma, which in turn enhances the etching. This model, although quite crude, can be used to understand the relative effects of all 4 input variables on all the output functions.

7.3.6 Optimization of the process

a. The optimized recipe for the highest selectivity over the resist

If second order effects can be neglected, it is now relatively easy to determine a process that will yield, e.g. the highest selectivity over the resist. It can be seen in Table 7.4b that the maximum selectivity for each input variable occurs at the lowest power, the highest pressure, the highest total flow rate and the central oxygen content. The process is optimized for maximum selectivity over the resist at these level settings. This recipe, represented by level settings 1, 3, 3, 2 for power, pressure, total flow rate and oxygen content respectively, is not one of the experiments included in the original $L_9 3^4$ orthogonal matrix, but running this recipe yielded a selectivity over the resist of 4.44, higher than any of the selectivities that resulted from the 9 matrix experiments.

b. Examining the influence of the input variables on the selectivity

Further information can be obtained from the results by plotting the output function averages as a function of level settings. This is shown in Fig. 7.4, using the selectivity over the resist again as an example. It can be seen that the effects of both power and pressure have a monotonical trend, and that by extending the level settings beyond those chosen for the original matrix, it should be possible to achieve even higher selectivities. In the case of total flow rate, it appears that the level setting 2 (35 sccm) represents a minimum in the selectivity, and that a higher selectivity could be achieved by going to a flow of more than the setting 3 (50 sccm) or less than the setting 1 (20 sccm). However, examination of the selectivity difference for the total flow rate shows that this variable has a relatively minor influence on the response any way, and the major improvement is to be found with the other three input variables. In the case of oxygen content, the level setting 2 (10%) resulted in a maximum in the selectivity.

c. Estimation of the random variation of the process

The two redundant experimental runs, which are repeats of the first run in the $L_9 3^4$ design, can be used to compute the random variation of the process. This is done by using the results of the two runs and the first run of the $L_9 3^4$ design to calculate the

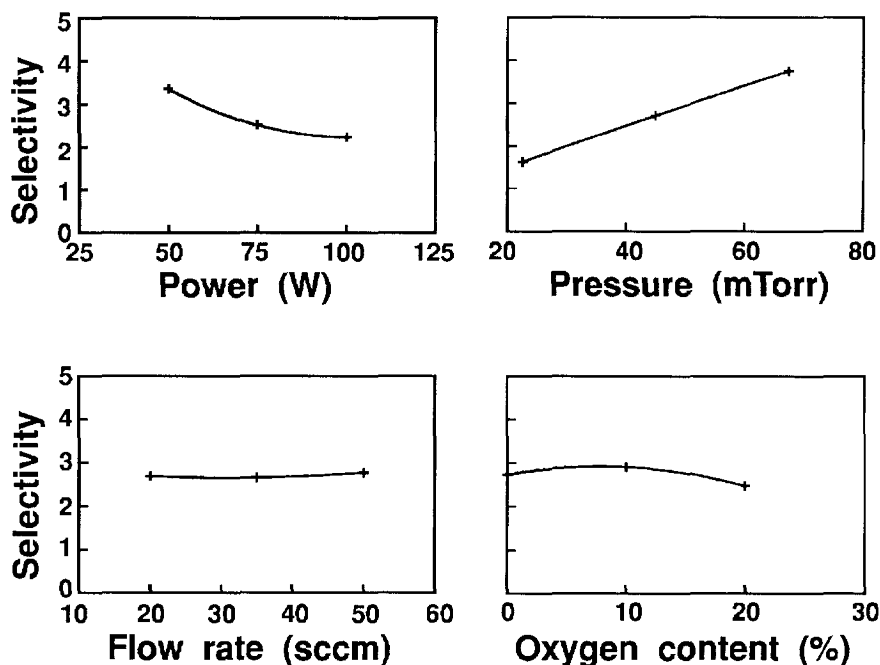

Fig. 7.4 *Effects of RF power, pressure, total gas flow rate and oxygen content on the selectivity of silicon etching over the resist.*

standard deviations, which are located in their corresponding columns of Table 7.4a. The relative significance of the output function averages can then be determined by comparison with the standard deviations. For experiments of this type, an output function difference of 2 to 3 standard deviation is required for the results to be statistically significant. Take the selectivity over the resist as an example, the standard deviation of the selectivity is 0.097. By comparing the standard deviation with the 4 selectivity differences ΔSr (1.13, 2.12, 0.1 and 0.43), it can be concluded that of the 4 selectivity differences, ΔSr's for power, pressure and oxygen content are significant while ΔSr for flow rate is not. In other words, the effects of total flow rate on the selectivity is not significant and can, therefore, be ignored.

d. Considerations of multi-objective optimization

In practice, there is usually more than one output function to be optimized. In the example presented above, the selectivity over the resist has been the sole objective of optimization. However, the etch rate and uniformity are also important for the membrane etching-through process. In examining the averages and differences for etch

rates and uniformities shown in Table 7.4b, with the goal of having the most selective, fastest and most uniform process, the recipes summarized in the Table 7.5 could be chosen. The numbers in the brackets indicate the relative importance ranking of the input variables on that corresponding output function, with 1 being the most important. These have been determined by comparing the output function difference among the 4 input variables. For instance, ΔSr for pressure (2.12) > ΔSr for power (1.13) > ΔSr for oxygen content (0.43) > ΔSr for flow rate (0.1), which results in the ranking of 2, 1, 4, 3 for power, pressure, total flow rate and oxygen content, respectively.

Table 7.5 The optimized recipes for selectivity, etch rate and uniformity

highest selectivity	1 (2)	3 (1)	3 (4)	2 (3)
maximum etch rate	3 (2)	3 (1)	1 (3)	1 (4)
minimum non-uniformity	3 (2)	1 (1)	1 (3)	1 (4)

It can be seen that both the total flow rate and oxygen content have less influence on the three output functions than the other two input variables. Therefore, the settings for the total flow rate and oxygen content should be chosen based on the consideration of which output function is the most important. Since the selectivity is the most important in the membrane etching-through process, the setting of the two input variables were chosen as 3 and 2 respectively, to ensure the highest selectivity while not significantly degrading etch rate and uniformity. The determination of the power and pressure is not easy since both are very important to all the three output functions. A level setting most favourable of one (or two) output function is most undesirable to the other two (or one) output functions. For example, taking level setting 3 of pressure can result in the highest selectivity and etch rate but the highest non-uniformity, while level setting 1 of power the highest selectivity but the lowest etch rate and the highest non-uniformity. As a result, compromise is unavoidable. In the membrane etching-through process, since the selectivity is the most important, the settings for power and pressure must be selected as 1 and 3, respectively, at the cost of reduced etch rate and increased non-uniformity. Nevertheless, it was found that these settings of 1, 3, 3, 2 for the highest selectivity resulted in an etch rate of 3205 Å/min, a non-uniformity of 6.5% with an anisotropy of 0.64, which were quite satisfactory for the intended application.

7.3.7 Discussions

It has been demonstrated that orthogonal design is a powerful tool of plasma process characterization and optimization. The number of experiments is much less than the corresponding factorial design and is also considerably less than other fractional factorial designs (such as Box-Behnken and FCC designs). The data analysis is very simple and straightforward, and does not need sophisticated algorithms, which can be performed by hand in a reasonable time or programmed easily into a personal computer.

However, some issues need to be considered in applying the method:

1. Care should be taken in choosing the level settings of the input variables. If the settings are too coarse, it is possible that a process minimum or maximum could be missed. On the other hand, if the level settings are too close together, the effects of that input variable will be too small to appear significant. Thus understanding of plasma chemistry, previous experience with the process, results from one dimensional search and results from smaller orthogonal matrices or screening designs need to be brought together in selecting the orthogonal matrix to run and the level settings to use.

2. The differences between output function averages in the orthogonal analysis contain information on both random fluctuations in the process and process drift, in addition to the desired effects of the input variations. Thus it is important to repeat one of the experiments one or more times during the orthogonal runs in order to estimate the uncertainties. Furthermore, it is very helpful to select level settings of the input variables that will give variations of the output functions larger than those errors. If the output functions are found to be very insensitive to an input variable, that input variable can be frozen and the effects of other input variables can be focused on more closely in a follow-up experiment.

3. If the process under development is unstable, it is possible to get misleading results. Generally speaking, the outputs must be smooth, continuous functions of the input variables for the orthogonal matrix to be useful.

4. The orthogonal design and data analysis described above cannot account for interactions between input variables. However, the interaction is common in real plasma etching. When strong interactions take place, the output function is more dependent on the interactions than on the absolute value of either variable. Interaction between variables can be detected by using one column of the orthogonal table to analyze the output function variations due to the interaction [7.16]. If it is already known or suspected that two input variables might interact, it is possible to incorporate this

knowledge into the orthogonal experiment directly. For example, in the process development described above, the fourth column of the design is for the O_2 content (the percentage of oxygen flow rate to the total gas flow rate) instead of O_2 flow rate. This is simpler than to run a design which contains 3 columns for the SF_6 flow rate, the O_2 flow rate and the interaction between them. In most instances, knowledge of the effect of various input variables upon the process, and which input variables are likely to be interactive are known and should be properly used in the orthogonal design.

5. Orthogonal design is also valuable for process control. In this case, it is more important to guarantee the stability and reproducibility of the process rather than the maximum throughput. As a consequence, the process should be chosen in a region where the output averages are weak functions of the input variables.

7.4 Modelling and optimization of silicon trench etching processes using Response Surface Methodology (RSM)

As shown in the previous section, orthogonal design can be used to qualitatively characterize a plasma etching process and to select level settings of input variables for the desired output functions of a process. However, there are some limitations with the method:

1. The selection of level settings is limited to discrete level settings of input variables pre-determined. However, a setting which results in the most desirable output functions may not necessarily be the same as one of the pre-determined settings. Therefore, important optimizing input level settings may be ignored.

2. Multi-objective optimization is rather difficult, if not impossible to perform, as shown in Section 7.3.6. This is due to the discrete nature of the obtained output functions as a result of experimental trials, which are bound to be discrete. The discreteness of the output functions do not allow the application of available optimization algorithms to find optimum settings for multi-objectives, as these usually require continuous output functions.

Therefore, an alternative must be sought with which continuous output functions can be obtained, so that any optimizing level setting between those pre-determined settings can be found and multi-objective optimization is possible. One of the alternatives is the Response Surface Methodology (RSM).

RSM is a statistical approach in which data from suitably designed experiments are used

to construct polynomial response models, the coefficients of which are determined by regression techniques. The methodology consists of experimentally measuring the process responses at a specified set of conditions (the experimental design), fitting the responses to a mathematical function and statistically evaluating the quality of the experimental data and process representation by the mathematical models. Parametric models are fitted to each response and are used to numerically explore and optimize the process. The contour or 3-dimensional plots of each response give a visual representation of the effects of the variation of input variables.

In this section, RSM will be explored to characterize and optimize the SF_6/O_2 chemistry for deep silicon trench-etching process, which is of importance for the fabrication of high-aspect ratio micromechanical structures and for trench isolation of IC's.

7.4.1 Response surface designs for quadratic model

A full quadratic model, which includes linear, two-factor interactions and quadratic terms for curvature, has been found to most adequately represent the real world of plasma etching processes [7.7][7.14]. The general form of the full quadratic model is:

$$Y = b_0 + \sum_{i=1}^{f} b_i X_i + \sum_{\substack{i=1 \\ (j>i)}}^{f-1} \sum_{j=2}^{f} b_{ij} X_i X_j + \sum_{i=1}^{f} b_{ii} X_i^2, \tag{7.2}$$

where Y denotes the process response and the X_i the input variables. In general, such a full quadratic model for f factors (input variables) contains one constant term, f linear terms, f(f-1)/2 interaction terms and f quadratic terms. Thus with 4 factors, which is the case of the intended SF_6/O_2 chemistry, the model is:

$$\begin{aligned} Y = {} & b_0 + b_1X_1 + b_2X_2 + b_3X_3 + b_4X_4 + b_{12}X_1X_2 + b_{13}X_1X_3 + b_{14}X_1X_4 \\ & + b_{23}X_2X_3 + b_{24}X_2X_4 + b_{34}X_3X_4 + b_{11}X_1^2 + b_{22}X_2^2 + b_{33}X_3^2 + b_{44}X_4^2 \end{aligned} \tag{7.3}$$

a. Choosing experimental design for the model

In principle, the number of experimental runs in the design must exceed that of coefficients in the model. If the number of trials and coefficients are the same, the solution will have no degrees of freedom for error estimation, and a "perfect" (i.e. fitting the data completely) but usually erroneous fit will be obtained. Furthermore, replicating data points in the design, as discussed in the orthogonal design, are

necessary to calculate experimental errors. The number of factor levels must also be adequate to support the model under consideration. A minimum of 3 levels is needed for the above quadratic model. Alternatively, a minimum of 2 (or 4) levels is needed for a linear (or cubic) model.

Therefore, the 4 factor, 3 level Box-Behnken design has been chosen for the process development. The design, together with the experimental results, is shown in Table 7.6. In this design there are 30 trials in total with 6 central replicating runs for experimental error estimation.

b. Using coded level settings

As can be seen in Table 7.6, the input variables are standardized to a common range of -1 to 1, with -1, 0 and 1 being the lower, central and upper setting, respectively. This is in contrast to the orthogonal design, in which the level settings need not be normalized. There are several advantages to use coded variables rather than the original input variables [7.19]:

1. It facilitates the construction of experimental designs. Normalization removes the units of measurement of the input variables and results in standardized distances measured along the axes of the coded variables in k-dimensional space.

2. When fitting polynomial models, it eases computation and increases accuracy in estimating the model coefficients.

3. It facilitates evaluation of the relative significance of each input variable and the terms of the polynomial.

The following transformation can be used to scale the input variables for their coded settings:

$$x_i = (X_i - \overline{X}_i)/S_i \qquad (7.4)$$

where x_i is the coded setting for original setting of X_i ; $\overline{X}_i$ is the average value of X_i and S_i is the standard deviation of X_i.

Table 7.6 4-factor, 3-level Box-Behnken design for SF_6/O_2 process optimization and experimental results

No.	Designs	R_{Si} (μm/min)	$S_{Si/SiO2}$	U (%)	A
1	1 1 0 0	0.720	13.4	3.2	0.594
2	1-1 0 0	0.310	5.2	1.7	0.834
3	-1 1 0 0	0.381	17.5	7.2	0.730
4	-1-1 0 0	0.217	6.8	4.0	0.827
5	0 0 1 1	0.167	3.8	8.2	0.958
6	0 0 1-1	0.535	11.0	3.9	0.539
7	0 0-1 1	0.292	7.7	6.0	0.930
8	0 0-1-1	0.456	14.9	5.5	0.519
9	0 0 0 0	0.468	9.9	4.5	0.751
10	0 0 0 0	0.546	12.9	5.0	0.654
11	1 0 0 1	0.296	5.0	3.7	0.885
12	1 0 0-1	0.554	9.5	3.0	0.551
13	-1 0 0 1	0.210	7.9	12.0	0.967
14	-1 0 0-1	0.467	17.7	7.6	0.501
15	0 1 1 0	0.509	13.2	6.0	0.648
16	0 1-1 0	0.527	19.6	5.9	0.548
17	0-1 1 0	0.233	5.2	3.3	0.877
18	0-1-1 0	0.251	6.0	2.1	0.776
19	0 0 0 0	0.412	9.7	5.0	0.685
20	0 0 0 0	0.388	9.4	5.4	0.695
21	1 0 1 0	0.445	7.7	4.3	0.730
22	1 0-1 0	0.473	9.2	2.9	0.645
23	-1 0 1 0	0.502	17.9	5.8	0.837
24	-1 0-1 0	0.352	14.2	4.6	0.664
25	0 1 0 1	0.381	10.2	7.3	0.953
26	0 1 0-1	0.603	19.6	4.7	0.490
27	0-1 0 1	0.076	1.6	6.7	0.658
28	0-1 0-1	0.292	6.1	2.0	0.639
29	0 0 0 0	0.541	12.4	6.8	0.672
30	0 0 0 0	0.466	11.3	8.3	0.679

7.4.2 Experimental details

The same RIE machine as described in Section 7.3.2 was used. The range of all input variables are listed in Table 7.7. As can be seen the range of oxygen content is considerably extended to 35%, compared with that in the previous design of Section 7.3.2 (20%). This is the consequence of the insight into the influence of oxygen content

on etching anisotropy, i.e. higher oxygen content results in better anisotropy, which is one of the conclusion obtained from the previous orthogonal design. The remaining three input variables (i.e. power, pressure and total flow rate) are in the same ranges as those used in the orthogonal design. The mask used was thermal silicon dioxide, in view of that the selectivity of silicon etching over oxide is much higher than over resist according to the results of the orthogonal design, so that very deep (> 10 μm) silicon trenches can be etched.

Table 7.7 *Ranges of input variables corresponding to their coded level settings.*

Level setting	Input variables			
	Power (W)	Pressure (mTorr)	Flow rate (sccm)	O_2 content (%)
-1	50	22.5	20	5
0	75	45	35	20
1	100	67.5	50	35

7.4.3 Experimental results and least square regression (LSR) analysis

The responses of the 30-run Box-Behnken design, including etch rate, selectivity over the oxide, uniformity and anisotropy, are listed in Table 7.6, together with the 4-factor, 3-level Box-Behnken design.

The data obtained for a response surface design can be analyzed using Least Squares Regression (LSR) analysis, which determines the model coefficients by minimizing the residual variance [7.19]. In Appendix A1 the principle of LSR is described. Using a nonlinear regression analysis program "NONLIN" [7.20], the coefficients for each of the 4 responses, together with the ANOVA (ANalysis Of VAriance) results are obtained. As an example, Appendix A2 shows the output file of NONLIN for the etch rate.

a. Statistical analysis of the estimations for the coefficients

For each coefficient, NONLIN displays, in addition to the final (maximum likelihood) estimates, the standard errors of the estimated coefficient values, the "t" statistic

comparing the estimated coefficient values with zero and the significance of the t statistic. These information are very useful to test the probability that the actual value of any coefficient could be zero, and thus the term of the model containing the coefficient can be eliminated without significantly affecting the accuracy of the regression.

In Appendix A2 the "t" statistic is computed by dividing the estimated value of a coefficient by its standard error. This statistic is a measure of the likelihood that the actual value of the parameter is not zero. The larger the absolute value of t, the less likely it is that the actual value of the coefficient could be zero. The "Prob (t)" value is the probability of obtaining the estimated value of the coefficient if the actual coefficient value is zero. The smaller the value of Prob (t), the more significant the coefficient and the less likely that the actual coefficient value is zero. Looking at Prob (t)'s corresponding to each coefficient, it is found that coefficients b3, b14, b23, b24 and b11 have a Prob (t) of 83%, 99%, 100%, 96% and 91%, respectively, implying that the terms of the model containing these coefficients can be eliminated.

Therefore, a second LSR analysis was carried out without those terms in the model. The results are shown in Appendix A3. Now it is clear that none of the coefficients is likely zero.

b. The ANalysis-Of-VAriance (ANOVA) to test the significance of the model

The procedure of testing the significance of the model is described in Appendix 4. A model is said to be significant if not all the coefficients of the model is zero. An ANOVA table is generated with NONLIN, which provides statistics about the overall significance of the model being fitted, referring to Appendix A3. The Prob (t) in the table indicates the probability that all the coefficients of the model are zero (in other words, the response can be represented properly by the mean value of all the experimental results and the model is not significant). For example, in the ANOVA table of Appendix A3, Prob (t) is 0.001%, indicating that the etch rate model is most significant.

The "proportion of variance explained (R^2)" in appendix A3 indicates how much better the model predicts the dependent function than just using the mean value of the dependent function. If the model perfectly predicts the observed data, the value of this statistic will be 1 (100%). The "adjusted coefficient of multiple determination (R_a^2)" in Appendix A3 is an R^2 statistic adjusted for the number of coefficients in the model and the number of data observations. It is a more conservative estimate of the percentage of variance explained, especially when the sample size is small compared to the number

of coefficients. From Appendix A3, it is seen that R^2 and R_a^2 are 93% and 89%, respectively, indicating that the obtained model predicts the observed data very well.

c. Testing lack of fit of the fitted model using replicated observations

The F value and Prob (F) in the ANOVA table are to test the null hypothesis $H_0 : b_1 = b_2 = ... = b_{44} = 0$ in the case of the 4-factor quadratic model. Rejecting the hypothesis by large F value (or low Prob (F)) means only that it could be inferred that at least one of coefficients in H_0 is not zero. This inference is not the same as saying that the fitted model adequately describes the behaviour of the response over the experimental ranges of the variables. For example, higher order effects of the input variables may play important role and thus a quadratic model is not adequate. A procedure for checking the adequacy of the fitted model is called testing lack of fit of the fitted model. The procedure is outlined in the Appendix A5 and it is shown that the quadratic model describes the etch rate behaviour of the plasma adequately.

d. Summary of the models

Following the procedure outlined above, the 4 quadratic models for the etch rate, selectivity, uniformity and anisotropy are obtained and evaluated. Table 7.8 summarizes the coefficients of the 4 models and Table 7.9 and Table 7.10 list the ANOVA tables, R^2 and R_a^2 of the 4 models. From the 3 tables it is concluded:

1. All the Prob (F)'s in the ANOVA tables are very small ($\leq$ 0.006%), meaning all the fitted models are significant. It is not likely that all of the coefficients for any one of the models are zero.

2. All the F values which test the lack of fit of the models are rather small ($\leq$ 4.9), meaning that the quadratic models fit the observed data very well. It is not likely that any higher order effects of the input variables are significant.

3. The fitted models for etch rate and selectivity explain most part of total variations of the observed values very well ($R_a^2 \geq$ 89.38%), while those for uniformity and anisotropy less well ($R_a^2 \leq$ 78.12%). This is probably due to the fact that the former two responses are relatively easy to precisely measure but the latter two are not. Therefore, less measurement errors have been introduced in the former data.

Table 7.8 Summary of the coefficients for the 4 quadratic models

Coefficient	Etch rate	Selectivity	Uniformity	Anisotropy
b_0	0.4643	11.1944	5.5538	0.7039
b_1	0.05575	-2.6667	-1.8642	-0.02392
b_2	0.1452	5.2167	1.2108	-0.05400
b_3	0	-1.0667	0.3750	0.04225
b_4	-0.1238	-3.5500	1.4333	0.1760
b_{12}	0.06150	0	0	0
b_{13}	-0.04450	-1.3000	0	0
b_{14}	0	1.3250	-0.9250	0
b_{23}	0	-1.4000	0	0
b_{24}	0	-1.2250	0	0.1110
b_{34}	-0.05100	0	0.9500	0
b_{11}	0	0	0	0.02647
b_{22}	0	0	-1.1468	0
b_{33}	-0.02513	0	-0.6005	0
b_{44}	-0.07675	-1.6111	0.9120	0

7.4.4 Discussions

Since it has been confirmed that the 4 models are significant and adequate, it is now possible to examine the major effects of all the input variables on the responses by looking at the models, i.e. inferring the relative importance of the input variables to a specific response by comparing the absolute value of the coefficients for the linear terms of the models. Whether the responses will increase with the input variables or *vice versa* can be known from the sign of the coefficients. Also the interactions among the input variables and the second order effects (curvature of the response surface) can be known. Fig. 7.5 shows the 3-dimensional plots of all the responses as a function of two input variables, with the remaining two variables being set to their central levels (level

Table 7.9 *The ANOVA tables, R^2 and R_a^2 of the etch rate and selectivity models.*

Etch rate

Source	DF	Sum of Squares	Mean Square	F value	Prob (F)
SSR	10	0.5645	0.05645	25.40	0.00001
SSE SS_{PE} SS_{LOF}	19 5 14	0.04222 0.01770 0.02452	0.02222	0.4948	
Total	29	0.6067			

$R^2 = 0.9304$, $R_a^2 = 0.8938$

Selectivity

Source	DF	Sum of Squares	Mean Square	F value	Prob (F)
SSR	9	623.0939	69.2327	28.66	0.00001
SSE SS_{PE} SS_{LOF}	20 5 15	48.3211 11.0933 37.2278	2.4161	1.1186	
Total	29	671.4150			

$R^2 = 0.9280$, $R_a^2 = 0.8956$

settings = 0).

a. Etch rate

From Table 7.8, it is seen that b_2 and b_4 are much larger than b_1, while b_3 is zero. This indicates that in the sense of first order effects, the etch rate is mainly determined by the pressure and oxygen contents and is little by the power, while the flow rate has no influence on the etch rate. b_1 and b_2 are positive (the etch rate increases with the power and pressure), while b_4 is negative (the etch rate decreases with the oxygen content). b_{22}, b_{33} and b_{44} are non-zero and all negative, meaning that the second order effects of the pressure, flow rate and oxygen content are significant and that all the three variables

Table 7.10 *The ANOVA tables, R^2 and R_a^2 of the uniformity and anisotropy models.*

Uniformity

Source	DF	Sum of Squares	Mean Square	F value	Prob (F)
SSR	9	112.1694	12.4633	8.04	0.00006
SSE	20	31.0175	1.5509	0.6569	
SS_{PE}	5	10.4413			
SS_{LOF}	15	20.5762			
Total	29	143.1869			

$R^2 = 0.7834$, $R_a^2 = 0.6859$

Anisotropy

Source	DF	Sum of Squares	Mean Square	F value	Prob (F)
SSR	6	0.4893	0.08155	18.26	0.00001
SSE	23	0.1027	0.004466	4.9016	
SS_{PE}	5	0.005509			
SS_{LOF}	18	0.0921			
Total	29	0.5920			

$R^2 = 0.8265$, $R_a^2 = 0.7812$

result in convex response surfaces. The fact that b_{12}, b_{13} and b_{34} are non-zero is an indication that there exist interactions between power and pressure, power and flow rate and flow rate and oxygen content.

b. Selectivity

From Table 7.8, it is seen that the power, pressure and oxygen content play major roles in determining the selectivity, while the effect of flow rate is minor. The selectivity increases with the pressure but decreases with the remaining three variables. The second order effects of the oxygen content are significant and there exist interactions between

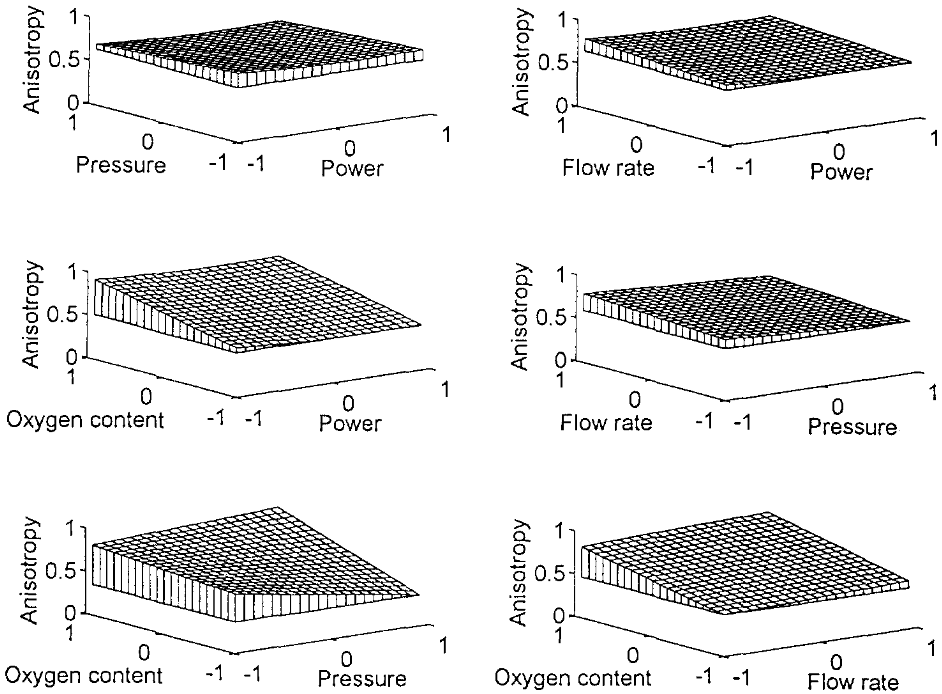

Fig. 7.5 *3-dimensional plots of the responses as a function of 2 of the 4 input variables, with the remaining 2 variables set to level 0 (central level).*

power and flow rate, power and oxygen content, pressure and flow rate and pressure and oxygen content.

c. Uniformity

From Table 7.8, it is seen that the same 3 variables that are dominant in determining the selectivity (power, pressure and oxygen content) are important in determining the uniformity. The non-uniformity is improved with increasing power but degraded with the remaining three variables. The second order effects of pressure, flow rate and oxygen content are significant. There exist interactions between power and oxygen content and between flow rate and oxygen content.

d. Anisotropy

From Table 7.8, it is seen that all the 4 variables are equally important in determining

the anisotropy. The anisotropy increases with the flow rate and oxygen content but decreases with the power and pressure. The second order effects of the power are significant. There exist interactions between pressure and oxygen content.

From above discussion, it is concluded that in the SF_6/O_2 chemistry, the pressure and oxygen content are most important in determining the etching characteristics. The power is less important and the flow rate is the least significant. All these features are in good agreement with those of a chemistry in which ion-enhanced chemical etching is the major etching mechanism, which has been confirmed by many authors for the SF_6/O_2 chemistry [7.21][7.22]. The conclusions are also in agreement with those obtained by the orthogonal design method.

7.4.5 Optimization of the SF_6/O_2 chemistry for desired applications

Mathematical optimization concerns the minimization or maximization of functions. Many algorithms have been developed for unconstrained optimization, in which searching of the minimum is not subject to any constrain. The principle algorithms are the Nelder-Mead simplex search method [7.23] and the BFGS quasi-Newton method [7.24]. For constrained optimization, in which minimizing process is subjected to constrains, variations of Sequential Quadratic Programming (SQP) [7.25] are used.

However, in such a practical design problem as plasma etching process development, a single objective with several hard constrains rarely adequately represents the problem being faced. More often the problem is a multi-objective optimization, i.e. a vector of objectives, $\mathbf{f}(\mathbf{x}) = \{f_1(\mathbf{x})...f_m(\mathbf{x})\}$ must be traded-off in some way. The relative importance of this objectives is not generally known until the system's best capabilities are determined and trade-offs between the objectives fully understood. The necessity of such trade-offs is obvious in the development of the SF_6/O_2 process. As modelled in the previous section, increasing (or decreasing) any input variable is always in favour of one or more response, while not in favour of the remaining responses. For example, high pressure is beneficial to high etch rate and selectivity, but harmful to uniformity and anisotropy; high oxygen content can improve anisotropy but degrade the remaining 3 responses. Therefore, multi-objective optimization is essential to the plasma process development. The principle of multi-objective optimization is described in Appendix A6.

a. Optimization results

Deep silicon trench etching represents one of the most challenging processes to plasma etching process development. It requires high etch rate, high selectivity over the mask, good uniformity and anisotropy. All these 4 requirements must be met simultaneously.

Using the 4 models obtained by the RSM, optimization of the SF_6/O_2 process for deep silicon trench etching has been carried out by applying the Goal Attainment (GA) method in the Optimization Toolbox of Matlab® Numeric Computation Software [7.26-7.27], which deals with the multi-objective optimization problem.

Suppose an etching process with the characteristics listed in Table 7.11 is required, executing the GA method results in the optimized input variables as power = 1, pressure = 1, flow rate = -0.0324 and oxygen content = 1. Performing a confirming etching test results in the etching characteristics listed also in Table 7.11. In the optimization, the absolute values of the weighting factors have been set to be the same as the goals with the signs for etch rate, selectivity and anisotropy being negative and that for uniformity being positive (referring to Appendix A6). Moreover, the boundaries of the input variables are limited from -1 to 1. It can be seen that the testing results is in good agreement with the design goals. The deviation of the testing results from the goal values is within 10%. The results described here confirm that the GA method is very powerful in optimizing a plasma process provided that adequate models for the objectives are available. Fig. 7.6 shows 15 μm silicon trench using the optimized process with 2.25 μm PSG mask.

Table 7.11 The goal, predicted responses by GA method and experimental results of the trench process

	Etch rate (μm/min)	Selectivity	Uniformity (%)	Anisotropy
Goals	0.5	5	5	0.9
Predicted results	0.4738	8.8	5.13	0.9381
Test results	0.4780	7.98	5.59	0.8362

7.4.6 Transferability of the optimized process

An attempt was made to transfer the optimized input level settings of the power, pressure, total flow rate and oxygen content to the DRYTEK 384T etcher, described in Chapter 2. This is because the optimized etch rate of silicon with the Alcatel machine is still not very high (about 5000 Å/min), as indicated in Table 7.11. With such an etch rate a silicon trench of e.g. more than 20 μm would take very long time, although not impossible. Due to its much higher plasma density, DRYTEK machine usually exhibits much higher etch rates than the Alcatel counterpart.

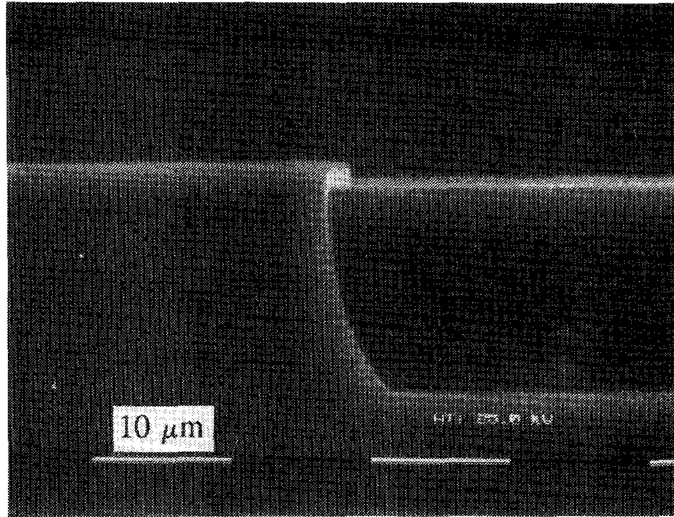

Fig. 7.6 *SEM photograph showing 15 μm deep trench etching with 2.25 μm PSG mask using the optimized process of 100 W, 67.5 mTorr, 34.5 sccm total gas flow rate and 35% oxygen content.*

Therefore, an etching test was carried out with the DRYTEK machine using 150 W RF power, 150 mTorr pressure, 86 sccm total flow rate and 35% oxygen content. The power and pressure levels are at the upper ranges of the process windows of the two variables, beyond these limits, an unstable plasma results. It was found that the etch conditions result in an etch rate of 1.56 μm/min, a selectivity of 7.8, a uniformity of 4.5% and an anisotropy of 0.9. It is seen that a much higher etch rate is indeed obtained with the DRYTEK machine with the remaining 3 etching characteristics similar to those obtained with the Alcatel machine. Note the selection of the input level settings of the DRYTEK machine is solely based on the insight to the process obtained previously with Alcatel machine, without any optimization specifically carried out for the DRYTEK machine. Nevertheless, the etching results of the DRYTEK machine indicate that the optimized level settings are reasonably transferrable.

7.4.7 Limitation of the RSM

Although the quadratic model obtained in the RSM can represent the plasma etching characteristics quite adequately, the results are applicable only within the ranges of the original experimental settings. Any attempt to extrapolate the model and make it suitable

for the prediction of the responses outside the ranges may result in misleading or even absurd results. This can be understood by realizing that the quadratic model represents, in fact, an oval, which at any rate should not be the real response of plasma processes to any input variable in the complete variable space. In this aspect process modelling based on neural networks may be one of the solutions [7.28].

7.5 Conclusions

In this chapter, plasma process development using statistical experimental design and data analysis is described, with the SF_6/O_2 plasma process for deep silicon trench etching being an example. Using orthogonal experimental design, the dependence of etching characteristics on instrumentational variables of plasma etching processes can be understood qualitatively, with much fewer experimental runs than factorial designs and fractional factorial designs. The data analysis associated with the design is rather simple and straightforward. An optimized process can be obtained using the level settings as suggested by the data analysis. However, due to the discreteness of the experimental results, it is not possible to find out any optimizing level which is not one of the originally pre-determined level settings for the experiment. Also multi-objective optimization is very difficult.

With Response Surface Methodology (RSM), plasma etching characteristics can be expressed as continuous functions of instrumental variables, using polynomial models. Statistical analysis can be used to test the significance and adequacy of the models. Quantitative relationship between input variables and output responses are obtained. Existing optimizing methods, such as the Goal Attainment method, can be used to obtain input level settings for desired applications.

References

[7.1] D. Edelson and D. Flamm, "Computer simulation of a CF_4 plasma etching silicon," *J. Appl. Phys.*, Vol. 56, pp. 1522-1531, 1984.

[7.2] M. J. Kushner, "Monte-Carlo simulation of electron properties in rf parallel plate capacitively coupled discharges," *J. Appl. Phys.*, Vol. 54, pp. 4958-4965, 1983.

[7.3] G. Z. Yin and D. W. Jillie, "Orthogonal design for process optimization and its application in plasma etching," *Solid State Technol.*, Vol.30 (5), pp. 127-132, May 1987.

[7.4] G. E. P. Box and N. R. Draper, *Empirical Model-Building and Response*

Surface, John Wiley & Sons, New York, 1987.

[7.5] K. K. Low and S. W. Director, "An efficient methodology for building macromodels of IC fabrication process," *IEEE Trans. Computer-Aid Design*, Vol. 8, pp. 1299-1313, 1989.

[7.6] P. E. Riley and D. A. Hanson, "Study of etch rate characteristics of SF_6/He plasmas by response surface methodology: effects of inter-electrode spacing," *IEEE Trans. Semicond. Manufact.*, Vol. 2, pp. 178-182, 1989.

[7.7] P. E. Riley, A. P. Turley and W. J. Malkowski, "Development of a multistep SiO_2 plasma etching process in a minibatch reactor using response-surface methodology," *J. Electrochem. Soc.*, Vol. 136, pp. 1112-1119, 1989.

[7.8] E. Gogolides and H. H. Sawin, "N^+-polysilicon etching in CCl_4/He discharge: characterization and modelling," *J. Electrochem. Soc.*, Vol. 136, pp. 1147-1154, 1989.

[7.9] K. J. McLaughlin, S. W. Butler, T. F. Edgar and I. Trachtenberg, "Development of techniques for real-time monitoring and control in plasma etching," *J. Electrochem. Soc.*, Vol. 138, pp. 789-799, 1991.

[7.10] G. S. May, J. Huang and C. J. Spanos, "Statistical experimental design in plasma etch modelling," *IEEE Trans. Semicond. Manufac.*, Vol. 4, pp. 83-98, 1991.

[7.11] W. G. Cochran and G. M. Cox, *Experimental Design*, John Wiley & Sons, New York, 1957.

[7.12] O. Kempthorn, *The design and Analysis of Experiments*, Robert E. Krieger Publishing Co., Huntington, New York, 1979.

[7.13] R. N. Kackar, "Off-line quality control, parameter design and the Taguchi method," *J. Quality Technol.*, Vol. 17, pp. 176-188, 1985.

[7.14] M. W. Jenkins, M. T. Mocella, K. D. Allen and H. H. Sawin, "The modelling of plasma etching process using response surface methodology," *Solid State Technol.*, Vol. 29 (4), pp. 175-182, 1986.

[7.15] G. E. P. Box, W. B. Hunter and J. S. Hunter, *Statistics for Experimenters*, John Wiley & Sons, New York, 1978.

[7.16] W. J. Diamond, *Practical Experiments Designs*, Van Nostrand Reinhold Co., New York, 1981.

[7.17] R. P. van Kampen, M. J. Vellekoop, P. M. Sarro and R. F. Wolffenbuttel, "Application of electrostatic feedback to critical damping of an integrated silicon capacitive accelerometer," *Sensors and Actuators*, Vol. 43, pp. 100-106, 1994.

[7.18] Z. Chu, P. M. Sarro and S. Middelhoek, "Silicon three-axis tactile sensor," in *The Proc. 8th Intern. Conf. Solid-State Sensors and Actuators (Transducer'95)*, 1995, pp. 656-659.

[7.19] A. I. Khuri and J. A. Cornell, *Response Surfaces - Designs and Analysis,* Marcel Dekker, Inc., New York, 1987, pp. 46-53.

[7.20] P. H. Sherrod, *NONLIN - Nonlinear regression Analysis Program*, 4410 Gerald Place, Nashville, TN 37205 - 3806, U. S. A. Internet: 76166.2640@compuserve.com

[7.21] T. Syau, B. J. Baliga and R. Hamaker, "Reactive ion etching of silicon trenches using SF_6/O_2 gas mixtures," *J. Electrochem. Soc.*, Vol. 138, pp. 3076-3081, 1991.

[7.22] R. Pinto, K. V. Ramanathan and R. S. Babu, "Reactive ion etching in SF_6 gas mixtures," *J. Electrochem. Soc.*, Vol. 134, pp. 165-175, 1987.

[7.23] J. A. Nelder and R. Mead, "A simplex method for function minimization," *Computer Journal*, Vol. 7, pp. 308-313, 1964.

[7.24] D. F. Shanno, "Conditioning of quasi-Newton methods for function minimization," *Mathematics of Computing*, Vol. 24, pp. 647-656, 1970.

[7.25] P. E. Gill, W. Murray and M. H. Wright, *Practical Optimization*, Academic Press, London, 1981.

[7.26] *MATLAB® User's Guide*, The MATH WORKS Inc., Mass., U. S. A., 1993.

[7.27] Andrew Grace, *Optimization Toolbox for Use with MATLAB®*, The MATH WORKS Inc., Mass., U. S. A., 1994.

[7.28] G. S. May, "Manufacturing ICs the neural way," *IEEE Spectrum*, pp. 47-51, Sept. 1994.

Chapter 8 Conclusions

8.1 General conclusions

Silicon micromachining is essential to the fabrication of micromechanical structures, which are required by silicon-based sensors and actuators. Plasma etching is an important alternative to conventional wet etching due to its superior etching characteristics to those of wet etching, such as small feature size, good linewidth control, independence of crystal orientation and ability to achieve sidewall profile control. Although many plasma etching processes exist for the fabrication of various microelectronic devices, especially high-density integrated circuits, plasma etching processes for silicon micromachining need to be developed to meet the requirements for the fabrication of silicon micromechanical structures, which are rather different from those for conventional IC fabrication. Moreover, by using the unique sidewall profile controllability of plasma etching, novel microstructures can be fabricated and, therefore resulting in new sensing and actuating devices.

In the development of plasma etching techniques for surface micromachining, etching selectivity over the underlying layer and uniformity are two major concerns. In Chapter 3 it is shown that a high etching selectivity of silicon nitride over polysilicon can be achieved by using a CHF_3-based chemistry with N_2 addition. The high selectivity is the result of the enhancement of silicon nitride etching upon N_2 addition and the formation of a etch-retarding thin polymer layer on the surface of polysilicon. Proper post-processing using *in situ* O_2 plasma treatment is required to remove this polymer layer to ensure good electrical contact of the polysilicon layer with the subsequently deposited conductive layer. When multi-layer structural membranes need to be patterned, multi-step etching approach is necessary. This is demonstrated in the patterning of a polysilicon/silicon nitride/polysilicon sandwich structure. The top two layers of the sandwich need to be etched, while the etching to the lower polysilicon must be minimized. The developed two-step etching process uses a 70 sccm CF_4 + 10 sccm SF_6 + 10 sccm O_2 plasma to etching the top polysilicon layer with high etch rate, and a 7.5 sccm CHF_3 + 42.5 sccm N_2 chemistry to *in situ* etching the silicon nitride layer with high selectivity over the lower polysilicon and with good uniformity. Analysis indicates that although a single step etching, using the same chemistry as for the top polysilicon etching, could be used to etch the top two layers, this would result in unacceptable etching to the lower polysilicon and high non-uniformity.

Surface non-planarity as a result of patterning of thick sacrificial films in surface

micromachining can result in severe problems of step coverage and stress concentration of structural films. These problems are relieved by a local planarization technique, developed in Chapter 4, which uses phosphosilicate glass (PSG) spacers along the sidewall of sacrificial PSG patterns. The spacer is formed by anisotropy etching-back of an extra PSG layer using a 162 sccm CHF_3 + 18 sccm C_2F_6 plasma chemistry. The original sharp corners of PSG patterns are rounded-off with the spacer formation. When a genuine double clamped beam instead of a step-up one is desired, or when multi-layer surface micromachining would result in severe surface non-planarity, filling trenches in silicon substrate by PSG provides a proper solution, as described in Chapter 4. Filling silicon trenches by PSG is achieved by a two-layer resist coating scheme, in which an image reversal photoresist is used, followed by a blank plasma etching back, in which O_2 is used to match the etch rate of the resist to that of the PSG.

Bulk silicon etching for micromachining using plasma is very promising since it is not crystalline orientation dependent. The ability of sidewall profile control with plasma etching, in which adding Cl_2 to a CF_4 plasma is shown to change the sidewall profile of silicon etching significantly, is demonstrated in Chapter 5. Using a 10 sccm Cl_2 addition to 210 sccm CF_4, in combination with a composite mask of resist and silicon oxide, a vertical sidewall profile is obtained for selective epitaxial growth (SEG) applications. Controlled degree of bowing in the etched sidewall is achieved using 50 sccm Cl_2 addition to 170 sccm CF_4 with silicon oxide masks. This enables the fabrication of recessed silicon micro-tips with a curvature of radius less than 100 Å, which find applications for vacuum microelectronic devices.

By combining anisotropic and isotropic etching properties of plasmas, a new micromachining technique - SIMPLE (Silicon Micromachining by Plasma Etching) is developed. The technique, described in Chapter 6, is based on a Cl_2 plasma with BCl_3 addition, which etches lightly n-doped silicon epitaxial layer anisotropically but a heavily n-doped buried layer underneath laterally. Free-standing single crystal micromechanical structures with high aspect ratio (4) and small separation (2 μm) can be formed in the single plasma etching. The technique is compatible with standard IC processing and therefore, on-chip integration of microstructures with electronic circuitry is possible. Because dry etching is used in the releasing of the structure from the substrate, sticking problems associated with wet sacrificial etching in conventional surface micromachining is eliminated.

Appropriate characterization and optimization of plasma etching chemistries require empirical modelling based on statistical experimental design and data analysis. This is demonstrated in Chapter 7, in which orthogonal design and response surface methodology (RSM) are used to develop a SF_6 + O_2 process for silicon etching.

Orthogonal designs provide mostly qualitative characterization of the process, with the minimum number of experimental runs. RSM results in polynomial models for each etching characteristics, allowing multi-objective optimization of the etching process using existing algorithms, at a cost of more experimental runs than orthogonal designs require.

8.2 Perspective

With the rapid development of microsystem technology, plasma etching is expected to play more and more important role in silicon micromachining. In addition to applying plasma etching in a conventional way (i.e. to achieve small feature size), for micromachining, new application areas of plasma etching are increasingly explored. Using plasma etching to replace the conventional wet anisotropic through-wafer etching is an example. Since plasma etching is not dependent on crystal orientation and can achieve vertical sidewall profile, bulk micromachining using plasma etching will provide much more opportunities to new device design than wet etching. To achieve through-wafer plasma etching, not only the input instrumental variables of plasma etching process need to be properly determined, but also new type of machines need to be developed to meet the very demanding requirements for the etching characteristics. For example, new plasma etching machines specialized for very deep (up to several hundred microns) silicon etching are appearing. These machines can etch silicon with very high etch rate ($> 2\mu m/min$), very high selectivity (> 50 for resist and > 200 for oxide) and with vertical sidewall profiles. To achieve these, new machine configurations, such as ICP (Inductive Coupled Plasma) or ECR (Electron Cyclotron Resonance) sources and low temperature ($\sim$ -100°C) electrodes, are used. New etching chemistries need to be investigated to ensure the very challenging etching characteristics.

Another interesting development of plasma etching in micromachining will be the lateral etching of sacrificial layer, for example PSG, to release microstructures in surface micromachining. This dry sacrificial etching will eliminate the sticking problem associated with wet sacrificial etching in conventional surface micromachining. To achieve high lateral etch rate for the sacrificial etching, high plasma density must be maintained, which may require also very specialized plasma etching set-up. High lateral etching selectivity over the structural layer, the substrate and masking materials is a prerequisite for the process to be useful in practice, which makes the process development very challenging.

Many plasma etching characteristics which were not desired for conventional microfabrication should be re-examined and even intendedly enforced, so as to provide

etching characteristics and open opportunities for novel device fabrication. This will motivate many new areas of research in terms of both plasma etching and device design. On one hand, with the increasing research and development activities on microsystem, many new sensors and actuators based on silicon will be required, therefore putting forward continuously new requirements for plasma etching research. On the other hand, successful development of new plasma etching processes will promote the advancement of the research and development of silicon sensing and actuating devices.

Appendix

Appendix A1 Principle of the least square regression

Let us assume provisionally that N observations of the response are expressible by means of the quadratic model:

$$Y_u = b_0 + \sum_{i=1}^{f} b_i X_{ui} + \sum_{\substack{i=1 \\ (j>i)}}^{f-1} \sum_{j=2}^{f} b_{ij} X_{ui} X_{uj} + \sum_{i=1}^{f} b_{ii} X_{ui}^2 + \varepsilon_u \quad \text{(A1.1)}$$

In Eq. (A1.1), Y_u denotes the observed response for the *u*th trial, X_{ui} represents the level of factor i at the *u*th trial, b_0, b_i, b_{ij} and b_{ii} are unknown coefficients, and ϵ_u represents the random error in Y_u. It is assumed that ϵ_u have zero mean and common variance σ^2, are mutually independent in the statistical sense and are normally distributed.

The method of LSR selects as estimates for the unknown coefficients in Eq. (A1.1), such that the quantity

$$R(b_0, b_i, b_{ij}, b_{ii}) = \sum_{u=1}^{N} \left(Y_u - b_0 - \sum_{i=1}^{f} b_i X_i - \sum_{\substack{i=1 \\ (i>j)}}^{f-1} \sum_{j=2}^{f} b_{ij} X_i X_j - \sum_{i=1}^{f} b_{ii} X_i^2 \right)^2$$

(A1.2)

is minimized. The coefficient estimates b_0, b_i, b_{ij} and b_{ii} are the solutions to the n_b + 1 normal equations, with n_b being the total number of the coefficients, written as:

$$X'X\beta = X'Y \quad \text{(A1.3)}$$

and

$$Y = Xb + \varepsilon, \quad \text{(A1.4)}$$

which is the matrix notation of Eq. (A1.1). The least squares estimates, β, of the elements of **b** in Eq. (A1.4) are

$$\beta = (X'X)^{-1}X'Y \tag{A1.5}$$

where **X'** is the transverse of **X** and $(\mathbf{X'X})^{-1}$ is the inverse of **X'X**.

Appendix A2 Output file of NONLIN for the etch rate

Title Estimate the influence of PWR,P,F,O on the ERSi

Variable PWR ! Power in Watts
Variable P ! Pressure in mTorr
Variable F ! Total Gas Flow in sccm
Variable O ! % O2 in Total Gas Flow
Variable ERSi ! Etch Rate of Si in micron/min

Parameters b0,b1,b2,b3,b4,b12,b13,b14,b23,b24,b34,b11,b22,b33,b44

Function ERSi=b0+b1*PWR+b2*P+b3*F+b4*O+b12*PWR*P+b13*PWR*F
+b14*PWR*O+b23*P*F+b24*P*O+b34*F*O+b11*PWR^2+b22*P^2+b33*F^2
+b44*O^2

---- Final Results ----

Number of observations = 30
Maximum allowed number of iterations = 50
Convergence tolerance factor = 1.000000E-010
Stopped due to: Both parameter and relative function convergence.
Number of iterations performed = 2
Final sum of squared deviations = 4.21719E-002
Standard error of estimate = 0.0530232
Average deviation = 0.0282111
Maximum deviation for any observation = 0.0803333
Proportion of variance explained (R^2) = 0.9305 (93.05%)
Adjusted coefficient of multiple determination (Ra^2) = 0.8656 (86.56%)
Durbin-Watson test for autocorrelation = 1.799

---- Descriptive Statistics for Variables ----

Variable	Minimum value	Maximum value	Mean value	Standard dev.
PWR	-1	1	0	0.6432675
P	-1	1	0	0.6432675
F	-1	1	0	0.6432675
O	-1	1	0	0.6432675
ERSi	0.076	0.72	0.4014333	0.1446369

---- Calculated Parameter Values ----

Parameter	Initial guess	Final estimate	Standard error	t	Prob(t)
b0	1	0.465666667	0.02164664	21.51	0.00001
b1	1	0.05575	0.01530648	3.64	0.00241
b2	1	0.145166667	0.01530648	9.48	0.00001
b3	1	0.00333333333	0.01530648	0.22	0.83054
b4	1	-0.12375	0.01530648	-8.08	0.00001
b12	1	0.0615	0.02651161	2.32	0.03487
b13	1	-0.0444999999	0.02651161	-1.68	0.11395
b14	1	-0.00025000	0.02651161	-0.01	0.99260
b23	1	2.1660E-011	0.02651161	0.00	1.00000
b24	1	-0.0015	0.02651161	-0.06	0.95563
b34	1	-0.051	0.02651161	-1.92	0.07358
b11	1	-0.0023333333	0.02024857	-0.12	0.90979
b22	1	-0.0557083333	0.02024857	-2.75	0.01485
b33	1	-0.0254583334	0.02024857	-1.26	0.22787
b44	1	-0.0770833333	0.02024857	-3.81	0.00172

---- Analysis of Variance ----

Source	DF	Sum of Squares	Mean Square	F value	Prob(F)
Regression	14	0.5645035	0.04032168	14.34	0.00001
Error	15	0.04217192	0.002811461		
Total	29	0.6066754			

Appendix A3 The output file of NONLIN for the etch rate when some terms of the model are removed as suggested by the "t" statistics of Appendix A2

Title Estimate the influence of PWR,P,F,O on the ERSi

Parameters b0,b1,b2,b4,b12,b13,b34,b22,b33,b44

Function ERSi = b0+b1*PWR+b2*P+b4*O+b12*PWR*P+b13*PWR*F+;
b34*F*O+b22*P^2+b33*F^2+b44*O^2

---- Final Results ----

Number of observations = 30
Maximum allowed number of iterations = 50
Convergence tolerance factor = 1.000000E-010
Stopped due to: Both parameter and relative function convergence.
Number of iterations performed = 2
Final sum of squared deviations = 4.23518E-002
Standard error of estimate = 0.0460173
Average deviation = 0.0276694
Maximum deviation for any observation = 0.0816667
Proportion of variance explained (R^2) = 0.9302 (93.02%)
Adjusted coefficient of multiple determination (Ra^2) = 0.8988 (89.88%)
Durbin-Watson test for autocorrelation = 1.861

---- Descriptive Statistics for Variables ----

Variable	Minimum value	Maximum value	Mean value	Standard dev.
PWR	-1	1	0	0.6432675
P	-1	1	0	0.6432675
F	-1	1	0	0.6432675
O	-1	1	0	0.6432675
ERSi	0.076	0.72	0.4014333	0.1446369

---- Calculated Parameter Values ----

Parameter	Initial guess	Final estimate	Standard error	t	Prob(t)
b0	1	0.464333333	0.01587748	29.24	0.00001
b1	1	0.05575	0.01328405	4.20	0.00044
b2	1	0.145166667	0.01328405	10.93	0.00001
b4	1	-0.12375	0.01328405	-9.32	0.00001
b12	1	0.0615	0.02300865	2.67	0.01462
b13	1	-0.0445000001	0.02300865	-1.93	0.06738
b34	1	-0.051	0.02300865	-2.22	0.03841
b22	1	-0.055375	0.0173929	-3.18	0.00467
b33	1	-0.025125	0.0173929	-1.44	0.16407
b44	1	-0.07675	0.0173929	-4.41	0.00027

---- Analysis of Variance ----

Source	DF	Sum of Squares	Mean Square	F value	Prob(F)
Regression	9	0.5643235	0.06270261	29.61	0.00001
Error	20	0.04235183	0.002117592		
Total	29	0.6066754			

Appendix A4 The calculation of F statistics to test the significance of the model

The last line of the Analysis of Variance table (Appendix A3) indicates the total variation in a set of data, which is called the total sum of squares (SST). It is computed by summing the squares of the deviations of the observed Y_u's about their average value,

$$\bar{Y} = (Y_1 + Y_2 + \cdots + Y_N)/N \qquad \text{(A4.1)}$$

thus,

$$SST = \sum_{u=1}^{N} (Y_u - \bar{Y})^2 \qquad \text{(A4.2)}$$

The quantity SST has associated with it N - 1 degrees of freedom since the sum of the deviations, $Y_u - \bar{Y}$, is equal to zero.

The total sum of squares can be partitioned into two parts; the sum of squares due to regression (SSR) and the sum of squares unaccounted for by the fitted model (SSE). The formula for calculating SSR is

$$SSR = \sum_{u=1}^{N} \left(\hat{Y}(X_u) - \bar{Y}\right)^2 \qquad \text{(A4.3)}$$

The deviation $\hat{Y}(X_u) - \bar{Y}$ is the difference between the value predicted by the fitted model for the *u*th observation and the overall average of the Y_u's. If the fitted model contains p coefficients, the number of degrees of freedom associated with SSR is p - 1. The SSE is

$$SSE = \sum_{u=1}^{N} \left[Y_u - \hat{Y}(X_u)\right]^2 \qquad \text{(A4.4)}$$

The quantity SSE is also called the sum of squares of the residuals. The number of degrees of freedom for SSE is defined as N - p which is the difference between that for SST and that for SSR, i.e. (N - 1) - (p - 1) = N - p. The SSR and SSE are listed in the first and second row, respectively, of the ANOVA table in Appendix A3.

The usual test of the significance of the fitted regression equation is by calculating the value of the F-statistic

$$F = \frac{SSR/(p-1)}{SSE/(N-p)} \qquad \text{(A4.5)}$$

and comparing the F value to the table value, $F_{\alpha, p-1, N-p}$, which is the upper 100α percent point of the F-distribution with p - 1 and N - p degrees of freedom, respectively. The

result is indicated in the ANOVA table by Prob (F). The lower the Prob (F), the more significant the model and the less likely that the actual values of all the coefficients are zero.

The "proportion of variance explained (R^2)" in Appendix A3 indicates how much better the model predicts the dependent function than just using the mean value of the dependent function. This is also known as the coefficient of multiple determination:

$$R^2 = SSR/SST \tag{A4.6}$$

If the model perfectly predicts the observed data, the value of this statistic will be 1 (100%). The "adjusted coefficient of multiple determination (R_a^2)" in Appendix A3 is an R^2 statistic adjusted for the number of coefficients in the model and the number of data observations. It is a more conservative estimate of the percentage of variance explained, especially when the sample size is small compared to the number of coefficients. It is computed using the formula:

$$R_a^2 = 1 - \frac{SSE/(N-p)}{SST/(N-1)} \tag{A4.7}$$

From Appendix A3, it is seen that R^2 and R_a^2 are 93% and 89%, respectively, indicating that the obtained model predicts the observed data very well.

Appendix A5 Test the lack of fit of the model

In general, to say the fitted model is inadequate or is lacking in fit is to imply the proposed model does not contain a sufficient number of terms. This inadequacy of the model is due to either or both of the following causes:

1. Factors (other than those in the proposed model) that are omitted from the proposed model but affect the response.

2. The omission of higher-order terms involving the factors in the proposed model which are needed to adequately explain the behaviour of the response.

In the following analysis, it is assumed that the inadequacy is due to the second cause, i.e. the omission of higher order terms in the fitted model. This is because in most plasma modelling situation the factors have been determined by consideration of underlying principle of plasma process and previous knowledge of chemistry. Therefore, it is not likely that new factors should be introduced into the experimental design upon

detecting inadequacy of the fitted model.

The test for adequacy (or zero lack of fit) of the fitted model requires two conditions be met regarding the collection (design) of the data values:

1. The number of distinct design points, n, must exceed the number of terms in the fitted model. If the fitted model contains p terms, then $n > p$.

2. An estimate of the experimental error variance that does not depend on the form of the fitted model is required. This can be achieved by collecting at least two replicate observations at one or more of the design points and calculating the variation among the replicates at each point.

When the above two conditions are met, the residual sum of squares, SSE, can be partitioned into two sources of variation: the variation among the replicates at those design points where replicates are collected, and the variation arising from the lack of fit of the fitted model. The sum of squares due to the replicate observations is called the sum of squares for pure error (SS_{PE}) and is calculated using

$$SS_{PE} = \sum_{l=1}^{n} \sum_{u=1}^{r_l} (Y_{ul} - \overline{Y}_l)^2 \qquad (A5.1)$$

where Y_{ul} denotes the uth observation at the lth design point ($u = 1, 2, \ldots, r_l \geq 1$, $l = 1, 2, \ldots, n$). $\overline{Y}_l$ is defined as the average of the r_l observations at the lth design point. The sum of squares due to lack of fit (SS_{LOF}) is found by subtraction

$$SS_{LOF} = SSE - SS_{PE} \qquad (A5.2)$$

or, alternatively, if $\hat{Y}_l$ is the predicted value of the response at the lth design point, then

$$SS_{LOF} = \sum_{l=1}^{n} r_l(\hat{Y}_l - \overline{Y}_l)^2 \qquad (A5.3)$$

The degrees of freedom associated with SS_{PE} in Eq. (A5.1) is $N_r - n$, where N_r is the total number of replicated observations, so that the degrees of freedom associated with

SS_{LOF}, obtained by subtraction, is (N - p) - (N_r - n).

In the etch rate example, there is only one design point (settings 0,0,0,0) with 6 replicates. Therefore, l = 1, r_l = 6 and SS_{PE} is

$$SS_{PE} = \sum_{u=1}^{6} (Y_u - \bar{Y})^2, \tag{A5.4}$$

which is found to be 0.0177. Therefore, SS_{LOF} = SSE - SS_{PE} = 0.0422 - 0.0177 = 0.0245.

The test of the null hypothesis of adequacy of fit (or lack of fit is zero) involves calculating the value of the F-ratio

$$F = \frac{SS_{LOF}/[(N-p) - (N_r-n)]}{SS_{PE}/(N_r-n)} \tag{A5.5}$$

and comparing the value with a table value of F. Lack of fit can be detected at the α level of significance if the value F exceeds the table value, $F_{\alpha, (N-p)-(Nr-n), Nr-n}$, where the latter quantity is the upper 100α percentage point of the central F-distribution. In the etch rate example,

$$F = \frac{0.0245/(19 - 5)}{0.0177/5} = 0.4614 \tag{A5.6}$$

which is less than the table value $F_{0.1, 14, 5}$ = 3.25. Therefore, we infer that there is no evidence to indicate that the fitted model exhibits lack of fit at the α = 0.1 level of significance. In other words, the quadratic model is adequate to fit the etch rate data.

Appendix A6 Principles of multi-objective optimization

Multi-objective optimization is concerned with the minimization of a vector of objectives **f**(**x**) which may be the subject of a number of constrains or bounds. Mathematically it is expressed as:

$$\min_{\mathbf{x} \in \Re^n} \mathbf{f}(\mathbf{x})$$

subject to:

$$g_i(\mathbf{x}) = 0 \qquad i = 1, \ldots, m_e$$

$$g_i(\mathbf{x}) \leq 0 \qquad i = m_e+1, \ldots, m$$

$$\mathbf{x}_l \leq \mathbf{x} \leq \mathbf{x}_u$$

Since $f(x)$ is a vector, if any of the components of it are competing, there is no unique solution to this problem. Instead, the concept of non-inferiority [A6.1] must be used to characterize the objectives. A non-inferior solution is one in which an improvement in one objective requires a degradation of another. In two-dimensional representation, the set of non-inferior solutions lies on the curve between C and D of Fig. A6.1. Since any point in the variable space that is not a non-inferior point represents a point in which improvement can be obtained in all the objectives, it is clear that such a point is of no value to solve the problem. Multi-objective optimization is, therefore, concerned with the generation and selection of non-inferior solution points.

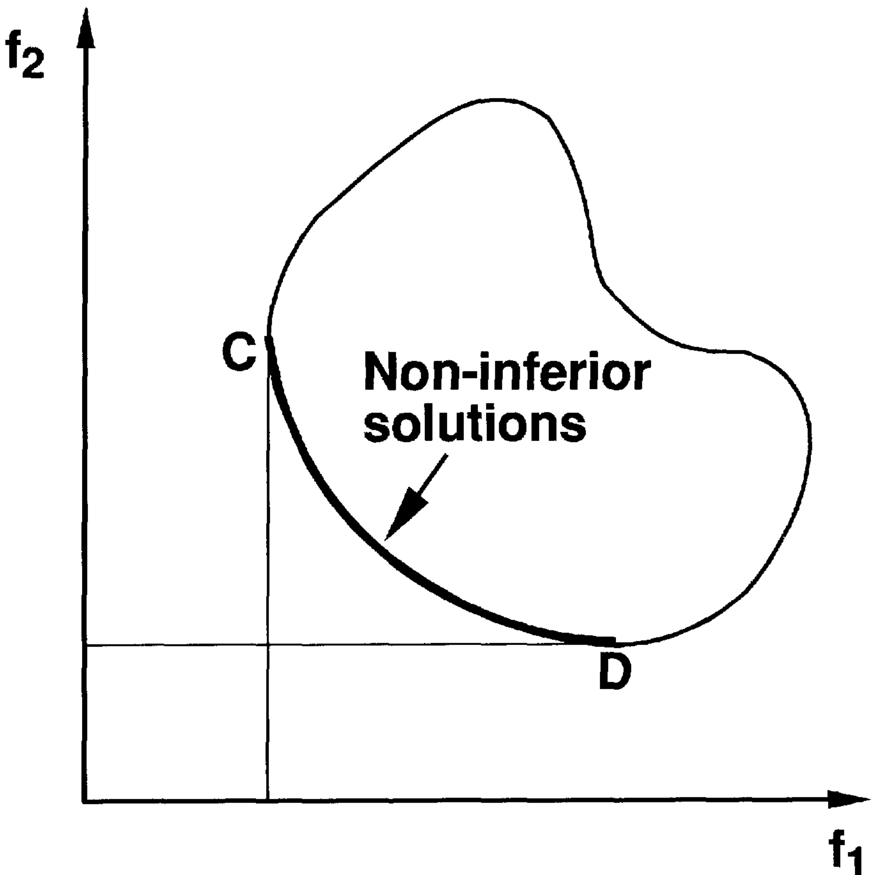

Fig. A6.1 *2-dimensional representation of non-inferior solutions.*

Of the various methods of multi-objective optimization, the Goal Attainment method [A6.2] is described next and will be found to be most useful for the optimization of the SF_6/O_2 process. The method involves expressing a set of design goals, $\mathbf{f}^* = \{f_1^*, \ldots, f_m^*\}$, which is associated with a set of objectives, $\mathbf{f}(\mathbf{x}) = \{f_1(\mathbf{x}), \ldots, f_m(\mathbf{x})\}$. The problem formulation allows the objectives to be under- or over-achieved, enabling the designer to be relatively imprecise about initial design goals. The relative degree of under- or over-achievement of the goal is controlled by a vector of weighting coefficients, $\mathbf{w} = \{w_1, \ldots, w_m\}$ and is expressed as a standard optimization problem using the following formulation:

$$\begin{aligned} &\text{minimize } \gamma \\ &\gamma \in \Re,\ \mathbf{x} \in \Omega \\ &f_i(\mathbf{x}) - w_i\gamma \leq f_i^* \quad i = 1, \ldots, m \end{aligned}$$

The term $w_i\gamma$ introduces an element of slackness into the problem which otherwise imposes that the goals be rigidly met. The weighting factor, $\mathbf{w}$, enables the designer to express a measure of the relative trade-offs among the objectives. For instances, setting $\mathbf{w}$ equal to the initial goals indicates that the same percentage under- or over-attainment of the goals is achieved. Hard constrains can be incorporated into the design by setting a particular weighting factor to zero (i.e., $w_i = 0$). The method provides a convenient intuitive interpretation of the design problem, which is solvable using standard optimizing procedures. Due to its ability and flexibility, the method has been chosen for the optimization of the plasma etching process for deep silicon trench etching.

References

A6.1 Y. Censor, "Pareto optimality in multiobjective problems," *Appl. Math. Optimiz.*, Vol. 4, pp. 41-59, 1977.

A6.2 P. J. Feming, "Application of multi-objective optimization to compensator design for SISO control systems," *Electron. Lett.*, Vol. 22, pp. 258-259, 1986.

Summary

Integrated silicon sensors are very promising in realizing high performance, low cost information processing systems, due to the integration of sensing and actuating elements with signal processing circuits in a single silicon chip. Silicon micromachining is an essential step in the fabrication of various silicon-based micromechanical structures required for integrated silicon sensors. Plasma etching, a key technique of pattern transfer in integrated circuit manufacturing, is a very important alternative to wet chemical etching techniques conventionally dominating in silicon micromachining. This is because plasma etching has a number of advantages over the traditional wet etching, such as the ability of achieving very small ($\sim \mu m$) feature size and independency on crystal orientation of the substrate. The former is important in surface micromachining, while the latter provides more flexibility for bulk micromachining. Moreover, plasma etching can yield unique micromachining techniques which, due to the nature of dry processing, can circumvent some fundamental problems of using wet chemicals, such as sticking in surface micromachining. This thesis presents plasma etching techniques which have been developed for the fabrication of integrated silicon sensors.

Chapter 1

In this chapter the potential of integrated silicon sensors and the fast-growing silicon micromachining technology are highlighted. An overview of three major silicon micromachining techniques is given, i.e. bulk micromachining, surface micromachining and wafer-to-wafer bonding, as well as some emerging techniques, such as micromachining using SOI substrates, porous silicon, epitaxial lateral overgrowth and ion-beam or laser-assisted etching. The necessity of using plasma etching for micromachining is discussed and the motivation of plasma etching research for the application is put forward.

Chapter 2

In this chapter some theoretical and practical aspects of the plasma etching techniques are discussed. After a brief introduction to the basic characteristics of plasma, the two most important processes in a plasma, i.e. production of species and development of self-bias at the RF-electrode, are described in detail. Mechanisms which are considered to be responsible for the etching are discussed and some typical types of plasma reactors are described. Major plasma etching chemistries, including F-atom dominant, unsaturated etchant and chlorine/bromine based, are discussed. The most important developments of plasma etching for micromachining, as described in literature, are also

summarized. Process control strategy and method of process optimization are described and finally problems encountered when using plasma etching are pointed out.

Chapter 3

This chapter describes plasma etching process development for the patterning of a polysilicon/silicon nitride/polysilicon sandwich structure, which is used as the structural membrane of a surface micromachined tactile image sensor and a tuneable interferometer. A silicon nitride plasma etching chemistry selective over polysilicon is developed using CHF_3 + N_2 gas mixtures. A multi-step process is designed for the etching of the sandwich structure, using a CF_4 + SF_6 + O_2 plasma to etch the top polysilicon layer and the CHF_3 + N_2 plasma to etch the nitride layer. Thus the top two layers of the membrane can be patterned, while keeping the attack of the lower polysilicon layer minimized. However, a thin polymer layer will be formed on the polysilicon surface if the nitride layer above is etched using the CHF_3 + N_2 chemistry, causing electrical insulation between this polysilicon layer and the subsequently deposited conductive layer. Special post-processing after the nitride plasma etching using *in-situ* O_2 plasma treatment has been found to be effective in removing the polymer layer.

Chapter 4

In this chapter two planarization techniques for surface micromachining using plasma etching are described. A local planarization technique is developed to improve the step coverage of structural layers on steep sacrificial PSG steps. The technique involves depositing an extra PSG layer followed by an anisotropic plasma etching-back. PSG spacers are formed along the sidewalls of the sacrificial PSG pattern, rounding-off the original sharp corners of the pattern. A CHF_3 + C_2F_6 plasma is optimized for the etching-back. A global planarization technique providing fully planarized PSG filling in large area silicon trenches is developed using two-layer resist coating and plasma etching-back. An image reversal photoresist is used in the two-layer resist system and optimized conditions are found for the resist patterning and thermal cure. The plasma etching-back uses a CHF_3 + C_2F_6 + O_2 process in which O_2 content is varied to match the etch rates of the PSG and photoresist.

Chapter 5

This chapter describes single crystal silicon plasma etching processes for Selective Epitaxial Growth (SEG) and silicon micro-tip fabrication, in which gas mixtures of CF_4 + Cl_2 are used. The sidewall profile of the silicon etching (or the degree of bowing)

can be changed and the etching selectivity over the resist or silicon dioxide mask can be improved, by increasing the content of Cl_2 in the gas mixture. A vertical sidewall profile is achieved for SEG application with 10 sccm Cl_2 addition in 210 sccm CF_4 using a composite mask of resist and oxide. A controlled degree of bowing is realized for silicon micro-tip fabrication when the Cl_2 addition is 50 sccm in 170 sccm CF_4 using an oxide mask.

Chapter 6

In this chapter a silicon micromachining technique based on plasma etching - SIMPLE is presented and tested. The SIMPLE technique combines the advantages of both conventional bulk micromachining (thick structural layers) and surface micromachining techniques (small lateral dimensions). It involves anisotropic etching of lightly n-doped silicon epitaxial layers and isotropic etching of heavily n-doped buried layers using a $Cl_2 + BCl_3$ plasma. Thus high aspect ratio single crystal silicon microstructures can be fabricated with close separation (μm) in a single plasma etching. The technique does not depend on wet chemicals to remove the sacrificial layer, therefore eliminating sticking problems. It is compatible with integrated circuit fabrication processes and, therefore, on-chip integration of micromechanical structures with electronic circuitry can be achieved. The $Cl_2 + BCl_3$ plasma etching chemistry is optimized to obtain the maximum lateral etching of the n^+-buried layer while keeping the etching of the lightly n-doped epitaxial layer anisotropic.

Chapter 7

This chapter presents general methods of optimizing plasma etching processes using statistical experimental design and data analysis, using a $SF_6 + O_2$ plasma as an example. Practical constraints on the design of experiment are described and some of the common experimental designs are given. Using an orthogonal design, the $SF_6 + O_2$ plasma is optimized for the etching-through of silicon membranes, which is required for the fabrication of many bulk-micromachined devices. The plasma is further characterized using the Response Surface Methodology (RSM), which yields a series of quadratic models of the process responses as a function of input variables. Based on the models a multi-objective optimization scheme is used to optimize the plasma process for deep silicon trench etching applications.

Chapter 8

In this chapter the conclusions of this research and some perspectives of future development are given.

Samenvatting

Door de integratie van sensoren en actuatoren met signaalverwerkende circuits op een enkele silicium chip, kunnen geïntegreerde complete informatie verwerkende systemen worden gefabriceerd van hoge kwaliteit tegen lage kosten. Silicium micromachining is een essentiele proces stap bij de fabricage van verschillende micromechanische structuren in silicium, die nodig zijn voor geïntegreerde siliciumsensoren. Plasma etsen, een sleuteltechniek bij het overbrengen van patronen tijdens de fabricage van geïntegreerde circuits, is een zeer belangrijk alternatief voor de natte, chemische etstechnieken die van ouds de micromechanica domineren. Dit komt door de voordelen die plasma-etsen biedt ten opzichte van het traditionele natte etsen; zoals de zeer kleine afmetingen van de structuren (~ μm) en het etsen onafhankelijk van de kristaloriëntatie van het substraat. Het eerste punt is van belang bij surface-micromachining. Het laatste geeft meer flexibiliteit bij bulk-micromachining. Verder biedt plasma-etsen unieke mogelijkheden doordat door de droge ets enkele fundamentele problemen van het natte etsen, zoals sticking, voorkomen kunnen worden. In dit proefschrift worden plasma-etstechnieken gepresenteerd die zijn ontwikkeld voor de fabricage van geïntegreerde siliciumsensoren.

Hoofdstuk 1

In dit hoofdstuk worden de mogelijkheden van geïntegreerde siliciumsensoren behandeld en wordt de snel groeiende micromachiningtechnologie toegelicht. Een overzicht wordt gegeven van de drie voornaamste silicium micromachiningtechnieken, namelijk; bulk-micromachining, surface-micromachining en wafer-to-wafer bonding. Ook worden enkele opkomende technieken behandeld, zoals micromachining door gebruik te maken van SOI substraten, poreus silicium, epitaxiale, laterale overgroei en ion-beam of laser ondersteund etsen. De noodzaak van het gebruik van plasma-etsen voor micromachining wordt behandeld, evenals de motivering voor plasma-etsonderzoek voor deze toepassing.

Hoofdstuk 2

In dit hoofdstuk worden een aantal theoretische en praktische aspecten van plasma-etstechnieken besproken. Na een korte introductie in de basiseigenschappen van plasma's worden de twee meeste belangrijke processen in een plasma in detail behandeld; te weten het ontstaan van reactieve elementen en het ontstaan van self-bias aan de RF elektrode. Mechanismen die verantwoordelijk worden geacht voor het etsproces worden behandeld en enkele typische voorbeelden van plasma-reactoren

worden beschreven. Ook wordt er aandacht besteed aan de belangrijkste plasma samenstellingen, waaronder plasma's in welke fluor dominant is, onverzadigd etsen en etsen op basis van chloor/broom. De meest belangrijke ontwikkelingen op het gebied van plasma-etsen voor micromachining, zoals die beschreven worden in de literatuur, worden ook samengevat in dit hoofdstuk. Verder worden de wijze van procesbeheersing en een methode voor procesoptimalisatie beschreven. Als laatste worden mogelijke problemen toegelicht die tijdens het plasma-etsen op kunnen treden.

Hoofdstuk 3

Dit hoofdstuk beschrijft de plasma-etsprocesontwikkeling voor het aanbrengen van het patroon in een meerlaags structuur samengesteld uit polysilicium/siliciumnitride/ polysilicium, welke wordt toegepast als membraan in een surface-micromachined tactiele sensor en in een instelbaar interferentiefilter. Een siliciumnitride plasma-ets is ontwikkeld die selectief is ten opzichte van polysilicium, door gebruik te maken van een $CHF_3 + N_2$ gasmengsel. Het proces bestaat uit verschillende stappen om de gestapelde structuur te etsen. Een plasma bestaande uit; $CF_4 + SF_6 + O_2$, is gebruikt om de bovenste polysilicium laag te etsen en een $CHF_3 + N_2$ plasma voor het etsen van het nitride. Hierdoor worden de twee bovenste lagen geëtst en wordt de aantasting van de onderste laag tot een minimum beperkt. Echter, een dun polymeer zal zich vormen op de onderste polysiliciumlaag, als gevolg van de nitride ets met CHF_3 en N_2. Dit zal een elektrische isolatie veroorzaken tussen deze polylaag en de daarna gedeponeerde geleidende laag. Een extra processtap volgende op de nitride plasma-ets bestaande uit een in-situ O_2 plasma behandeling, was voldoende om dit polymeer te verwijderen.

Hoofdstuk 4

Twee planarisatie technieken voor surface-micromachining worden beschreven die gebruik maken van plasma-etsen. Een lokale planarisatietechniek is ontwikkeld voor de verbetering van de stapbedekking van structurele lagen over hoge stappen van het sacrificial PSG. De techniek behelst het deponeren van een extra PSG laag gevolgt door terugetsen met behulp van een anisotropische plasma-ets. Extra PSG zijwanden vormen zich langs de rand van het PSG patroon die de originele scherpe randen afronden. Een $CHF_3 + C_2F_6$ plasma is geoptimaliseerd voor het terugetsen. Door gebruik te maken van een fotolaklaag en terugetsen met plasma, is een globale planarisatietechniek verkregen die geëtste sleuven kan vullen met PSG. Er wordt een patrooninverterende fotolak gebruikt en optimale omstandigheden zijn bepaald voor het aanbrengen van het patroon in de fotolak en het uitbakken. De plasma terugets maakt gebruik van een $CHF_3 + C_2F_6 + O_2$ mengsel, waarbij de hoeveelheid O_2 wordt gevarieerd om een gelijke etssnelheid van PSG en fotolak te verkrijgen.

Hoofdstuk 5

Dit hoofdstuk beschrijft het monokristallijn silicium plasma-ets proces voor Selectieve Epitaxiale Groei (SEG) en de fabricage van een microtip in silicium waarbij gebruik wordt gemaakt van een CF_4 + Cl_2 mengsel. Het profiel van de zijwand van het silicium etsproces (of de helling) kan worden veranderd en de etsselectiviteit ten opzichte van fotolak of het siliciumdioxide masker kan worden verbeterd door een toename van de hoeveelheid Cl_2 aan het mengsel. Een verticale zijwand voor SEG toepassingen is mogelijk met 10 sccm Cl_2 toegevoegd aan 210 sccm CF_4, gebruikmakend van een samengesteld masker uit fotolak en oxide. Een gecontroleerde helling voor de silicium microtip is bereikt door een toevoeging van 50 sccm Cl_2 aan 170 sccm CF_4 en het gebruik van een oxide masker.

Hoofdstuk 6

In dit hoofdstuk wordt een silicium micromachining techniek, SIMPLE, gepresenteerd en getest, die gebaseerd is op plasma-etsen. De SIMPLE techniek combineert de voordelen van bulk-micromachining (dikke structurele lagen) en surface-micromachining (kleine laterale dimensies). Het bestaat uit het anisotroop etsen van een licht n-gedoteerde silicium epitaxiale laag en isotroop etsen van een zwaar n-gedoteerde begraven laag met behulp van een Cl_2 + BCl_3 plasma. Hiermee kunnen monokristallijne siliciumstructuren worden verkregen met een grote hoogte-breedte verhouding en kleine onderlinge afstanden (μm) in een enkele plasma etsstap. Deze techniek gebruikt geen natte etsen voor het verwijderen van sacrificial-lagen, waardoor er geen problemen kunnen optreden als sticking. Het proces is compatibel met de fabricage van geïntegreerde circuits en het is dus mogelijk micromechanische structuren te combineren met elektronica op dezelfde chip. De samenstelling van het Cl_2 + BCl_3 plasma is geoptimaliseerd om een maximale, laterale etssnelheid te verkrijgen van de begraven laag, terwijl de ets van de licht n-gedoteerde epitaxiale laag anisotroop blijft.

Hoofdstuk 7

Methodes worden gepresenteerd voor het optimaliseren van plasma-ets processen met behulp van statistisch experimenteel ontwerpen en data analyse. Hierbij wordt SF_6 + O_2 plasma als een voorbeeld gebruikt. Praktische beperkingen bij het ontwerpen van experimenten worden besproken en een aantal veelvoorkomende experimentele ontwerpen worden gegeven. Gebruikmakend van orthogonaal ontwerpen, is het SF_6 + O_2 plasma geoptimaliseerd voor het etsen van silicium membranen, wat gebruikt wordt bij de fabricage van veel sensoren gemaakt met bulk-micromachining. Het plasma is verder gekarakteriseerd met behulp van de Response Surface Methodology (RSM). Dit

levert een serie kwadratische modellen van de proces gedragingen op als een functie van de invoervariabelen. Met deze modellen als basis wordt met behulp van een meervoudig-doel-optimalisatie-methodologie het plasma proces geoptimaliseerd voor het etsen van sleuven in silicium.

Hoofdstuk 8

In dit hoofdstuk worden de conclusies gepresenteerd die het gevolg zijn van dit onderzoek en worden enkele toekomstperspectieven gegeven.

Acknowledgement

This thesis is the result of my Ph.D. study in the past four years, which could not be completed without the help and support of many people, especially the members of the Laboratory for Electronic Instrumentation, Department of Electrical Engineering, Delft University of Technology and the staff of the Delft Institute of Microelectronics and Submicrontechnology (DIMES). I would like to express my sincere gratitude to all of them.

In particular I would like to thank:

Professor Dr. Ir. S. Middelhoek, my thesis advisor, for giving me the opportunity to study in this laboratory towards the Ph.D. degree and for creating a most stimulating and pleasant research environment.

Dr. Ir. R. F. Wolffenbuttel, who is my project supervisor, for his continuous support, guidance and stimulation.

Dr. P. J. French, who is most helpful in solving technological problems involved in my research, for his support and many scientific and linguistic advices.

Dr. P. M. Sarro for her support in performing the research in DIMES, advices and encouragement.

M. Laros, who maintains plasma etching equipments in DIMES and guided me in both general IC processing and plasma etching, for his great enthusiasm and devotion.

H. W. van Zeijl for his assistance in photolithography and advice in using image reversal resist and H. Schellevis for providing baseline plasma process of silicon trench etching. The contributions of the other DIMES staff members of IC process group are also greatly appreciated.

B. P. van Drieënhuizen and J. F. L. Goosen, who are my fellow Ph.D. students, for their help in solving technical problems, sharing their expertise of many computer programs and softwares and linguistic assistance. The translation of the summary of this thesis into Dutch by J. F. L. Goosen is mostly appreciated.

A. Burtsev, a visiting undergraduate student in DIMES, for his carrying out the plasma

etching experiment for the process characterization using Response Surface Methodology (Chapter 7 of this thesis).

G. de Graaf for his technical support and I. Egmond and E. Sharabi for their administrative support.

Dr. Y. S. Raptis and Professor E. Anastassakis of National Technical University, Greece for their help in strain profile characterization, and Dr. G. Vegh of Technical University of Budapest, Hungary for his performing spreading resistance measurement.

The Delft University of Technology, the Dutch Organization for Scientific Research (NWO) for their financial support to travel abroad.

Mr. G. G. Lee, my late uncle, for his great enthusiasm in helping me to come to the Netherlands for the Ph.D. study.

My parents for their never-ending encouragement and support.

My wife Wen Jing for her understanding and patience during these years, which enabled me to complete the research and to write the thesis.

List of Publications related to this research

Journal papers

Y. X. Li, P. J. French and R. F. Wolffenbuttel, "Effects of plasma etching chemistry and post-processing on the mechanical adhesion and electrical contact of double polysilicon layer structures," *IEEE Trans. Electron Devices*, Vol. 42, pp. 64-70, 1995.

Y. X. Li, P. J. French and R. F. Wolffenbuttel, "Plasma planarization for sensor applications," to be published in *J. Microelectromechanical Systems*, Vol. 4, Sept. 1995.

Y. X. Li, P. J. French and R. F. Wolffenbuttel, "Selective reactive ion etching (RIE) of silicon nitride over silicon using CHF_3 with N_2 addition," to be published in *J. Vac. Sci. Technol.*, Vol. B13, Sept/Oct 1995.

A. Burtsev, Y. X. Li, H. W. van Zeijl and C. I. M. Beenakker, "Development of silicon trench plasma etching process using response surface methodology (RSM)," submitted to *Microelectronic Engineering*.

Y. X. Li, M. R. Wolffenbuttel, P. J. French, M. Laros, P. M. Sarro and R. F. Wolffenbuttel, "Reactive ion etching (RIE) techniques for micromachining applications," *Sensors and Actuators*, Vol. A41-42, pp. 317-323, 1994.

Y. X. Li, M. Laros, P. M. Sarro, P. J. French and R. F. Wolffenbuttel, "Plasma etching of polysilicon/nitride/polysilicon sandwich structure for sensor applications," *Microelectronic Engineering*, Vol. 21, pp. 341-344, 1993.

Y. X. Li, M. Laros, P. M. Sarro, P. J. French and R. F. Wolffenbuttel, "Process design for plasma etching of polysilicon/silicon nitride/polysilicon sandwich structures for sensor applications," *Microelectronic Engineering*, Vol. 20, pp. 321-328, 1993.

Conference proceedings

Y. X. Li, P. J. French, P. M. Sarro and R. F. Wolffenbuttel, "Fabrication of a single crystalline siliocn capacitive lateral accelerometer using micromachining based on single step plasma etching," in *The Proc. 8th IEEE International Workshop on Micro Electro Mechanical Systems (MEMS'95)*, 1995, pp 398-403.

Y. X. Li and R. F. Wolffenbuttel, "Development of deep silicon plasma etching process for sensor applications," to be published in *The Proc. SPIE - the Intern. Soc. Opt. Eng. (Micromachining and Microfabrication Process Technology)*, Texas, U. S. A., Oct. 1995.

D. Poenar, Y. X. Li and R. F. Wolffenbuttel, "Dry etching of deep trenches in Si," to be published in *Micro Mechanics Europe 1995*, Copenhagen, Denmark, Sept. 1995.

Y. X. Li, P. J. French and R. F. Wolffenbuttel, "Reactive ion etching (RIE) techniques for sensor applications," in *The Proceedings of the Dutch Conference on Sensor Technology 1994*, 1994, pp. 323-326.

J. A. Foerster, Y. X. Li, M. Bartek, P. J. French and R. F. Wolffenbuttel, "Fabrication of recessed micro-tips in silicon for sensor applications," in *The Proceedings of Micro Mechanics Europe 94*, 1994, pp. 198-201.

Y. X. Li, P. J. French, H. Schellevis, P. M. Sarro and R. F. Wolffenbuttel, "SIMPLE - a fabrication technique for SIlicon Micromachining by single step PLasma Etching," in *The Book of Abstracts of EUROSENSORS VIII Conference*, Toulouse, France, Sept. 1994, p. 112.

M. Bartek, P. J. French, P. Gennissen, Y. X. Li and R. F. Wolffenbuttel, "Epitaxial layer optimization for smart silicon sensors by placing read-out electronics in SEG silicon," in *The Book of Abstracts of EUROSENSORS VIII Conference*, Toulouse, France, Sept. 1994, p. 213.

J. F. L. Goosen, P. J. French, Y. X. Li, D. Poenar, B. P. van Drieënhuizen and R. F. Wolffenbuttel, Surface micromachining module compatible with BIFET electronic processing, in *The Book of Abstracts of EUROSENSORS VIII Conference*, Toulouse, France, Sept. 1994, p. 108.

M. R. Wolffenbuttel, Y. X. Li, D. Poenar, P. J. French, P. P. L. Regtien and R. F. Wolffenbuttel, "Multilayer membranes for a tactile imaging sensor, using surface micromachining and RIE," in *The Proceedings of the 7th International Conference on Solid-State Sensors and Actuators (Transducer'93)*, 1993, pp. 284-287.

About the author

Yuan Xiong Li was born in Fujian, P. R. China, on December 8, 1963. He received the B.Sc. degree in semiconductor physics and device physics from Hefei University of Technology, P. R. China in 1982, and the M.Sc. degree in integrated circuit design and processing from Shanghai Institute of Metallurgy, Academia Sinica, P. R. China in 1986, with his thesis work concerning the design and processing technology of high frequency dual gate MOSFET's. From 1986 to 1991, he was a research associate in the same institute , where he was engaged in research on high speed CMOS technology and ASIC design. Since September 1991 he has been at the Laboratory for Electronic Instrumentation, Department of Electrical Engineering, Delft University of Technology, working toward the Ph.D. degree on the subject of micromachining technology for sensor applications.